UNIVERSIDAD COMPLUTENSE DE MADRID
FACULTAD DE FARMACIA

TESIS DOCTORAL

Optimización del metabolismo de polihidroxialcanoatos de *Pseudomonas putida* KT2440 mediante abordajes de biología sintética y de sistemas

Synthetic and systems biology approaches towards the optimization of polyhydroxyalkanoates metabolism in *Pseudomonas putida* KT2440

MEMORIA PARA OPTAR AL GRADO DE DOCTOR

PRESENTADA POR

María Tsampika Manoli

Directores

María Auxiliadora Prieto Jiménez
Juan Nogales Enrique

Madrid

UNIVERSIDAD COMPLUTENSE DE MADRID

FACULTAD DE FARMACIA

DEPARTAMENTO DE BIOQUÍMICA Y BIOLOGÍA MOLECULAR

Optimización del metabolismo de polihidroxialcanoatos de *Pseudomonas putida* KT2440 mediante abordajes de biología sintética y de sistemas.

Synthetic and systems biology approaches towards the optimization of polyhydroxyalkanoates metabolism in *Pseudomonas putida* KT2440

TESIS DOCTORAL

MARIA TSAMPIKA MANOLI

DIRECTORES:

MARÍA AUXILIADORA PRIETO JIMÉNEZ

JUAN NOGALES ENRIQUE

CONSEJO SUPERIOR DE INVESTIGACIONES CIENTÍFICAS

CENTRO DE INVESTIGACIONES BIOLÓGICAS MARGARITA SALAS

MADRID, 2020

CSIC

Consejo Superior de Investigaciones Científicas

UNIVERSIDAD COMPLUTENSE DE MADRID

FACULTAD DE FARMACIA

DEPARTAMENTO DE BIOQUÍMICA Y BIOLOGÍA MOLECULAR

Optimización del metabolismo de polihidroxialcanoatos de *Pseudomonas putida* KT2440 mediante abordajes de biología sintética y de sistemas.

Synthetic and systems biology approaches towards the optimization of polyhydroxyalkanoates metabolism in *Pseudomonas putida* KT2440

TESIS DOCTORAL

MARIA TSAMPIKA MANOLI

DIRECTORES:

MARÍA AUXILIADORA PRIETO JIMÉNEZ

JUAN NOGALES ENRIQUE

CONSEJO SUPERIOR DE INVESTIGACIONES CIENTÍFICAS

CENTRO DE INVESTIGACIONES BIOLÓGICAS MARGARITA SALAS

MADRID, 2020

CSIC

CONSEJO SUPERIOR DE INVESTIGACIONES CIENTÍFICAS

To my loving family and friends

To Fran

Στην αγαπημένη μου οικογένεια και φίλους

Μην ψάχνεις πια αλλού εδώ είναι το ταξίδι.

ACKNOWLEDGEMENTS

Since the first time I read a doctoral thesis, these first pages were the ones I liked the most. Now, it is my turn to thank all the people that contributed to the realization of this work. First of all, I would like to specially acknowledge my Thesis directors, Auxi and Juan, for their help and support during all these years and for keeping me motivated. Thanks to Auxi for introducing me into the inspiring world of PHA and to Juan for transmiting its passion towards *Pseudomonas* metabolism and robustness.

Secondly, I would like to thank the sources of my research funding from European Union´s Horizon 2020 research and innovation program under grant agreements number 633962 (P4SB project) and 814418 (SinFonia project). I would also acknowledge support from the Community of Madrid P2018NMT_4389 (Nanobiocargo) and the Spanish Ministry of Science, Innovation and Universities, BIO2017-83448-R_TECMABIO project and BIO2014-59528-JIN _RobDcode. Special thanks to the Spanish National Research Council (CSIC), the Biological Research Center Margarita Salas (CIB) and its facilities for all the scientific support.

Furthermore, special appreciation to our mentors and contributors to the scientific support, José Luis García, Eduardo Díaz, Manuel Carmona, Pedro García, Ernesto García, Jesús Sanz, Beatriz Maestro, Beatriz Galán and Gonzalo Durante. I would like to deeply thank all the past and present members of Rubenes big family for all the help, and motivation throughout all these years. In advance, my sincere gratitude goes to my labmates. During all these years, I was rewarded with a cheerful, helpful and friendly group of fellow students and postdocs. Special tribute to all the Rubenes that we also spent time outsite the laboratory, contributing funny moments to this adventure.

I would like to thank Dr. Eduardo Espeso for helping and motivating me all these years in Madrid. Special thanks to my friends throughout the world and my family for supporting and loving me during these challenging moments. Finally, last but not least, I would like to thank Fran, for being my companion in this interesting trip.

Contents

ABBREVIATIONS

ACADs	Acyl-CoA dehydrogenases
ACP	Acyl-carrier protein
ACS1	Acyl-CoA synthase 1
ADIPATE	Adipic acid
ALE	Adaptive laboratory evolution
ATP	Adenosine triphosphate
BCPY	Biomass-coupled product yield
BSA	Bovine serum albumin
C11:1	Undecenoic acid
CA	Catabolite activity
CDW	Cell dry weight
cfu	Colony forming unit
CoA	Coenzyme A
COBRA	Constraint-based reconstruction and analysis
CRISPR	Clustered regularly interspaced short palindromic repeats
14DBO	1,4-Butanediol
DBTL	Design-build-test-learn
DHAP	Dihydrixyacetone phosphate
ED	Entner-Doudoroff
EDTA	Ethylenediaminetetraacetic acid
EG	Ethylene glycol
EMP	Embden Meyerhof Parnas
ESI	Electrospray ionization
FBA	Flux balance analysis
FDA	Food and drug regulation administration
G3P	Glycerol-3-phosphate
GAPs	Granule associated proteins
GC-MS	Gas chromatography-mass spectrometry
GEMs	Genome-scale models
GENREs	Genome-scale network reconstructions
GFP	Green fluorescent protein
GOI	Gene of interest
GRAS	Generally recognized as safe
4HBz	Sodium 4-hydroxybenzoic acid

HV1	Host vector system safety, level 1
IPTG	Isopropyl-β-D-thiogalactopyranoside
ICL	Isocitrate lyase
ICD	Isocitrate dehydrogenase (dimeric)
IDH	Isocitrate dehydrogenase (monomeric)
KDPG	2-Keto-3-deoxy-6-P-gluconate
KO	Knockout mutants
LB	Luria-Bertani medium
lcl-PHA	Long-chain-length polyhydroxyalkanoates
mcl-PHA	Medium-chain-length polyhydroxyalkanoates
MCS	Multicloning site
MDI	4-4-Methylene diphenyl diisocyanate
MS	Mass sprectrometry
N.A.	Not determined
NAD	Nicotinamide adenine dinucleotide
NADP	Nicotinamide adenine dinucleotide phosphate
N.D.	Not detected
OD	Pptical density
ORF	Open reading frame
PA	Polyamides
PAC	Phenylacetic acid
PBAT	Polybutylene adipate terephthalate
PBS	Phosphate buffered saline
PBS polymers	Polybutylene succinate
PCA	Protocatechuic acid
PCR	Polymerase chain reaction
PDHC	Pyruvate dehydrogenase complex
PET	Polyethylene terephthalate
PE	Polyethylene
PP	Polypropylene
PPP	Pentose phosphate pathway
P(3HB)	Poly(3-hydroxybutyrate)
P(3HHx)	Poly(3-hydroxyhexanoate)
P(3HHp)	Poly(3-hydroxyheptanoate)
P(3HO)	Poly(3-hydroxyoctanoate)
P(3HD)	Poly(3-hydroxydecanoate)
P(3HDD)	Poly(3-hydroxydodecanoate)

P(3HTD)	Poly(3-hydroxytetradecanoate)
P(3HV)	Poly(3-hydroxyvalerate)
P(3HO-*co*-3HHx)	Poly(3-hydroxyoctanoate-*co*-3-hydroxyhexanoate)
P(3HB-*co*-3HHx)	Poly(3-hydroxybutyrate-*co*-3-hydroxyhexanoate)
P(3HB-*co*-3HV)	Poly(3-hydroxybutyrate-*co*-3-hydroxyvalerate)
PHA	Polyhydroxyalkanoates
PIDH	Prokaryotic isocitrate dehydrogenases
PLA	Polylactic acid
PTT	Polytrimethylene terephthalate
PU	Polyurethane
(*R*)-HA	(*R*)-3-Hydroxyacyl-carboxylic acid (free monomers)
(*R*)-HA-CoA	(*R*)-3-Hydroxyacyl-CoA
RBS	Ribosome binding site
RT-PCR	Reverse transcription polymerase chain reaction
rpm	Revolutions per minute
scl-PHA	Short-chain-length polyhydroxyalkanoate
SDS-PAGE	Sodium dodecyl sulfate-polyacrylamide gel electrophoresis
SEVA-DS	Standard european vector architecture database
sgRNA	Single guide RNA
TCA	Tricarboxylic cycle
TEM	Transmission electron microscopy
TPHTA	Terephthalic acid
Tris	Tris(hidroximetil)aminometano
U	Enzymatic activity unit
wt	Wild type
X-gal	5-Bromo-4-chloro-3-indolyl-β-D-galactopyranoside
$Y_{p/s}$	Product yield

SUMMARY

Pseudomonas putida KT2440 is a model environmental bacterium attracting considerable interest as a cell-factory through synthetic and systems biology approaches. Its metabolism has been extensively characterized and a high-quality metabolic model is available (*i*JN1441), allowing for the systems evaluation of its metabolic capabilities. Among its biotechnological applications, KT2440 is widely used for the production of polyhydroxyalkanoates (PHA), also known as bacterial polyesters or bioplastics. This family of polyesters presents interesting properties for replacing fossil fuel-based plastics. PHA metabolism in *P. putida* is mediated through the PHA polymerase (PhaC) and the PHA depolymerase (PhaZ) that synthesizes and degrades PHA, respectively, in a continuous cycle. The PHA are accumulated in the cytoplasm as carbon and energy stores, and contrary to oil-based plastic, they are produced from renewable resources. PHA metabolism goes beyond solely having a role in carbon storage since recent findings have highlighted its function as a balancing route that increases *P. putida* fitness during environmental perturbations.

In the first Results chapter, validations of the PHA cycle in conferring robustness to *P. putida* will be described in depth. In order to assess the effect of blocking the PHA turnover in the cell, a *phaZ* null strain was constructed. We then validated a library of strains expressing *phaZ* over a range of levels in this Δ*phaZ* background. To investigate the impact of tuning *phaZ* expression on *Pseudomonas* metabolism, key physiological parameters were analyzed under PHA production conditions. A variety of physiological responses were observed, resulting in changes in cell number, cell size, PHA accumulation and production of extracellular *(R)*-Hydroxyalkanoic acids (*(R)*-HAs) as compared between wild type and *phaZ* null strains. These observations suggest a rerouting of the cellular carbon flux when the PHA cycle is disrupted. Overall, *phaZ* variant strains shown important differences including growth rate, octanoate consumption rate, residual octanoate and a panel of extracellular metabolites. To get a glance of the overall metabolism, these experimental data were contextualized into the *in silico* metabolic model (*i*JN1411). The systems impact of the PHA cycle in the physiology of this model bacterium, including the presence of a residual oxidative metabolism under stationary growth phase, associated to high flux through PHA cycle will be discussed.

In the second Results chapter, studies were carried out to address the physiological roles of the prokaryotic isocitrate dehydrogenase isoenzymes (PIDH) in *P. putida* and the role of functional redundancy as mechanism of metabolic robustness in

this bacterium. PIDH is an ancient and highly diverse enzyme. There are many examples in the literature of works characterizing the biochemical and enzymatic properties of these enzymes in a variety of microorganisms. However, it is not clear why two PIDH are present in pseudomonads in terms of microbial physiology, since this is a characteristic more commonly observed and studied in psychrophiles. The results for the purification and enzymatic characterization of the two PIDH from *P. putida* is presented. The key amino acid residues for catalytic activity of the monomeric PIDH (*idh*) were verified by site-directed mutagenesis experiments. In order to study the impact of having two PIDH, the expression levels of both genes were assessed by qRT-PCR experiments under different growth conditions. Finally, in order to study the role of the two PIDH in *P. putida* physiology and metabolism, different isocitrate dehydrogenase deletion mutants were designed. After several tries, we were capable to obtain only the dimeric PIDH (*icd)* deletion mutant, suggesting that monomeric *idh* could be an essential gene in *P. putida.*

The third Results chapter delves into the creation of biofactories producing PHAs from complex and poor PHA substrates. In particular, PHA substrates generated from the breakdown of lignin and the fossil fuel-based plastics, polyethylene terephthalate (PET) and polyurethane (PU). We present a set of *in silico* growth-coupled PHA overproducer *P. putida* strains, using monomers derived from the hydrolysis of these polymers, as carbon sources. We applied an iterative DBTL cycle in order to achieve this goal. The model of *P. putida*, *i*JN1411, was used as a computational platform to *in silico* designing of growth-coupled strains. Subsequently, these *in silico* designs were implemented, evaluated and optimized *in vivo*. Cutting edge synthetic biology approaches were used to generate the high number of gene knockouts and knockins required to systematically remove all potential competing pathways and to reroute the carbon flux towards PHA biosynthesis. The effect on PHA production of the iterative rounds of model-guided genetic modifications was subsequently evaluated by means of high-throughput physiological experiments. Finally, we discuss the impact of synthetic and systems approaches towards the industrial production of PHA from other inexpensive substrates such as sugars and glycerol using *P. putida* as a bacterial chassis.

RESUMEN

Pseudomonas putida KT2440 es una bacteria modelo en biotecnología que suscita mucho interés como catalizador celular, y que es susceptible de ser optimizado mediante herramientas de biología sintética y de sistemas. Su metabolismo se ha caracterizado ampliamente y se cuenta con un modelo metabólico muy preciso (*i*JN1411), que permite la evaluación de sus capacidades metabólicas mediante una aproximación de biología de sistemas. Entre las aplicaciones biotecnológicas, KT2440 se ha usado ampliamente para la producción de PHA. Esta familia de poliésteres presenta propiedades interesantes para reemplazar a los plásticos de origen petroquímico. El metabolismo de PHA en *P. putida* está mediado por la PHA sintasa (PhaC) y la PHA despolimerasa (PhaZ), que sintetiza y degrada el PHA, respectivamente, en un ciclo continuo. Los PHA se producen a partir de fuentes renovables y se acumulan en el citoplasma bacteriano como fuente de reserva de carbono y energía. Sin embargo el metabolismo de PHA va más allá de ser una mera reserva de carbono, ya que estudios recientes han determinado su función como un ciclo "amortiguador", capaz de mejorar la adaptación del microorganismo ante diferentes perturbaciones ambientales.

En el primer capítulo de la sección de Resultados se describe en profundidad la evaluación del carácter amortiguador del ciclo de PHA, validándose su capacidad de conferir robustez metabólica a *P. putida*. Con el fin de evaluar el efecto del bloqueo del ciclo continuo de PHA en la fisiología de la bacteria, se ha construido una cepa mutante donde se ha delecionado el gen *phaZ*. Se ha validado una librería de cepas derivadas de la mutante Δ*phaZ* con diferentes niveles de expresión del gen *phaZ*. Para investigar el impacto de la variación en la producción de PhaZ en el metabolismo de *Pseudomonas*, se han determinado en cada cepa diferentes parámetros fisiológicos en condiciones de producción de PHA. Estos resultados sugieren un cambio del flujo de carbono cuando se interrumpe el ciclo de PHA. En general, las cepas con diferente expresión de *phaZ* han mostrado cambios importantes, como por ejemplo, la tasa de crecimiento, la tasa de consumo de octanoato, el octanoato residual y la presencia de metabolitos extracelulares. Para relacionar estos resultados con el metabolismo general del carbono, estos datos experimentales se han contextualizado *in silico* en el modelo metabólico *i*JN1411, incluyendo la presencia del metabolismo oxidativo residual, durante la fase estacionaria del crecimiento asociada en el alto flujo mediante el ciclo de PHA. Por último, se discute en profundidad el impacto del ciclo de PHA en la fisiología de esta bacteria modelo.

En el segundo capítulo de los Resultados, se estudia cómo la redundancia funcional puede ser un mecanismo de robustez en relación con los roles fisiológicos de las isoenzimas de la isocitrato deshidrogenasa prokariota (PIDH). La PIDH es una enzima ancestral y muy diversa en cuanto a su origen y estructura primaria. Existen gran cantidad de trabajos disponibles sobre la caracterización de las propiedades bioquímicas de estas enzimas en una variedad de organismos. Sin embargo, no está claro cuál es la relevancia de la existencia de dos PIDH diferentes en las bacterias de género *Pseudomonas*, ya que esto es una característica observada principalmente en psicrófilos. En este capítulo, se presentan los resultados de la purificación y caracterización enzimática de las dos PIDH de *P. putida*. Los aminoácidos clave para la actividad catalítica en la *idh* monomérica se verifican mediante mutagénesis dirigida. Para estudiar el impacto de la presencia de dos PIDH, se han evaluado los niveles de expresión de ambos genes mediante experimentos de qRT-PCR en diferentes condiciones de crecimiento. Finalmente, para estudiar el papel de las dos PIDH en la fisiología y metabolismo de *P. putida*, se diseñaron diferentes mutantes de deleción de la isocitrato deshidrogenasa. Los resultados indican que sólo se puede obtener el mutante de deleción de la *icd* dimérica, lo que sugiere que la *idh* monomérica podría ser un gen esencial en *P. putida*.

El tercer capítulo de Resultados profundiza en la creación de factorías celulares para producir PHA a partir de sustratos complejos. En particular, los sustratos generados a partir de la descomposición de la lignina y de los plásticos basados en combustibles fósiles, cómo el tereftalato de polietileno (PET) y el poliuretano (PU). Presentamos un conjunto de cepas de *P. putida* super-productoras de PHA capaces de utilizar *in silico* hidrolizados PET y PU como fuentes de carbono. Se adoptan abordajes de vanguardia de biología sintética y de sistemas integrados en ciclos interactivos de optimización de Diseño, Construcción, Prueba, y Aprendizaje (DBTL). El modelo de *P. putida*, *i*JN1411, se utilizó como plataforma computacional para lograr la producción de PHA acoplada al crecimiento. Además, estos diseños *in silico* fueron implementados, evaluados y optimizados *in vivo*. Para ello se utilizan técnicas clásicas de biología molecular para delecionar un gran número de genes necesarios e introducir otros, para eliminar sistemáticamente todas las vías potencialmente competidoras con nuestro diseño *in silico*, y redirigir el flujo de carbono hacia la biosíntesis de PHA. El efecto de las rondas iterativas de modificaciones genéticas guiadas por el modelo *i*JN1411 sobre la producción de PHA, se evalúan mediante experimentos fisiológicos. Finalmente, se discute el posible impacto de las herramientas de biología sintética y de sistemas en la producción industrial de PHA a partir de sustratos sostenibles como azúcares y glicerol, utilizando *P. putida* como chasis bacteriano.

1. INTRODUCTION

1 INTRODUCTION

1.1 Plastic pollution, moving towards a sustainable society

The term “plastic” originates from the Greek word “plastikos” (πλαστικός), used to describe something capable to mold or suitable for molding. Nowadays, plastic is a term used to describe a very large family of materials with diverse characteristics, properties and uses. Thanks to their versatility, the plastic materials provide personalized solutions for a huge variety of necessities and applications. Their massive production and their inappropriate waste management during the last decades, led to plastic pollution of lands, seas, oceans etc., causing environmental worries. Nowadays, the European Commission takes the challenge to transform the European economy into a circular and efficient strategy as far as it concerns the use of resources. New challenges must be addressed concerning the indiscriminate plastic abandonment (“littering”) and the options at the end of life of certain types of plastic wastes (especially plastic packaging), if we want to take advantage of their full potential in efficient and circular economy in the use of resources (https://ec.europa.eu/environment/circular-economy/index_en.htm).

In 2017, the global plastic production reached up to almost 350 million tons with 64.4 million tons only produced in Europe. China (50.1%) is the major producer of plastics followed by Europe (18.5%) and North America (17.7%). These data were obtained from market studies provided by PlasticsEurope (PEMRG) and Converted Market and Strategy GmbH and can be downloaded in th following link: (https://www.plasticseurope.org/application/files/6315/4510/9658/Plastics_the_facts_2018_AF_web.pdf).

Nowadays, plastics can be based on fossil or biological origins. A quite new bio-based plastic terminology is referred to bio-based “drop in” polymers (e.g. PET). They are chemically identical to petrochemical counterparts but derived from biomass and they are usually no biodegradable. They differ from the biodegradable new bio-based plastics such as PHA (polyhydroxyalkanoate) and PLA (polylactic acid). Recent economic studies have revealed that bio-based polymers can create new business opportunities and stable growth in new plastic markets (Prieto, 2016). Currently, bioplastics represent roughly one percent of the 359 million tons of plastic produced annually. However, as demand is rising, and more sophisticated biopolymers, application and products are emerging while the market is continuously growing. According to the latest market data compiled by European Bioplastics in cooperation with the research institute nova-Institute, global bioplastics production capacity tend to increase from around 2.11 million

tons in 2019 to approximately 2.43 million tons in 2024 (see Figure 1 and the following link https://www.european-bioplastics.org/market/).

Bio-based drop-in PET (polyethylene terephthalate), PE (polyethylene), PP (polypropylene) polymers and new biopolymers, PLA and PHA show the highest growth rates on the market. The most capital investment is expected to take place in Asia and South America due to better access to feedstock and a favourable political framework. Synthetic and systems biology approaches will provide improved strains that can utilize low-cost substrates such as glucose, glycerol, and lignin-derived compounds for bio-based polymers widespread production (Prieto, 2016).

The durability of plastics is not always considered as a virtue, since it may impede the up-cycling of these materials in terms of circular economy and sustainably. PLA, PHA and succinate (PBS) polymers are the most common bio-based polymers since they have been successfully applied in the biodegradable plastic industry. The biodegradability of these polymers has been utilized to solve environmental issues, such as waste and public pollution. In this Doctoral Thesis, *P. putida* strain metabolism was redesigned in order to transform recalcitrant plastic wastes derivatives into new-high added alternatives, such as the bio-plastics, PHA by using synthetic and systems biology approaches.

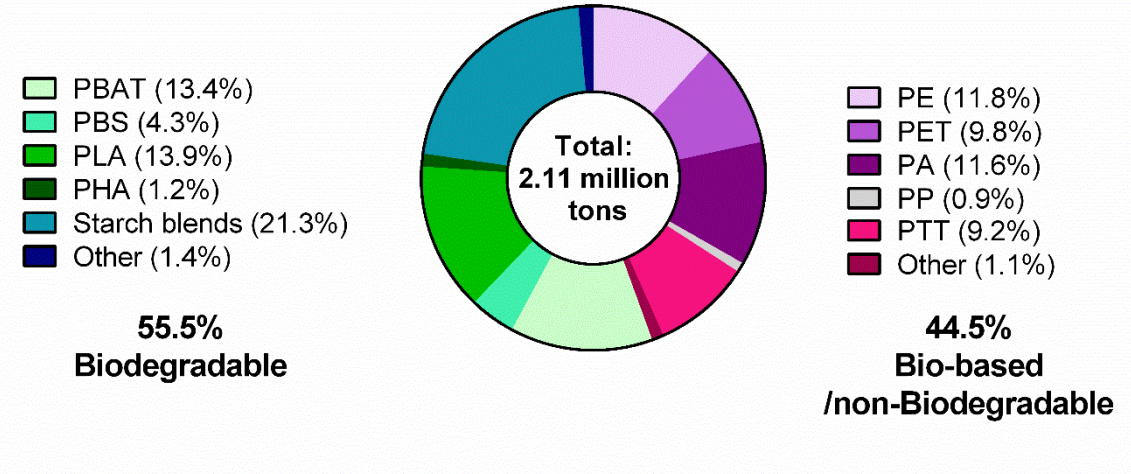

Figure 1. Global production capacities of bioplastics in 2018 (by material type); among the biodegradable bio-based plastics, the PBAT (polybutylene adipate terephthalate), PBS (polybutylene succinate), PLA (polylactic acid), PHA (polyhydroxyalkanoates), starch blends and others are presented. Among the bio-based non-biodegradable, PE (polyethylene), PET (polyethylene terephthalate), PA (polyamides), PP (polypropylene), PTT (polytrimethylene terephthalate) and others are distinguished. The figure was adapted from the Bioplastics Market update 2019 (European Bioplastics, nova-Institute, 2019).

1.2 General characteristics of polyhydroxyalkanoates

1.2.1 A general overview of PHA

PHA were first described in 1926 by M. Lemoigne in France, who reported the presence of poly(3-hydroxybutyrate) (P(3HB)) in the cytoplasm of *Bacillus megaterium* (Lemoigne, 1926). PHA are naturally produced in a great range of bacteria (>300 species) and are non-toxic and biodegradable. They are biocompatible without producing noxious effects to the human body. There have been found in many Gram-negative and Gram-positive genera, as well as some archaea and consist of 3-*(R)*-hydroxyalkanoate monomers (Han *et al.*, 2010).

PHA are accumulated in the cell cytoplasm under nutrient imbalances, including carbon excess coupled with a limitation of at least one nutrient such as nitrogen, oxygen, or phosphorus (Lee *et al.*, 2000; Poblete-Castro *et al.*, 2012). PHA are not solely a source of carbon and energy during nutrient starvation, but rather a key element in resource balancing (De Eugenio *et al.*, 2010a). Depending on the microorganism, the PHA production could reach up to 90% of cell dry weight (Kniewel *et al.*, 2017).

These insoluble and highly hydrophobic intracellular inclusions are well known as PHA granules or carbonosomes that traditionally have been proposed to be coated by a layer of proteins and phospholipids (Jendrossek and Pfeiffer, 2014). The presence of phospholipids though is still a controversial issue and is under discussion (Pötter and Steinbüchel, 2006; Bresan *et al.*, 2016). On the contrary, the presence of proteins on the surface of PHA granules is widely accepted. The so-called granule associated proteins (GAPs) play structural, biosynthetic, catabolic and regulatory functions. These include PHA synthases, depolymerases and a group of low weight molecular proteins called phasins. Other proteins such as transcriptional regulators, hydrolases or reductases can also be found on the surface of the granule (Jendrossek and Pfeiffer, 2014).

The PHA synthases are key enzymes in the biosynthesis of these polyesters; they transform the *(R)*-hydroxyalkanoate-CoA (*(R)*-HA-CoA) thioesters monomers in a polyester chain by liberating one CoA molecule. The resulting polyester molecule is further degraded into free monomers *(R)*-HAs by PHA depolymerases (see section 1.4.4 and 1.4.5 for more details).

The phasins are amphipathic proteins located in the interphase between PHA and the cytoplasm. In general, the phasins play regulatory and functional roles, by regulating the formation, the localization, the number and size of the granules (Moldes *et al.*, 2004; Galán *et al.*, 2011). Phasins have attracted much interest as biotechnological tools, as

immobilization platforms (Wong and Rehm, 2018), biomedical (tissue engineering) and drug delivery (biosurfactant properties) applications (Parlane *et al.*, 2017). A detailed description of these enzymes in *P. putida* could be found in 1.4.4 and 1.4.5 sections.

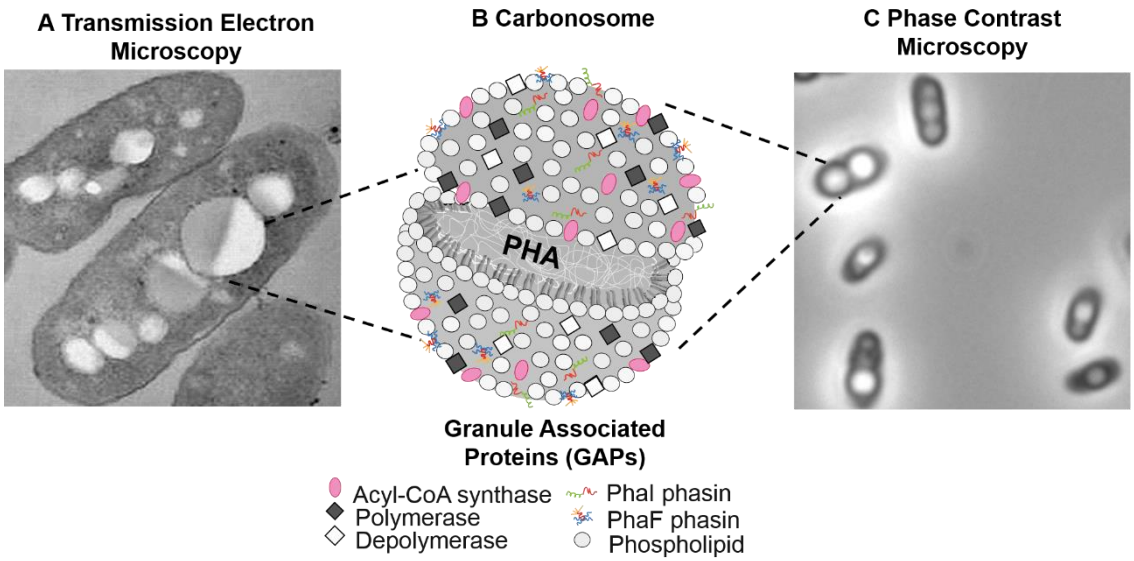

Figure 2. PHA production and granule schematic structure. The presence of granules is observed by Transmission electron microscopy (TEM) and phase contrast microscopy pictures of *P. putida* KT2440 growing under PHA production conditions, **A. and C**., respectively. **B.** Schematic representation of a PHA granule from *P. putida* KT2440. The hydrophobic polymer core (PHA) is surrounded by a layer of granule-associated proteins (GAPs) (Galán *et al.*, 2011).

1.2.2 Mechanical, thermal and chemical properties of PHA

The PHA monomeric composition can be influenced by several factors including among others i) the genetic background of the producer organism, ii) the carbon source used which influence the metabolic pathway used and iii) the PHA synthases substrate specificity (Sudesh *et al.*, 2000). As far as it concerns the PHA synthase stereospecificity, only monomers with *R* configuration have been reported until now (De Eugenio *et al.*, 2010a). PHAs are built of 3-hydroxyfatty acid monomers ((*R)*-HAs) where the carboxyl group of one monomer forms an ester bond with the hydroxyl group of the following monomer.

Depending on the total number of carbon atoms within a PHA monomer, they can be classified into short chain length (scl-PHA; 3 to 5 carbon atoms; such P(3HB)), medium chain length (mcl-PHA; 6 to 14 carbon atoms, such as P(3HO)) and long chain length (lcl-PHA; 15 or more carbon atoms) (Li *et al.*, 2016). Several bacteria produce scl-PHA including the model bacterium *Cupriavidus necator* H16 (Kniewel *et al.*, 2017). The mcl-PHA producers belong mainly from the genus *Pseudomonas* (Rai *et al.*, 2011),

whereas lcl-PHA are more scarcely found, such as that produced by a local isolate of *P. aeruginosa* MTCC (Singh and Mallick, 2009). For the purpose of this Doctoral Thesis, we will focus on the mcl-PHA production from *Pseudomonas putida* KT2440.

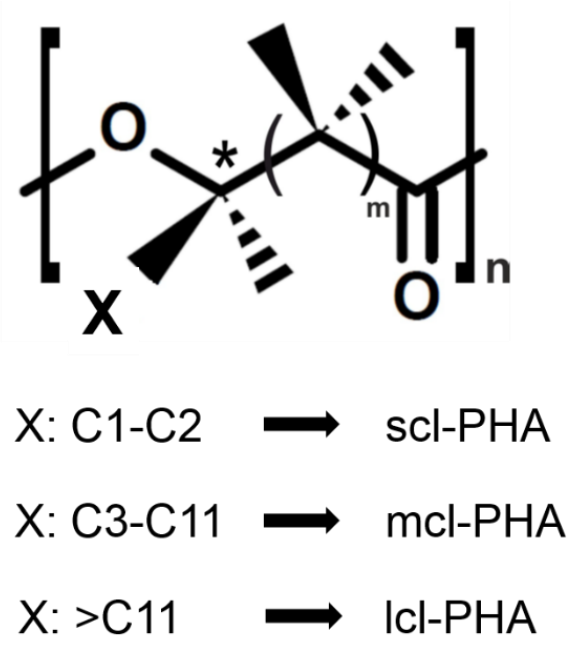

Figure 3. PHA chemical structure. Classification is based on the length of the aliphatic side chain (X) and has been divided into short-length PHAs (scl-PHAs), medium-chain length PHAs (mcl-PHAs) and long-chain length PHAs (lcl-PHAs) depending on the number of carbons. All monomeric units have an asymmetric carbon centre (*) and *R* enantiomer configuration.

Given their natural origin and their physicochemical properties, PHA have attracted much attention as alternative polymeric materials. However, several disadvantages, such as high production costs and incompatibility to thermal approaches due to susceptibility to thermal degradation, limit their application as thermoplastics (Raza *et al.*, 2018). Therefore, it became needed to modify the thermomechanical properties of these polymers, in order to improve their processability.

The diversity of the PHA lays on the side substitution on the position 3. More than 150 different monomer constituents have been described including unsaturated, aliphatic and aromatic groups among others (Zinn *et al.*, 2001). PHA may be composed by only one type of monomer (homopolymers) or by various types of monomers, called copolymers or heteropolymers (Olivera *et al.*, 2010). Depending on the monomer composition and the length of the side chain, the thermomechanical and physicochemical properties such as stiffness, brittleness, melting point, glass transition temperature, degree of crystallinity and resistance to organic solvents may vary. scl-PHA tend to be stiff and brittle with a high degree of crystallinity (60-80%), while mcl-PHA are elastic with low crystallinity (25%), low tensile strength, high elongation to break, low

melting point and glass transition temperature below room temperature (Anjum *et al.*, 2016). A summary of the thermal and mechanical properties of two prototype PHA polymers are listed in the Table 1.

PHA	Monomer Content	σ_t MPa	ε_b %	T_m ºC	T_g ºC	Reference
P(3HB)	100%	40	3-8	173-180	5-9	(Sudesh *et al.*, 2000; Anjum *et al.*, 2016)
P(3HHx-*co*-3HO)	(12-88%)	9	380	61	-31	(Valappil *et al.*, 2006)

Table 1. Thermal and mechanical properties of some representative polymers from the PHA family. T_m, melting temperature; T_g, glass transition temperature. E, Young's modulus; σ_t, tensile strength; ε_b, elongation at break. 3HB: 3-hydroxy-butyrate, 3HHx: 3-hydroxy-hexanoate, 3HO: 3-hydroxy-octanoate.

1.3 An introduction to *Pseudomonas putida:* a model bacterium in biotechnology

Pseudomonas spp, is a continuously growing genus (approximately 300 species) of Gram negative, aerobic, bacillus, belonging to γ-proteobacteria class (Stanier *et al.*, 1966). First description of the genus was due to the professor Migula of the Karlsruhe Institute in Germany at 1894-1900. The etymology of *Pseudomonas* derived from the Greek terminology pseudes (ψευδές) which means false and the monas (μονάς) which means one unit (Palleroni, 2010). There are rod-shaped, non-sporulating, motile with polar flagella bacteria (Nikel *et al.*, 2014b).

One of the early discoveries of the genus was its remarkable metabolic versatility and adaptability to endogenous and exogenous stresses. L.E. Den Dooren in 1926, first observed the ability of *Pseudomonas* to degrade a great range of substrates such as carbohydrates, organic acids, aromatic, amino acids, alcohols and nitrogen compounds (Stanier *et al.*, 1966; Clarke, 1982). Furthermore, *Pseudomonas* spp. could be tolerant to harmful agents present in soils such as disinfectants, detergents, organic solvents and heavy metals (Jimenez *et al.*, 2002; dos Santos *et al.*, 2004). However, pseudomonads are not tolerant to extreme changes concerning temperature and hydrogen ion concentrations resulting in the absence of thermophilic and acidophilic strains included in this genus (Palleroni, 2010). Finally, among the variety of *Pseudomonas* species, can be distinguished some human and plant pathogens, such as *P. aeruginosa* and *P. syringae,* respectively, due to the production of virulence factors (Morris *et al.*, 2008; Gellatly and Hancock, 2013).

P. putida is a “paradigm of a class of cosmopolitan bacteria” isolated from a variety of environments such as soils, plant rhizosphere and water (Nelson *et al.*, 2002; dos Santos *et al.*, 2004). *P. putida* KT2440 (KT stands for Kenneth Timmis) strain derives from the toluene-degrading organism initially isolated in Japan (1960 from an undergraduate student Hosokawa) and designated *as P. arvilla* mt-2 (mt-2, stands for “*meta*-toluate degrader, isolate 2”) and later renamed to *P. putida* mt-2 (Nakazawa, 2002; Timmis, 2002). This strain harbours the TOL plasmid pWW0, which encodes a pathway for toluene and *m*/*p*-xylene biodegradation (Williams and Murray, 1974). Recently, genomic, phylogenetic and catabolic re-assessment of the *P. putida* clade supports the delineation of 4 new species *P. alloputida* sp. nov., *P. inefficax* sp. nov., *P. persica* sp. nov. and *P. shirazica* sp. nov. The *P. putida* KT2440 is reclassified in cluster Pp5, as *P. alloputida* KT2440 (derived from the Greek allos “άλλος”, meaning another *putida*) (Keshavarz-Tohid *et al.*, 2019).

The *P. putida* KT2440 is the best-characterized strain of its species and it is classified by the FDA (Food and Drug Regulation Administration) as HV1 (Host vector system safety level 1) certified strain, suggesting that it is safe to use in a P1 or ML1 environment, but it should not be used as food additive (Kampers *et al.*, 2019). Taking advantage this characteristic, *P. putida* KT2440 was converted to a model organism for biotechnological, environmental and industrial applications such as biodegradation and chemical biotransformation studies (Nikel *et al.*, 2014b). For the purpose of this Doctoral Thesis, we are going to focus our attention and describe in depth the production, characteristics and the PHA metabolism in *P. putida* KT2440.

1.3.1 Available synthetic biology tools in *P. putida* KT2440

Since the publication and the recent revision of the *P. putida* KT2440 genome, much effort has been invested in exploiting these capacities in biotechnological applications (Nelson *et al.*, 2002; Belda *et al.*, 2016). Some of the synthetic biology challenges are the removal of non-desirable traits and the enhancement of the advantageous ones, the insertion of new activities and understand the functionality of complex genetic and metabolic circuits (Nikel *et al.*, 2014b; Nikel *et al.*, 2016).

1.3.1.1 Plasmid availability and genome integration tools

A “Standard European Vector Architecture” database (SEVA-DB, http://seva.cnb.csic.es) is available, where a wide variety of pSEVA plasmid collection is listed (Silva-Rocha *et al.*, 2013; Martínez-García *et al.*, 2015). Many of these plasmids are used in *P. putida*, since it is easily genetically manipulated and can maintain a range of plasmids, containing common broad-host-range multicopy replicons including pBBR1, pRO1600/ColE1 and RK2. On the average, in *P. putida* the plasmid copy number is higher than in *E. coli* (Cook *et al.*, 2018). However, since *P. putida* is naturally resistant to some antibiotics (such as Ampicillin), care must be taken on selecting bacterial markers present in these vectors (Martínez-García and de Lorenzo, 2011).

As far as it concerns the genomic integration approaches using transposons elements, the most studied bacterial transposition systems have been Tn*5* and Tn7 (Choi and Kim, 2009; Hickman and Dyda, 2016). In this work, the site-directed Tn*7*-mediated insertion system was used, which it is targeted at high frequency into the *att*Tn*7* site and it integrates unidirectionally as a single copy located downstream of the *glmS* gene (Lambertsen *et al.*, 2004; Silva-Rocha and de Lorenzo, 2014). Recently, serine recombinases were also tested in *P. putida* KT2440 as a promising tool for high efficiency integration system (Elmore *et al.*, 2017).

1.3.1.2 Gene expression approaches and functional parts

Nowadays, synthetic biology approaches are searching for the best combination of biological parts such as promoters, ribosome binding sites (RBS), coding sequence of the gene(s) of interest, terminators, in order to meet the desired performance criteria for the metabolic engineering purposes. Several advanced cloning methods have been reported so far, such as Sequence and Ligation-Independent Cloning (SLIC) (Li and Elledge, 2012), Gibson DNA assembly (Gibson *et al.*, 2009), BioBricks or BglBricks standards (Anderson *et al.*, 2010; Lee *et al.*, 2011) and Modular Cloning assembly system (Golden Gate-MoClo), among others (Engler *et al.*, 2008; Weber *et al.*, 2011). The latter system is based on type IIs restriction endonuclease, that cleave DNA outside of the recognition site, allowing up to 256 overhangs by producing a 4 nucleotide overhang. These unique overhangs allow multiple DNA fragments assemblies in a single reaction mix (Engler *et al.*, 2008).

Prior metabolic engineering studies in *P. putida* have majorly relied on the *lac* family promoters (*lac*, *lacUV5*, *tac*, *trc*) from *E. coli* (Borrero-de Acuña *et al.*, 2014; Johnson and Beckham, 2015; Elmore *et al.*, 2017). Additionally, works are available on

using native promoters such as *rrn* (Wang *et al.*, 2010), P_m (Gemperlein *et al.*, 2016) or PP_1099 promoter (Lin *et al.*, 2016). For chromosomal expression, constitutive promoters libraries have been described in *P. putida* with variable expression levels (Zobel *et al.*, 2015; Elmore *et al.*, 2017; Cook *et al.*, 2018). In this concept, a library of synthetic promoters with various upstream elements, -35 and -10 sequences and different ribosome binding sites have been tested in *P. putida* KT2440 (Elmore *et al.*, 2017). In this Doctoral Thesis, P_m/*XylS* native activator, induced by 3-methylbenzoate, P_{lac}/*LacI* heterologous activator, induced by IPTG or constitutive promoters have been used (Zobel *et al.*, 2015; Tiso *et al.*, 2016).

1.3.1.3 Genome editing approaches

In many Gram negative bacteria, different markless and scarless gene editing methods have been proposed. These approaches remove any antibiotic marker and require the application of a counterselection system, for instance the sucrose sensitivity conferred by *sacB* gene (Schäfer *et al.*, 1994). pK18*mobsacB* strategy has been widely used in *P. putida* and it was also applied in this Doctoral Thesis (Cai *et al.*, 2009; Galán *et al.*, 2011). Additionally, deletion strategies that apply a counterselection system based on 5-fluorouracil, in order to function, require a strain carrying the *upp* deletion, a gene encoding for uracil phosphoribosyltransferase (Graf and Altenbuchner, 2011).

Furthermore, similar homologous recombination process is realized by the cleavage of the chromosome with unique endonuclease I-Sce-I sites from *Saccharomyces cerevisiae*, added to the segment of interest by the vector system (Martínez-García and de Lorenzo, 2011, 2012). Recently, this system has been updated into new pSEVA variants called as pSEVAn28S, where n means different antibiotic resistance marker such as Amp, Kan, Cm, Sm, Tc and Gm. This novelty also includes the Gibson assembly implementation (Gibson *et al.*, 2009), in order to avoid the use of T4 DNA ligase (Aparicio *et al.*, 2015). With this system 11 chromosomal deletions, accounting for 300 genes, were performed in *P. putida* KT2440, resulting in EM42 and EM383 strains, genetically upgraded strains, as far as it concerns growth properties and stress survival capabilities (Martínez-García *et al.*, 2014).

Other scarless gene knockout approaches include the *λ*/Red based deletions (Luo *et al.*, 2016), customized mini-Tn*5* transposons with the Flp-FRT recombination system (Leprince *et al.*, 2012) and the use of CRISPR/Cas9 (Tan *et al.*, 2018). The latter technique is based on Cas9 nuclease from *Streptococcus pyogenes* that uses a single guide RNA (sgRNA) to target any DNA sequence, widely used in Gram negative and Gram positive bacteria (Cobb *et al.*, 2015).

Finally, random knockouts via transposon mediated-insertional mutagenesis strategies have been traditionally used to study relevant genes to a biological function. This approach results in a single locus mutations that can be identified by insertion mapping (Cebolla and Arévalo-Rodríguez, 2010). A collection of *P. putida* KT2440 mutant strains obtained by mini Tn*5* transposons elements is available, known as *Pseudomonas* Reference Culture Collection and it can be found in the following link: (https://www.gbif.es/coleccion/pseudomonas-reference-culture-collection-estacion-experimental-del-zaidin/) (de Lorenzo et al., 1990; Herrero et al., 1990; Duque et al., 2007). With this approach, *in silico* proposed conditional essential genes in *P. putida* KT2440 (*i*JN746 (Nogales *et al.*, 2008), *i*JP850 (Puchałka *et al.*, 2008)) have been evaluated (Molina-Henares *et al.*, 2010).

1.3.2 Available genome-scale metabolic models

With available publications of full genome sequence, it was possible to identify the gene products and the reactions that make up an organism. Thus, it was feasible reconstruct on a genome-scale, metabolic networks (known as GENREs) for a target organism in a biochemically manner (Monk *et al.*, 2014). Network reconstruction is a long and laborious process and it consists in collecting all the available biochemical, genetic, genomic (BiGG) information and then organizes it into a mathematical format yielding mechanistic genotype-phenotype relationships for microbial metabolism (Figure 4). Since the first GENRE, many more *in silico* models have been followed including that for human metabolism (Edwards and Palsson, 1999). The scope and content of network reconstructions continues to grow by including more and more information about the given organism such as, the entire transcription and translation apparatus of a cell and the structural information about the metabolic enzymes (Palsson, 2015).

Networks consist of compounds (nodes; represented as rows in a matrix) and reactions (links; represented by columns). When many reactions are known to share reactants and products, they can be graphically linked together and mathematically represented. Mathematical representation is based on the stoichiometric coefficients that count the molecules that are consumed and produced by a biochemical reaction and it can be organized in a stoichiometric matrix format **S** (a table). This means that all steady states of a network can be described by a linear equation, **Sv=0**, where **v** is a vector of fluxes through chemical reactions. Every reaction can also be given upper and lower bounds, which define the allowable fluxes of the reactions (Orth *et al.*, 2010; Palsson, 2015).

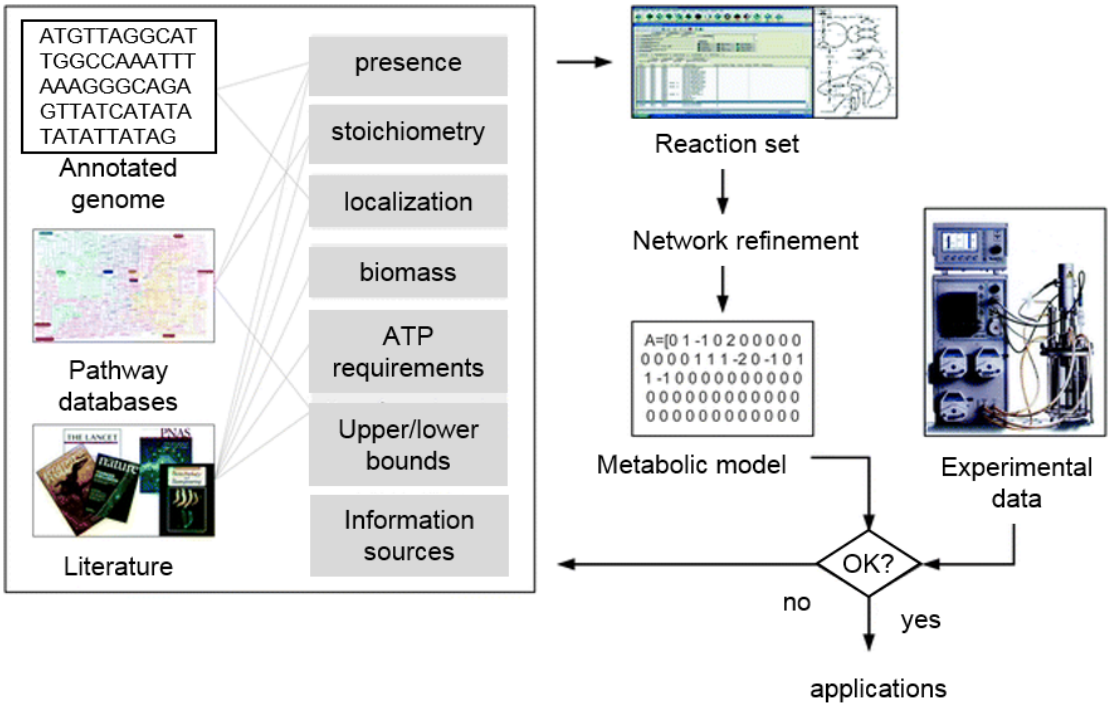

Figure 4. The iterative process of metabolic network reconstruction. The process starts with gathering the current knowledge about the microorganism from multiple sources of information. Next the construction and debugging of the reaction set, the building of a stoichiometric matrix, and the comparison of the *in silico* simulation results using experimental data are carried out. Once the experimental data (i.e., measured rates) are in agreement with the *in silico* predictions, the model can be used for further applications like, e.g., development of metabolic engineering strategies. Adapted from (Baart and Martens, 2012).

The metabolic reconstruction could be divided in four main steps. First, based on the available genome annotated sequence and information of a given organism, can be obtained the draft reconstruction. Second, reconstruction complementation and manual curation process can be done by adding the detailed biochemical, genetic data and known metabolic functions. Third, by adding available detailed physiological data, deletion phenotypes (phenomics), the construction is converted into mathematical format. Finally, the reconstruction is validated against various data sets such as fluxomics, metabolomics, proteomics and transcriptomics (Palsson, 2015).

Nowadays, there are many different reconstructions published and publicly available majorly from prokaryotic microorganism of specific environmental and bioprocessing interest (Kim *et al.*, 2012; Gu *et al.*, 2019). There are available some practical protocols for GENRE and integration of transcriptomics data from our group (Nogales, 2014; Nogales and Agudo, 2015)

*P. putida´*s metabolism has been extensively characterized and eight genome-scale models (known as GEMs) are available including *i*JN746 (Nogales *et al.*, 2008), *i*JP850 (Puchałka *et al.*, 2008), PpuMBEL1071 (Sohn *et al.*, 2010), *i*JP962 (Oberhardt *et al.*, 2011), *i*EB1050 (Belda *et al.*, 2016), PpuQY1140 (Yuan *et al.*, 2017), *i*JN1411

(Nogales *et al.*, 2017) and *i*JN1462 (Nogales *et al.,* 2020). An analytic comparison of the characteristics of each of the above-mentioned metabolic models is provided (Nogales *et al.,* 2017). These genome-scale models have been widely used for studying key metabolic features of *P. putida* such as aromatic and PHA metabolism. The potential carbon, nitrogen, sulphur, phosphorous and iron sources supporting *in silico* growth were tested. Furthermore, using these models, identification of processes non-essential for *P. putida* growth and tolerance to different stressors are feasible. The *i*JN1411 metabolic model was widely used during this Doctoral Thesis.

1.3.3 Design-build-test-learn cycle

DBTL (Design-Build-Test-Learn, Figure 5) cycles are interactive designs combining the advances in systems and synthetic biology towards rational genetic modifications and strains high-throughput phenotyping leading to conclusions, further understanding and additional hypothesis generation (Liu *et al.*, 2015). The Design stage includes the initial steps of experimental configuration, starting from the problem definition, adequate host selection to *in silico* modelling simulations using a variety of available novel software tools. The Build stage begins by applying synthetic biology processes towards host modification and optimization using recombinant DNA technology and different parts assembly approaches. To Test, high-throughput analyses can be realized, testing growth performance, gene and protein expression, PHA production, quantifying the metabolome among others. The Learn stage involves the data analysis in order to identify behaviour patterns and to reach to the conclusions. These steps can be repeated several times in order to reach the corresponding process performance. Furthermore, the goal of these DBTL cycle is the process automation. In this Doctoral Thesis, DBTL approaches were used in distinct Results chapters, in order to achieve the planned objectives.

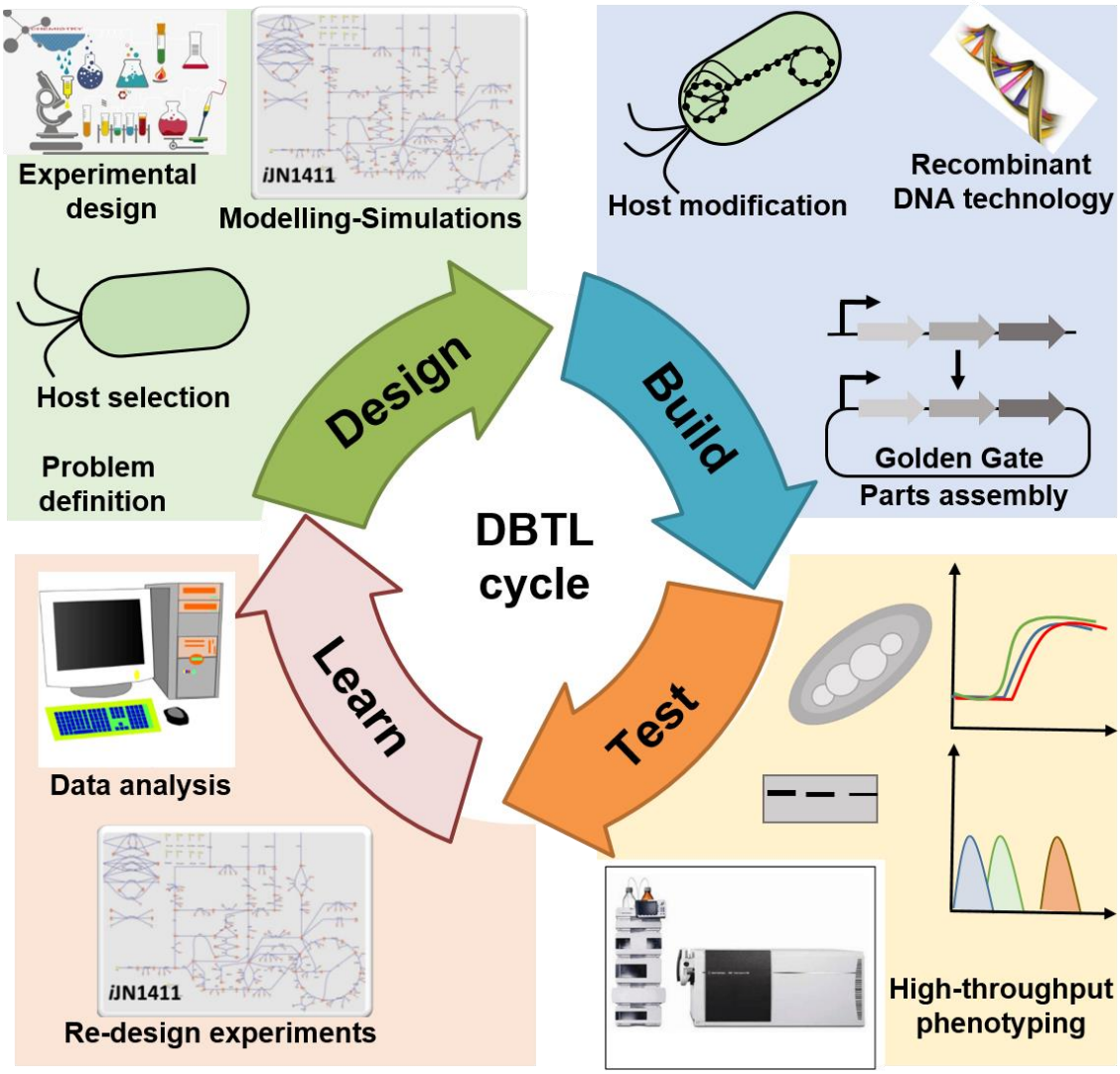

Figure 5. Iterative design of DBTL (Design-Built-Test-Learn) cycle.

1.4 Metabolic pathways involved in mcl-PHA production in *P. putida*

1.4.1 mcl-PHA synthesis from structurally related substrates

In pseudomonads, structurally PHA-related substrates like fatty acids are catabolized through β-oxidation pathway. The fatty acids can be incorporated into PHA directly as β-oxidation intermediates (*(R)*-HA-CoA) avoiding their complete oxidation to acetyl-CoA, yielding monomer chains of equal or shorter length than those of the carbon source applied (Durner *et al.*, 2000). The fatty acid catabolism and the involved enzymes in this route (Fad) are conserved in distinct bacterial species and have been widely studied in the bacterial model *E. coli*.

A detailed β-oxidation pathway in *P. putida* and its connection with PHA metabolism is shown in the Figure 6 and the Supplementary Table S1. In short, the fatty acids are activated into acyl-CoA through the acyl-CoA synthetase (FadD). Subsequently, an acyl-CoA dehydrogenase (FadE) catalyzes the formation of a double bond yielding an enoyl-CoA. In the next step, a tetrameric complex formed by FadBA proteins carries out the hydration, oxidation and thiolysis processes. This complex comprises five enzymatic reactions (enoyl-CoA hydratase, 3-hydroxyacyl-CoA dehydrogenase, cis-Δ^3-trans-Δ^2-enoyl-CoA isomerase, 3-hydroxyacyl-CoA epimerase, and 3-ketoacyl-CoA thiolase) and it is responsible for the removal of two carbon units of the acyl-chain (Pramanik *et al.*, 1979). The intermediates of the β-oxidation enoyl-CoA, *(S)*-3-hydroxyacyl-CoA and 3-ketoacyl-CoA, can be converted into *(R)*-HA-CoA, PHA synthase substrates, through a stereospecific trans-enoyl-CoA hydratase (PhaJ), an epimerase (FadB), or a 3-oxoacyl-ACP reductase (FabG), respectively (Kniewel *et al.*, 2017).

In *P. putida* KT2440, two fatty acid transporter genes, long-chain fatty acid transporter (*fadL*; PP_1689) and short-chain fatty acid transporter (PP_3124) initializing the pathway have been identified (Wang and Nomura, 2010).

FadD (EC 6.2.1.3) is an ATP, CoA and Mg^{2+} dependent enzyme, widely distributed among the organisms and exhibits a broad substrate specificity. This is a cytoplasmic membrane-associated protein that activates exogenous fatty acids into metabolically active CoA thioesters, when they are transported across the cytoplasmic membrane. Two key studies were performed in *Pseudomonas* species reporting two *fadD* gene homologues in *P. putida* U (named as FadD1 and FadD2) (Olivera *et al.*, 2001a) and *P. putida* GPo1 (named as Acs1 and Acs2) (Ruth *et al.*, 2008). FadD1 was proposed to be an enzyme involved in the physiological fatty acid degradation, while the FadD2 was a cryptic gene, induced when the FadD1 was inactivated (Olivera *et al.*, 2001a). Furthermore, the Acs1 and Acs2 shared 94% and 92% identity to FadD1 and FadD2 of *P. putida* U, respectively. By fluorescent microscopy experiments the Acs1 has been mainly associated with the PHA granules, activating the *(R)*-HAs released by the PHA depolymerase during the PHA degradation process, whereas the Acs2 was located in the cellular membrane (Ruth *et al.*, 2008). Finally, in *P. putida* KT2440, three genes encoding putative FadD enzymes (FadD-I; PP_4549, 94% identity to FadD1 of *P. putida* U, FadD-II; PP_4550, 91% identity to FadD2 from *P. putida* U and fadDx; PP_2213) were identified, where the FadD-I was proposed to be the principal one (Wang and Nomura, 2010).

The second step of fatty acid degradation in *P. putida* KT2440 is realized by acyl-CoA dehydrogenases, FadE. They belong to a large family of flavoproteins and show

activity towards a broad range of substrates. The substrate specificity of FadE classifies the enzyme into short, medium, long or very long chain acyl-CoA dehydrogenases. However, the boundary of classification is not tight as substrate specificities of particular enzymes may overlap (Ghisla and Thorpe, 2004). The reaction of dehydrogenation presents the rate limiting step in the β-oxidation, since FadE have the lowest activity among all β-oxidation enzymes in *E. coli* (Lu *et al.*, 2003). Initial works in *P. putida* KT2440 identified PP_2216 as a specific acyl-CoA dehydrogenase for short chain aliphatic fatty acyl-CoAs (McMahon *et al.*, 2005) and the PP_0368 as an inducible phenylacyl-CoA dehydrogenase (McMahon and Mayhew, 2007). Recently, *in silico* analysis of its genome sequence revealed 21 putative acyl-CoA dehydrogenases (ACADs), four (PP_1893, PP_2039, PP_2048 and PP_2437) of which were functionally characterized by mutagenesis studies. The PP_1893 (FadE) and PP_2437 (FadE2) were proposed to directly participate in fatty acid degradation, while the 19 remaining putative ACADs have a redundant role or overlap in terms of function when *P. putida* KT2440 is grown on aliphatic fatty acids (Guzik *et al.*, 2014).

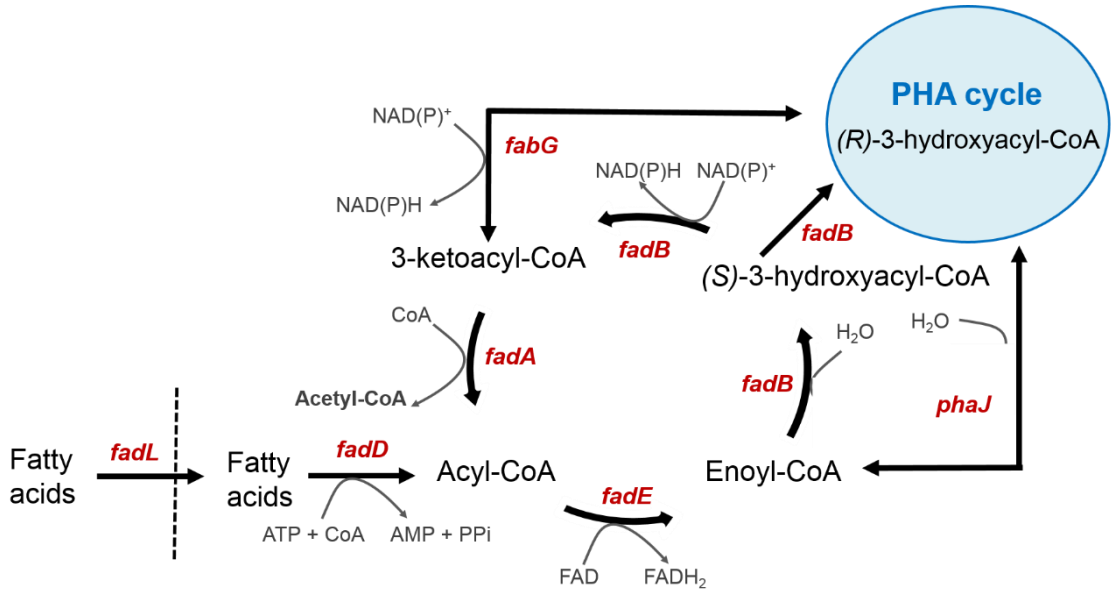

Figure 6. Fatty acid β-oxidation pathway and its connection with PHA metabolism. Diagram with the main metabolic steps involved in the β-oxidation pathway (black lines), the proposed connection with PHA metabolism, the responsible genes involved in these metabolic pathways (red color) and the reaction exchanges (gray color) are shown.

The FadBA complex is encoded by two set of genes located in two different operons, in *P. putida* KT2440, *fadB* and *fadA* (PP_2136 and PP_2137), *fadBx* and *fadAx* (PP_2214 and PP_2215). The first set seems to play a more important role since its lack causes a defective β-oxidation pathway yielding polymers with longer chain monomers (Ouyang *et al.*, 2007). Various isoenzymes have been proposed to carry out some of the steps performed by the FadBA complex (Olivera *et al.*, 2001b).

As far as it concerns the fatty acid catabolism regulation, in *Pseudomonas* spp. PsrA regulator was reported to transcriptionally control the *fad* genes and not an orthologue of FadR regulator in *E. coli* (Kang *et al.*, 2008; Fonseca *et al.*, 2014).

1.4.1.1 The connection of the β-oxidation pathway to PHA cycle

In the β-oxidation pathway, the acyl-CoA is sequentially oxidized into enoyl-CoA, *(S)*-3-hydroxyacyl-CoA and *(R)*-3-ketoacyl-CoA. All of these intermediates are proposed to be converted to PhaC1 substrate *(R)*-HA-CoA by a stereospecific trans-enoyl-CoA hydratase (PhaJ), an epimerase (FadB) and/or a 3-oxoacyl-ACP reductase (FabG), respectively (Figure 6) (Ren *et al.*, 1998).

PhaJ is one of the proposed enzymes linking β-oxidation to PHA synthesis and catalyzes a stereospecific hydration reaction from trans-2-enoyl-CoA to *(R)*-3- HA-CoA. Studies in pseudomonads have suggested that the PhaJ enzyme can contribute to the monomer supply for PHA biosynthesis from fatty acids precursors (Vo *et al.*, 2008). Four *phaJ* genes have been identified in *P. aeruginosa*, where only the PhaJ1 was found to be specific for scl-enoyl-CoAs (C4-C6) and the other three PhaJs were specific for mcl-enoyl-CoAs (C6-C12) (Tsuge *et al.*, 2003). From database search, three homologues of $phaJ1_{pa}$, $phaJ3_{pa}$ and $phaJ4_{pa}$ were found in *P. putida* and named as *phaJ1* (PP_4552), *phaJ3* (PP_0580) and *phaJ4* (PP_4817), respectively. Only the *phaJ4* showed higher expression levels when growing in fatty acids. Additionally, PhaJ4 enzyme substrate specificity was shown to be mcl-enoyl-CoAs like PhaJ4 from *P. aeruginosa* (Fiedler *et al.*, 2002; Wang and Nomura, 2010; Sato *et al.*, 2011).

Another linker between β-oxidation and PHA synthesis was previously proposed to be a NADPH-dependent-3-ketoacyl-ACP reductase, FabG. This is a reversible enzyme, known to catalyze the conversion of 3-ketoacyl-CoA into *(R)*-HA-CoA and vice versa (Nomura *et al.*, 2005). Initial studies on *E. coli* have shown that $FabG_{Ec}$ and $FabG_{pa}$ (from *P. aeruginosa*) were capable to generate *(R)*-HA-CoA precursors from 3-ketoacyl-CoA in the presence of PHA synthase (Taguchi *et al.*, 1999; Ren *et al.*, 2000). In pseudomonads, its contribution to PHA biosynthesis via β-oxidation pathway is yet unclear. In fact, an overexpression of *fabG* and *phaJ* in *P. putida* strain resulted in controversial results, with negative and positive effect on PHA biosynthesis, respectively. This *fabG* negative effect could be due to the reversible conversion of *(R)*-HA-CoA into 3-ketoacyl-CoA (Vo *et al.*, 2008).

Finally, FadB a putative epimerase was proposed to connect β-oxidation and PHA synthesis by converting *(S)*-HA-CoA to *(R)*-HA-CoA. Despite the assigned epimerase activity in *E. coli* (Pramanik *et al.*, 1979), its role is not physiologically relevant in

pseudomonads. Thus, FadBA does not seem to possess the putative epimerase function to provide *(R)*-enantiomer of HA-CoA efficiently and that other linking enzymes are required to efficiently channel intermediates of β-oxidation towards mcl-PHA biosynthesis (Fiedler *et al.*, 2002). More studies need to be done to verify this.

1.4.2 mcl-PHA synthesis from non-PHA-related carbon sources

Non-structurally related substrates such as acetate, ethanol, sugars (glucose, fructose and sucrose), glycerol and aromatic molecules can be oxidized to acetyl-CoA and channeled towards PHA formation via *de novo* fatty acid synthesis (1.4.3 section). When these substrates were applied for growth and PHA production, the composition of the resulting polyester is independent of the carbon source applied. Under these conditions, it was reported that the polyester produced by *Pseudomonas* spp. is composed mainly by *(R)*-3-hydroxydecanoate. However, in less extent other saturated and unsaturated monomer types were also observed. A variety of non-PHA related carbon sources have been applied in this Doctoral Thesis, such as glucose, sucrose, glycerol and aromatic substrates. For this purpose in the following introduction sections the metabolism of some of these carbon sources will be described in more detail.

1.4.2.1 Glucose metabolism

In *Pseudomonas* spp., fructose seems to be the only carbohydrate to be transported intracellularly via PEP-PTS system (Durham and Phibbs, 1982). However, glucose and other sugars enter the periplasmic space via the porine (OprB), which is located in the external membrane (Saravolac *et al.*, 1991).

Even though the metabolism of glucides in *Pseudomonas* spp. is not preferential, the glucose metabolism is quite complex, since three convergent peripheral pathways exist, able to transform it into the 6-phospho-gluconate (6PG) intermediate (Figure 7 and Supplementary Table S2) (del Castillo *et al.*, 2007; Rojo, 2010). The glucose can be i) directly phosphorylated to glucose-6-P in the cytoplasm or ii) transformed into gluconate in the periplasm and then phosphorylated to 6PG intracellularly, iii) or continue the oxidation process up to 2-ketogluconate, then intracellularly phosphorylated and reduced into 6PG.

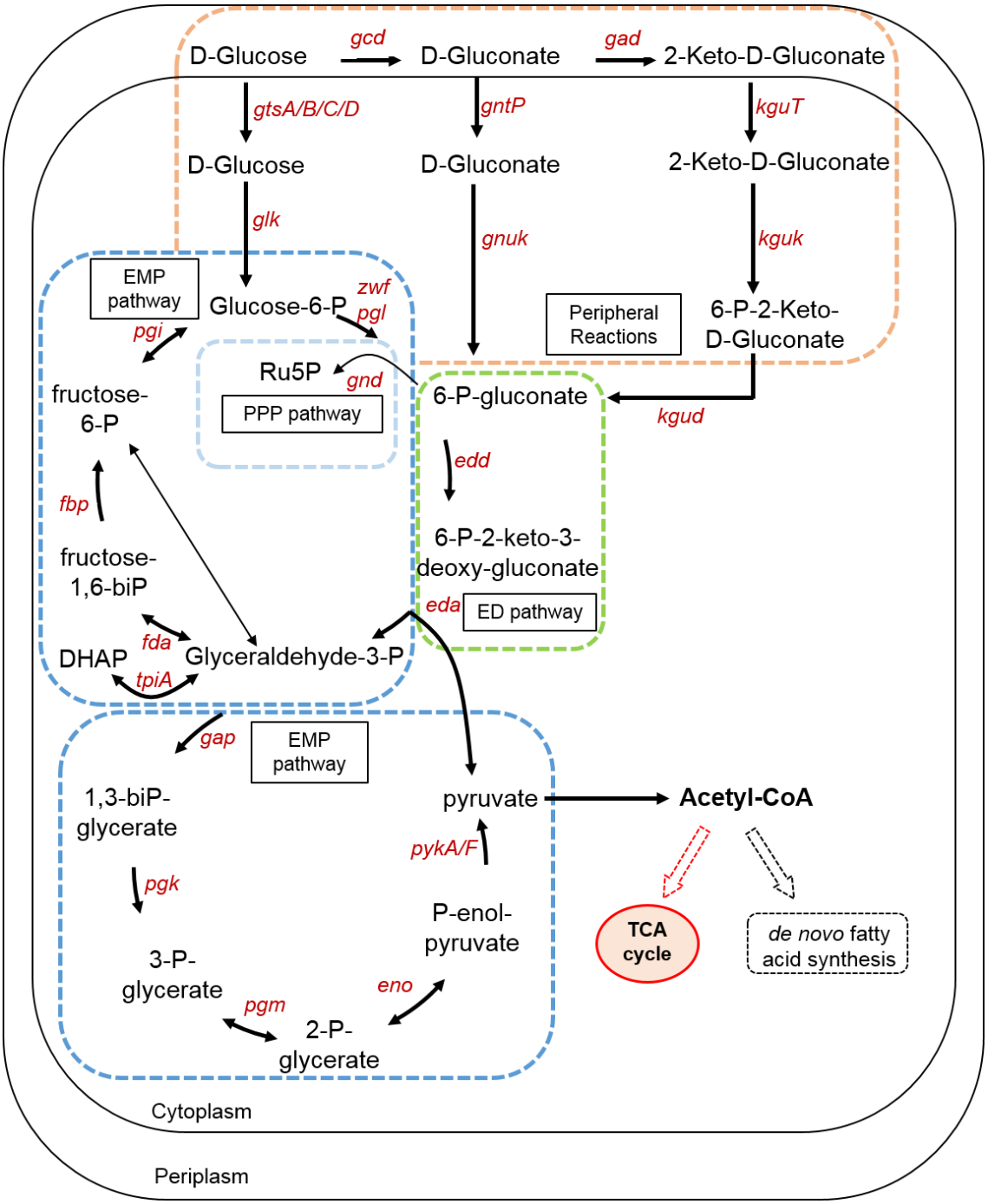

Figure 7. Diagram of glucose catabolism in *Pseudomonas*. The EMP (Embden-Meyerhof-Parnas Pathway; shown in blue color square), the ED (Entner-Doudoroff; shown in green color square), the peripheral pathways (shown in orange color square) are indicated. The responsible genes involved in these metabolic pathways (shown in red color) are annotated. Acetyl-CoA is a key branch point to Tricarboxylic acid cycle or to other biosynthetic pathways like the *de novo* fatty acid synthesis. The figure is adapted from (Kukurugya *et al.*, 2019).

Majorly, pseudomonads metabolize the glucose through the Entner-Doudoroff (ED) pathway due to the absence of phosphofructokinase enzyme, that catalyzes the phosphorylation of fructose-6-phosphate to fructose-1,6-biphosphate (Nikel *et al.*, 2015). ED starts by transforming 6PG to 2-keto-3-desoxy-6-phosphogluconate (KDPG) by the

6-phoshogluconate dehydratase (Edd). Then, KDPG is hydrolyzed to glyceraldehyde-3-phosphate and pyruvate by the KDPG aldolase (Eda). The glyceraldehyde-3-phosphate after a series of steps is transformed to pyruvate (EMP, Embden–Meyerhof-Parnas process). ^{13}C mapping experiments confirmed that glucose-derived carbons were catabolized through a cyclic flux connection from the ED pathway towards the upper EMP pathway and the non-oxidative PP pathway (Kohlstedt and Wittmann, 2019; Kukurugya *et al.*, 2019). Finally, pyruvate is descarboxylated to acetyl-CoA by pyruvate dehydrogenase complexes (PDHCs) and it enters the tricarboxylic cycle (TCA) or derived to other biosynthetic pathways such as the *de novo* fatty acid synthesis.

1.4.2.2 Sucrose metabolism

From industrial point of view, sugarcane based sucrose is cheaper and environmentally friendlier substrate compared to corn based glucose, which is the most common carbon source for *E. coli* industrial fermentation processes. However, most industrial strains, including *P. putida* cannot utilize sucrose as sole carbon source compared to some enteropathogenic *E. coli* strains such as EC3132 (Jahreis *et al.*, 2002) and W (Sabri *et al.*, 2013).

In *E. coli,* two gene clusters are responsible for sucrose degradation including the *scr* regulon that encodes for sucrose phosphotransferase system (PTS) and the *csc* regulon, encoding a sucrose non-PTS utilization system (Schmid *et al.*, 1988; Jahreis *et al.*, 2002). Even though, the *scr* regulon could be found either on plasmid, transposon or on the chromosomal DNA, the *csc* regulon is only located on the chromosome. For the purpose of this Doctoral Thesis, we will focus on the latter regulon. The sucrose permease, CscB transports sucrose into the cell and it is further hydrolyzed intracellularly into glucose and fructose by the action of sucrose hydrolase/invertase, CscA. Finally, the generated sugars are phosphorylated intro glucose-6-phosphate and fructose-6-phosphate by glucokinase, Glk and sucrose fructokinase, CscK, respectively. The transcriptional repressor, CscR negatively regulates the *csc* catabolic genes in the absence or at low sucrose concentration (<2 g/L) (Sabri *et al.*, 2013).

Recently, sucrose fermenting strains were obtained by introducing the *cscA cscB* genes from *E. coli* W to *P. putida* KT2440 (Löwe *et al.*, 2017b). Furthermore, PHA production from sucrose has been achieved by *P. putida cscAB* and *Synechococcus elongatus cscB* synthetic mixed cultures (Löwe *et al.*, 2017a).

1.4.2.3 Glycerol metabolism

Glycerol is a simple polyol compound, relatively cheap and readily available substrate for a variety of bioprocesses. The biochemistry, genetics and biotechnology of glycerol utilization in *Pseudomonas* spp. were recently reviewed by Poblete-Castro and colleagues (Poblete-Castro *et al.*, 2019).

glp regulon, is involved in glycerol metabolism in Gram negative bacteria and shares a common regulatory theme. Glycerol-3-phosphate (G3P) is the inducer for the *glp* regulon in *E. coli*, *P. aeruginosa* and *P. putida* (Escapa *et al.*, 2013; Nikel *et al.*, 2014a). In *P. putida*, glycerol cross the bacterial external membrane via porine OprB (Figure 8 and Supplementary Table S3). From the periplasm, glycerol is transported to cytoplasm via glycerol transporter/facilitator, GlpF. In the cytoplasm, glycerol is phosphorylated to glycerol-3-phosphate (G3P) via glycerol kinase, GlpK. Then, G3P dehydrogenase, GlpD transforms G3P to dihydroxyacetone-phosphate DHAP, which is latter channeled into key glycolytic intermediates via Entner-Doudoroff metabolism (Escapa *et al.*, 2013; Poblete-Castro *et al.*, 2019).

In some *P. putida* species, apart from the direct, ATP-dependent phosphorylation of intracellular glycerol, it can be oxidized into dihydroxyacetone (DHA) by the glycerol dehydrogenase (GldA). Then, it can be further phosphorylated to DHAP using as phosphoryl donor, the phosphoenolpyruvate (PEP) and generate pyruvate by the DHA kinase, DhaKLM (Poblete-Castro *et al.*, 2019).

glpF, *glpK* and *glpD* expression levels were significantly higher when the cells were grown on glycerol, confirming that all of these enzymes are involved in glycerol metabolism (Wang and Nomura, 2010). The long lag phase observed by the cells grown using glycerol as sole carbon source, is due to the need of inducing the expression of *glp* genes for the efficient glycerol utilization. GlpR represses glycerol catabolism and it is responsible for the long lag-phase (Escapa *et al.*, 2013).

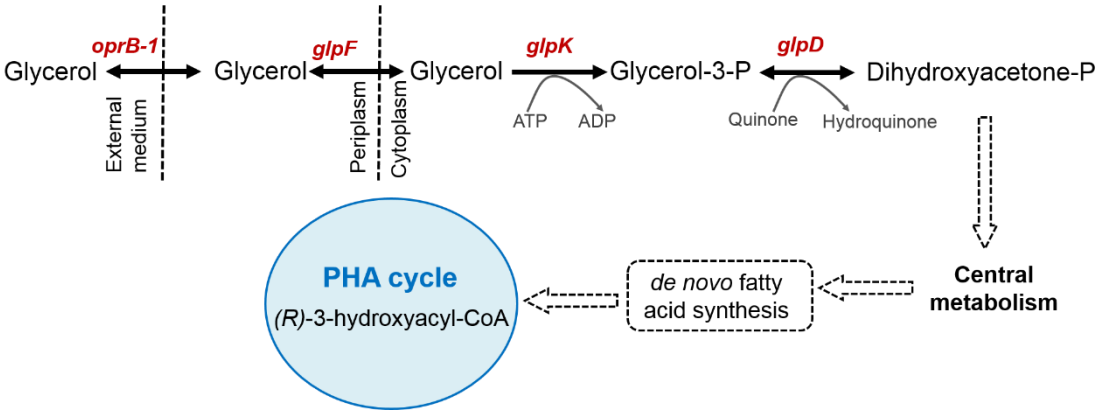

Figure 8. Conserved pathways for glycerol metabolism. The coding genes involved in glycerol metabolism (shown in red) are GlpF, glycerol facilitator (transporter); GlpK, glycerol kinase; GlpD, glycerol-3-P dehydrogenase

1.4.2.4 Aromatic degradation

The aromatic degradation is a mechanism highly studied, the different aromatic substrates are converted in mono-, di- or tri-hydroxylate derivatives via the incorporation of oxygen atoms by the distinct types of oxygenases. Then, the dioxygenases breakdown the aromatic ring of these hydroxylate intermediates. The obtained products can be easily oxidized up to central metabolic intermediates (Jimenez *et al.*, 2002). The variety of aromatic compounds could be channeled into 5 central pathways, including 3-oxoadipate (β-ketoadipate) pathway via protocatechuate (ferulate, vanillate, *p*-coumarate, *p*-hydroxybenzoate), catechol (benzoate), the homogentisate pathway (phenylalalanine, tyrosine) the phenylacetyl-CoA pathway (phenylacetate and phenylalakanoate) or gallic acid degradation pathway (Jimenez *et al.*, 2002; dos Santos *et al.*, 2004; Nogales *et al.*, 2011) (Figure 9). The classical strategies of aerobic degradation involve the activation of aromatic compounds to dihydroxylated intermediates and their dioxygenolytic ring-cleavage (the enzymes involved in these pathways are listed in the Supplementary Table S4).

For the purpose of this Doctoral Thesis, we will focus on the β-ketoadipate pathway, which is composed of two *ortho*-cleavage branches, one for protocatechuate (*pca* genes) and other for catechol (*cat* genes) degradation. The protocatechuate branch pathway is widely conserved among bacteria (Jimenez *et al.*, 2002; Jiménez *et al.*, 2004) and the *pca* genes in sequenced *Pseudomonas* spp. (except in *P. mendocina)* have been identified (Jiménez *et al.*, 2010). These genes are organized in three different clusters in *P. putida* KT2440. The protocatechuate is cleaved to a carboxy-*cis*,*cis*-muconate by protocatechuate 3,4-dioxygenase, PcaGH, which is further converted to γ-

carboxymuconolactone by the action of 3-carboxy-*cis*,*cis*-muconate cycloisomerase, PcaB. Then, it is converted to β-ketoadipate enol-lactone by 4-carboxymuconolactone decarboxylase, PcaC. By the action of 3-oxoadipate enol-lactonase, PcaD it is transformed to β-ketoadipate and by the two-component complex PcaI/PcaJ is transformed to β-ketoadipyl-CoA. Finally, the beta-ketoadipyl-CoA thiolase, PcaF, generates acetyl-CoA and succinyl-CoA.

One of the most widely spread peripheral pathways is of the *p*-hydroxybenzoate degradation to protocatechuate by the 4-hydroxybenzoate 3-monooxygenase, PobA. Other common carbon sources are the phenylpropenoids such as ferulate, which is converted to Feruloyl-CoA by the action of feruloyl-CoA synthetase, Fcs and further to vanillin by enoyl-CoA hydratase, Ech. Then, vanillin generates protocatechuate through vanillin dehydrogenase, Vdh and vanillate O-demethylase, VanAB (Jimenez *et al.*, 2002; Jiménez *et al.*, 2004, 2010).

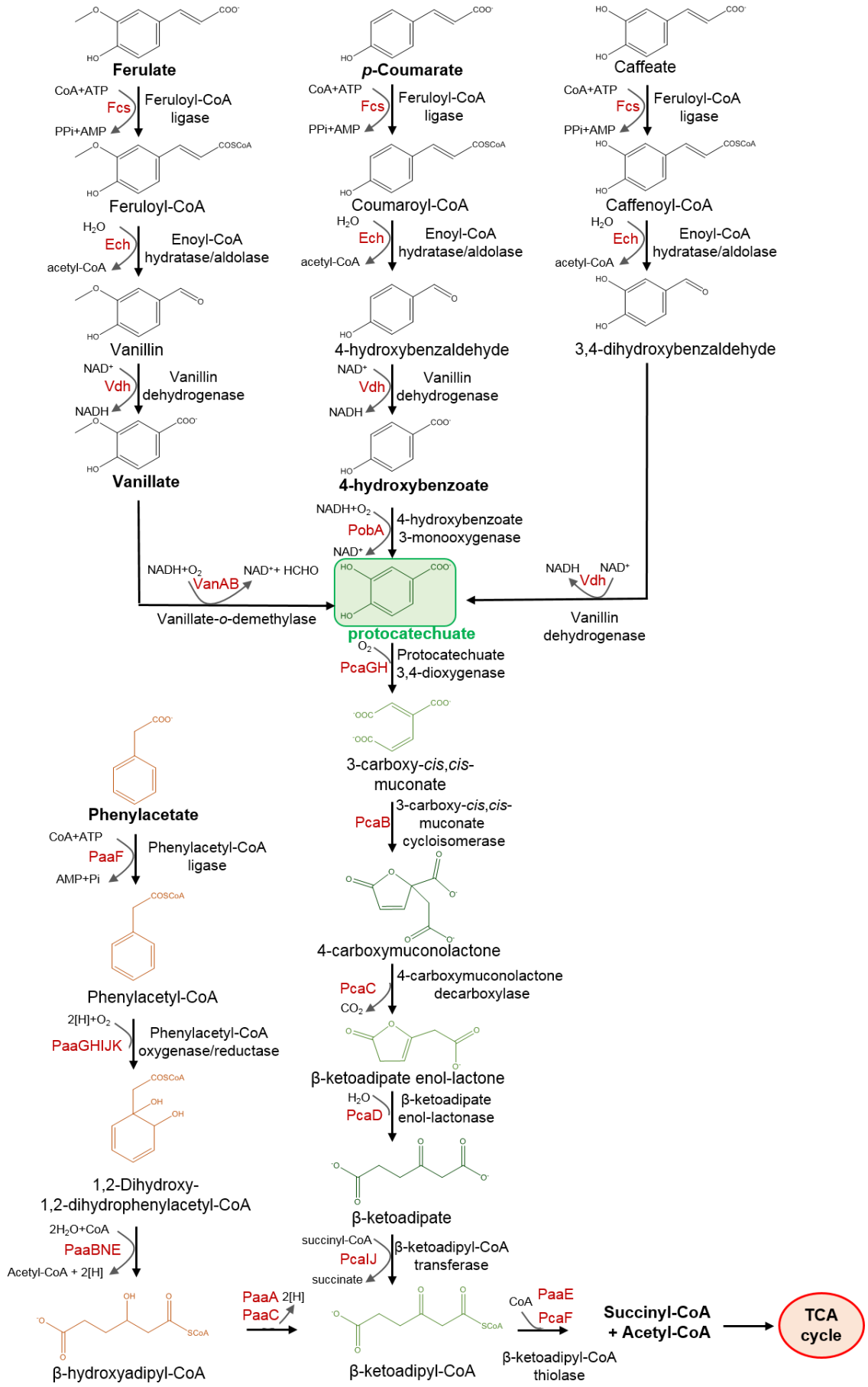
Ferulate
CoA+ATP
Fcs
Feruloyl-CoA ligase
PPi+AMP
Feruloyl-CoA
H2O
Ech
Enoyl-CoA hydratase/aldolase
acetyl-CoA
Vanillin
NAD+
Vdh
Vanillin dehydrogenase
NADH
Vanillate
p-Coumarate
Coumaroyl-CoA
4-hydroxybenzaldehyde
4-hydroxybenzoate
Caffeate
Caffenoyl-CoA
3,4-dihydroxybenzaldehyde
NADH+O2
PobA
4-hydroxybenzoate 3-monooxygenase
NAD+
NADH+O2
VanAB
NAD++ HCHO
Vanillate-o-demethylase
protocatechuate
NADH
NAD+
Vdh
Vanillin dehydrogenase
O2
PcaGH
Protocatechuate 3,4-dioxygenase
3-carboxy-cis,cis-muconate
PcaB
3-carboxy-cis,cis-muconate cycloisomerase
4-carboxymuconolactone
PcaC
CO2
4-carboxymuconolactone decarboxylase
β-ketoadipate enol-lactone
H2O
PcaD
β-ketoadipate enol-lactonase
β-ketoadipate
succinyl-CoA
PcaIJ
β-ketoadipyl-CoA transferase
succinate
β-ketoadipyl-CoA
CoA
PaaE
PcaF
β-ketoadipyl-CoA thiolase
Succinyl-CoA + Acetyl-CoA
TCA cycle
Phenylacetate
CoA+ATP
PaaF
Phenylacetyl-CoA ligase
AMP+Pi
Phenylacetyl-CoA
2[H]+O2
PaaGHIJK
Phenylacetyl-CoA oxygenase/reductase
1,2-Dihydroxy-1,2-dihydrophenylacetyl-CoA
2H2O+CoA
PaaBNE
Acetyl-CoA + 2[H]
β-hydroxyadipyl-CoA
PaaA 2[H]
PaaC

Figure 9. Pathways for the aromatic catabolism in *P. putida* KT2440. The β-ketoadipate (shown in green colors) and the phenylacetate (shown in orange colors) degradation pathways are shown. The names of the metabolites and the reaction exchanges (shown in grey color) are shown. The coding genes (shown in red) involved in this process are listed in the Supplementary Table 4. The metabolites used in this Doctoral Thesis are shown in bold letters. The central metabolite protocatechuate is shown in green color. This figure was adapted from Jiménez and collaborators (Jiménez *et al.*, 2004; Nogales *et al.*, 2007).

1.4.2.5 Tricarboxylic acid cycle

Tricarboxylic cycle (TCA) is a conserved catabolic pathway for energy and reducing power generation (Figure 10 and Supplementary Table S5). The name of TCA or citric acid cycle is due to the first step in this pathway characterized by the attachment of acetyl-CoA to citrate by the action of citrate synthase, GltA. This cycle is also known as Szent-Gyorgyi-Krebs or just Krebs cycle, named after the scientists who described it (Krebs and Johnson, 1980).

The central acetyl-CoA generated from the fatty acid, glucose, aromatics degradation, or other convergent pathways, can be either channeled to TCA cycle or redirected to other biosynthetic pathways, such as for PHA production. The pyruvate generated by EMP and ED pathways is a common source of acetyl-CoA, which is converted to this molecule by the action of PDHC (de Kok *et al.*, 1998). In every turn of TCA cycle, one molecule of acetyl-CoA is converted to two CO_2 molecules, a total of four molecules of $NAD(P)^+$, respectively, and one molecule of GDP is phosphorylated to GTP. The reduced NAD(P)H molecules serve as electron donors for oxidative phosphorylation.

Finally, a truncated form of TCA cycle, known as glyoxylate cycle, converts the acetyl-CoA to biosynthetic intermediates (succinate, glyoxylate, malate) without the loss of CO_2 leading to biomass formation (Walsh and Koshland, 1984).

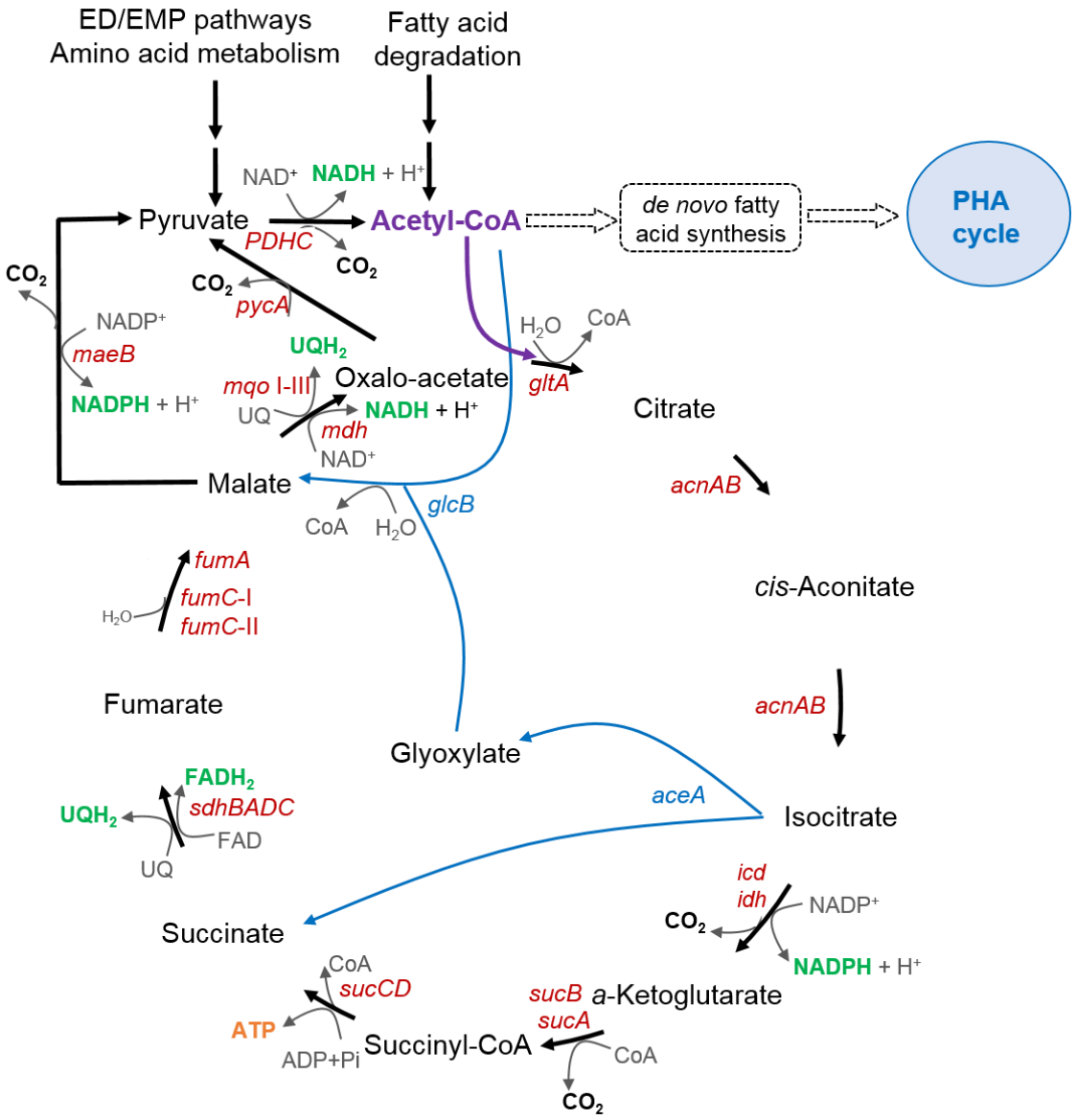

Figure 10. Tricarboxylic cycle (TCA). The involved coding genes (with red color) and the reaction exchanges (with grey color) are shown. The reducing power produced in each reaction is shown with green color and the ATP produced in orange color. The glyoxylate shunt is shown with blue color. The figure is adapted from Kukuruya and collaborators (Kukurugya et al., 2019). Additional information about the enzymes involved in this process is provided in the Supplementary Table S5.

1.4.3 *de novo* fatty acid synthesis

Non-PHA related substrates such as carbohydrates can act as indirect precursors of PHA through their complete oxidation to acetyl-CoA and they can be channeled towards the *de novo* synthesis pathway (Figure 11 and Supplementary Table S6). The genetic and biochemical characterization of the *de novo* fatty acid biosynthesis in pseudomonads have been principally analyzed in *P. aeruginosa*. However, recently

several aspects of the fatty acid biosynthesis in different bacteria has been revised, focusing on different metabolic engineering approaches and their structure elucidation (Beld *et al.*, 2015).

The *de novo* fatty acid intermediates are activated by the acyl carrier protein (ACP). The fatty acid synthesis starts with the acetyl-CoA carboxylation into malonyl-CoA by the acetyl-CoA carboxylase, AccABCD complex (Best and Knauf, 1993). Then, the malonyl-CoA is transtioesterified into malonyl-ACP thanks to the malonyl-CoA:ACP transacylase, FabD (Kutchma *et al.*, 1999). The generated malonyl-ACP is further condensed into 3-ketoacyl-ACP by different 3-ketoacyl-ACP synthases: first, is condensed by an acetyl-CoA molecule, thanks to FabH, then in successive rounds of elongation a new molecule of malonyl-ACP is condensed with the 3-acyl-ACP formed by FabB or FabF (Campbell and Cronan, 2001; Schweizer, 2004). FabB has been also proposed to catalyze decarboxylation of malonyl-ACP into acetyl-ACP (Cronan and Rock, 2008). The following steps include the reduction of 3-ketoacyl-ACP into *(R)*-3-hydroxyacyl-ACP by a 3-ketoacyl-ACP reductase, FabG and the formation of a double bond into enoyl-ACP by 3-hydroxyacyl-ACP dehydratase, FabA or FabZ (Heath and Rock, 1996; Sullivan *et al.*, 2002). Finally, one enoyl-ACP reductase, FabI, FabK or FabL transforms the enoyl-ACP into 3-acyl-ACP (Hoang and Schweizer, 1999). In *P. putida* KT2440 has not been identified the gene that codifies for the enoyl-ACP reductase activity, however it has been proposed to probably contain a FabK or Fab-type enoyl-ACP reductase (Schweizer, 2004).

1.4.3.1 *de novo* fatty acid synthesis connection to PHA cycle

Hydroxyacyl-ACP intermediates can be transformed into *(R)*-HA-CoAs by the specific transacylase PhaG, present in most pesudomonads (Rehm *et al.*, 1998). PhaG was reported as a 3-hydroxyacyl-acyl carrier protein (ACP)-CoA transferase, able to transfer the 3-hydroxyacyl group from ACP to CoA moiety in *P. putida* KT2440 and *P. aeruginosa* (Rehm *et al.*, 1998; Fiedler *et al.*, 2000; Hoffmann *et al.*, 2000; Hoffmann and Rehm, 2004; Tobin *et al.*, 2007). However, recently PhaG was proposed to function as a 3-HA-ACP thioesterase. The existence of at least one 3-hydroxyacyl-CoA ligase is needed in order to convert 3-hydroxyalkanoate substrates into 3-HA-CoA thioester PHA precursors (Q. Wang *et al.*, 2012). Based on homology studies, PP_0763 gene was predicted to encode a medium-chain-fatty acid CoA ligase and its transcription levels were highly upregulated when cells were grown under PHA producing conditions (Q. Wang *et al.*, 2012). In order to verify this, *phaG* (PP_1408) and PP_0763 genes from *P. putida* were cloned and co-expressed with the engineered *phaC1* (STQK) synthase from

Pseudomonas sp. 61-3 in recombinant *E. coli*. The latter strain resulted in about 4-fold higher PHA production from non-fatty acid carbon sources than that in *P. putida* KT2440 (Q. Wang *et al.*, 2012).

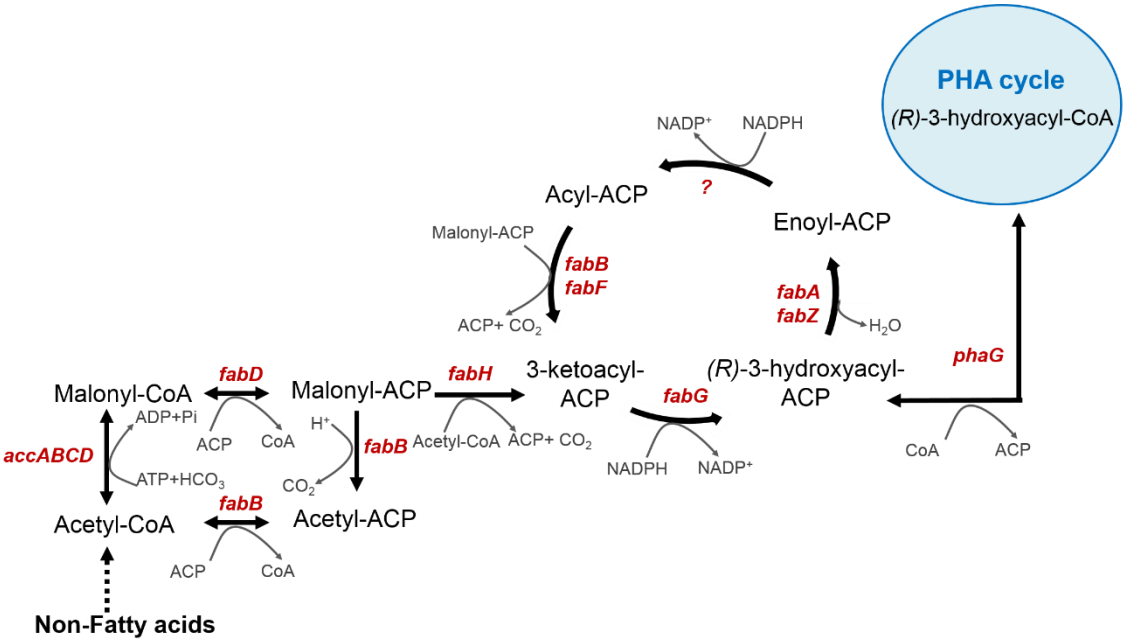

Figure 11. *de novo* fatty acid biosynthesis and its connection with PHA metabolism. Diagram with the main metabolic steps involved in the *de novo* fatty acid biosynthesis (black lines), the proposed connection with PHA metabolism, the responsible genes involved in these metabolic pathways (red color) and the reaction exchanges (gray color) are shown.

1.4.4 The PHA cycle

The PHA metabolism in *P. putida* KT2440 is mediated through two PHA synthases, PhaC1 (PP_5003) and PhaC2 (PP_5005) and the PHA depolymerase, PhaZ (PP_5004) that synthesize and degrade the PHA, respectively.

More than 60 genes codifying for PHA synthases in 45 bacterial species have been cloned and have been characterized (Rehm, 2003). These enzymes can be divided into four classes according to the substrate specificity, the amino acid primary sequence and the subunits composition (Zou *et al.*, 2017). In general, synthase of class I (e.g. *Cupriavidus necator;* formally known as *Ralstonia eutropha*), class III (e.g. *Allochromatium vinosum*) and class IV (e.g. *Bacillus megaterium*) preferentially use *(R)*-HA-CoA thioesters comprising 3 to 5 carbon atoms. The class II PHA synthases (PhaC1 and PhaC2) are mainly observed in pseudomonads and preferentially utilize CoA thioesters of various *(R)*-3-hydroxy acids comprising of 6 to 14 carbon atoms. Several studies in other *Pseudomonas* species confirmed that the *phaC2* synthase is functional *in vivo* but the specificity of both synthases may be distinct (Arias *et al.*, 2008).

Regarding the enzymes responsible for the PHA depolymerization, there are two types: the extracellular depolymerases and the intracellular ones. Several, non-PHA producer microorganisms secrete extracellular depolymerase that allows them to obtain carbon and energy sources from the degradation of the exogenous PHA. Generally, the microorganisms that produce PHA, have an intracellular depolymerase. For instance, the intracellular degradation of the scl-PHA has been studied extensively in *C. necator* H16 and *Rhodospirillum rubrum*. Functional genomic analyses confirm the complexity of the PHB hydrolysis process (Handrick *et al.*, 2004; Pohlmann *et al.*, 2006).

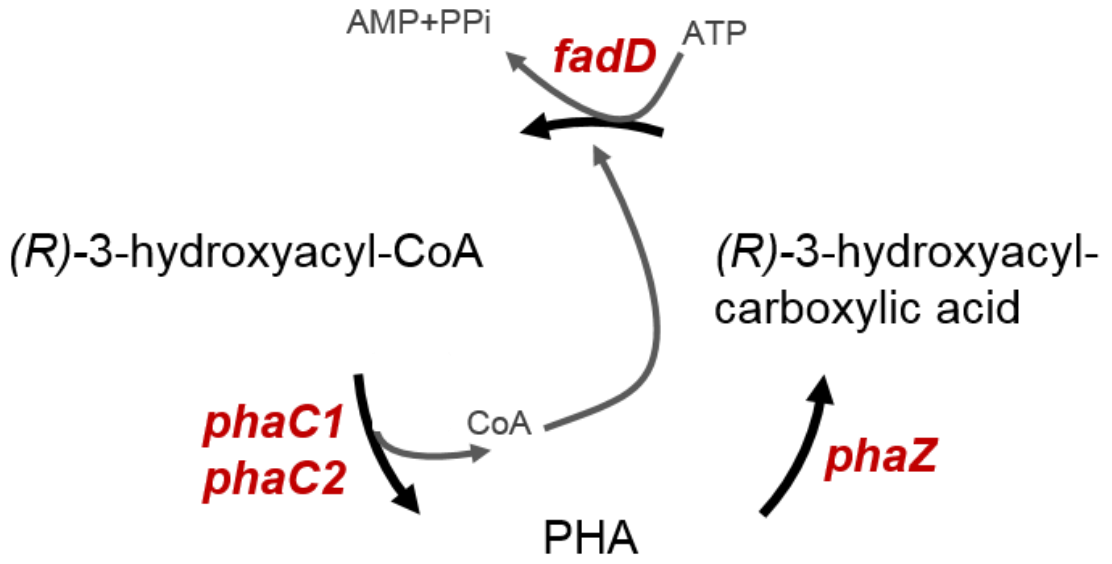

Figure 12. PHA cycle in *P. putida*. The key players are the PHA synthases (PhaC1, PhaC2), PHA depolymerase (PhaZ) and Acyl-CoA synthetase (FadD). The *(R)*-HA-CoA is substrate for PhaC synthases and for the enzymes responsible for the fatty acid metabolism. The responsible genes involved in this cycle and the reaction exchanges are shown in red and grey color, respectively.

The first intracellular mcl-PHA depolymerase PhaZ was described in *P. putida* GPo1 and its enzymatic activity was confirmed *in vivo* on the defective *phaZ* mutant (GPo500). In fact, the mutant was able to accumulate efficiently, however, no polymer degradation occurred during the stationary phase (Huisman *et al.*, 1991). Similar experiments and conclusions have been obtained from *P. putida* U and *P. putida* KT2442 (De Eugenio *et al.*, 2007; De Eugenio *et al.*, 2010a). The first biochemical characterization of PhaZ from *P. putida* KT2442 was carried out in our laboratory (De Eugenio *et al.*, 2007). The PhaZ preferentially hydrolyzes mcl-PHAs containing aliphatic and aromatic monomers. The enzyme behaves as a serine hydrolase that is inhibited by phenyl-methylsulfonyl fluoride. The three-dimensional structure of PhaZ was modeled, complexed with a 3-hydroxyoctanoate dimer. Using this model, the enzyme appears to be built up from a core of a/β hydrolase-type domain capped with a lid structure with an

active site containing a catalytic triad buried near the connection between domains (Figure 13, (De Eugenio *et al.*, 2007)).

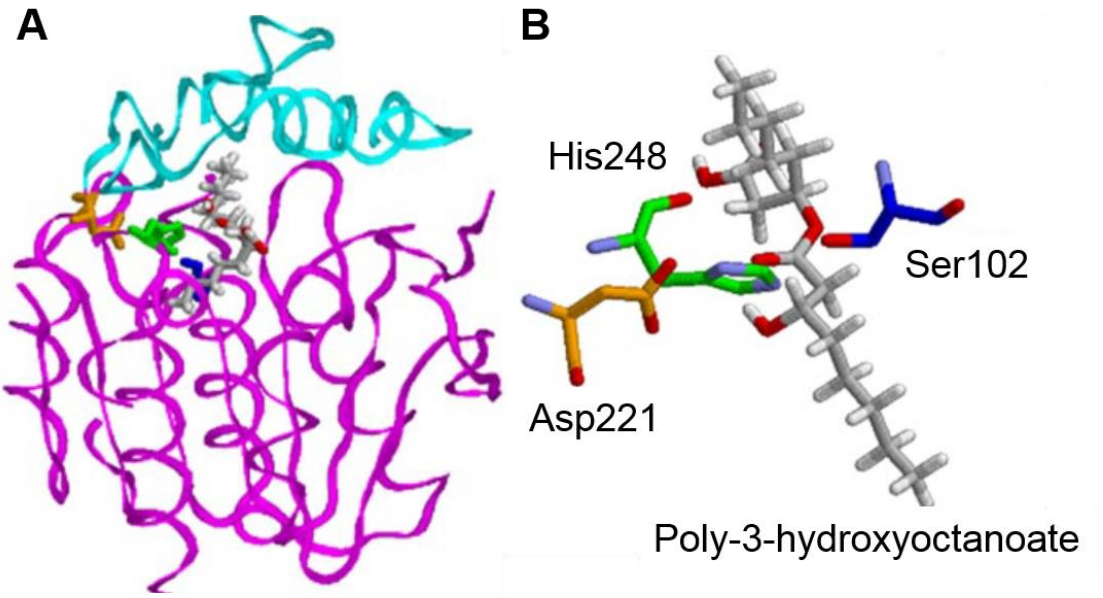

Figure 13. Model of the three-dimensional structure of PhaZ using CumD hydrolase as template. A. ribbon diagram, depicting the core domain (magenta) and the lid domain (cyan). Residues Ser102 (blue), His248 (green), and Asp221 (orange), and a docked theoretical dimer of HO are depicted in wire frame representation; **B.** schematic representation of the catalytic triad around the substrate. Adapted from (De Eugenio *et al.*, 2007)

Key proteins of the PHA machinery are the phasins. They lack enzymatic activity but have been identified as the major GAPs in PHA granules (Prieto *et al.*, 1999). *P. putida* KT2440 contains two phasins, PhaF (PP_5007) and PhaI (PP_5008), which are present in all known mcl-PHA-accumulating bacteria (Prieto *et al.*, 2016). PhaF (26 kDa) has two different modules connected by a leucine zipper domain. The N-terminal domain consists of a long amphipathic a-helix that can bind to the PHA granule (Maestro *et al.*, 2013). The C-terminal module is predicted to contain a superhelical structure that can interact with the nucleoid and is related to *pha* cluster transcriptional regulation (1.4.5 section). The N-terminal and leucine zipper domains share sequence similarity with PhaI phasin (15 kDa) (Moldes *et al.*, 2004). Recently, the formation of PhaF and PhaI complexes was confirmed and the involvement of leucine zipper domain for these interactions was established (Tarazona *et al.*, 2019a).

These modular proteins have multiple functions. The crucial role of PhaF/PhaI for granule formation and segregation between daughter cells during division has been described (Galán *et al.*, 2011). Recently, PhaF has been demonstrated to function as a surfactant protein stabilizing PHA granules in the hydrophilic environments, as occurs in the cytoplasm of bacterial cells (Tarazona *et al.*, 2019b). In this sense, the interfacial

activity of PhaF domain confirmed the potential of these proteins to interact and stabilize the surface of very different hydrophobic materials (Mato *et al.*, 2019).

1.4.5 PHA metabolism regulation

The *pha* gene cluster is well conserved among the mcl-PHA producer strains and contains 2 operons, *phaC1ZC2D* and *phaFI*, that are transcribed in opposite directions (Figure 14) (Prieto *et al.*, 2007). The PhaD (PP_5006) is a TetR family transcriptional regulator and so far, PhaD was not found in the granule surface, between the GAPs. The intergenic regions of the *pha* cluster vary depending the species (as observed in *P. corrugata*, *P. mediterranea*, *P. aeruginosa*) suggesting that the transcription control differs between the strains (Prieto *et al.*, 2007).

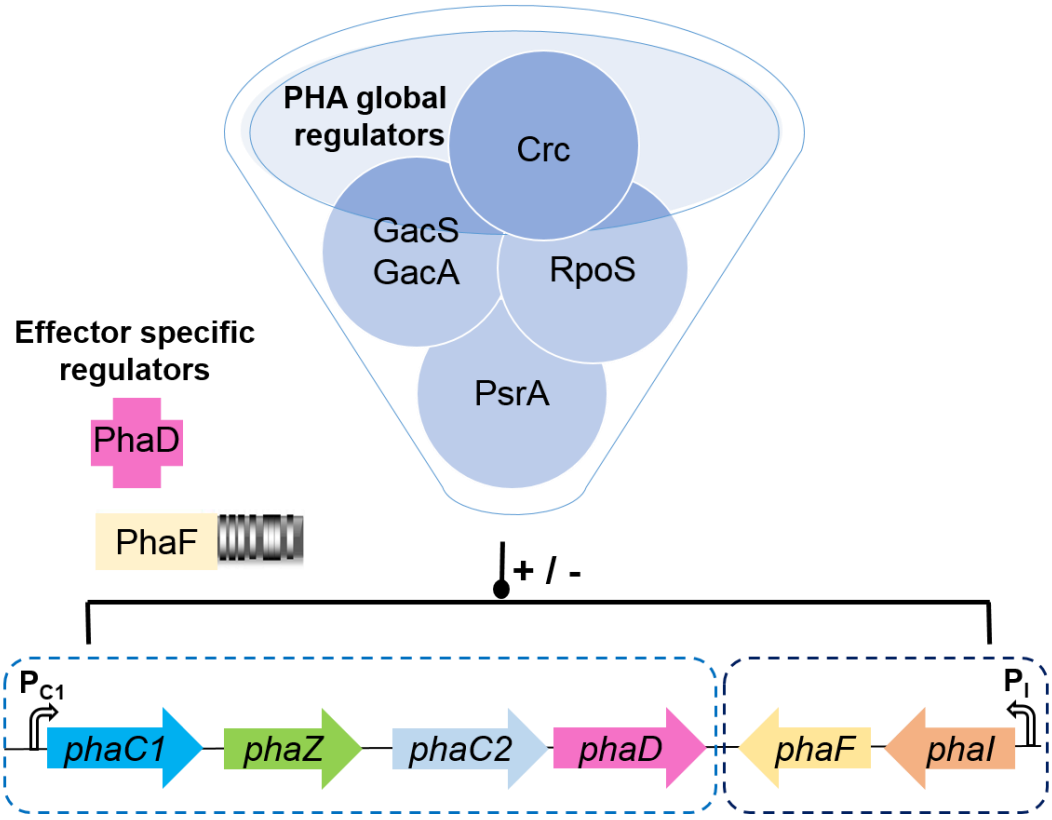

Figure 14. Genetic organization of *pha* cluster in *P. putida* KT2440. The complex PHA global regulators such as GacS/GacA, PsrA, RpoS, Crc are demonstrated. Both operons, *phaC1ZC2D* and *phaIF*, are under the control of the regulator PhaD.

PHA are widely investigated concerning its structure versatility, physicochemical properties, biodegradability, sustainable and optimization production possibilities (Chen, 2009; Rehm, 2010; Gao *et al.*, 2011; Li *et al.*, 2016). However, the molecular mechanisms behind the PHA metabolism regulation are not yet clear, due to the complexity of this regulation system at different levels (genetic, post-trascriptional,

enzymatic and global regulators). Furthermore, the PHA accumulation could depend on the carbon source(s), the specificity of the PHA synthase and the metabolic pathways involved. The PhaC synthase substrates derive from the β-oxidation and *de novo* fatty acid synthesis. Thus, we can assume that regulating factors affecting the enzymes involved in these pathways could be involved in the PHA synthesis regulation, too.

PhaF regulates the expression of the entire transcriptomic profile of *pha* genes, due to its DNA binding abilities and putative histone-like functionality (Galán *et al.*, 2011; Dinjaski and Prieto, 2013). The co-existence of polycistronic transcription units by the identification of five functional promoters upstream of the *phaC1*, *phaZ*, *phaC2*, *phaF* and *phaI* genes has been proposed by using *lacZ* translational fusions (De Eugenio *et al.*, 2010b). However, by RT-qPCR experiments, the P_{C1} and P_I have been demonstrated to be the most active (De Eugenio *et al.*, 2010b).

PhaD transcriptionally activates the *pha* genes by binding to 25 and 29 bp target regions of the P_{C1} and P_I promoters, respectively (De Eugenio *et al.*, 2010b). In different *Pseudomonas* strains, variable transcription levels of *phaF*, *phaFI* have been observed, related to the PhaD role (Sandoval *et al.*, 2007). The effector of PhaD remains unknown, however, CoA intermediates of fatty acid β-oxidation or TCA cycle have been proposed to be possible PhaD effectors. A clear carbon source dependence has been also demonstrated (De Eugenio *et al.*, 2010a).

Finally, the PHA production is modulated by the presence of global regulators (Figure 14) including Crc (catabolite repression response), PsrA, RpoS/RpoN and GacS/GacA (Prieto *et al.*, 2016). In brief, Crc is a global regulator facilitating the hierarchical and sequential use of carbon sources when the growth medium contains several at non-growth-limiting concentrations/conditions (Rojo, 2010). Crc is influenced by the carbon source used and the culture C/N ratio. In fact, low ratios, (balanced medium conditions) which are not optimal for PHA accumulation, provoke Crc-dependent repression response. However, high ratios, such as nitrogen limitation that favors PHA accumulation, suppress this response (La Rosa *et al.*, 2014). Crc is associated with Hfq protein and controls gene expression post-transcriptionally, promoting an inhibition in the translation of RNAs containing an AAnAAnAA motif (where n represents any nucleotide), known as Catabolite Activity (CA) motif, located close to the translation start site. Crc regulation motifs, resembling the canonical CA were predicted close to the translation initiation sites of *phaC1*, *phaF* and *phaI* mRNAs. Only that of *phaC1* appeared to be functional (La Rosa *et al.*, 2014).

PsrA is a TetR family transcription regulator that negatively regulates genes related to β-oxidation fatty acid metabolism by binding to the promoter region of *fadBA,* inhibiting its expression (Fonseca *et al.*, 2014). *psrA*Δ deletion mutant in *P. putida* presents a more

active β-oxidation pathway, resulting in an increase of scl-monomers and in all the conditions tested demonstrated less PHA content than the wild type strain. Finally, the PsrA affect global gene expression including activation of stationary phase sigma factor *rpoS* in *P. aeruginosa* (Kang *et al.*, 2008) and *P. putida* (Kojic and Venturi, 2001).

1.5 PHA-related features influencing bacterial fitness and stress resistance

Apart from their primary storage function, PHA play a variety of roles such as balanced the use of available energy and carbon sources and survival under environmental stresses (Figure 15). The PHA related functions are for example maintaining anoxic photosynthesis and the sulfur cycle in photosynthetic microorganisms (Rothermich *et al.*, 2000), acting as carbon and energy source triggering spore formation and germination in *Bacilli* (Slepecky and Law,1961), encystment in *Azotobacter vinelandii* (Segura *et al.*, 2003), allowing energy production and NADH oxidation of nitrogen-fixing bacteria such as *Rhizobium eti* (Encarnacion *et al.*, 2002), controlling the exopolysaccharide production *in Azospirrilum brasilense* (Kadouri *et al.*, 2003a; Kadouri *et al.*, 2005) and microbial biofilm formation in *P. aeruginosa* (Castro-Sowinski *et al.*, 2010). Furthermore, PHA play an important role in syntrophic interactions between consortia of organisms in different ecosystems such as *Azospirillum* and other rhizosphere bacteria by keeping plant and microorganism symbiosis (Kadouri *et al.*, 2005). Finally, PHA were reported to contribute to fitness of non PHA producer bacteria such as the obligate predator *Bdellovibrio bacteriovorus* (Martínez *et al.*, 2013) by providing energy source.

In the recent years, there is much interest on the involvement of PHA in bacterial stress resistance, reviewed by (Singh Saharan *et al.*, 2014; Obruca *et al.*, 2018). However, there are controversial studies on a variety of bacteria on whether just the presence of PHA granule (Goh *et al.*, 2014), or the ability to accumulate and/or mobilize the PHA could attribute to stress resistance. For example, PHA accumulation has been related to resistance to a variety of environmental stresses such as high and low temperatures, desiccation, ultraviolet radiation, osmotic pressure and oxidative stress as observed by *Azospirillum brasilense* (Kadouri *et al.*, 2002; Kadouri *et al.*, 2003a; Kadouri *et al.*, 2003b), *Aeromonas hydrophila* (Zhao *et al.*, 2007) and *E. coli* (Wang *et al.*, 2009). Additionally, ethanol and acid-pH value resistance were observed in *A. hydrophila* (Zhao *et al.*, 2007) and *E. coli* (Wang *et al.*, 2009), respectively. According to these, it could be concluded that PHA related roles towards stress resistance are regardless of the

microorganisms and the specific stressor. However, the particular protective mechanism of PHA is still unknown and it is likely that not just one single mechanism is responsible to these physiological PHA funcitons (Obruca *et al.*, 2018).

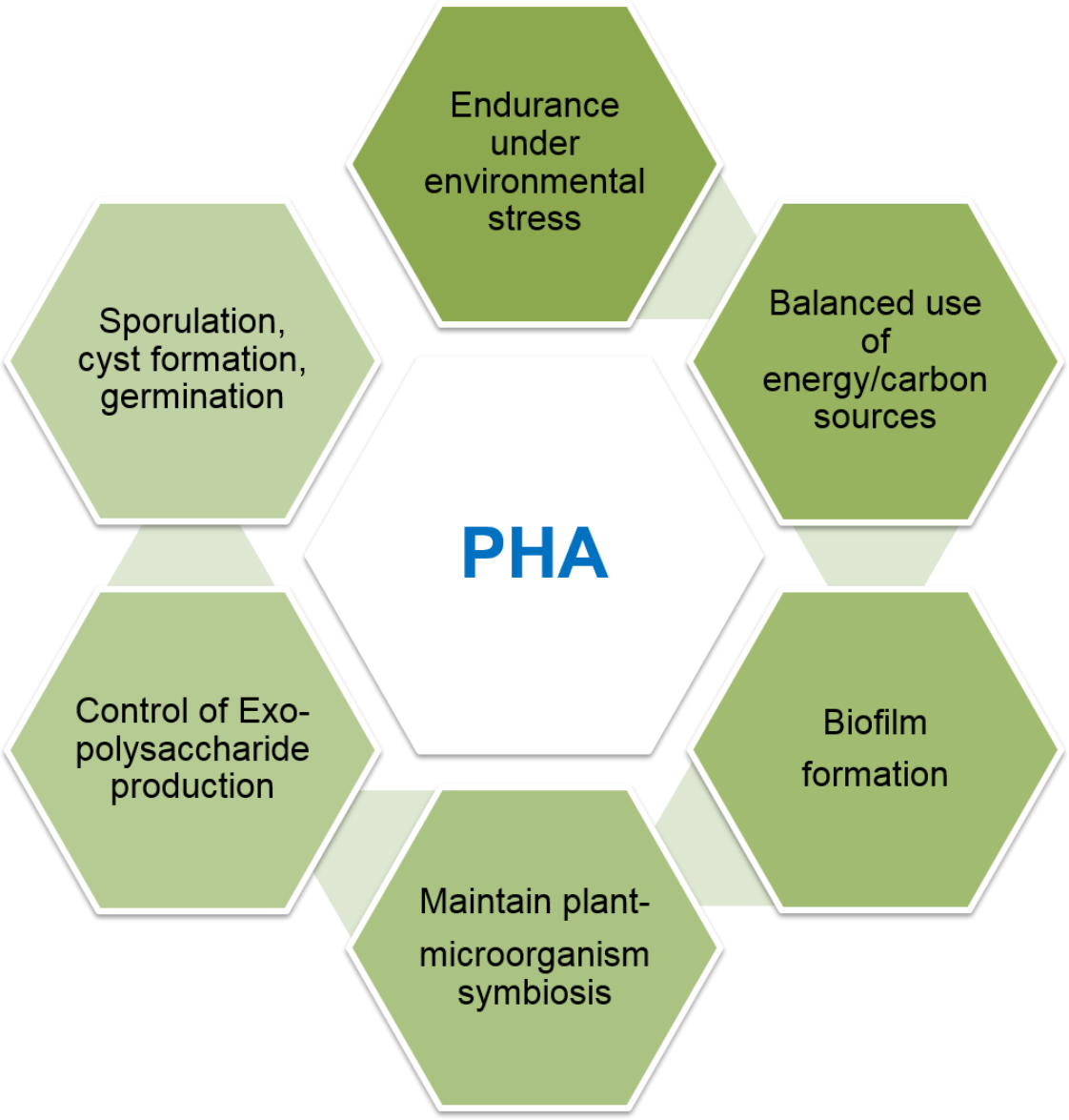

Figure 15. Physiological functions of PHA. With the goal of surviving in nutrient-poor ecosystems, bacteria use PHA metabolism to increase their ability to endure physical and chemical stresses. PHA can be used as a carbon source under nutrient deficiency conditions, and function as a source of energy (reducing equivalents) that can be mobilized to respond to the stress. Figure modified from (Prieto et al., 2016).

1.6 PHA cycle as a robustness cycle

Futile cycles occur in microorganisms inducing a considerable energy burden for the cell, operating when the reactions act in an antagonistic fashion, promoting the dissipation of energy. Such cycles fall into two main categories, those involving simultaneous phosphorylation and dephosphorylation reactions, and those involving transport reactions in the opposite direction.

PHA metabolism is not an unidirectional metabolic process, where the PHA are either polymerized or depolymerized but an “ongoing” cycle, where there is a simultaneous polymerization and degradation of PHA polymer in order to facilitate the turnover of the polymer (Ren *et al.*, 2009; De Eugenio *et al.*, 2010a). PhaZ is active even under conditions where it would appear not to be required (Ren *et al.*, 2009). Cells facing carbon excess and nutrient limitation direct the PHA metabolism to store the extra carbon in the form of polyesters by PHA synthases. Under balanced C/N ratio, PHA metabolism is directed to the hydrolysis pathway releasing *(R)*-HAs monomers to the extracellular medium by the action of the PhaZ depolymerase. The released monomers are then activated to HA-CoAs by a granule-associated acyl-CoA synthetase (FadD) via ATP-dependent reaction (Figure 12). This metabolite is a substrate for PhaC as well as for the fatty acid metabolism. Depending on the metabolic state of the cell, *(R)*-HA-CoA is either incorporated into nascent PHA polymer chains or used by the fatty acid metabolism to make the stored carbon available to the central metabolism.

Robustness is understood as the inherent property that allows systems to maintain their functions despite external and internal perturbations. It is a systems-level phenomenon ubiquitously observed in nature (Kitano, 2004, 2007). Recent work from our group, identified metabolic robustness cycles in *P. putida* KT2440 using the *in silico* genome-scale metabolic model *i*JN1411 (Nogales *et al.*, 2017). Such cycles are more than conventional futile cycles and act as metabolic capacitors responsible for connecting catabolism and anabolism with central metabolism (Figure 16, cycles shown in green). These metabolic capacitors provide a pre-processed source of energy and anabolic building blocks while balancing and optimizing the redox state. Thus, such buffering cycles provide metabolic robustness and fitness under changing environmental conditions.

PHA cycle has been traditionally considered as a futile cycle (Ren *et al.*, 2009; De Eugenio *et al.*, 2010a). However, based on the canonical definition of futile cycles, PHA cannot be considered as a such. In any case, it was not clear which was the metabolic advantage of the PHA cycle, as a great amount of energy was wasted (Ren *et al.*, 2009;

De Eugenio *et al.*, 2010a; Escapa *et al.*, 2012). PHA cycle was identified among these robustness cycles. It has been proposed to be highly expressed under exponential growth phase irrespectively of the nutritional scenario (Nogales *et al.*, 2017). This means that during nutrient imbalance conditions, the cells can adapt rapidly without the need to induce complex cascades of gene expression (Ren *et al.*, 2009). Additionally, PHA cycle has been proposed to regulate the fatty acid flux towards the fatty acid oxidation pathway (Ren *et al.*, 2009). Similarly, work from our group demonstrated that an active PHA cycle has a great impact on a variety of physiological processes such as cell size and number of individuals as function of carbon/nitrogen availability and biomass formation (De Eugenio *et al.*, 2010a; Escapa *et al.*, 2012).

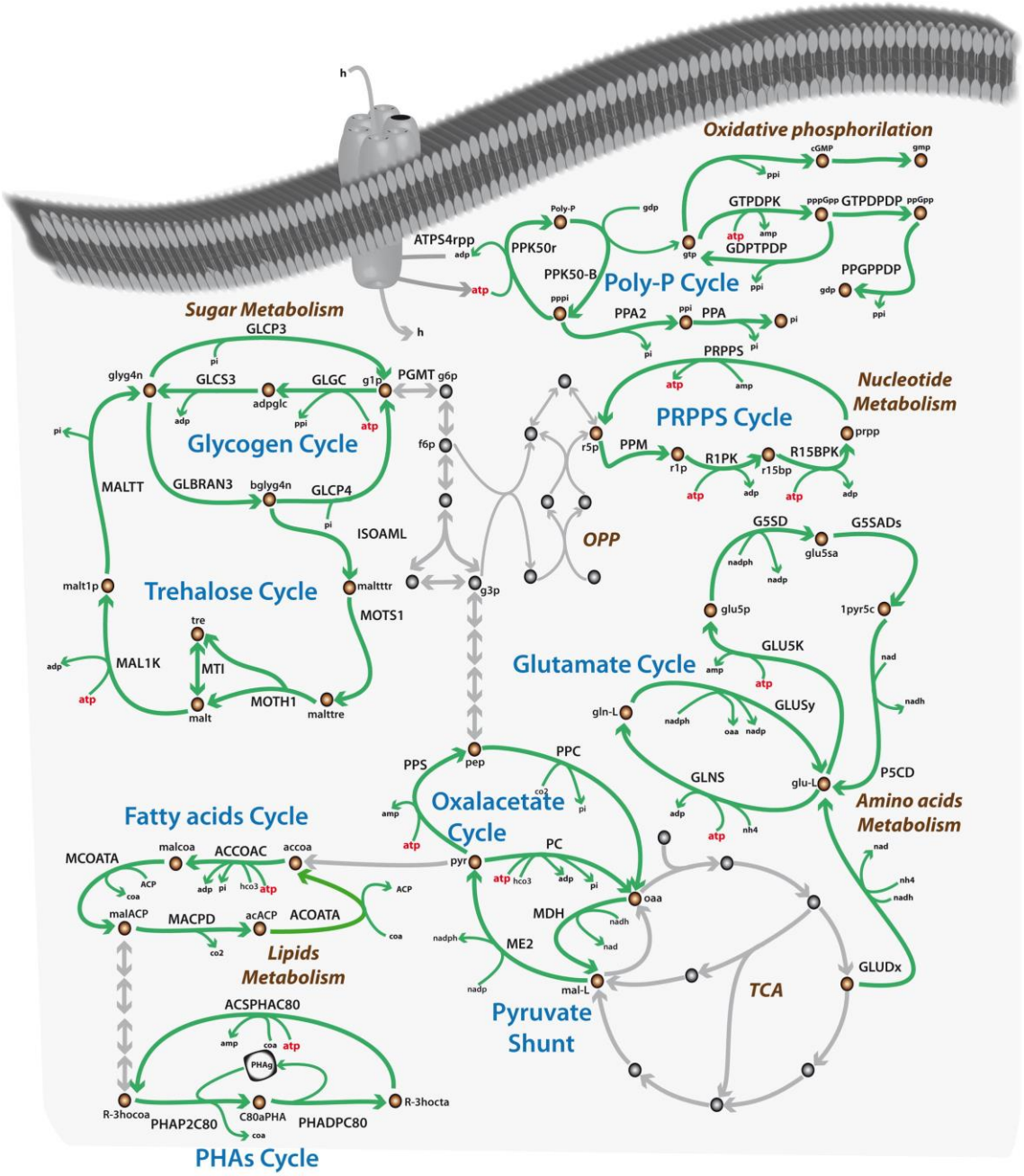

Figure 16. PHA cycle a "robustness cycle"; adapted from Nogales *et al.*, 2017

2. OBJECTIVES

2 OBJECTIVES

The objectives proposed for this Doctoral Thesis are listed:

1. Validation of PHA cycle as robustness cycle in *P. putida* KT2440
i. Physiological analysis of mutant strains in *pha* genes by high throughput phenotyping and gene expression studies.
ii. Study the impact of the PHA cycle on the overall metabolism of *P. putida* KT2440

2. Study of the functional redundancy of isocitrate dehydrogenase in *P. putida* as a mechanism of robustness

3. Model-driven design and optimization of PHA production through system and synthetic biology using aromatics derived from the hydrolysis of recalcitrant polymers.

3. MATERIALS AND METHODS

3 MATERIALS AND METHODS

3.1 Bacterial strains

The bacterial strains used in this Doctoral Thesis are listed in the Table 2. Their genotype and most relevant characteristics are mentioned.

Strains	Genotype/ Relevant characteristics	Reference
P. putida		
KT2440	Rf^r, TOL plasmid-cured, spontaneous restriction deficient derivative of *P. putida* mt-2	(Bagdasarian *et al.*, 1981)
KT40Z	KT2440 derivative strain, Δ*phaZ* deletion mutant	This work
KT2440 Δ*pha*	KT2440 derivative strain, Δ*pha* cluster deletion mutant	https://www.ncbi.nlm.nih.gov/sra/?term=SRX3133083
M0	Gm^r, *P. putida* KT40Z, with genomic insertion via Tn*7* using pMM5	This work
M1	Gm^r, *P. putida* KT40Z, with genomic insertion via Tn*7* using pMM8	This work
M2	Gm^r, *P. putida* KT40Z, with genomic insertion via Tn*7* using pMM14	This work
M3	Gm^r, *P. putida* KT40Z, with genomic insertion via Tn*7* using pMM11	This work
M4	Gm^r, *P. putida* KT2440, with genomic insertion via Tn*7* using pMM12	This work
MM3	KT2440 derivative strain, Δ*mmgF*	This work
MM4	KT2440 derivative strain, Δ(*mmgF scpC*)	This work
MM6	KT2440 derivative strain, Δ(*mmgF scpC sucC sucD*)	This work
MM8	KT2440 derivative strain, Δ(*mmgF scpC sucC sucD aceA*)	This work
MM9	KT2440 derivative strain, Δ(*mmgF scpC sucC sucD aceA glcB*)	This work
MM11	KT2440 derivative strain, Δ(*mmgF scpC sucC sucD aceA glcB icd*)	This work
MM12	KT2440 derivative strain, Δ(*mmgF scpC sucC sucD aceA glcB icd phaZ*)	This work
MM13	KT2440 derivative strain, Δ(*mmgF scpC sucC sucD aceA glcB icd phaZ PP_3190*)	This work

MM14	KT2440 derivative strain, Δ(*mmgF scpC sucC sucD aceA glcB icd phaZ PP_3190 ocd*)	This work
MM15	KT2440 derivative strain, Δ(*mmgF scpC sucC sucD aceA glcB icd phaZ PP_3190 ocd hutF*)	This work
MM16	KT2440 derivative strain, Δ(*mmgF scpC sucC sucD aceA glcB icd phaZ PP_3190 ocd hutF PP_3533*)	This work
MM18	KT2440 derivative strain, Δ*icd*	This work
MM19	KT2440 derivative strain, Δ(*mmgF scpC sucC sucD aceA glcB icd phaZ PP_3190 ocd hutF PP_3533 pha* cluster)	This work
MT1	Km^r, MM19 strain with pMM55	This work
MT2	Km^r, KT2440 Δ*pha* strain with pMM55	This work
MT9	Km^r Gm^r, MM19 strain with pMM55 and pMM66	This work
MT10	Km^r Gm^r, KT2440 Δ*pha* strain with pMM55 and pMM66	This work
MT11	Gm^r, KT2440 with pMM66	This work
E. coli		
DH5a	Cloning host; F^- λ^- *endA1 glnX44*(AS) *thiE1 recA1 relA1* spoT1 *gyrA96*(Nal^R) *rfbC1 deoR nupG purB20* Φ80(*lacZ*ΔM15) Δ(*lacZYA-argF*)U169, hsdR17($r_K^-m_K^+$),	(Grant *et al.*, 1990)
DH10B	Cloning host; F-, *mcrA* Δ(*mrr hsdRMS-mcrBC*) Φ80d*lac*ΔM15 Δ*lacX74 deoR recA1 araD139* Δ(*ara-leu*)7697	Invitrogen, Thermo Fisher Scientific, USA
CC118λ*pir*	Rf^r,Sp^r Cloning host; Δ*(ara-leu), araD,* Δ*lacX74, galE, galK, phoA20, thi-1, rpsE, rpoB, argE* (*Am*), *recA1,* lysogenized with λ*pir* phage	(Herrero *et al.*, 1990)
HB101	Helper strain; F^- λ^- *hsdS20*(r_B^- m_B^-) *recA13 leuB6*(Am) *araC14* Δ(*gpt-proA*)62 *lacY1 galK2*(Oc) *xyl-5 mtl-1 rpsL20*(Sm^R) *glnX44*(AS)	(Boyer and Roulland-Dussoix, 1969)
PIR2	Cloning host; F- Δ*lac*169 *rpo*S(am) *rob*A1 *cre*C510 *hsd*R514 *end*A *rec*A1 *uidA*(Δ*Mlu I*)*::pir*	(Zobel *et al.*, 2015)
DH5aλ*pir*	Cloning host; DH5a lysogenized with λ*pir* phage	(Zobel *et al.*, 2015)
BL21 (λDE3)	B F^- *ompT gal dcm lon hsdS*$_B$($r_B^-m_B^-$) λ(DE3 [*lacI lacUV5-T7p07 ind1 sam7 nin5*]) [*malB*$^+$]$_{K\text{-}12}$(λ^S)	Novagen, Merck KGaA, Germany

Table 2. Strains used in this study

3.2 Plasmids

The plasmids used in this Doctoral Thesis are listed in the Table 3. The most relevant characteristics are mentioned.

Plasmids	Relevant characteristics	Reference
pRK600	Cm^r, ColE1 *oriV* RK2 Mob$^+$ Tra$^+$ donor of transfer functions	(Kessler *et al.*, 1992)
pK18*mobsacB* derivative vectors		
pK18*mobsacB*	Km^r, pMB1, *oriV*, Mob$^+$, *lacZa*, *sacB*; vector for allelic exchange homologous recombination mutagenesis	(Schäfer *et al.*, 1994)
pMM4	Km^r, pK18*mobsacB* derivative vector used for *phaZ* deletion	This work
pMM15	Km^r, pK18*mobsacB* derivative vector used for *aceA* deletion	This work
pMM16	Km^r, pK18*mobsacB* derivative vector used for *glcB* deletion	This work
pMM19	Km^r, pK18*mobsacB* derivative vector used for *icd* deletion	This work
pMM22	Km^r, pK18*mobsacB* derivative vector used for PP_3190 deletion	This work
pMM24	Km^r, pK18*mobsacB* derivative vector used for *hutF* deletion	This work
pMM25	Km^r, pK18*mobsacB* derivative vector used for *ocd* deletion	This work
pMM26	Km^r, pK18*mobsacB* derivative vector used for *PP_3533* deletion	This work
pMM51	Km^r, pK18*mobsacB* derivative vector used for PP_4012 inactivation with Ser133Ala, Asn136Ala, Arg140Ala	This work
pEMG deletion strategy vectors		
pEMG	Km^r, plasmid used for deletions; ori R6K *oriV*, *lacZα* fragment with two flanking I-SceI recognition sites	(Martínez-García and de Lorenzo, 2011)
pEMGTS1-TS2	Km^r, pEMG derivative vector used for *pha* cluster deletion	Arantxa Mato
pSW-I	Amp^r, helper plasmid used for deletions; ori RK2, *oriV*, xylS, Pm→I-SceI	(Wong and Mekalanos, 2000)

pET29a (+) derivative vectors		
pET29a (+)	Km^r, Expression vector. F1 ori, T7 promoter/lac operator, N-terminal S•Tag™/thrombin configuration, and optional C-terminal His6-tag sequence	Novagen, Merck KGaA, Germany
pMM27	Km^r, pET29a (+) derivative vector for production of PP_4011-His$_6$ tag sequence	This work
pMM28	Km^r, pET29a (+) derivative vector for production of PP_4012-His$_6$ tag sequence	This work
pMM42	Km^r, pET29(+) derivative vector for production of PP_4012 mut-His$_6$ tag sequence, with point mutations to Ser133Ala, Asn136Ala, Arg140Ala	This work
sucrose degradation vectors		
pSEVA23*cscAcscB*	Km^r, J23106-BCD12-*cscA*-B0015; J23116-B0033m-*cscB*-B0015; for sucrose degradation	Juan Nogales lab
pSEVA621	Gm^r, ori RK2 used for the cloning of *cscAcscB* genes for sucrose degradation	SEVA collection
pMM66	Gm^r, pSEVA621 derivative vector; J23106-BCD12-*cscA*-B0015; J23116-B0033m-*cscB*-B0015; for sucrose degradation	This work
pBG derivative vectors and those used in PhaZ library construction		
pTnS-1	Amp^r, ori R6K, TnSABC+D operon	(Choi *et al.*, 2005)
pTn*7*-M	Km^r Gm^r, ori R6K, Tn7L and Tn7R extremes, standard multiple cloning site	(Zobel *et al.*, 2015)
pBG	Km^r Gm^r, ori R6K, Tn7L and Tn7R extremes, BCD2-*msfgfp* fusion	(Zobel *et al.*, 2015)
pBG28	Km^r Gm^r, ori R6K, pBG derivative vector with **14a** synthetic promoter	(Zobel *et al.*, 2015)
pBG37	Km^r Gm^r, ori R6K, pBG-derivative vector with **14c** synthetic promoter	(Zobel *et al.*, 2015)
pBG42	Km^r Gm^r, ori R6K, pBG-derivative vector with **14g** synthetic promoter	(Zobel *et al.*, 2015)
pBG51	Km^r Gm^r, ori R6K, pBG-derivative vector with **14d** synthetic promoter	(Zobel *et al.*, 2015)
pGEM-Teasy	Amp^r, ori ColE1, *lacZa* used for cloning BCD2-*phaZ* fusion	Promega, Wisconsin, USA
pMM3	Amp^r, pGEM-Teasy derivative vector, BCD2-*phaZ* fusion	This work

pMM5	Km^r Gm^r, ori R6K, pBG-derivative vector with BCD2-*phaZ* fusion	This work
pMM8	Km^r Gm^r, ori R6K, pBG28-derivative vector with BCD2-*phaZ* fusion	This work
pMM11	Km^r Gm^r, ori R6K, pBG37-derivative vector with BCD2-*phaZ* fusion	This work
pMM12	Km^r Gm^r, ori R6K, pBG42-derivative vector with BCD2-*phaZ* fusion	This work
pMM14	Km^r Gm^r, ori R6K, pBG51-derivative vector with BCD2-*phaZ* fusion	This work
Golden Gate cloning vectors level 0		
pICH41295	Sm^r, ori pMB1/ColE1, golden gate cloning vector **level 0**_ promoter region	Addgene, USA
pICH41308	Sm^r, ori pMB1/ColE1, golden gate cloning vector **level 0**_ coding sequence region	Addgene, USA
pICH41276	Sm^r, ori pMB1/ColE1, golden gate cloning vector **level 0**_ terminator region	Addgene, USA
pRK154	Sm^r, pICH41295 derivative vector, λT0-SynPro16 promoter	This work
pSS14	Sm^r, pICH41276 derivative vector, λT1 terminator	This work
pRK106	Sm^r, pICH41276 derivative vector, rnpB-T1 terminator	This work
pRK107	Sm^r, pICH41276 derivative vector, rpoCterm terminator	This work
pSS68	Sm^r, pICH41308 derivative vector *phaF* gene	This work
pSS70	Sm^r, pICH41308 derivative vector*, phaC1* gene	This work
pMM32	Sm^r, pICH41308 derivative vector*, phaG* gene	This work
pMM33	Sm^r, pICH41308 derivative vector*, PP_0763*	This work
Golden Gate cloning vectors level 1		
pICH47732	Amp^r, ori pUC/RK2, golden gate cloning vector **level 1** position 1	Addgene, USA
pICH47742	Amp^r, ori pUC/RK2, golden gate cloning vector **level 1** position 2	Addgene, USA
pICH47751	Amp^r, ori pUC/RK2, golden gate cloning vector **level 1** position 3	Addgene, USA
pICH47761	Amp^r, ori pUC/RK2, golden gate cloning vector **level 1** position 4	Addgene, USA
pICH47772	Amp^r, ori pUC/RK2, golden gate cloning vector **level 1** position 5	Addgene, USA

pICH54033	Amp^r, ori pUC/RK2, golden gate cloning vector **level 1** position 3; dummy	Addgene, USA
pMM34	Amp^r, pICH47732 derivative vector **level 1** position 1; T0-SynPro16-*phaC1*-λT1	This work
pMM35	Amp^r, pICH47742 derivative vector **level 1** position 2; T0-SynPro16-*phaF*-rnpB-T1	This work
pMM37	Amp^r, pICH47772 derivative vector **level 1** position 5; T0-SynPro16-PP_0763-λT1	This work
pMM38	Amp^r, pICH47761 derivative vector **level 1** position 4; T0-SynPro16-*phaG*-rnpB-T1	This work
Golden Gate cloning vectors level 2		
pAGM4723	Km^r, ori ColE1/pVS1, golden gate cloning **vector level 2**	Addgene, USA
pICH49299	Amp^r, ori pUC/RK2, golden gate vector **level 2 end-linker (open construct),** position 5	Addgene, USA
pMM55	Km^r, pAGM4723 derivative **vector level 2**; *phaC1*; *phaF*; dummy 3; *phaG*; PP_0763	This work

Table 3. Plasmids used in this study.

3.3 Media and growth conditions

E. coli and *P. putida* strains were grown routinely for DNA manipulations and for pre-cultures in lysogeny broth (LB) medium (Sambrook and Russell, 2001) at 37°C and 30°C, respectively. The appropriate selection antibiotics, gentamicin (10 µg/ml), chloramphenicol (34 µg/ml), ampicillin (100 µg/ml), kanamycin (50 µg/ml), streptomycin (75 µg/ml) were added when needed. Additionally, IPTG (0.5-1 mM) and Xgal (40 µg/ml) were added when needed.

Standard growth experiments of *P. putida* in defined medium were performed in M63 minimal medium (13.6 g of KH_2PO_4/L, 2 g $(NH_4)_2SO_4$/L, 0.5 mg $FeSO_4$ •7H_2O/L, adjusted to pH 7.0 with KOH) (Miller, 1972), plus the carbon source needed in each case. For PHA accumulation, *P. putida* strains were grown in M63 0.1 N nitrogen-limited minimal medium (13.6 g of KH_2PO_4/L, 0.2 g $(NH_4)_2SO_4$/L, 0.5 mg $FeSO_4$•7 H_2O/L, adjusted to pH 7.0 with KOH), supplemented with the needed carbon source for 24 h at 30°C under vigorous shaking at 200 rpm, as previously described (De Eugenio *et al.*, 2010a). In both cases, the medium was supplemented with 1 mM $MgSO_4$ and 1 X solution of trace elements (Goodies) (composition 1000 X dissolved in 1N HCl: 2.78 g/L

of $FeSO_4 \cdot 7H_2O$, 1.98 g/L of $MnCl_2 \cdot 4H_2O$, 2.81 g/L of $CoSO_4 \cdot 7H_2O$, 1.47 g/L $CaCl_2 \cdot 2H_2O$, 0.17 g/L of $CuCl_2 \cdot 2H_2O$, 0.29 g/L of $ZnSO_4 \cdot 7H_2O$).

For *P. putida* growth experiments, fresh LB pre-cultures cells were washed twice with 0.85% saline solution (NaCl), adjusted to an optical density at 600 nm of 0.3 in the corresponding medium either M63 0.1 N or M63 plus the needed carbon source. Culture growth (50 ml) was monitored in shaking Erlenmeyer flasks (at 200 rpm) of 250 ml using a portable spectrophotometer (Fischer Scientific, Pennsylvania, USA) at 600 nm for 24-48 h. In all the experimental approaches described, the cultures occupied no more than 20% of the volume of the flask and special care was taken to control the C/N ratio, in order to compare between different growth conditions when different carbon sources were applied. For PHA mobilization experiments, the C/N ratio was varied between 1-3 mol/mol, whereas for PHA accumulation experiments, the C/N ratio was maintained at 40 mol/mol (Table 4).

For the cultivation in 96-microwell plates, 200 µl aliquots were distributed in the microwells. The plates were incubated at 30°C for 24-48 h, with 20 seconds of heavy orbital shaking every 15 min using a Multiskan Ascent Incubator (Thermo Scientific, Waltham, MA, USA) that monitors optical density at 630 nm every 15 min.

Substrate	Nº carbons	Concentration (mM)	Nitrogen Limitation	C/N ratio (mol/mol)
Octanoate	8	7.5	No	2
		15	Yes	40
Glucose	6	10	No	2
		20	Yes	40
4-Hydroxybenzoic acid (4HBz)	7	5	No	1.12
		10	Yes	23.33
p-Coumaric acid	9	3.9	No + EDTA	1.12
Vanillic acid	8	4.4	No + EDTA	1.12
Ferulic acid	10	3.5	No + EDTA	1.12
Phenylacetatic acid	8	4.4	No + EDTA	1.12
4HBz + octanoate	7 / 8	5 / 3	No	2
4HBz + 10 undecenoic acid	7 / 11	5 / 3	No	2.26
Glycerol + octanoate	3 / 8	20 / 1	No	2.26
Glycerol + glucose	3 / 6	20 / 1.3	No	2.26
Sucrose	12	5	No	2
Succinate	4	15	No	2

Table 4. Carbon sources used in this work. The concentration, the medium and the C/N ratio are listed.

3.4 Synthetic biology DNA techniques

The revisited KT2440 genome complete nucleotide sequence is accessible in the data bank ((Belda *et al.*, 2016); https://www.ncbi.nlm.nih.gov/nuccore/NC_002947.4). Standard molecular biology techniques were performed as previously described (Sambrook and Russell, 2001). All oligonucleotides used for PCR amplification are listed in Table S 7. Plasmid DNA Isolation were made using the High Pure Plasmid Isolation Kit (Roche, Mannheim, Germany) following the manufacturer's protocol. Genomic extractions of *P. putida* KT2440 were performed with the illustraTM bacteria genomicPrep Mini Spin Kit (GE Healthcare, Buckinghamshire, UK) or PureLink® Genomic DNA kit (Invitrogen). DNA agarose gel bands, PCR products and digestion products were purified with illustraTM GFX PCR DNA and Gel Band Purification Kit (GE Healthcare, Buckinghamshire, UK) or QIAquick Gel Extraction Kit (Quiagen) and QIAquick PCR Purification Kit (Quiagen). DNA concentrations were measured with Nano Drop® 2000 Spectrophotometer (Thermo Scientifc, Massachusetts, USA). The enzymes Phusion DNA polymerase, T4 DNA ligase, EcoRI-HF, BamHI-HF, XbaI, HindIII-HF, NotI-HF, NcoI-HF, DraIII-HF, PacI, SpeI and CutSmart buffer were acquired from New England Biolabs (NEB, Ipswich, Massachusetts). For cloning confirmation, the DNA Taq polymerase (Biotools, Madrid, Spain) was used. The GoldenGate-MoClo enzymes, BpiI and BsaI, and Buffer G were acquired from Thermo Scientific (Massachusetts, USA). The GoldenGate-MoClo Toolkit (Kit 1000000044) was purchased from Addgene (Massachusetts, USA).

3.4.1 Preparation and transformation of competent strains

Preparation of chemically competent *E. coli* cells was carried out using the RbCl method and their transformation was followed as described previously (Sambrook and Russell, 2001). *P. putida* strains were transformed following the Choi et al. protocol with some modifications (Choi *et al.*, 2006). *P. putida* KT2440 strains were grown overnight in 20 ml of LB at 30°C. These cultures were pelleted at 3000 x*g* for 20 minutes at 4°C, washed five times with 300 mM sucrose and resuspended in 500 µl of 300 mM sucrose. 100 µl of cell suspension was mixed with 100 ng of desired plasmid and transferred to a 2 mm gap electroporation cuvette. After a pulse of 25 µF, 2.5 kV and 200 Ω (Gene Pulser/Pulse Controller (Bio-Rad)), 900 µl of fresh room temperature LB was added and transferred to a 100 x 16 mm round-bottom polypropylene tube and incubated for 1 hour

at 30°C and 200 rpm. Different dilutions were plated on LB 1.5% agar medium with corresponding antibiotic selection and grown at 30°C for 18 hours.

3.4.2 Plasmid transfer by conjugation

To perform a conjugation transfer, we need to bring together the donor cell that bears the plasmid of interest, the recipient strain, which is the target bacterium, and a helper bacterial strain to assist and catalyze the mating process. The mating helper is an *E. coli* strain that provides the conjugation machinery, which is normally derived from a RK2 or RP1 plasmid that involves the mobilization (*mob*) and transfer (*tra*) functions supplied *in trans*. There are two basic types of helper strains, which express the above mentioned functions either on a plasmid (such as HB101 carrying pRK600) or genome integrated (such as S17λ*pir*). In this Doctoral Thesis, the former type of helper strain was used, and three bacterial strains in the mating process need to be included, offering the possibility of changing the donor *E. coli* strain. The donor strain should contain the *pir* gene as λ*pir* lysogen such as CC118λ*pir* or DH5aλ*pir* in order to favor counter selection of transconjugants as needed (Martínez-García *et al.*, 2017).

Triparental mating was performed following the protocol described by Herrero and collaborators (Herrero *et al.*, 1990), using *E. coli* DH10B with pMM series plasmids as donor strain, *E. coli* HB101 pRK600 as helper strain and *P. putida* KT2440 as recipient strain. The LB pre-inoculum strains were washed twice using 0.85% saline solution and then 100 µl of each strain were mixed in an eppendolf. As a negative control, the mixed strains without the recipient one was used. Then, on nonselective LB agar plate, we placed filters of 0.22 µm pores (Merck) and 100 µl of the mixture of the strains were placed on top of the filters. The plate was incubated for 10 hours in 30°C. Placing the conjugation mixture on a solid support facilitates *oriT*-mediated conjugation by immobilizing cells in close proximity to one another. The filter was used to facilitate the recovery of cells, and nonselective medium was required to avoid killing nontransformed recipient cells (Choi and Schweizer, 2006). The counterselection against *E. coli* was achieved by using *Pseudomonas*-selective rich media such as cetrimide-containing agar or minimal M63 medium supplemented with 0.2% citrate or 5 mM benzoate (*E. coli* donor cells cannot use citrate or benzoate as sole carbon and energy source). In all the cases, the corresponding antibiotic was added in order to inactivate any nontransformed *P. putida* cells.

3.4.3 Plasmid insertion via Tn*7* transposon system

Broad host range mini-Tn*7* vectors facilitate integration of single-copy genes into bacterial chromosome at a neutral and naturally evolved site. The TnsABCD transposase components of Tn*7* catalyze site and orientation-specific insertion with high frequency into bacterial chromosomes at Tn*7* attachment (*att*Tn*7)* sites. With very few exceptions these sites are located downstream of a highly conserved *glmS* gene coding essential glucosamine-6-phosphate synthetase (Choi *et al.*, 2005; Choi and Schweizer, 2006).

This method was carried out by four-parental mating. 4 ml of overnight LB precultures of *E. coli* CC18λ*pir* bearing pMM series of plasmids (Table 3) strain (donor strain), *E. coli* HB101 pRK600 (helper strain), *E. coli* DH5αλ*pir* pTnS-1 (leading transposase strain) and *P. putida* (recipient strain) were washed twice with 0.85% of saline solution and then 100 µl of each strain were mixed in an eppendolf. The same mating protocol was used as described previously. The transconjugants were selected on cetrimide agar containing 10 µg/ml gentamicin plates and incubated at 30°C for 18 hours. A negative control of the *E. coli* parental strains without the recipient *P. putida* strain was also plated. The next day, few colonies were picked on LB kanamycin (to verify the loss of the plasmid) and LB gentamicin and incubated at 30°C for 18 hours (having Tn*7* transposon chromosomically integrated). Few LB gentamicin resistant and LB kanamycin sensitive clones were selected in order to verify the correct insertion of the transposon into the *att* Tn*7* site and checked via colony PCR and sequencing (primers 5-Pput-*glmS*UP and 3-Tn7L, Supplementary Table S7).

3.4.4 Construction of *P. putida* deletion mutants

During this Thesis, two deletion strategies based on the pK18*mobsacB* and pEMG were used.

The gene of interest was inactivated by allelic exchange homologous recombination using the mobilizable plasmid pK18*mobsacB* (Schäfer *et al.*, 1994). The PCR primer pairs used for these constructions are listed in the Supplementary Table S7. The PCR primer pairs were designed in order to amplify approximately 500-800 bps regions upstream (Z1) and downstream (Z3) of the gene that will be deleted to serve as recombination arms of homology. We added proper restriction enzyme sites upstream of Z1 and downstream of Z3, in order to clone the fragment Z1Z3 into pK18*mobsacB*. The two purified fragments Z1, Z3 were used in order to obtain a Z1Z3 fusion fragment (overlapping PCR). The obtained Z1Z3 fragment and the plasmid pK18*mobsacB* were digested with the appropriate restriction enzymes and further gel purified. Finally, the

purified fragment and plasmid were ligated using T4 DNA ligase (New England Biolabs) overnight at 16°C. These deleted genes were cloned into the corresponding unique sites of pK18*mob*sacB plasmid and transformed into chemically competent *E. coli* DH10B. The transformants were plated on LB plates with kanamycin (50 µg/ml), 0.5 mM IPTG and 40 µg/ml Xgal for selection and blue/white screening. Colony PCR was used to verify selected white colonies using the F24, R24 primer pair. From selected candidates we performed plasmid isolation and the correct sequence of the cloned inserts was confirmed by DNA sequencing.

The resultant plasmid was used to delete the target gene to the host chromosome via homologous recombination. Triparental mating was performed following protocol described before, using *E. coli* DH10B with pMM series of plasmids (Table 3) as donor strain, *E. coli* HB101 pRK600 as helper strain and *P. putida* KT2440 as recipient strain. For the first recombination selection process, the cells were plated on cetrimide agar containing 50 µg/ml kanamycin, that permitted only the selection of *P. putida* strains (Zobel *et al.*, 2015). The resulted recombinant strains were confirmed by PCR and the selected colonies were grown in LB during 6 hours and then plated on M63 10 mM citrate selective plates supplemented with 5% sucrose. The *sacB* counterselection marker from *Bacillus subtilis* confers sucrose sensitivity to Gram negative bacteria. Almost all sucrose-resistant colonies will have been cured from pK18*mobsacB* plasmid (Schäfer *et al.*, 1994). Transconjugants sucrose resistant and kanamycin sensitive were isolated and the second crossover event was confirmed by PCR, using external primers of the arms of homology region (for example Z1-For, Z3-Rev) and DNA sequencing. A schematic representation of the process is represented in Figure 17.

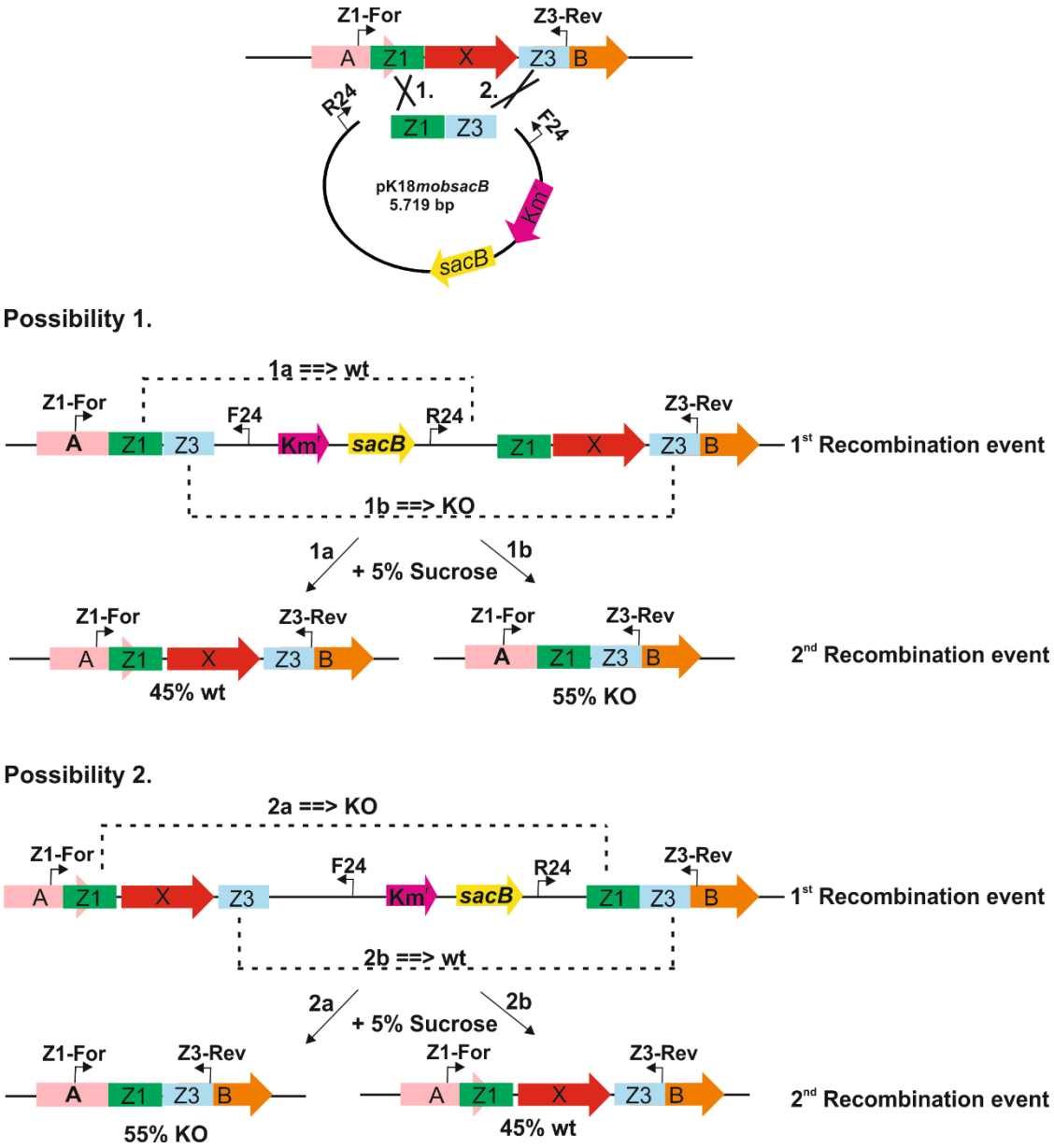

Figure 17. schematic representation of pK18*mobsacB* strategy. The two possibilities of recombination events are represented. Z1 (green color), Z3 (blue color) upstream and downstream arms of homology regions. With dot lines the different options of having restored wilt type phenotype (45% possibility; shown as wt) and gene knock out (55% possibility; shown as KO) are shown.

For the *pha* cluster deletion, the pEMG knockout system was used, with some modifications (Martínez-García and de Lorenzo, 2011). The pEMG system is based on similar principles of markerless gene replacements by a double-strand break in the chromosome, than the pK18*mobsacB* strategy. As far as it concerns the design of the homology regions (called as TS1 and TS2 regions, upstream and downstream of to be deleted gene (s), respectively), the delivery vector (pEMG) and the first recombination event transconjugants are the same as in the case of pK18*mobsacB* strategy.

The key event in the procedure is the generation of a single break in target genome through conditional expression of the I-Sce-I endonuclease. The site recognized by this enzyme is an 18 bp sequence (5´-TAGGGATAACAGGGTAAT-3´) that is not present in any of the >1700 microbial genomes known thus far. The I-Sce-I sites are entered in the chromosome of the bacterium upon co-integration of the recombinogenic vector. Under these conditions, surviving cells must have recombined the sequences that flank the I-Sce-I site to restore chromosomal integrity. The constructing vector pEMG incorporates two I-Sce-I sites flanking a *lacZa* poly-linker. This vector functions in concert with the I-Sce-I producing pSW(I-SceI) plasmid that allows the accumulative edition of the genome of *P. putida* (Martínez-García and de Lorenzo, 2011).

Thus, *P. putida* transconjugants of the first recombination event were transformed with pSW-I via electroporation. The selection plates were LB + 500 µg/ml Amp and 15 mM 3-methylbenzoate (3MB) and incubated on 30ºC for 16 h. We should note here, that KT2440 is naturally resistant to ampicillin but such concentration allows plasmid selection. Additionally, the I-Sce-I endonuclease expression is dependent on a 3MB inducible promoter system. Single colonies were picked on LB + 500 µg/ml Amp and LB + Km to screen for kanamycin sensitive clones. Similar to pK18*mobsaB* strategy, several kanamycin sensitive clones were checked for the knockout phenotypes, using external primers to the homology region (FdPHA and RdPHA, Supplementary Table S7). To confirm, the integrity of the homology region, DNA sequencing of the PCR product was also performed. Under non-selective cultivation *Pseudomonas* loses the pSW-I plasmid quite fast. For this purpose, several single colonies were checked for 500 µg/ml Amp sensitivity to verify pSW-I plasmid loss.

3.4.5 GoldenGate-MoClo protocol

Golden Gate cloning method is based on the use of type IIS restriction enzymes combined with restriction-ligation. Extremely high cloning efficiency is obtained using a simple one-pot incubation of multiple undigested entry constructs and a destination vector in the presence of restriction enzyme and ligase. MoClo (modular cloning system) allows any multigene construct of choice to be made by using a defined set of pre-made vectors and a defined assembly strategy. Basic genetic elements like promoters, coding sequences and terminators are cloned at level 0 modules. Each module is flanked by two BsaI restriction sites specific for each modules type, with cleavage sites designed to allow sets of compatible modules to be assembled in one step in a level 1 destination vector (using BsaI enzyme). The resulting level 1 constructs contain transcriptional units, which are then assembled six at a time in level 2 constructs using a second type IIS

enzyme, BpiI. The cloning process can then be repeated to add more transcription units to the resulting construct by alternating the type IIS enzyme (s) for cloning.

GoldenGate-MoClo plasmids were constructed following the Weber et al. protocol with some modifications (Weber *et al.*, 2011). For Level 0 plasmid construction, every part was PCR amplified with oligonucleotides designed with the Benchling platform (www.benchling.com) with the following characteristics: a tail containing the BpiI recognition site followed by the corresponding 4-nt fusion site, 21 bp of minimal length for target complementarity, 50°C of minimal Tm for that region and a maximal Tm difference of ± 1.5°C between both oligonucleotides. If a part contained a BpiI/BsaI recognition site, it would be eliminated introducing by PCR amplification silent samesense point mutations in the restriction site sequences. PCR products were purified using gel purification kit following manufacturer instructions. Digestion-ligation reaction was set up by pipetting in one tube 100 ng of destination vector and the corresponding DNA amount of PCR product to maintain 2:1 insert-vector molar ratio, 10 U of BpiI, 400 U of T4 DNA ligase and 1 mM ATP in commercial Buffer G in a final reaction volume of 20 µl. The reaction was incubated in a thermocycler for four cycles of restriction-ligation at 37°C for 10 minutes and 16°C for 10 minutes and then heat inactivation at 65°C for 20 minutes. The final step is of great importance, thus, omitting this inactivation would lead to re-ligation of some of the insert and plasmid backbone fragments when the reaction vessel is taken out of the thermal cycler and would lead to a higher proportion of colonies containing incorrect constructs 100 µl of chemically competent *E. coli* DH5α were transformed with 5 µl of reaction mix. Transformed cells were grown overnight at 37°C in LB 1.5% agar supplemented with 75 µg/ml streptomycin, 0.5 mM IPTG and 40 µl/ml X-gal. Blue-white selection was carried out and four white colonies were transferred to 4 mL of liquid LB medium with 75 µg/ml streptomycin for plasmid purification. The extracted plasmids were digested for an hour at 37°C with BsaI to check the presence of the correct insert in an agarose 0.7% gel. Two plasmids with the correct insert size were sequenced with RK81-RK82 (Supplementary Table S7) to verify sequence integrity.

The position and orientation of each gene in a final construct determines which level 1 destination vector has to be chosen for assembly of a transcription unit. A total of 14 vectors are available (pL1F1-7, pL1R1-7) for cloning of genes either forward or reverse orientation at each of seven possible positions. These level 1 vectors differ only by the sequence of the fusion sites. The two external fusion sites (BpiI cleavage sites) of each vector are designed to be compatible with the fusion sites of the vectors from the position before and after. The downstream fusion site of the vector at position 7 is compatible to the upstream fusion site of vector at position 1 (TGCC). Thus, multigene

constructs with more than seven genes can be assembled without the need for additional cloning vectors. In practice, a gene that is planned to be cloned at position 8 in a multigene construct is simply cloned in a position 1 destination vector etc. For Level 1 plasmid construction of transcription units, the reaction mix was composed by 100 ng of destination vector (pL1F-1 to pL1F-7 depending on the CDS position), a promoter plasmid part, a CDS plasmid part and a terminator plasmid part in a 2:1 donor vector-destination vector molar ratio. 10 U of BsaI, 400 U of T4 DNA ligase and 1 mM ATP in Buffer G in a final reaction volume of 20 µl. The reaction was incubated in a thermocycler for four cycles at 40°C for 10 minutes and 16°C for 10 minutes, then at 50°C for 10 minutes and heat inactivation at 80°C for 20 minutes. 100 µl of chemically competent *E. coli* DH10B were transformed with 5 µl of the reaction. Transformed cells were grown overnight at 37°C in LB 1.5% agar supplemented with 100 µg/ml ampicillin, 0.5 mM IPTG and 40 µl/ml X-gal. Blue-white selection was carried out and four white colonies were transferred to 4 mL of liquid LB medium with 100 µg/ml ampicillin to do a plasmid purification. The extracted plasmids were digested for an hour at 37°C with BpiI to check the presence of the correct insert in a 0.7% agarose gel. Two plasmids with the correct insert size were sequenced with RK155-RK156 to verify sequence integrity (Table S7).

Level 2 vectors contain two inverted BpiI recognition sites for insertion of level 1 modules. The upstream fusion site (TGCC) is compatible to a gene cloned in a level 1 vector, whereas the downstream fusion site consists of a universal sequence (GGGA). This design allows cloning of two to six genes in the same vector. Using more genes in this step would lead to incorrect clones because the same fusion sites would be present in different modules. The last gene is fused to the vector by using a compatible linker. There are two types of linkers, the “closed” construct, where no further genes can be added (pELE-1-7) and the “opened” construct for cloning of further genes (pELB1-7 and pELP1-7). Level 2 reactions were carried out with 100 ng of destination vector (pL2), the corresponding end-linker vector (depending on the number of transcriptions units and if the construct was “opened” or “closed”), the vector/s with each transcription unit in a 2:1 donor vector-destination vector molar ratio. 10 U of BpiI, 400 U of T4 DNA ligase and 1 mM ATP in Buffer G in a final reaction volume of 20 µl. The reaction was incubated in a thermocycler for four cycles at 37°C for 10 minutes and 16°C for 10 minutes and then heat inactivation at 65°C for 20 minutes. 100 µl of chemically competent *E. coli* DH10B were transformed with 5 µl of the reaction. Transformed cells were grown overnight at 37°C in LB 1.5% agar supplemented with 50 µg/ml kanamycin. Red-white selection was carried out and four white colonies were transferred to 4 mL of liquid LB medium with 50 µg/ml kanamycin to do a plasmid purification. The extracted plasmids were digested for an hour at 37°C with DraIII-HF and other control enzymes in order to

check the presence of the correct inserts in an agarose 0.7% gel. During each step of the part construction, apart from the control digestion process, sequencing (with the listed oligonucleotides in Supplementary Table S7) of all the included parts was realized.

An example of the hierarchical cloning levels of GoldenGate-MoClo used in this work is shown in Figure 18. In all the cases, the SynPro16 promoter was used with an upstream λT0 terminator which was introduced into the Golden Gate-MoClo pL0-PU plasmid (Tiso *et al.*, 2016). Genes encoding PhaC1, PhaF, PhaG and PP_0763 enzymes from *P. putida* KT2440 were cloned intro the pL0-SC plasmid from the Golden Gate-MoClo kit. The terminator λT1, rnpB-T1 and rpoC-term were cloned into the pL0-T plasmid from the Golden Gate-MoClo kit.

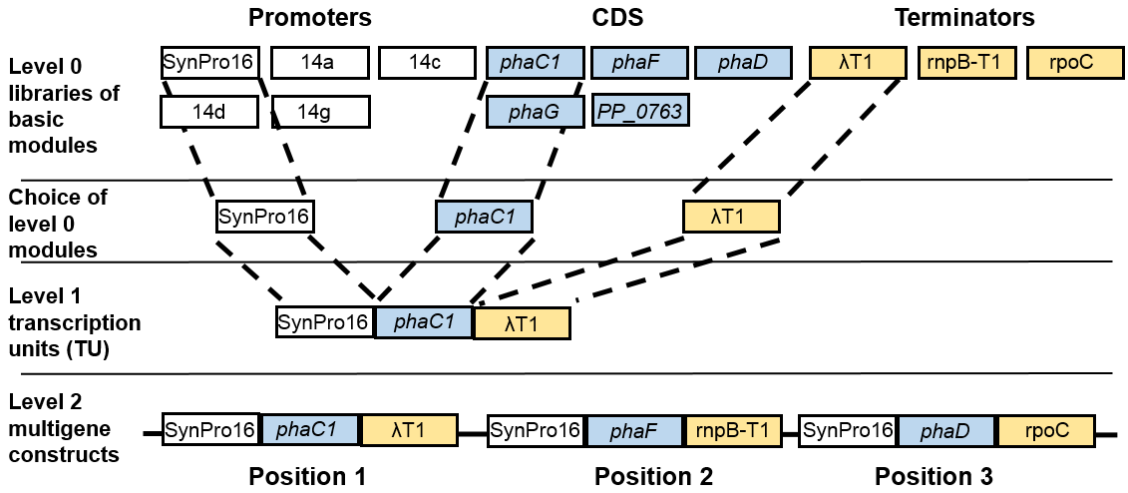

Figure 18. The hierarchical cloning levels of GoldenGate-MoClo. Representation of different possible combinations that can be carried out from Level 0 parts to form Level 1 transcription units and the subsequent assembly of three Level 1 transcription units to form a Level 2 multigene assembly plasmid.

3.5 Molecular biology RNA techniques

3.5.1 RNA extraction

For the RNA extraction process, standard molecular biology techniques were followed (Escapa *et al.*, 2012). The RNA samples were obtained from at least three independent cultures, grown under PHA mobilization and PHA accumulation conditions (more details in each Results chapter). After 6 h of growth (mid-exponential phase), 7 ml were harvested by centrifugation at 3000 x*g* for 10 min at 4°C. The cell pellets were rapidly frozen in dry ice and stored at -80°C until further use. Pellets were resuspended in TE buffer (10 mM Tris-HCl pH 7.5, 1 mM EDTA) containing 5 mg/ml of lysozyme. RNA was extracted using the High Pure RNA Isolation kit (Roche) following the manufacturer's

instructions. Extracted RNA was treated with DNase (Ambion) following the manufacturer´s instructions. RNA integrity was checked by agarose gel electrophoresis and was quantified with NanoDrop 2000® Spectrophotometer (Thermo Scientific, Massachusetts, USA). For further verification of DNA absence, a control PCR verifying the absence of amplification was performed.

3.5.2 Real time quantitative reverse transcription PCR assay

cDNA synthesis was proceeded by using Transcriptor First Strand cDNA Synthesis kit (Roche), following the manufacture´s recommendations. cDNA was synthesized from 1 µg of purified RNA using random hexamer-primed reactions. For the qRT-PCR assay, the protocol described by Revelles and collaborators was followed with some modifications (Revelles *et al.*, 2016). For the RT-PCR reaction, 1 µg of transcribed cDNA was used and a standard curve of differential dilutions (from 10^{-1} to 10^{-5}) of *P. putida* genomic DNA was realized. The sequence of the primers used for this study are listed in Table S7. Finally, the absolute quantification was chosen for our data analysis, showing the expression levels in nM concentration of DNA. This analysis was performed in three technical replicates from three independent biological samples and the size of each amplified gene was taken into account.

3.6 Physiological parameters quantification

3.6.1 Total biomass calculation

For total biomass calculation, 40 ml of culture medium were centrifuged, in previously tared 50 ml Falcon tubes, for 45 min at 3000 x*g* at 4°C. Cell pellets were rapidly frozen at -80°C and were freeze-dried for 24 h in a lyophilizer. Finally, the tubes were weighted and the cell densities were expressed in grams of cell dry weight (CDW) per liter. By residual biomass, it is referred to the total biomass free of PHA.

3.6.2 Cell viability calculation

Bacterial serial dilutions from 10^{-1} to 10^{-7} were made in salt solution (0.85% NaCl), in order to calculate the cell viability. Three different spots of each dilution from 10^{-3} to 10^{-7} were plated on LB solid medium. After the spot was dried off, the plates were

incubated O/N at 30°C and then the colony-forming units (cfu) were counted. For each strain and condition, at least three independent experiments were carried out.

3.6.3 Growth rate calculation

It is worth to notice that PHA content disturbs cells turbidimetry, thus, the optical density gives mixed information about cell growth plus PHA accumulation. Optical density can only be used to determine the growth rates in absence of PHA (from the linear part of the growth curve). Growth rates have been calculated based on the log10 of residual biomass (biomass free of PHA) data in different time points versus time. The curve slope was multiplied by a conversion factor (2.303) between Napierian logarithms.

3.7 Analytical procedures

3.7.1 Methanolysis process and GC-MS analysis for PHA determination

For composition and cellular PHA content, standard GC-MS techniques of the methanolysed polyester, previously described from our lab with some modifications were used (De Eugenio *et al.*, 2010a). 2-5 mg of lyophilized samples (culture pellets) were resuspended in 2 ml of methanol containing 15% sulfuric acid (Sigma-Aldrich, Merck, Germany) and 2 ml of chloroform containing 0.5 mg/ml 3-methylbenzoic acid (internal standard; Sigma-Aldrich, Merck, Germany) and then incubated using screw-capped tube at 100°C for 5-6 h. After cooling, 1 ml of distilled water was added to the mixture, to extract most cell debris and the sulfuric acid left. A two-phase extraction process was performed by removing completely the water phase to prevent fouling of the GC column. Finally, a small amount of Na_2SO_4 powder was added to dry the chloroform phase and to remove any water remains. The absence of sulfuric acid residues to the samples was verified by checking that the pH was 5. Then, the organic phase containing the resulting methyl esters of monomers was analyzed by GC-MS.

An Agilent (Waldbronn, Germany) series 7890A coupled with a 5975C MS detector (EI, 70 eV) and a split–splitless injector were used for analysis. An aliquot (1 µl) of organic phase was injected into the gas chromatograph at a split ratio of 1:50. During this work the DB-5HTDB-5HT column (400°C: 30 m x 0.25 mm x 0.1 µm film thickness) was used. Helium was used as carrier gas at a flow rate of 0.9 ml min^{-1}. The injector and transfer line temperature were set at 275°C and 300°C respectively. The oven temperature program was initial temperature 80°C for 2 min, then from 80°C up to 175°C at a rate of

5°C min^{-1}, for efficient separation of peaks. EI mass spectra were recorded in full scan mode (*m/z* 40–550). With this program, monomers from C4 to C14 were detected. The retention time for each monomer is 1.9 min (C4), 2.4 min (C5), 3.5 min (C6), 4.8 min (C7:1), 7.2 min (C8), 9.3 min (C9:1), 12.0 min (C10), 14.1 min (C11:1), 16.2 min (C12:1), 16.6 min (C12), 20.9 min (C14) and 6.1 (3MB, internal standard).

3.7.2 GC-MS and octanoate consumption quantification

For the quantification of extracellular octanoate using GC-MS, the lyophilized supernatants of the strains growing under PHA accumulation conditions were derivatized. Approximately 5 mg of lyophilized sample were weighted and 100 µl of pyridine (Sigma-Aldrich, Merck, Germany) and 50 µl of N´N´BSTFA (Bis(trimethylsilyl)trifluoroacetamide, Sigma-Aldrich, Merck, Germany) were added. The mixture was incubated for 45 min in sand bath at 70°C with agitation. Then, 50 µl of 10 mM n-decane (Sigma-Aldrich, Merck, Germany) dissolved in pyridine was added in the mixture, as an internal standard. A standard curve of sodium octanoate (Sigma-Aldrich, Merck, Germany) was performed with the same procedure. The used column was HP-5MS 5% Phenyl Methyl Silox (400°C: 30 m × 0.25 mm × 0.1 µm film thickness). The transfer line temperature was set at 280°C. The oven temperature program was initial temperature 80°C for 0 min, and then from 20°C min^{-1} up to 200°C for 0 min, the duration of the run was 6 min, for efficient separation of peaks. The retention time was 2.4 min and 4 min for the internal standard (decane) and sodium octanoate, respectively.

3.7.3 HPLC-MS and extracellular *(R)*-HAs quantification

P. putida strains were cultivated under PHA mobilization and accumulation conditions. After different time points, 40 ml of culture medium were centrifuged, in previously tared 50 ml Falcon tubes, for 45 min at 3000 x*g* at 4°C. Supernatants were rapidly frozen at -80°C and were freeze-dried for 24 h in a lyophilizer. Finally, the tubes were weighted for further calculations. The lyophilized supernatant was homogenized and was resuspended in solution methanol-water (50% v/v) at 10 mg/ml. Then, 25 µl were injected into the chromatographic system, for the determination of *(R)*-Hydroxyalkanoic acids (*(R)*-HAs; free monomers) content by using a Finnigan Surveyor pump coupled to a Finnigan LXQ TM ion trap mass spectrometer (Thermo Electron) (HPLC-MS).

The separation was performed on a 2.1×150 mm (3.5 µm particle size) XTerra MS C18 column (Waters) at a flow rate of 100 µL min^{-1} and an injection volume of 25 µL.

The mobile phase was 0.1% ammonium hydroxide in water (A), 0.1% ammonium hydroxide in methanol (B) and 0.1% ammonium hydroxide in acetonitrile (C). The following elution program was used as follows: at the start, 95% A and 5% B; after 3 min, the percentage of B was linearly increased to 95% in 20 min, then kept constant for 5 min, and after that, percentage of C was increased from 0 to 45% in order to clean the column. Finally, it was ramped to the original composition in 5 min, and then equilibrated for 10 min. The samples were introduced to the electrospray ionization (ESI) source in negative mode by continuous infusion by means of the instrument syringe pump at a rate of 3 mL min^{-1}. The source was operated at 4.5 kV and the capillary temperature was set to 200°C. All spectra were recorded in full scan mode (m/z 50-1500).

A standard curve of commercial 3-hydroxyoctanoic acid (HO; Sigma-Aldrich, Merck, Germany) was used, where we observed a deprotonated HO monomer (m/z 159) with retention time 15.4 min, a dimer adduct of HO-HO (m/z 603) with retention time 21.5 min, a trimer adduct of HO-HO-HO (m/z 887) with retention time 29.7 min and a tetramer adduct HO-HO-HO-HO (m/z 1171) with retention time 35.6 min (Figure 19). The samples analysis revealed mainly two peaks a deprotonated HO monomer (m/z 159) and a dimer adduct of HO-HO (m/z 603).

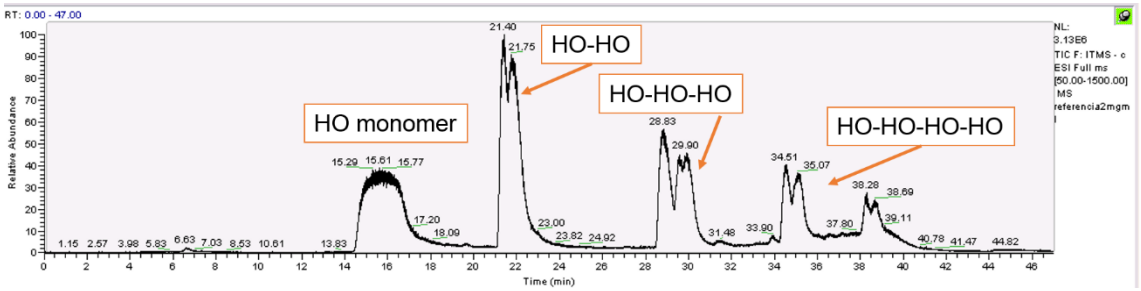

Figure 19. Identification of the P(HO-co-HX) hydrolysis products catalysed by PhaZ. LC-MS analysis of 2 mg/ml commercial 3-hydroxyoctanoic acid (HO). Four picks are identified the HO monomer, HO-HO dimer adduct, HO-HO-HO trimer adduct and HO-HO-HO-HO tetramer adduct.

3.7.4 HPLC for the identification of extracellular metabolites

Detection of metabolites using the method published by (Revelles *et al.*, 2016). The reference compounds used: fructose, acetate, citrate, succinate, pyruvate, propionate, malate, formate, fumarate, oxoalacetate, ketoglutarate, butyrate, glucose and sucrose (Sigma-Aldrich, Merck, Germany). The different compounds were quantified by HPLC (Agilent Series 1260 Infinity II, Agilent, CA, USA), on an Aminex HPX-87H column (Biorad, Hercules, CA, USA) at 40°C with a flow rate of 0.5 mL min^{-1} and an injection volume of 25 µl. The mobile phase was 2.5 mM H_2SO_4 applied in an isocratic regime and detection was performed with a refractive index detector.

Sucrose (rt = 8.4 min), ketoglutarate (rt =8.6 min), citrate (rt = 8.9 min), malate (rt= 9.5 min), oxoalacetate (rt = 9.6 min), pyruvate (rt=9.9 min), glucose (rt= 9.9 min), fructose (rt= 10.9 min), succinate (rt = 13.4 min), formate (rt = 15.7 min), fumarate (rt= 15.8 min), acetate (rt = 17.3 min), propionate (rt = 20.4 min), butyrate (rt= 25.8 min).

The presence of residual 4 Hydroxy benzoate (4HBz; Sigma-Aldrich, Merck, Germany) was quantified by HPLC (Agilent Series 1260 Infinity II, Agilent, CA, USA), on an ZORBAX Eclipse Plus C18 (Biorad, Hercules, CA, USA, Agilent, CA, USA) at room temperature with a flow rate of 0.51 mL min^{-1} and an injection volume of 25 µL. The mobile phase was 0.1% trifluoroacetic acid in water (A) and 0.1% trifluoroacetic acid in methanol (B). The following elution program was used as follows: at the start, 85% A and 15% B; after 11 min, the percentage of B was linearly increased to 50%. After that, it was ramped to the original composition in 2 min, and then equilibrated for 8 min. The mobile phase was 2.5 mM H_2SO_4 applied in an isocratic regime and detection was performed with a refractive index detector. The retention time of 4HBz was 13.5 min. A standard curve of 4HBz was done (1-5 mM). As a control, the medium without 4HBz was injected.

3.8 Proteins production, purification and detection

3.8.1 Analyses of PhaZ production

LB pre-cultures of the strains were grown until $OD_{600\ nm}$ 0.6 in fresh LB medium. Whole cell extracts were used for these immunological techniques of PhaZ production. Western blot was performed as described before (De Eugenio *et al.*, 2007). Briefly, 12.5% polyacrylamide gels were prepared. The primary anti-PhaZ antibody, 1:5000 (De Eugenio *et al.*, 2007) was used, previously washed O/N at 30°C with shaking 200 rpm with the sonicated KT40Z *phaZ* null strain. The secondary antibody was a commercially one, rabbit polyclonal antiserum against PhaZ, 1:10000 (GE Healthcare, England). Western blot analysis was performed with the ECL Western Blotting Detection Kit (GE Healthcare, England) according to the protocol described by the manufacturer. The expected PhaZ size is 31 kDa. The western blot signal intensities were quantified using Image J software and the resulting intensities were normalized to the M4 strain and taking into account the OD_{600nm} equivalent load of each sample.

3.8.2 Overproduction and purification of recombinant isocitrate dehydrogenase

In this work the dimeric *icd* (PP_4011) and monomeric *idh* (PP_4012) genes of *P. putida* KT2440 were cloned and enzymatically characterized. A mutated form of PP_4012, was obtained by site-directed mutagenesis on Ser133Ala, Asn136Ala, Arg140Ala. For kinetic properties characterization, they were heterologously overexpressed in *E. coli* using the traditional pET29a vectors and His-tagged protein versions were used in order to enable the protein purification. The PP_4011 fragment was obtained using MM152 and MM153 primers, while PP_4012 using MM154 and MM155 primers, and for PP_4012 mut MM223-MM224 primers were additionally used. The resulting PCR fragments were cloned in pET29a plasmid (Novagen) using BamHI-HF and HindIII-HF. For maintaining the plasmid and its sequence validation (using T7 prom and TT7 primers), hosts that do not contain the T7 RNA polymerase gene were initially used (DH10B), in order to avoid the production of proteins potentially toxic to the host cell. Once established the correct sequence of the inserts, plasmids were transferred into the expression hosts *E. coli* BL21(DE3).

The *E. coli* BL21 (λDE3) (pET29a (empty plasmid as negative control), pET29a-4011, pET29a-4012 and pET29a-4012 mut) strains pre-cultures were resuspended in fresh LB medium supplemented with kanamycin (50 µg/ml) with initial $OD_{600\ nm}$ of 0.05. When $OD_{600\ nm}$ reached 0.6, 1 mM of IPTG was added to induce recombinant protein synthesis under T*7* promoter control, and growth was continued at 37°C for 2 hours. The cells were harvested from a 100 ml culture by centrifugation at 3000 x g at 4°C for 20 min and washed twice with 0.85% saline solution and the pellets were frozen at -80°C until further use.

Cells were resuspended in buffer A (50 mM NaH_2PO_4, 50 mM Na_2HPO_4, 300 mM NaCl, 20 mM imidazole at pH 7.4 and 1 tablet of Roche cOmplete^{TM}, EDTA free, protease inhibitor cocktail per 50 ml culture) and disrupted by two passages using French press at 1000 psi. The soluble extract was obtained by a 30 min centrifugation at 10.000 x*g* at 4°C to remove cellular debris and was purified in small-scale using Ni-NTA, with macroporous silica support material, Spin columns (Quiagen; Catalog Number 31314). To previous equilibrated column (three passages with buffer A), the soluble extract was loaded (three passages) and several column washes were realized by increasing gradiently the imidazole concentration (20-500 mM (buffer B)). His-isocitrate dehydrogenase was eluted at 250 mM imidazole. The protein concentration was quantified by Bradford method using bovine serum albumin (BSA) as a standard (Bradford., 1976). Up to 250 mM imidazole does not interfere with the Bradford assay.

3.8.3 Isocitrate dehydrogenase enzymatic activity

ICDH (Isocitrate dehydrogenase, both *icd* and *idh*) activity was assayed at 30°C by following NAD(P)H formation spectrophotometrically at 340 nm. The assay mixture contained 25 mM Tris-HCl (pH 7.3), 5 mM $MgCl_2$, 0.6 mM $NADP^+$, 0.6 mM isocitrate, 10 mM succinate (to inhibit interfering of isocitrate lyase activity) and 0.05 mg of purified protein extract. For the calculations, we took into account the extinction coefficient of NADPH, 6.22 mM^{-1} cm^{-1}, which can be used to directly quantify the product formation. Enzyme activity is expressed as U/mg, where a Unit is defined as a µmol of NAD(P)H formed per minute per milligram of protein. To measure the K_M value for isocitrate we maintained a fixed concentration of $NADP^+$ (0.2 mM) varying the isocitrate concentrations from 0-0.6 mM. Similarly, to measure the K_M value for $NADP^+$ we maintained a fixed concentration of isocitrate (0.2 mM) varying the $NADP^+$ concentrations from 0-0.6 mM. The Km and Vmax values were obtained using Prism 6 software (GraphPad Software Inc., USA).

3.9 Microscopy

3.9.1 Optical microscopy

Cultures were routinely visualized with a 100 X phase-contrast objective (Nikon microscope) and images were taken with a connected camera Leica DFC345 FX. For cell size quantification, 40 individual cells from at least three individual experiments were quantified at different time points during the bacteria growth curve, using image J software.

3.9.2 Transmission electron microscopy

P. putida cells previously grown under the conditions of interest for 24 h were harvested and washed twice in 1 X PBS. Afterwards, cells were suspended in 2.5% (w/v) OsO_4 for 1 h, gradually dehydrated in ethanol (30, 50, 70, 90, and 100% (v/v); 30 min each) and propylene oxide (1 h), embedded in Epon 812 resin. Ultrathin sections (thickness 70 nm) were cut with a microtome using a Diatome diamond knife. The sections were picked up with 400 mesh cupper grids coated with a layer of carbon and subsequently observed in a Jeol-1230 electron microscope (JeolLtd, Akishima, Japan). The analysis of the biological samples was performed by CIB services.

3.10 Systems biology approaches

3.10.1 Constraint-based flux analysis

The *i*JN1411 model was exported from SimPHeny as an SBML file and analyzed with the COBRA Toolbox v2.0 within the MATLAB environment (The MathWorks Inc.) (Becker *et al.*, 2007; Schellenberger *et al.*, 2011). A recent update of this Toolbox is available (Heirendt *et al.*, 2019). Tomlab CPLEX and the GNU Linear Programming kit were used for solving the linear programming problems. The constraint-based model consists of a 2087 x 2826 matrix containing all the stoichiometric coefficients in the model of 2087 metabolites and 2826 reactions (S).

3.10.2 Flux balance analysis

Flux balance analysis (known as FBA) is a widely used approach for studying biochemical networks, in particular GENREs (genome-scale metabolic networks reconstructions). FBA calculates the flow of metabolites through the given metabolic network (Figure 20). Thus, FBA makes possible to analyze the phenotypes and capabilities of organisms with different environmental or genetic perturbations, to predict the growth rate of an organism or the rate of production of a metabolite of interest.

FBA is based on solving a linear optimization problem by maximizing or minimizing a given objective function Z subject to a set of constraints (Figure 20). The constraints S*v=0 correspond to a situation of steady-state mass conservation where the change in concentration of the metabolites as a function of time is zero. The vector v represents the individual flux values for each reaction. These fluxes are further constrained by defining lower and upper limits for flux values. For reversible reactions, an upper and lower bound of -1000 $mmol.gDW^{-1}.h^{-1}$ and 1000 $mmol.gDW^{-1}.h^{-1}$ were used respectively. A lower bound of 0 $mmol.gDW^{-1}.h^{-1}$ was used in case of irreversible reactions. For simulating condition-specific growth conditions, lower bounds of the corresponding exchange reactions were modified accordingly.

In FBA the metabolic reactions equations are solved using computational linear programming algorithms such as those included in the COBRA (constraint-based reconstruction and analysis) Toolbox (is a freely available MATLAB toolbox). COBRA methods emphasize describing the constrains that a system must satisfy rather than computing an explicit solution, by leading to the definition of a “solution space”, which contains the set of feasible solutions that satisfy all imposed constraints. Some of the

limitations of FBA are the fact that cannot predict the metabolite concentrations since it does not use kinetic parameters and it is only suitable for determining fluxes at steady state (Orth *et al.*, 2010).

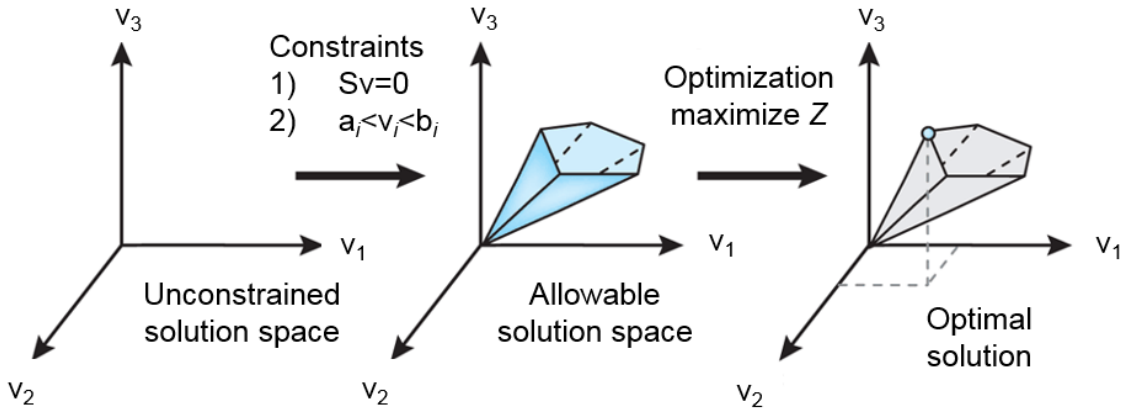

Figure 20. With no constraints, the flux distribution of a biological network may lie at any point in a solution space. When mass balance constraints imposed by the stoichiometric matrix S (labeled 1) and capacity constraints imposed by the lower and upper bounds (a_i and b_i) (labeled 2) are applied to a network, it defines an allowable solution space. The network may acquire any flux distribution within this space, but points outside this space are denied by the constraints. Through optimization of an objective function, FBA can identify a single optimal flux distribution that lies on the edge of the allowable solution space; adapted from (Orth et al., 2010).

3.10.3 Construction of condition specific models

For the *in silico* data contextualization, we used the experimental data collected under PHA accumulation conditions including the residual biomass, growth rate, octanoate uptake rate, extracellular *(R)*-HAs production, PHA production rate. Different condition-specific models were thus obtained and flux balance analysis (Orth *et al.*, 2010) and random sampling of Monte Carlo (Schellenberger and Palsson, 2009) were used for analysis. In Monte Carlo analysis, sampling mixed fractions of 0.53-0.58 were obtained, indicating that the solution space for these models was uniformly sampled. Finally, the median value from the distribution was used as the most probable flux value.

Randomized sampling of Monte Carlo has many advantages such as the ability to work with missing data, apply post-processing techniques, quantify uncertainty by knowing how limiting the imposed constraints are, and optimize experiments in order to reduce this uncertainty by shrinking the size of the solution space. This approach is based on that random set of points, which are chosen from the solution space to act as surrogate for the entire space. This means that many of the properties that can be

calculated for one candidate solution can then be calculated for point throughout the entire space. The obtained properties can be evaluated in statistical manner where we obtain the mean value of flux through each reaction. Summing up, Monte Carlo sampling allow us to analyze large-scale networks towards understanding the whole cell metabolism (Schellenberger and Palsson, 2009).

3.10.4 Data clustering

For the data clustering, experimental data, such as, growth rate, total biomass, residual biomass, PHA content, viable cells number, *(R)*-HAs free monomers content of the strains grown for 24h under PHA accumulation conditions were used. Each data were previously normalized to the corresponding wild type values. With value of 1, refers to no differences observed, values less or higher than 1 to a decrease or an increase compared to the wild type, respectively.

3.10.5 Growth-coupled overproducing strains

For growth-coupled overproducing strain designs, the Genetic Design through Local Search (GDLS) algorithm was used (Lun *et al.*, 2009). GDLS is a computational design tool for metabolic engineering that uses an efficient, low-complexity local search approach to identify favorable genetic designs using flux-balance metabolic models. GDLS was chosen over other strain design methods due to the complexity of our objective, e.g., to find growth-coupled designs of PHA overproducing strains from PHA-unrelated substrates, which could anticipate a large number of gene knockouts needed, and would require a large computational runtime due to the size of our model. GDLS is a heuristic algorithm method capable of handling large metabolic models while allowing a much larger number of genetic manipulations in the final design than other methods. In addition, GDLS runtime scales linearly in contrast to other globally-optimal search methods that scale exponentially. Moreover, GDLS employs a local search approach with multiple search paths to find a set of locally optimal strategies that allow for the analytical evaluation of the different paths. Similar to other strain design methods, GDLS implements reductions that simplify FBA models. Finally, GDLS was demonstrated to have as good performance as other globally optimal search methods such as OptFlux and Optknock with an order of magnitude of improvement in computational time for solutions that yield equal or comparable value. The function GDLS implemented in COBRA 2.0 was used (Schellenberger *et al.*, 2011).

In order to achieve an optimal biomass-coupled product yield (BCPY), GDLS runs were computed using minimum growth rate values up to 60% of that predicted for the wild-type model. Due to computing time limitations, the number of simultaneous knockouts (neighborhood parameters) tested were 2 to 4, and 3 was the value that showed a significant increase in PHA production in all designs described in the results. The number of paths used was tested from 1 to 10 depending of the computing complexity for each neighborhood value. Generally, a single path was selected by default for each case described in the results. The maximum number of knockouts and iterations were set to 50 and 70, respectively, by default. Those paths with the greatest BCPY value in the final design for each case were selected.

3.11 Statistical analysis and other software

Data sets were analyzed using Prism 6 (GraphPad Software Inc., USA) and Excel software. Comparisons among multiple groups were made using one-way or two-way analyzes of variance (ANOVA) test, depending on whether one or two different variables were considered, respectively. In addition, Tukey's multiple comparisons test was used. In every statistical analysis performed, the confidence interval was 95%.

For DNA processes (construct designs and DNA sequence alignments), Geneious and Benchling softwares were used and Prime 3 for the oligonucleotide design. For visualization of the DNA sequences chromatograms apart for the above-mentioned programs, Chromas software was used. For additional DNA sequence alignment, we based on Lalign Server (EMBnet- Expasy) and BLASTN in the NCBI server. For protein multiple sequences alignment CLUSTALW in the EMBL-EBI server was used. For identifying functional association networks, String web, part of the ELIXIR infrastructure, was used. For proteins crystal structure information the Protein Data Bank (PDB) was used. For isocitrate dehydrogenase available information, the comprehensive enzyme information system, BRENDA was used.

4. RESULTS

4 RESULTS

4.1 Chapter 1: Systems analysis and synthetic tuning of the PHA cycle in *P. putida* KT2440

PHA cycle is a continuous cycle, where polymerization and degradation of the polymer happens simultaneously. PHA are not only a source of carbon during carbon starvation but rather a key element in resource balancing that assures efficient growth. In this chapter, it was performed a thoroughly validation of PHA cycle as a robustness cycle in *P. putida* KT2440 (1.4.4 and 1.6 sections). A DBTL cycle was used by combining synthetic and systems biology advances (Figure 21). In order to study the impact of the PHA turnover and native *pha* regulation process on the central metabolism of *P. putida*, the *phaZ* depolymerase was deleted. Thus, the possibility to complete the PHA cycle was avoided by preventing the production of PHA degradation monomers. Then, a library of strains with tuned PhaZ production levels were constructed and further extensively phenotyped, in order to investigate the impact of the differential *phaZ* expression levels into *P. putida* physiology. To obtain an overall view of this impact on *Pseudomonas* metabolism, condition specific models were finally constructed allowing the *in silico* contextualization of the *in vivo* experimental data (Figure 21).

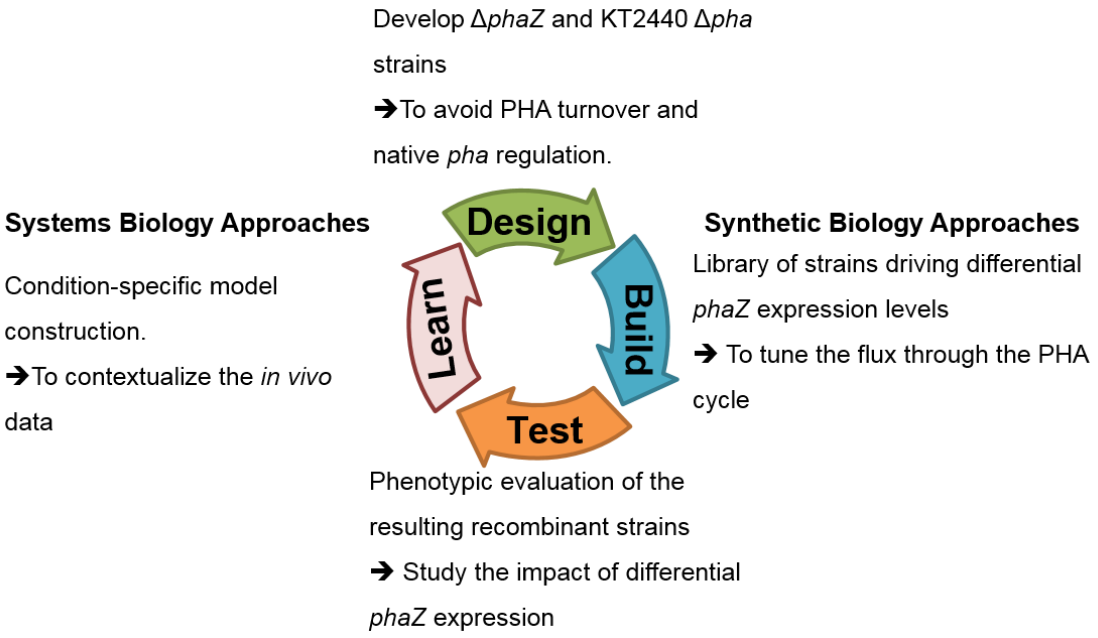

Figure 21. PHA cycle tuning using DBTL cycle.

4.1.1 Construction of a *P. putida* strain lacking the PHA cycle.

In order to study the impact of the PHA turnover process on the central metabolism of *P. putida*, the *phaZ* depolymerase was deleted using the pK18*mobsacB* strategy, resulting to KT40Z strain (Table 2 and 3.4.4 section). A schematic representation of the *phaZ* deletion process is shown in Figure 22A. The phenotype exhibited by the knockout strain was initially analyzed by electronic microscopy. As it could be expected, no effect on PHA production was observed and in the KT40Z background, cells were able to accumulate PHA as efficient as the wild type does after 24 h of growth under PHA accumulation conditions (Figure 22B).

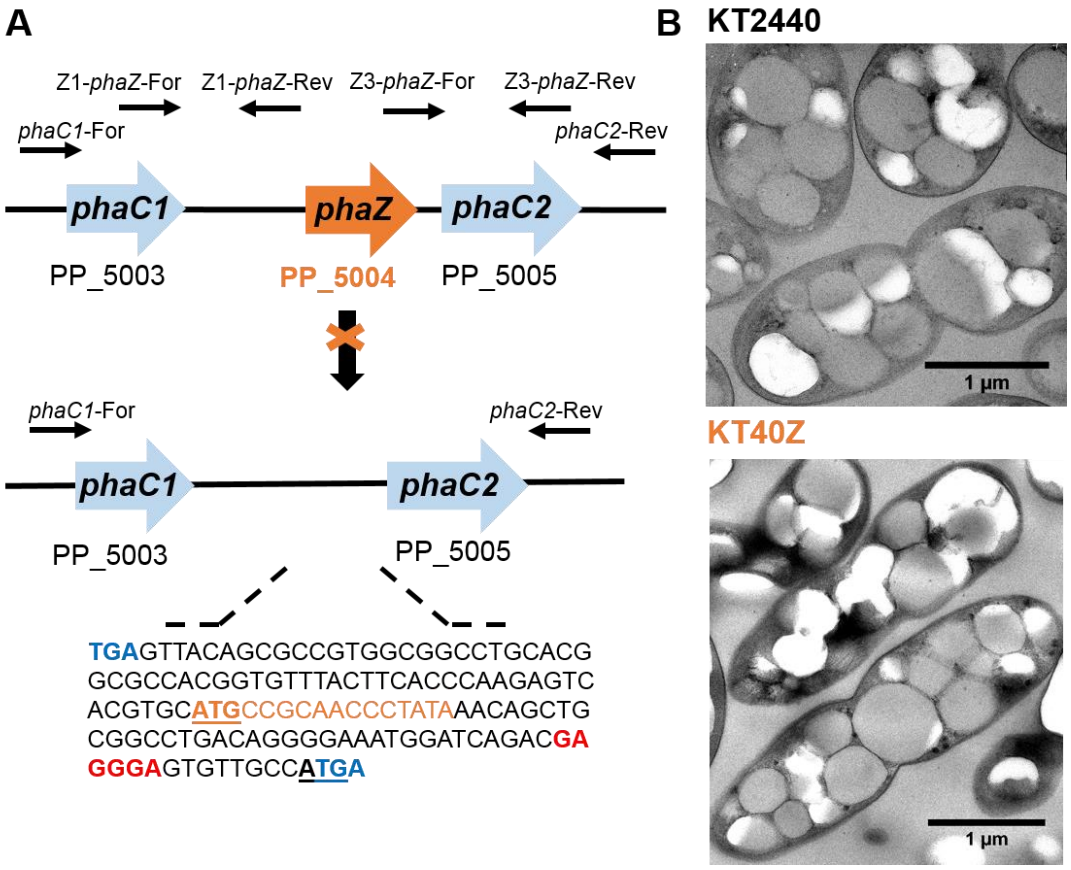

Figure 22. Construction of *phaZ* null depolymerase mutant. A. Schematic representation of the *phaZ* deletion mutant. The oligonucleotides used for the deletion process are shown with black arrows and detailed in the Supplementary Table S7. For this deletion the Z1-phaZ-For and Z1-phaZ-Rev primers were used to obtain the Z1 upstream homology region and the Z3-phaZ-For and Z3-phaZ-Rev resulting into the Z3 downstream homology region. For the second recombination process verification, the external phaC1-For and phaC2-Rev primers were used. The remaining nucleotide sequence after the deletion is shown. The stop codons and the start codons are shown with bold blue and bold underlined, respectively. The first stop codon corresponds to the *phaC1* gene and the second one to the *phaZ* gene. The first start codon corresponds to the *phaZ* and the second one to the *phaC2*. The Ribosome binding site (RBS) is shown in red color. The *phaZ* remaining nucleotide sequence is shown in orange color. **B.** TEM microscopy picture of wild type and KT40Z strains after 24 h of growth under PHA accumulation conditions. The scale bar is 1 µm.

Since the *phaZ* is co-transcribed with the *pha* genes, its deletion could result in putative polar effects, impacting on the expression of downstream *pha* genes. Additionally, if the PhaD transcriptional activator is not properly transcribed, it could decrease the transcription levels of the whole *pha* cluster (Figure 14, for a scheme of the regulatory system). In order to analyze the putative polar effects, the transcription levels of some of the downstream *pha* genes were verified by means of qRT-PCR. Since the transcription levels of phasins *phaFI*, as major GAPS proteins, were significantly higher than those of *phaC2* synthase, the phasins were selected for these analyses. The wild type and KT40Z strains were harvested after 6 h of growth (mid-exponential phase) under PHA mobilization and PHA accumulation conditions and qRT-PCR experiments were performed using total RNA.

It is worth to notice that, by PHA mobilization conditions, we refer to conditions where the PHA degradation is favored and no nutrient limitation is observed. However, under PHA accumulation conditions, the PHA storage is favored due to carbon excess and some nutrient limitation. In this chapter for simplicity, we refer as PHA mobilization conditions as cell growing on minimal M63 medium supplemented with 7.5 mM octanoate by maintaining the C/N ratio at 2 mol/mol. PHA accumulation conditions means growth on minimal M63 0.1N medium supplemented with 15 mM octanoate by maintaining the C/N ratio at 40 mol/mol.

As it could be expected, significantly higher phasin expression was found under PHA accumulation than in PHA mobilization conditions (Figure 23). Under this scenario, PHA is being synthetized and the requirement of phasins increase accordingly in order to allocate this PHA into the growing granules both in the wild type and *phaZ* strain. KT40Z strain showed 1.4 to 1.5 times higher *phaF* transcription levels compared to wild type under PHA mobilization and PHA accumulation conditions, respectively. Furthermore, KT40Z strain showed 1.4 and 1.2 times higher *phaI* transcription levels compared to wild type under PHA mobilization and PHA accumulation conditions, respectively (Figure 23). Thus, so far, it could be concluded that the KT40Z null mutant strain produced efiiciently PHA and there was no decrease in phasins transcription levels (Figure 22B and Figure 23).

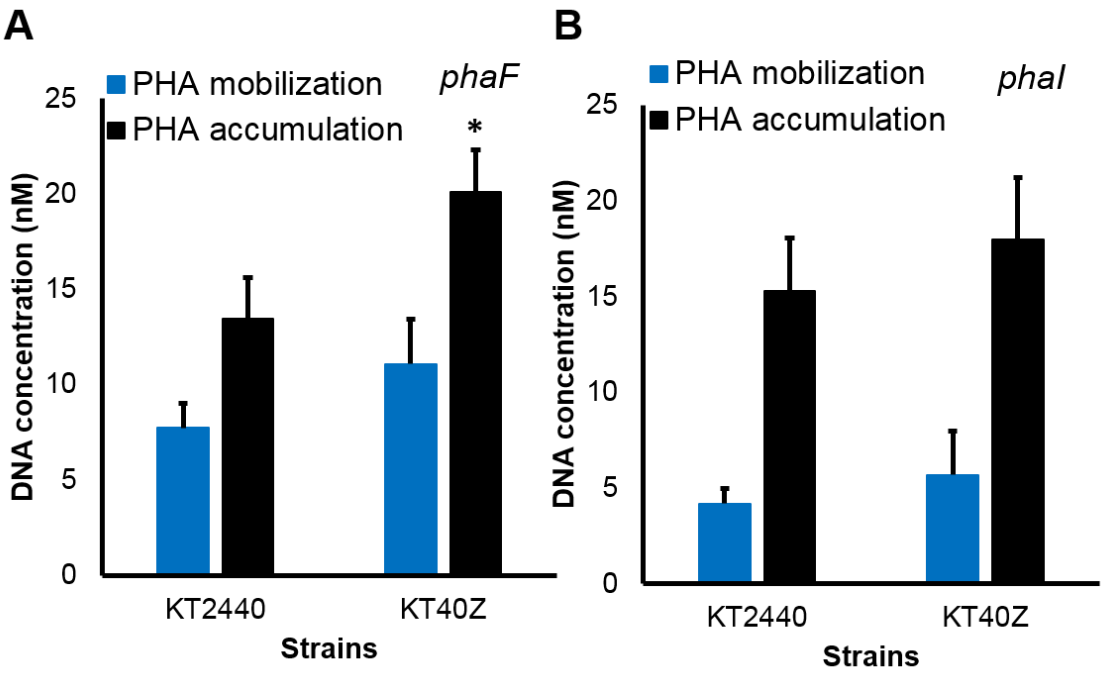

Figure 23. Phasins transcription levels by qRT-PCR experiments. Quantification of expression levels of KT2440 and KT40Z phasins phaF (A) and phaI (B). The expression levels of phasins under PHA mobilization conditions (blue bars) and PHA accumulation conditions (black bars) were monitored after 6 h of growth. One way ANOVA test analysis was performed and the significant differences compared to the wild type strain are shown (*, $p<0.05$).

4.1.2 Construction and validation of a library of strains driving differential *phaZ* expression levels.

In an attempt to finely tune the flux through the PHA cycle, a library of *P. putida* strains was constructed harbouring differential PhaZ production levels. For this purpose, a collection of vectors was obtained, expressing the *phaZ* gene under the control of constitutive synthetic promoters with different strength. For this collection construction, we based on a promoter library collection previously tested for optimal expression in *P. putida* KT2440 (Zobel *et al.*, 2015).

The pBG derivated version plasmids contain three modules; the synthetic promoter, the translational coupler or bicistronic element BCD2 and the reported gene, *msf::gfp*. The only variable in this system is the promoters strength. Bicistronic couplers were used in order to fix the translational efficiency by limiting the interaction of mRNA secondary structures with the 5´-untranslated regions of the gene of interest (GOI). BCD2 add a downstream region to the promoter and contains two Shine-Dalgarno sequences where the SD2 is translationaly coupled to the GOI. In our case, the BCD2-

msf-gfp was substituted by the BCD2-*phaZ.* The latter construct was obtained by a PCR amplification of *P. putida* genome with AvrII-BCD2-*phaZ* and *phaZ*-BamHI-Rev primers using phusion polymerase (Table S7). BCD2-*phaZ* construct was subcloned into the pBG-derived vectors using AvrII and BamHI-HF restriction enzymes, resulting to a panel of pBG-derived vectors expressing *phaZ* gene at different dosage (Table 3).

E. coli constructs verification was checked via plasmid sequencing. Further, genome integration of these constructs into the *P. putida* KT40Z was performed by using the Tn*7*-strategy (Materials and Methods 3.4.3 section). The resulting strains, that should theoretically account for increasing level of *phaZ* expression were called as M0-M4. A detailed description of the structural organization of the resulting pBG-derived plasmids is schematically represented in the Figure 24 and the sequences of the integrated synthetic promoters used in this work are listed in the Table 5.

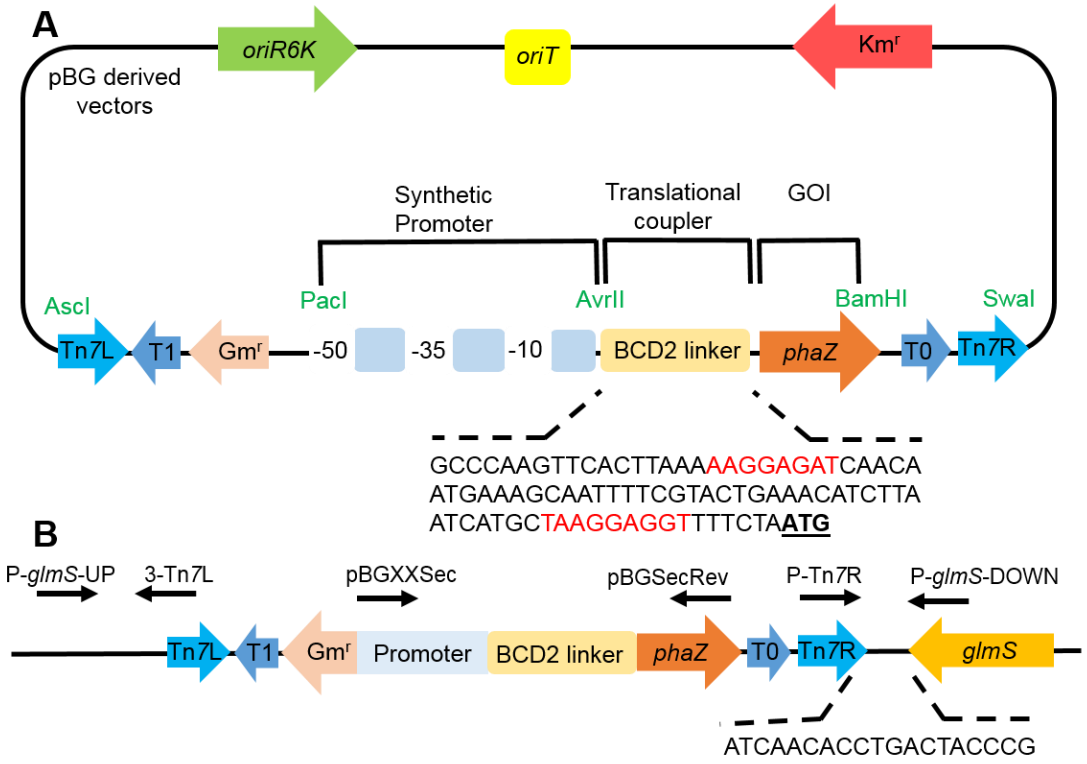

Figure 24. Structural organization of pBG-derived library collection vectors. A. Functional elements of the plasmid include, a backbone vector bearing a Km^r marker, origin of replication *oriR6K*, the origin of transfer *oriT* and a Tn*7* module cloned between AscI and SwaI sites that bears a Gm^r marker. Two terminators (T1 and T0), a SEVA version of MCS, and two Tn*7* sites recognized by transposase (which is provided *in trans*). Three modules were designed; a module carrying the synthetic promoter, BCD2 translational coupler, and the gene of interest (GOI), *phaZ.* The sequence of the leader peptide is indicated between SD1 and SD2 (Shine-Dalgarno sequence, shown in red letters). The restriction enzymes between each module are shown in green letters. The initial codon of *phaZ* gene is shown with bold underlined letters. **B.** Schematic representation of pBG-derived vectors chromosome integration after the *glmS* gene, on KT40Z strain. The primers used for the genome integration confirmation are shown with arrows (Table S7). The nucleotide sequence after the integration event is shown.

Strains	SEVA Promoter number	ID/ Promoter Sequence
M0	pBG	TTAATTAAGCGGATAACAATTTCACACAGGAGGCCGCCTAGG
M1	pBG28/14a	TTAATTAACTAGGTTGACATGGATATAATGTATGTACCTAGG
M2	pBG51/14d	TTAATTAATCTACTTGACATCCGACATTCGCGACTGTATAATAAGTTGGCCTAGG
M3	pBG37/14c	TTAATTAAGTGAATTGACATGTCAATTTTTATGTTGTATAATATAACTACCTAGG
M4	pBG42/14g	TTAATTAAGCCCATTGACAAGGCTCTCGCGGCCAGGTATAATTGCACGACCTAGG

Table 5. Sequences of integrated synthetic promoters. Restriction sites (shown in green) for PacI (TTAATTAA) and AvrII (CCTAGG), the conserved -35 (TTGACA) and -10 (TATAAT) regions of sigma -70 promoters (shown in red).

The library of *P. putida* strains accounting for increasing levels of PhaZ was further validated by means of western blot analysis (Figure 25 and materials and methods 3.8.1 section). In these experiments, *P. putida* M0-M4 strains were grown overnight in LB medium at 30ºC under vigorous shaking (250 rpm). Then, the cells were inoculated in fresh LB medium at inicial OD_{600nm} of 0.05. The cells were harvested at mid-exponential phase by reaching OD_{600nm} of 0.6. Different concentration of whole cell extracts were tested by Western blot experiments, shown as OD equivalent load (Figure 25A). The *phaZ* null strain, KT40Z was used as negative control. The expected size of PhaZ is of 31 kDa (De Eugenio *et al.*, 2007).

As it could be expected a positive correlation was found between the promotor strength and the PhaZ production levels, where M0; the lowest to M4; the highest promoter´s activity (Figure 25B). The wild type strain behaved similar to M0 strain, where no signal was observed in the Western blot experiments. Additionally, the KT2440, KT40Z and M4 strains, were tested under PHA mobilization and accumulation conditions. Only, the M4 strain was observed by Western blot experiments (data not shown). It can be concluded that M0-M4 strains can successfully produce differential PhaZ levels, higher than the native one.

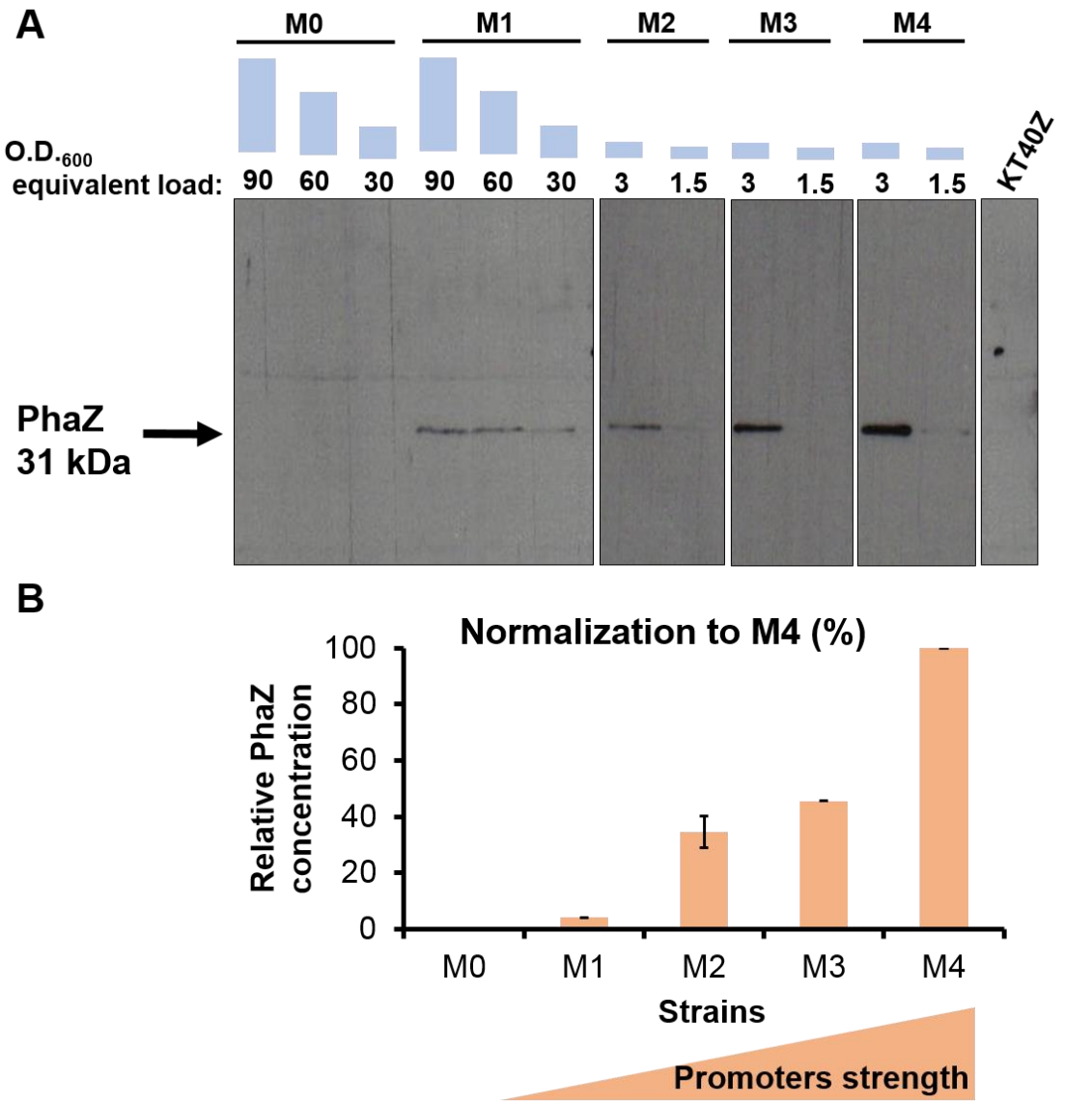

Figure 25. Construction of *P. putida* strains with tuning PhaZ production levels. **A.** Anti-PhaZ Western blots. Whole cell extracts of cells collected in mid-exponential phase ($O.D._{600}$=0.6). The OD equivalent load in each case is shown. **B.** relative PhaZ concentration in culture is indicated. The data where normalized to M4 strain. The library of strains named M0-M4, from the lowest (M0) promoter's activity to highest (M4). KT40Z was used as negative control. The signal intensities of PhaZ production levels were quantified using ImageJ software. Then, the data were normalized to the M4 production levels and taking into account the OD equivalent load in each case.

4.1.3 Increasing the level of flux through PHA cycle leads to significant physiological and phenotypical changes in *P. putida*.

To investigate the impact of the fine tuning expression of *phaZ* on *P. putida* metabolism, a battery of high-throughput phenotyping analyses under both PHA

mobilization and accumulation conditions were next carried out. The results were compared with a control strain, where the whole *pha* cluster was deleted KT2440 Δ*pha*).

Under PHA mobilization conditions, no major differences in cell size, growth and viable cell number were observed beween the analyzed strains (Figure 26). For instance, as it could be expected due to the lack of a functional *pha* cluster, the KT2440 Δ*pha* strain did not accumulate PHA, either on 8 or 24 h of growth (Table 6 and Figure 26C). Interestingly, similar behaviour was found in M2-M4 strains, due to the high depolymerase activity present in these strains, that completely avoid the net accumulation of PHA (Figure 26). In contrast, the wild type strain was able to accumulate small amounts of PHA at 8 h, but not at longer times where the degradation of the polymer is favoured (Figure 26C). In fact, after 24 h only negligible amount of PHA was detected, reaching up to 4% of CDW. Similar behaviour to the wild type was observed by the M0-M1 strains, confirming the results obtained by the Western blot experiments (Figure 25). Finally, the absence of PhaZ in the KT40Z strain promoted the accumulation of up to 29% PHA of the CDW.

Under PHA mobilization conditions, it would be expected to find *(R)*-HAs content in the supernatant of the strains, since the PHA degradation is favored. However, no significant amounts of (*R)*-HAs were detected in all the strains tested after 24 h of growth under these conditions, suggesting that the low C/N ratio favors the catabolism of the free acids.

Strains	Total Biomass (g/L)	PHA (% CDW)	PHA (g/L)	Residual Biomass (g/L)	Viable cells (10^8/ml)
KT2440	0.9 ± 0.1	4.0 ± 1.3	<0.1	0.8 ± 0.1	21.2 ± 3.9
KT40Z	0.9 ± 0.1	29.3 ± 6.0	0.2 ± 0.0	0.6 ± 0.1	17.7 ± 5.0
KT2440 Δ*pha*	0.9	<0.5	<0.1	0.9 ± 0.0	27.0 ± 0.0
M0	0.9 ± 0.0	7.6 ± 1.9	<0.1	0.8 ± 0.0	26.0 ± 8.5
M1	1.0 ± 0.1	1.6 ± 0.7	<0.1	1.0 ± 0.0	21.5 ± 4.9
M2	1.0 ± 0.2	<0.5	<0.1	1.0 ± 0.2	18.0 ± 0.0
M3	0.9 ± 0.1	<0.5	<0.1	0.9 ± 0.0	17.0 ± 0.0
M4	1.0 ± 0.0	<0.5	<0.1	0.9 ± 0.0	18.3 ± 3.8

Table 6. Physiological data after 24 h of growth under PHA mobilization condition. Total biomass, PHA content, Residual biomass, viable cell number were listed. Residual biomass is referred to biomass free of PHA.

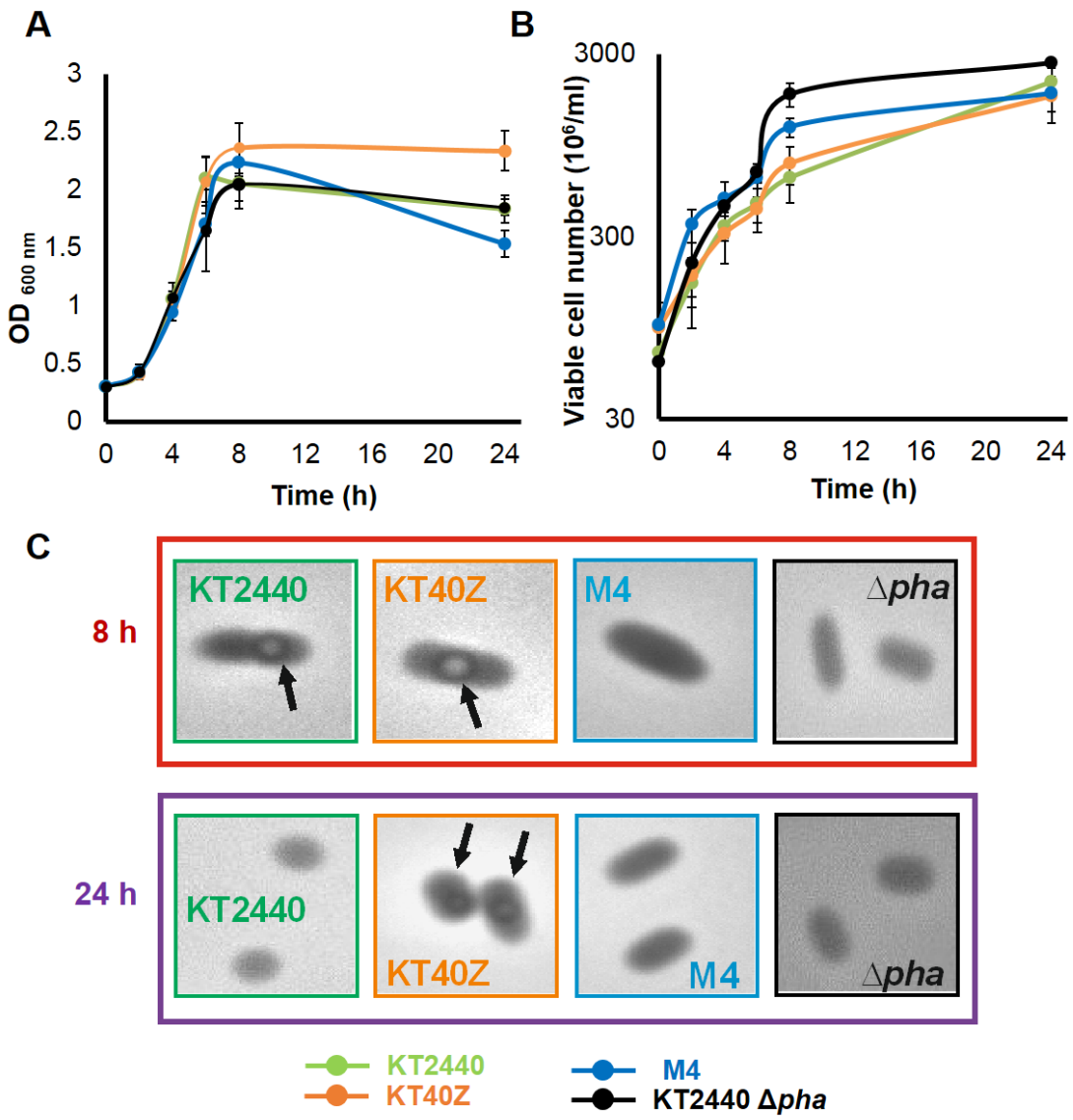

Figure 26. Growth characteristics of selected strains under PHA mobilization conditions. A. growth curves **B.** viable cell number throughout time**. C.** Optical microscopy picture after 8 and 24 h. The strains tested were KT2440 (in green), KT40Z (in orange), M4 (in blue) and KT2440 Δ*pha* (in black). The scale of the pictures correspond to 2 µm. The PHA granules are indicated with arrows.

Next, we studied the phenotype of the constructed strains on a variety of growth parameters under PHA accumulation conditions. Under these conditions, large differences were found regarding the PHA accumulation properties of the different cells (Figure 27). As it would be expected the KT2440, KT40Z and M1 strains reached up to 72% PHA under 24 h of growth under these conditions (Table 7). On the contrary, it was found that in those *P. putida* strains harbouring high constitutive PhaZ levels (e.g., M2-M4 strains), the trend was towards a decrease in cell density and smaller cell size. In fact, the M2-M4 strains after 8 h of growth were twice smaller than the wt strain (Figure 27D). The lack of PHA production resulted in one log increase in viable cell number of M2 to M4 and KT2440 Δ*pha* strains, when compared to both wild type and *phaZ* null

strains (Figure 27B). As far as it concerns the residual biomass, no major differences were observed among the strains, reaching between 0.4 to 0.7 g/L. Furthermore, since the PHA content alters the cells turbidimetry, the residual biomass was used in order to calculate the cell growth rate (3.6.3 section). It can be concluded that M2-M4 strains had higher viable cell number, but the cells were smaller, with similar residual biomass. Therefore, the cell size is not due to the presence of PHA.

In order to have a complete picture of the carbon cycle in the strains analyzed, we proceeded to monitor both, residual octanoate and secreted *(R)*-HAs after 24h of growth. Regarding the residual octanoate concentration, no significant amounts were detected in the culture supernatants of all the strains tested, after 24 h of growth under these conditions. With higher *phaZ* expression levels, more *(R)*-HAs content is expected in the supernatant of the strains (3.7.3 section), since the polymer degradation process is favored. In fact, M2-M4 strains produced up to 0.6 g/L of (*R)*-HAs compared to 0.2 g/L in the wild type strain (Table 7). As it would be expected, in absence of *phaZ* (in the KT40Z strain), no (*R)*-HAs production was observed.

Strains	Total Biomass (g/L)	PHA (% CDW)	PHA (g/L)	Residual Biomass (g/L)	*(R)*-HAs (g/L)	Viable cells (10^8/ml)	Growth Rate (h^{-1})
KT2440	1.3 ± 0.1	71.7 ± 3.1	1.0 ± 0.1	0.4 ± 0.0	0.2 ± 0.0	1.8 ± 0.6	0.31 ± 0.02
KT40Z	1.4 ± 0.0	72.3 ± 3.3	1.0 ± 0.1	0.4 ± 0.0	0.0 ± 0.0	1.2 ± 0.5	0.31 ± 0.01
KT2440 Δ*pha*	0.6 ± 0.1	0.0 ± 0.0	<0.01	0.6 ± 0.1	0.0 ± 0.0	22.3 ± 4.8	0.34 ± 0.00
M1	1.3 ± 0.1	70.2 ± 3.7	0.9 ± 0.1	0.4 ± 0.0	0.3 ± 0.0	4.1 ± 0.3	0.30 ± 0.01
M2	0.6 ± 0.0	0.3 ± 0.4	<0.01	0.6 ± 0.0	0.5 ± 0.1	16.5 ± 3.1	0.29 ± 0.00
M3	0.7 ± 0.1	0.4 ± 0.4	<0.01	0.7 ± 0.1	0.6 ± 0.0	16.8 ± 3.1	0.31 ± 0.00
M4	0.5 ± 0.0	0.7 ± 1.0	<0.01	0.5 ± 0.0	0.5 ± 0.0	15.4 ± 3.6	0.35 ± 0.02

Table 7. Physiological data after 24 h of growth under PHA accumulation conditions. Sodium octanoate (mM) was not detected in the culture supernatant of all the strains tested.

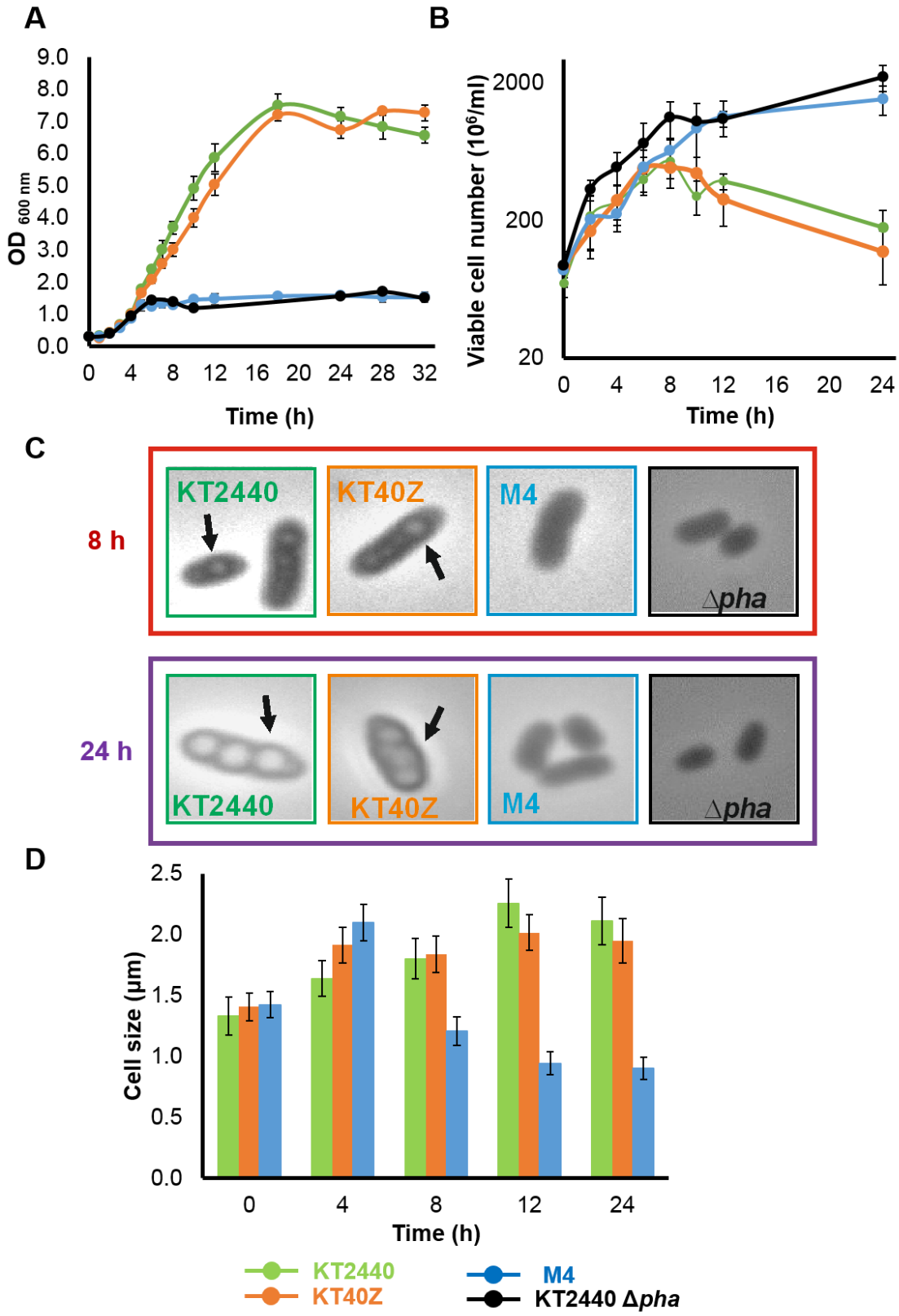

Figure 27. Growth characteristics under PHA accumulation conditions. A. growth curves **B.** viable cell number throughout time. **C.** Optical microscopy pictures after 8 and 24 h. The strains tested were KT2440 (in green), KT40Z (in orange), M4 (in blue) and KT2440 Δ*pha* (in black). The scale of the pictures correspond to 2 µm. The PHA granules are indicated with arrows.**D.** Cell size quantification.

Taking into account that the residual biomass production shown in the Table 7, it is very likely that other metabolites are released and increment of CO_2 production occurs. In order to investigate the accumulation of extracellular metabolites originated from an unbalanced carbon catabolism, the culture supernatants of all the strains after 24 h of growth under PHA accumulation conditions, were analyzed by HPLC (3.7.4 section). The presence of sucrose, citrate, pyruvate, glucose, fructose, malate, succinate, formate, acetate, propionate, butyrate, fumarate, oxaloacetate and ketoglutarate were checked. No significant amounts of these compounds were detected in the culture medium after 24 h of growth. Similar observations have been obtained previously by *pha* mutant strains (Escapa *et al.*, 2012).

In order to comparatively integrate the overall behaviour of the analyzed strains after 24 h of growth under PHA accumulation conditions, the quantified phenotype including: i) total and residual biomass, ii) PHA and *(R)*-HAs (free monomers) content and iii) growth rate were used as input for systematic clustering (Table 7 and Figure 27).

Accordingly, the strains can be classified into two main categories (Figure 28). On one hand, the strains that were able to produce PHA with no o low *(R)*-HAs production (like KT2440, M1, and KT40Z strains). On the other hand, those strains that did not produce PHA, since they had increased PhaZ production levels, which favored the increased depolymerization of PHA resulting on increased *(R)*-HAs production (like M2 - M3 - M4 strains). No PHA accumulation (M2-M4 and KT2440 Δ*pha* strains) led to one log increase in the viable cell number compared to the strains able to accumulate PHA (wild type and KT40Z). Due to PHA production, the strains had an increased total biomass, which led to a slight decrease in residual biomass compared to M2-M4 strains. No major differences were observed as far as it concerns the growth rate of all the strains tested. Furthermore, in the KT2440 Δ*pha* strain neither PHA or *(R)*-HAs production was observed, but a similar total and residual biomass to M2-M4 strains was obtained.

Strains	growth rate	Total Biomass	Residual Biomass	PHA	HAs	Viable cells
KT2440	1.0	1.0	1.0	1.0	1.0	1.0
KT40Z	1.0	1.1	1.1	1.1	0.0	0.7
KT2440 Δ*pha*	1.1	0.4	1.6	0.0	0.0	12.4
M1	1.0	1.0	1.0	0.9	1.9	2.3
M2	0.9	0.4	1.6	0.0	3.8	9.2
M3	1.0	0.5	1.8	0.0	4.2	9.4
M4	1.1	0.4	1.4	0.0	3.9	8.6

<1: decrease 1: no difference >1: increase

Figure 28. Data analysis. The data in each column were previously normalized to the corresponding wild type values. Comparison should be realized only among the data of each column. With value of 1 we refer to no differences observed when compared with the wild type (shown in grey color); values less than one to a decrease compared to the wild type (shown in red color); and with values higher to one an increase compared to the wild type (shown in green color).

4.1.4 Model-based phenotyping data contextualization highlights large metabolic changes in response to increasing flux through PHA cycle.

To further understand the effect of increasing the flux through the PHA cycle on the physiology of *P. putida*, the experimental data collected under PHA accumulation conditions (Tables 7-10) were contextualized, within the metabolic model (*i*JN1411) (Nogales *et al.*, 2017). For this, a serie of condition-specific models were constructed by using a step-by-step procedure for the integration of experimental data in genome-scale metabolic models based on GIMME (Nogales and Agudo, 2015). Firstly, it was noticed, after the careful analysis of the time series datasets collected, that up to three different growth phases could be considered under PHA accumulation conditions, likely corresponding to three different steady states (Figure 29). The phase A (between 0-5 h of growth; early exponential phase), where the bacteria majorly grew and there was slight PHA accumulation and/or *(R)*-HAs production. The phase B (between 5-10 h of growth; late exponential phase), where the bacteria were majorly producing PHA or *(R)*-HAs content and there was slight growth. The phase C (between 10-24 h of growth; stationary phase), where there was no o slight growth and/or PHA/*(R)*-HAs free monomers production. Therefore, due to the presence of these three consecutive steady states, three independent growth-phase condition models were constructed mimicking the early exponential, late exponential and stationary phases, respectively. This way, it was possible to simulate the whole growth curve by overlapping these three consecutive steady states.

To construct each growth-phase condition model, the experimental data were firstly transformed into flux rates ($mmol.gdw^{-1}.h^{-1}$), a compatible format for constraining the model. Subsequently, octanoate uptake rate, growth rate, initial residual biomass, PHA and *(R)*-HAs production rates for the three different phases (A, B, C) were applied as constraints into the *i*JN1411 model (material and methods section 3.10.3 and Figure 30). All the experimental data used for the *in silico* contextualization and for the condition specific model construction are listed in Tables 7-10. At time 0 the residual biomass of all the strain was between 0.08-0.09 g/L with no PHA and *(R)*-HAs observed in the culture pellet and supernatant, respectively. The octanoate concentration at t0 in culture supernatant was between 14.92-15.63 mM.

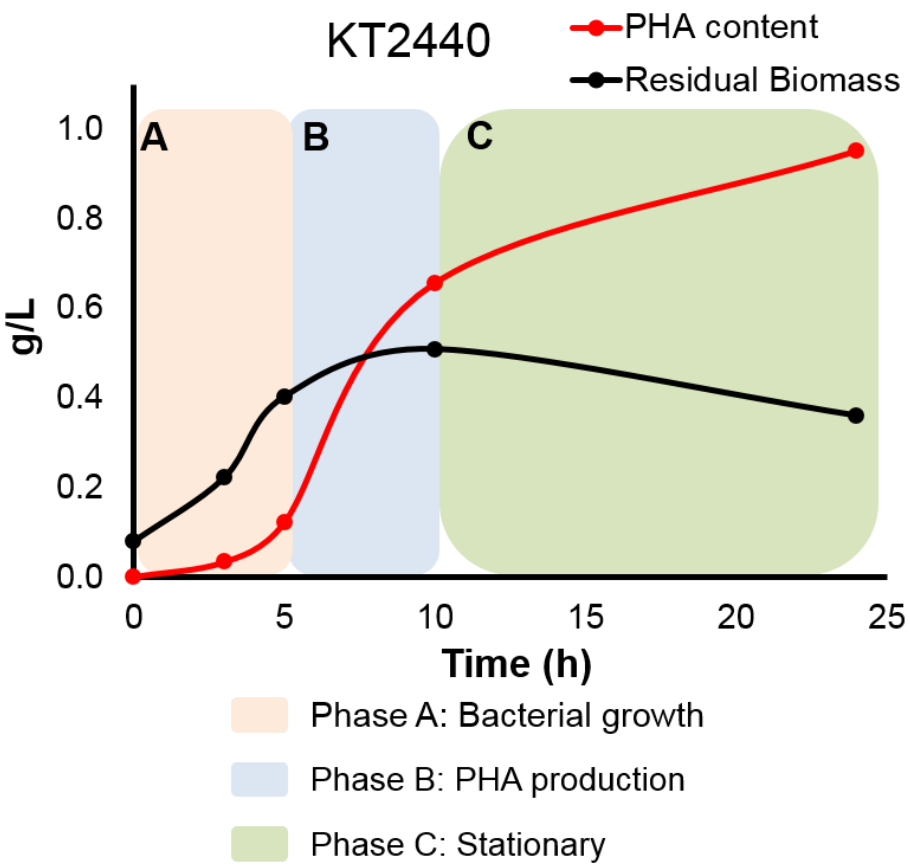

Figure 29. Growth phases representation. Experimental data of KT2440 growth under PHA accumulation conditions. The PHA content and Residual Biomass are shown in red and black color, respectively. The Phase A, B and C are shown in shaded pink, blue and green color, respectively.

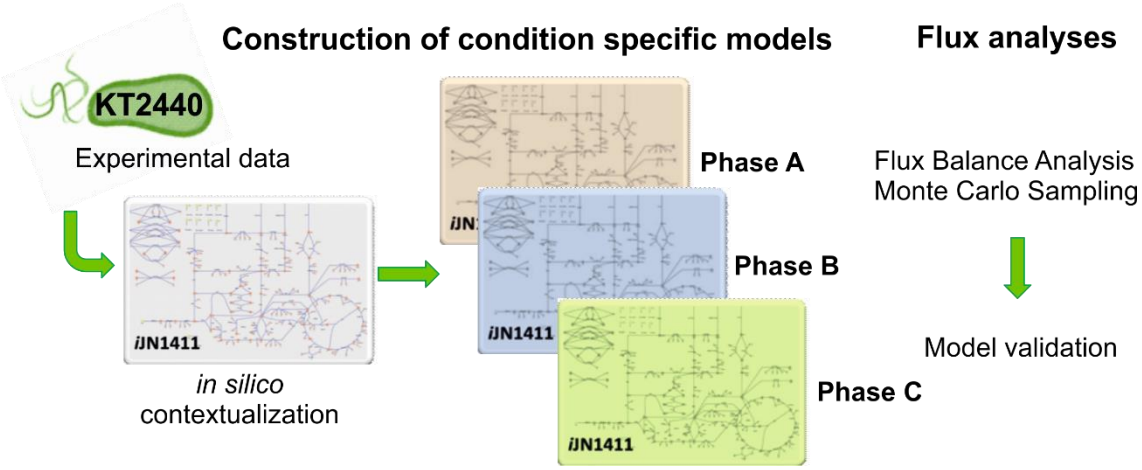

Figure 30. Schematic representation of the experimental data contextualization for the *P. putida* strains by using *i*JN1411 model. Condition specific models were constructed for the phase A (Early exponential phase; shown in pink), phase B (Late exponential phase; shown in blue) and phase C (Stationary phase; shown in green). In the resulted condition specific models, the metabolic states were analized by using Flux Balance Analysis (FBA) and Random sampling of Monte Carlo.

Strains	Total Biomass (g/L)	PHA (% CDW)	PHA (g/L)	Residual Biomass (g/L)	Octanoate concentration (mM)
KT2440	0.26 ± 0.02	13.25 ± 0.57	0.03 ± 0.00	0.22 ± 0.01	13.03 ± 1.21
KT40Z	0.25 ± 0.02	14.48 ± 0.86	0.03 ± 0.01	0.22 ± 0.02	14.71 ± 0.59
KT2440 Δ*pha*	0.26 ± 0.01	N.D.	N.D.	0.26 ± 0.01	15.05 ± 0.99
M1	0.26 ± 0.03	9.83 ± 0.40	0.02 ± 0.00	0.23 ± 0.03	13.52 ± 0.74
M2	0.23 ± 0.04	N.D.	N.D.	0.23 ± 0.03	14.63 ± 0.28
M3	0.23 ± 0.05	N.D.	N.D.	0.23 ± 0.04	15.39 ± 0.18
M4	0.25 ± 0.02	N.D.	N.D.	0.25 ± 0.02	14.80 ± 0.47

Table 8. Physiological data at t3 h used in the *in silico* contextualization process under PHA accumulation condition. N.D.: not detected

Strains	Total Biomass (g/L)	PHA (% CDW)	PHA (g/L)	Residual Biomass (g/L)	*(R)*-HAs (g/L)	Octanoate concentration (mM)
KT2440	0.52 ± 0.06	23.32 ± 2.54	0.12 ± 0.01	0.40 ± 0.05	0.17 ± 0.02	11.80 ± 1.44
KT40Z	0.51 ± 0.03	19.09 ± 1.95	0.10 ± 0.02	0.41 ± 0.02	0.00 ± 0.00	11.52 ± 1.34
KT2440 Δ*pha*	0.45 ± 0.01	N.D.	N.D.	0.45 ± 0.01	0.13 ± 0.01	13.64 ± 1.24
M1	0.52 ± 0.05	20.02 ± 2.16	0.11 ± 0.02	0.40 ± 0.03	0.21 ± 0.02	9.85 ± 1.10
M2	0.42 ± 0.03	N.D.	N.D.	0.42 ± 0.03	0.19 ± 0.00	12.35 ± 0.84
M3	0.40 ± 0.00	N.D.	N.D.	0.40 ± 0.00	0.16 ± 0.02	12.47 ± 0.08
M4	0.45 ± 0.06	N.D.	N.D.	0.45 ± 0.05	0.22 ± 0.01	11.88 ± 0.99

Table 9. Physiological data at t5 h used in the *in silico* contextualization process under PHA accumulation condition. N.D.:not detected

Strains	Total Biomass (g/L)	PHA (% CDW)	PHA (g/L)	Residual Biomass (g/L)	*(R)*-HAs (g/L)	Octanoate concentration (mM)
KT2440	1.22 ± 0.12	56.27 ± 2.75	0.67 ± 0.04	0.52 ± 0.08	0.21± 0.02	3.13 ± 0.64
KT40Z	1.08 ± 0.05	44.91 ± 3.45	0.48 ± 0.03	0.59 ± 0.05	0.00 ± 0.00	3.03 ± 0.54
KT2440 Δ*pha*	0.61 ± 0.06	N.D.	N.D.	0.61 ± 0.05	0.14 ± 0.01	7.16 ± 0.60
M1	1.01 ± 0.08	40.26 ± 2.29	0.42 ± 0.03	0.62 ± 0.03	0.37 ± 0.04	2.01 ± 0.48
M2	0.52 ± 0.01	N.D.	N.D.	0.52 ± 0.01	0.43 ± 0.04	6.32 ± 0.30
M3	0.51 ± 0.05	N.D.	N.D.	0.51 ± 0.04	0.48 ± 0.02	5.43 ± 0.35
M4	0.56 ± 0.05	N.D.	N.D.	0.56 ± 0.04	0.48 ± 0.04	6.55 ± 0.43

Table 10. Physiological data at t10 h used in the *in silico* contextualization process under PHA accumulation condition. N.D.: not detected

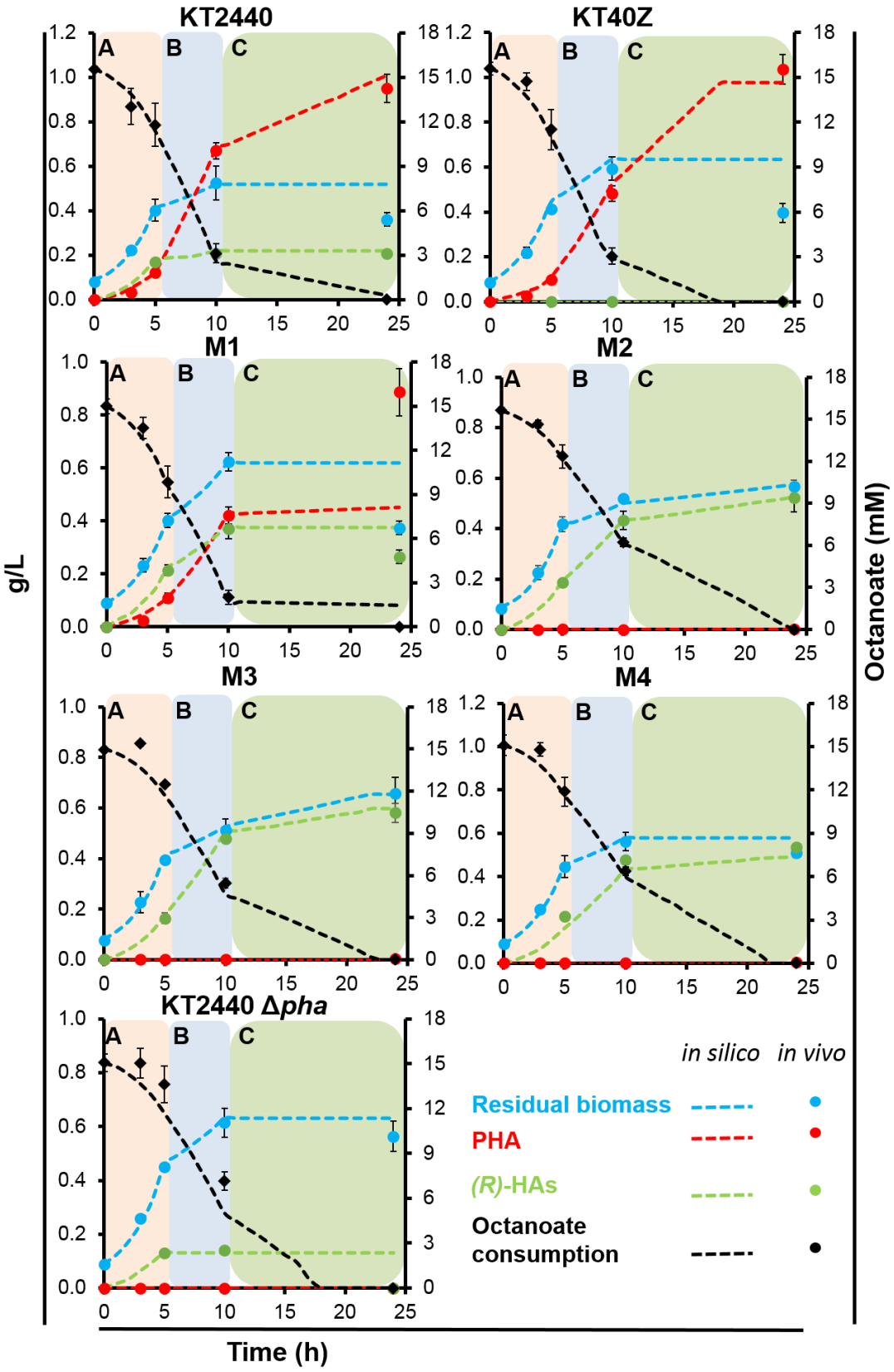

Figure 31. Condition specific model validation for KT2440, KT40Z, M1-M4 and KT2440 Δ*pha* strains using FBA analysis. The *in silico* and *in vivo* data were shown with lines and dots, respectively. Residual biomass data shown in blue color; PHA data shown in red color; *(R)*-HAs shown in green color and residual octanoate consumption (mM) shown in black color.

Using the condition-specific models for each phase, the computation of the growth curve, the consumption and production profiles of octanoate and PHA/*(R)*-HAs of each strain was carried out (Figure 31). A high level of agreement was demonstrated by interpolling and comparing the *in silico* data with the experimental ones. Therefore, it can be concluded that the condition specific models predict accurately what happens *in vivo*. Thus, these models became in unprecedent tools in order to study the impact of *phaZ* on *P. putida* metabolism under these environmental conditions. For this purpose, the solution space for each condition-specific model was further computed by Markov chain Monte Carlo sampling (Schellenberger and Palsson, 2009).

4.1.5 Model-based identification of residual oxidative metabolism under stationary phase associated to PhaZ activity.

In order to analyze the impact of increasing the *phaZ* dosage on *P. putida*, the solution space in each growth phase model was sampled by using Monte Carlo approach (materials and methods 3.10.3 section). Thus, the probabilistic flux value for each reaction was computed for each model. Random set of points were chosen from the solution space to act as surrogate for the entire space. The impact of PhaZ flux on the distribution of central metabolites at each individual growth phases (A, B, C), for KT40Z and M4 strains compared with the wild type strain, is shown in Figures 32-34. The flux distribution predictions for the rest of the strains are listed in Supplementary Tables S8-S10.

According to model prediction, depolymerase reaction deletion led to significant carbon flux distribution changes compared to wild type strain in phase A (early exponential). In fact, based on the flux analysis, KT40Z strain showed higher flux channeled through the TCA cycle (Figure 32A). Therefore, key reactions of TCA cycle, including citrate synthase (CS), aconitate dehydratase (ACONTa/b) and malate dehydrogenase (MDH) had between 1.8-2.2 times higher flux compared to the wild-type strain. Accordingly, in the KT40Z strain, this high activity of TCA cycle resulted in 1.7 higher ATP production compared to wild type (Supplementary Table S8 and Figure 32, bottom left). Finally, as a consequence of this high oxidative metabolism, KT40Z produced 3.2 times higher CO_2 and showed 2.2 fold higher respiration rate than the wild type stran (Table S8).

Additionally, during this phase, KT40Z showed a 1.3 fold higher flux through the glyoxylate shunt reactions e.g., isocitrate lyase (ICL) and malate synthase (MALS), respectively, thus providing higher levels of C4 metabolites from Acetyl-CoA. According to the model predictions, this excess of C4 metabolites was rerouted to biomass building

blocks and sugars via gluconeogenesis. In fact, 1.5-1.8 increased flux was predicted in this pathway when compared to the wild-type strain (glyceraldehyde-3-P-dehydrogenase, GAPD; phosphoglycerate kinase, PGK; phosphoglycerate mutase, PGM and phosphopyruvate hydratase, ENO reactions).

Interestingly, the lack of PhaZ function not only led to PHA cycle blockeage, but to a significant reduction of the flux through the PHA synthase (PHAP2C80). In addition, the *(R)*-HA-CoA, PHA synthase substrate, was not incorporated into nascent PHA, but instead it was funnelled to β-oxidation pathway through the reaction catalized by 3-oxoacyl-ACP reductase, FabG (RHACOAR80) and subsequently transformed in Acetyl-CoA, thus funnelling the TCA cycle and the oxidative metabolism described above.

From the other hand, by increasing the PhaZ concentration in phase A, no major differences were observed in the carbon flux distribution around TCA cycle and glycolysis compared to the wild-type strain (Figure 32B). Interestingly, model based predictions suggested different pathway providing *(R)*-HA-CoA. Thus, while 3-oxoacyl-ACP reductase (RHACOAR80) was predicted providing *(R)*-HA-CoA in M4 strain, enoyl-CoA hydratase, PhaJ (RECOAH3), acted as major source of *(R)*-HA-CoA in the wild type strain. Since, 3-oxoacyl-ACP reductase (RHACOAR80)-based pathway, closely assisted by enoyl-CoA dehydratase, FadB (ECOAH3) and 3-hydroxyacyl-CoA dehydrogenase, FadB (HACD3i), interchanges a mole of NADH by NADPH by a mole of *(R)*-HA-CoA produced, it is tempting to speculate that this alternative pathway in the M4 strain could be a consequence of a putative balancing of reducing equivalent. However, further experiments are needed in order to validate this exciting model-based hypothesis. On the other hand, this alternative pathway in the M4 strain could be simply a computational artefact due to the nature of FBA where multiple optimal solutions are allowed.

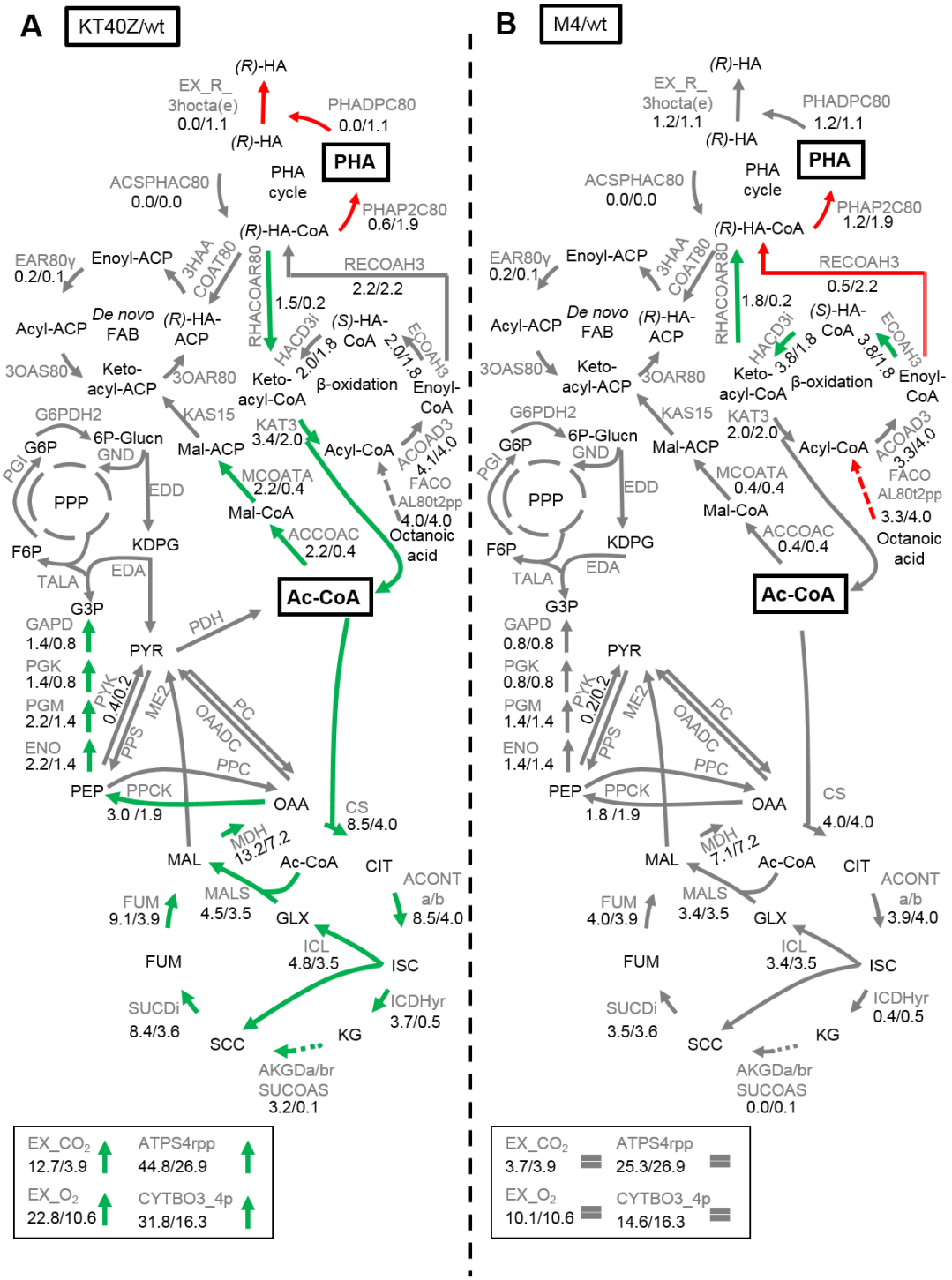

Figure 32. Impact of PhaZ depolymerase on the distribution of central metabolite fluxes, as determined by random samping of Monte Carlo in phase A (0-5 h). The diagrams summarize the reaction networks in cells growing under PHA accumulation conditions. Modifications in the carbon flux resulting from the deletion (**A**) or the overexpression (**B**) of the *phaZ* gene, are indicated by red arrows (reduced flux), thick green arrows (increased flux) and unaffected fluxes are shown in grey arrows. The numbers next to the arrows indicate the net flux (mmol.gCDW^{-1}. h^{-1}) in the mutant and wild-type strain (mutant/wild type). The model reactions are shown in grey color. Abbreviations in the figure: Gluc, glucose; Glucn, gluconate; 2K-Glucn, 2-keto-D-Gluconate; F6P, fructose-6-phosphate; G3P, glyceraldehyde-3-phosphate; KDPG, 2-dehydro-3-deoxy-6-phosphogluconate; PYR, pyruvate; Ac-CoA, acetyl-CoA; PEP,

phosphoenolpyruvate; OAA, oxaloacetate; CIT, citrate; ISC, isocitrate; KG, a-ketoglutarate; SCC, succinate; FUM, fumarate; MAL; malate; GLX, glyoxylate. For the model reaction nomenclature extra information can be found in the following link https://drive.google.com/file/d/1L-iVLsONX9qiReDmjVgRS_eDTL6sfJa9/view.

As far as it concerns the carbon flux distribution during the phase B (late exponential), no major differences were observed among KT40Z and wild type strains. Again, differential production of *(R)*-HA-CoA was found, with KT40Z strain using mainly the enoyl-CoA hydratase (RECOAH3) reaction, in contrast to wild type strain that synthetized *(R)*-HA-CoA through 3-oxoacyl-ACP reductase (RHACOAR80) reaction (Figure 33A and Supplementary Table S9).

However, M4 model saw significant differences with respect to the wild type model, in terms of flux distribution (Figure 33B and Table S9). Overall, the model predicts an important metabolism deceleration fuelled by a decrease in the uptake of octanoate (2.2 vs 3.8, respectively). Subsequently, a significant decrease in the flux through the β-oxidation pathway, PHA synthesis, TCA cycle, oxidative phosphorylation and gluconeogenesis was predisted (Figure 33B). As expected by the high depolymerase activity present in M4 strain, all the PHA synthetized was further hydrolysed and subsequently secreted to the medium. Interestingly, this observed metabolism deceleration does not impact on the growth rate and similar values were found in both strains. These results strongly suggest that as greater is the PhaZ activity, lower is the carbon spilling.

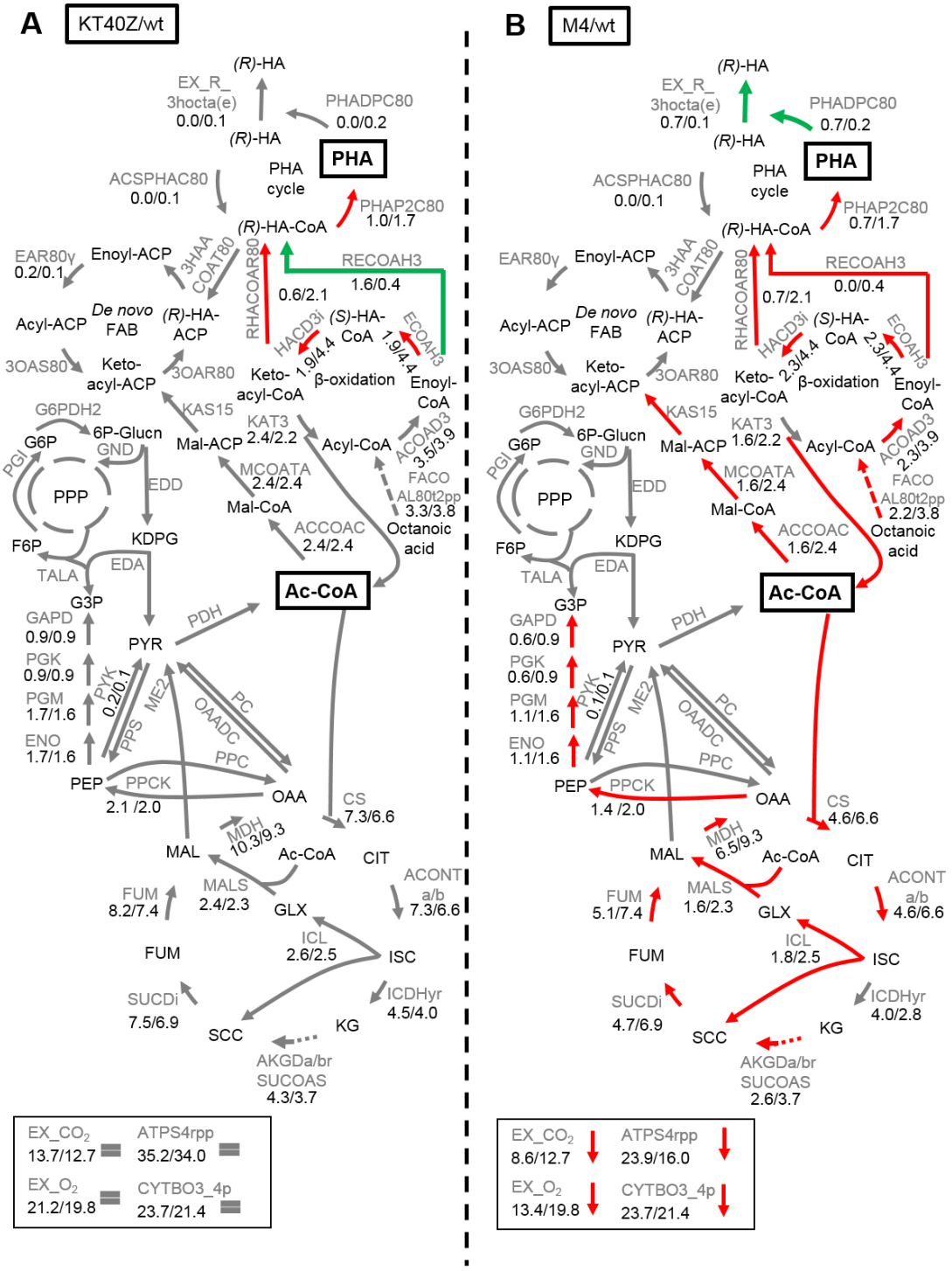

Figure 33. Impact of PhaZ depolymerase on the distribution of central metabolite fluxes, as determined by random samping of Monte Carlo in phase B (5-10 h). The diagrams summarize the reaction networks in cells growing under PHA accumulation conditions. Modifications in the carbon flux resulting from the deletion (**A**) or the overexpression (**B**) of the *phaZ* gene, are indicated by red arrows (decreased flux), thick green arrows (increased flux) and unaffected fluxes are shown in grey arrows. The numbers next to the arrows indicate the net flux (mmol.gCDW^{-1}. h^{-1}) in the mutant and wild-type strain (mutant/wild type). The model reactions are shown in grey color. Abbreviations in the figure: Gluc, glucose; Glucn, gluconate; 2K-Glucn, 2-keto-D-Gluconate; F6P, fructose-6-phosphate; G3P, glyceraldehyde-3-phosphate; KDPG, 2-dehydro-3-deoxy-6-phosphogluconate; PYR, pyruvate; Ac-CoA, acetyl-CoA; PEP,

phosphoenolpyruvate; OAA, oxaloacetate; CIT, citrate; ISC, isocitrate; KG, a-ketoglutarate; SCC, succinate; FUM, fumarate; MAL; malate; GLX, glyoxylate. For the model reaction nomenclature extra information can be found in the following link https://drive.google.com/file/d/1L-iVLsONX9qiReDmjVgRS_eDTL6sfJa9/view.

As observed during phase B, the wild type and KT40Z strains saw similar carbon flux distribution during phase C (stationary phase), indicating that the deletion of *phaZ* had little effect on the physiology of *P. putida* growing under PHA accumulation conditions (Figure 34A). In both strains, phase C was dominated by a basal metabolism drived by a reduced octanoate uptake and modest activity of β-oxidation and TCA cycle.

Interestingly, M4 strain maintained a very active metabolism in this phase characterized by high flux through β-oxidation driving a significant oxidation of Acetyl-CoA in the TCA cycle. As a direct consequence, M4 strain maintained a significant activity through oxidative phosphorylation resulting in high production of ATP levels in stationary phase (Figure 34B). In fact ATP production rate was 9.8 times higher in the M4 background strain than the wild type (Supplementary Table S10).

A summarized view of the *phaZ* tuning in key reactions of metabolism during the three phases is shown in Figure 35. The reactions focusing on the TCA cycle (Citrate synthase), ATP synthesis and CO_2 producion are shown for the different strains studied in this work. By increasing the PhaZ concentration, the trend was towards a decrease in the flux of these reactions during the phase A (early exponential phase) and no major differences compared to the other strains during the phase B (late exponential phase). These results are fully consistent with the metabolism deceleration observed in the M4 strain during these growth phases. Interestingly, the strains with higher PhaZ expression levels maintained flux through these reactions compared to the wild type and null *phaZ* depolymerase strain, during the phase C (stationary phase).

Summing up, based on the carbon flux distribution predictions (Figures 32-35 and Supplementary Tables S8-10), it could be concluded that the activity of PhaZ depolymerase has a great impact in the overall *P. putida* metabolism. In fact, in the absence of *phaZ,* significant carbon flux alterations were observed during the initial phases A and B. On the contrary, the increased doses of *phaZ* led to minor changes during the first two phases, but maintained significant higher oxidative metabolism during the phase C compared to wild type and KT40Z strains. These results demonstrate that by controlling the PHA cycle activity, the carbon metabolism of *P. putida* could be controlled to tailor potential biotechnological applications.

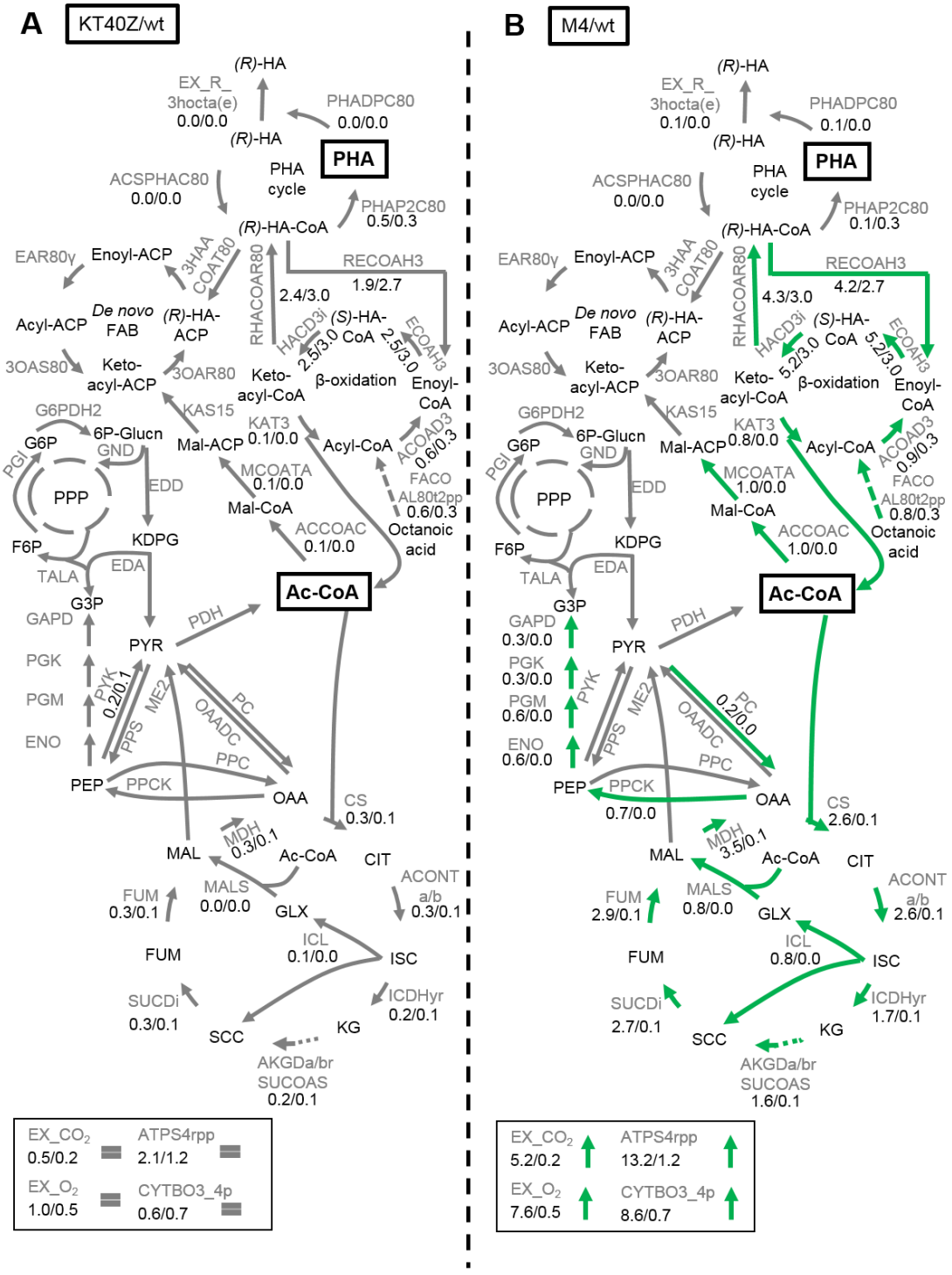

Figure 34. Impact of PhaZ depolymerase on the distribution of central metabolite fluxes, as determined by random samping of Monte Carlo in phase C (10-24 h). The diagrams summarize the reaction networks in cells growing under PHA accumulation conditions, Modifications in the carbon flux resulting from the deletion (**A**) or the overexpression (**B**) of the *phaZ* gene, are indicated by red arrows (decreased flux), thick green arrows (increased flux) and unaffected fluxes are shown in grey arrows. The numbers next to the arrows indicate the net flux (mmol.gCDW^{-1}. h^{-1}) in the mutant and wild-type strain (mutant/wild type). The model reactions are shown in grey color. Abbreviations in the figure: Gluc, glucose; Glucn, gluconate; 2K-Glucn, 2-keto-D-Gluconate; F6P, fructose-6-phosphate; G3P, glyceraldehyde-3-phosphate; KDPG, 2-dehydro-3-deoxy-6-phosphogluconate; PYR, pyruvate; Ac-CoA, acetyl-CoA; PEP,

phosphoenolpyruvate; OAA, oxaloacetate; CIT, citrate; ISC, isocitrate; KG, a-ketoglutarate; SCC, succinate; FUM, fumarate; MAL; malate; GLX, glyoxylate. For the model reaction nomenclature extra information can be found in the following link https://drive.google.com/file/d/1L-iVLsONX9qiReDmjVgRS_eDTL6sfJa9/view.

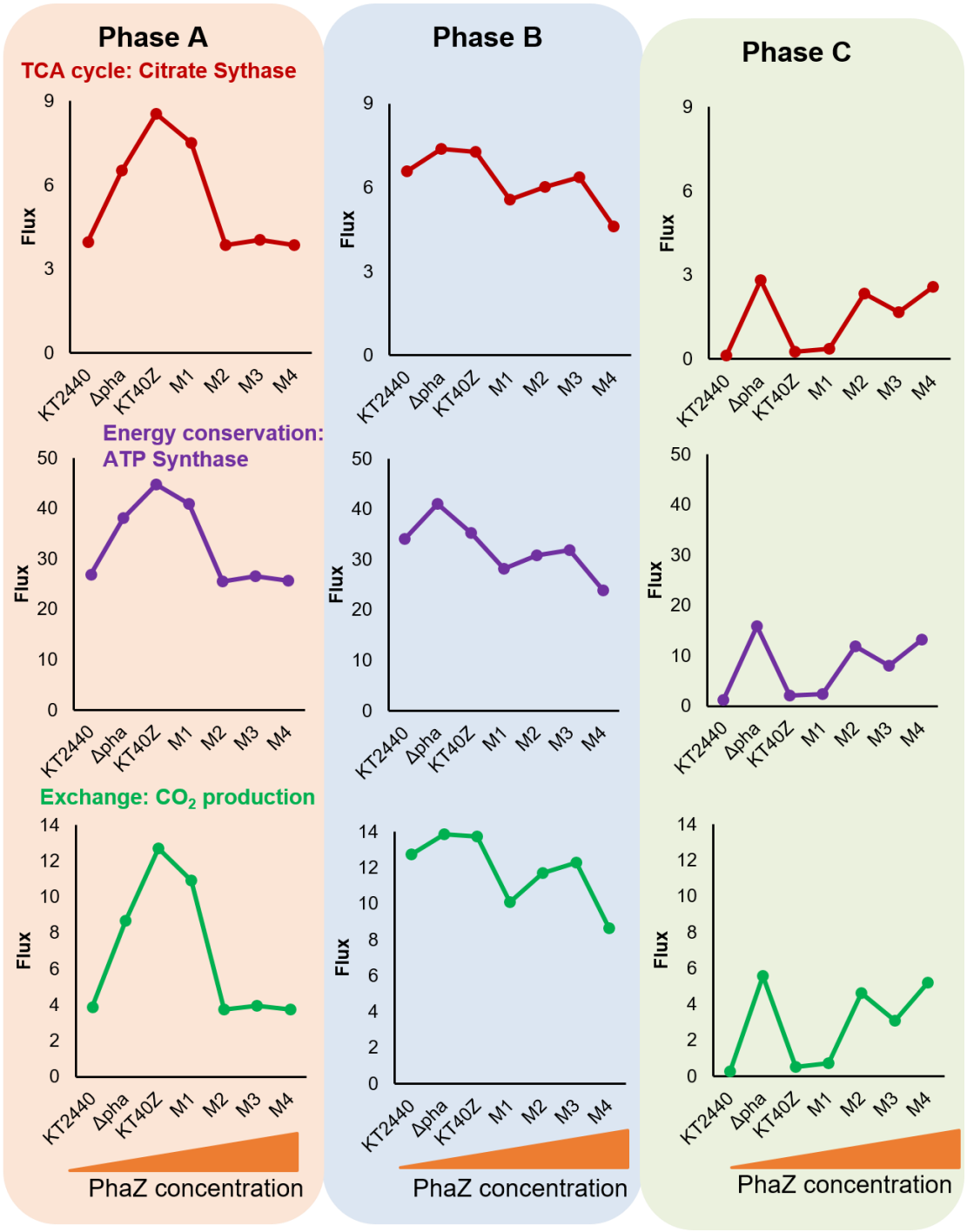

Figure 35. Impact of PhaZ depolymerase on the distribution of key metabolite fluxes, as determined by random samping of Monte Carlo in phases A-C. The reactions of citrate synthase, ATP synthase and CO_2 procuction are shown in red, purple and green color, respectively. Net flux: mmol.gCDW^{-1}. h^{-1}

4.2 Chapter 2: Study the role of enzyme duplication in the central metabolism (e.g. isocitrate dehydrogenases) in *P. putida* KT2440

Introduction

Functional redundancy can be defined as the existence of more than one similar or identical mechanisms that can replace each other when needed (e.g., response to environmental perturbations), thus assuring the integrity of the whole system. Gene functional redundancy, overlapping functions and diversity have been described as alternative mechanisms of robustness (Kitano, 2004; Nogales *et al.*, 2017).

Non-essential genes have been widely distributed along the subsystems present in the *in silico* genome-scale metabolic model, *i*JN1411. 75% of them provided robustness under genetic perturbations through the alternative and redundant mechanisms. Thereby, 59% of them had at least one isoenzymes, that could replace each other, such as isocitrate dehydrogenase (Nogales *et al.*, 2017).

Isocitrate dehydrogenase catalyzes the oxidative decarboxylation reaction of 2*R*, 3*S*-isocitrate to yield 2-oxoglutarate and CO_2 in the TCA cycle (Figure 36). It is a key enzyme in amino acid biosynthesis, fatty acids and steroid biosynthesis, vitamin production and energy metabolism (Sivaraman *et al.*, 2003). Furthermore, isocitrate dehydrogenase is an ancient enzyme widely studied in diverse organisms, focusing on characterizing and understanding its biochemistry, structure and evolution (Supplementary Table S11) (Dean and Golding, 1997; Zhu *et al.*, 2005).

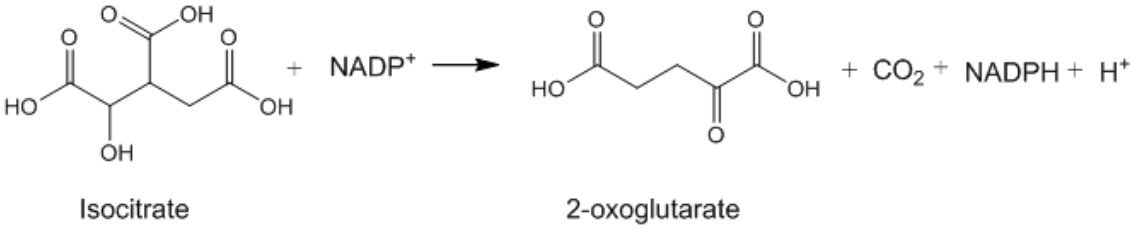

Figure 36. Isocitrate dehydrogenase reaction

There are two isocitrate dehydrogenases in living organisms; the NAD^+-dependent-IDH (EC 1.1.1.41; NAD^+-IDH) and the $NADP^+$-dependent isocitrate dehydrogenase (EC 1.1.1.42; $NADP^+$-IDH). The first type forms a heterooligomeric structure and it is majorly found in eukaryotic organisms, while the majority of prokaryotic organisms contain $NADP^+$-IDH. $NADP^+$-IDH could either form a dimeric structure composed of identical subunits of 40-50 kDa or a monomeric one with molecular weight of 80-100 kDa (Gálvez and Gadal, 1995; Wang *et al.*, 2015). For simplification, both dimeric and monomeric $NADP^+$-IDH will be referred as prokaryotic $NADP^+$-IDH (PIDH).

Regarding the presence of PIDH in bacteria, there are organisms that contain both monomeric and dimeric PIDH, such as in the case of the obligatory psychrophile *Colwellia maris* (Supplementary Table S11). Depending on the type of PIDH, different biochemical properties in response to cold, acetate, environmental stresses among others have been demonstrated. For instance, the monomeric PIDH was a cold inducible gene, an important feature for the survival of this bacterium at low temperatures, and contributing to the metabolic robustness of the cell (Ishii *et al.*, 1993; Suzuki *et al.*, 1995).

Interestingly, *P. putida* KT2440 contains both PIDH too, characteristic that will be studied in depth in this chapter. Construction and phenotyping of PIDH deletion mutants was performed. The biochemical properties of the purified PIDH enzymes were characterized. Finally, the proposed catalytic sites responsible for isocitrate binding were confirmed by site-directed mutagenesis experiments.

Results

4.2.1 *P. putida* encodes two transcriptionally active PIDH that are expressed under a wide variety of growth conditions

Several studies of PIDH are available in pseudomonads such as in *P. nautica* (Roy and Packard, 1998), *P. psychrophila* (Matsuo *et al.*, 2010), *P. fluorescens* (Hampton and Hanson, 1969; Alhasawi *et al.*, 2015) and *P. aeruginosa* (Crousilles *et al.*, 2018). However, it still remains unclear why mesophilic pseudomonads have two PIDH, a characteristic mainly observed in psychophilic bacteria (Ochiai *et al.*, 1979; Matsuo *et al.*, 2010). In *P. putida* KT2440 genome, two PIDH, have been annotated; the dimeric ICD (PP_4011) and the monomeric IDH (PP_4012) (Nelson *et al.*, 2002; Belda *et al.*, 2016). It is worth to mention that during this chapter, the dimeric and monomeric isocitrate dehydrogenase will be named as ICD and IDH, respectively.

Icd and *idh* genes are chromosomically located in tandem in opposite direction from each other (Figure 37). The dimeric *icd* is followed by the monomeric *idh*. This chromosomic arrangement of *P. putida* PIDH isoenzymes is conserved among pseudomonads including a 300-450 bps conserved intergenic region (Figure 37). However, this arrangement is different in the psychrophilic organisms, *Colwellia maris* and *Colwellia psychrerythraea* NRC1004. In these organisms, the two PIDH genes are located tandem in the same direction, with the dimeric type following the monomeric one by maintaining a 200-300 bp conserved intergenic region (Matsuo *et al.*, 2010). Some differences were observed in *Colwellia psychrerythraea* 34H, where two monomeric and one dimeric type PIDH have been described (Suzuki and Takada, 2016). Furthermore, *Mycobacterium tuberculosis* has two PIDH located in different chromosomic regions

(Murima *et al.*, 2016). Finally, the *Azotobacter vinelandii* has only a monomeric *idh* and *E. coli* a dimeric *icd*.

Sequence alignment analyses revealed that the ICD from *P. putida* KT2440 exhibited 89.1%, 91.6%, 75.4% and 75.9% of identity with the ICD of *P. aeruginosa* PAO1, *P. psychrophila*, *C. maris* and *E. coli*, respectively. On the other hand, the IDH from *P. putida* showed 66.3%, 82.1%, 66.6% and 77.9% of identity with the monomeric IDH of *P. aeruginosa* PAO1, *P. psychrophila*, *C. maris* and *A. vinelandii*, respectively.

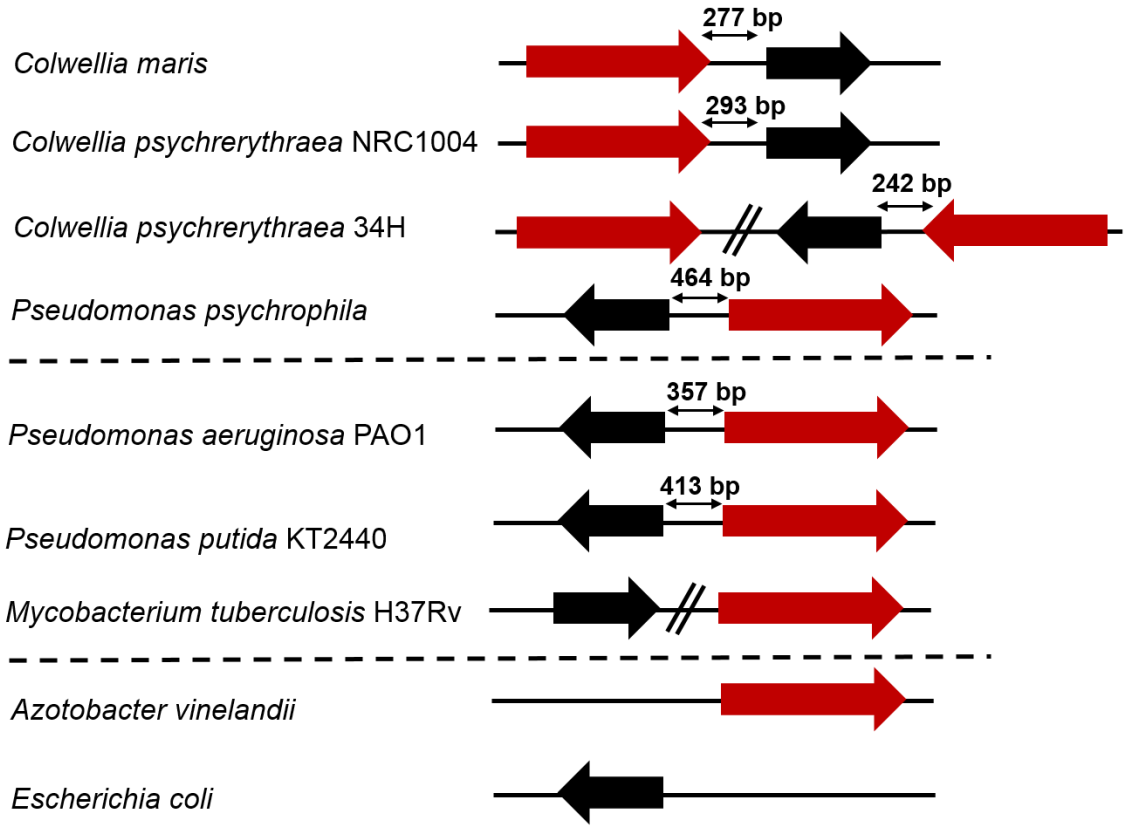

Figure 37. Example of location of isocitrate dehydrogenase on the chromosome DNA in several bacteria. The monomeric *idh* and the dimeric *icd* genes are shown in red and black color, respectively. The intergenic region is annotated. Locational data for PIDH coding genes from these bacteria have been reported previously (Maki *et al.*, 2006; Matsuo *et al.*, 2010).

Since this is the first study realized in *P. putida* KT2440, we first checked whether both PIDH coding genes are transcriptionally active under several growth conditions. Thus, in order to get a glance towards the transcription levels of both PIDH, available transcriptomic data of *P. putida* KT2440, collected from the literature under different growth conditions, including minimal medium supplemented by succinate, glucose, glycerol or fructose as sole carbon sources were used (Frank *et al.*, 2011; Kim *et al.*, 2013; La Rosa *et al.*, 2015; Bojanovič *et al.*, 2017). The careful analysis of these expression profiles revealed that in the majority of the conditions, the monomeric *idh* showed higher expression levels compared to the dimeric *icd* (Figure 38). Interestingly,

in the conditions were fructose or glycerol was applied as sole carbon source, *icd* demonstrated higher expression levels (Figure 38).

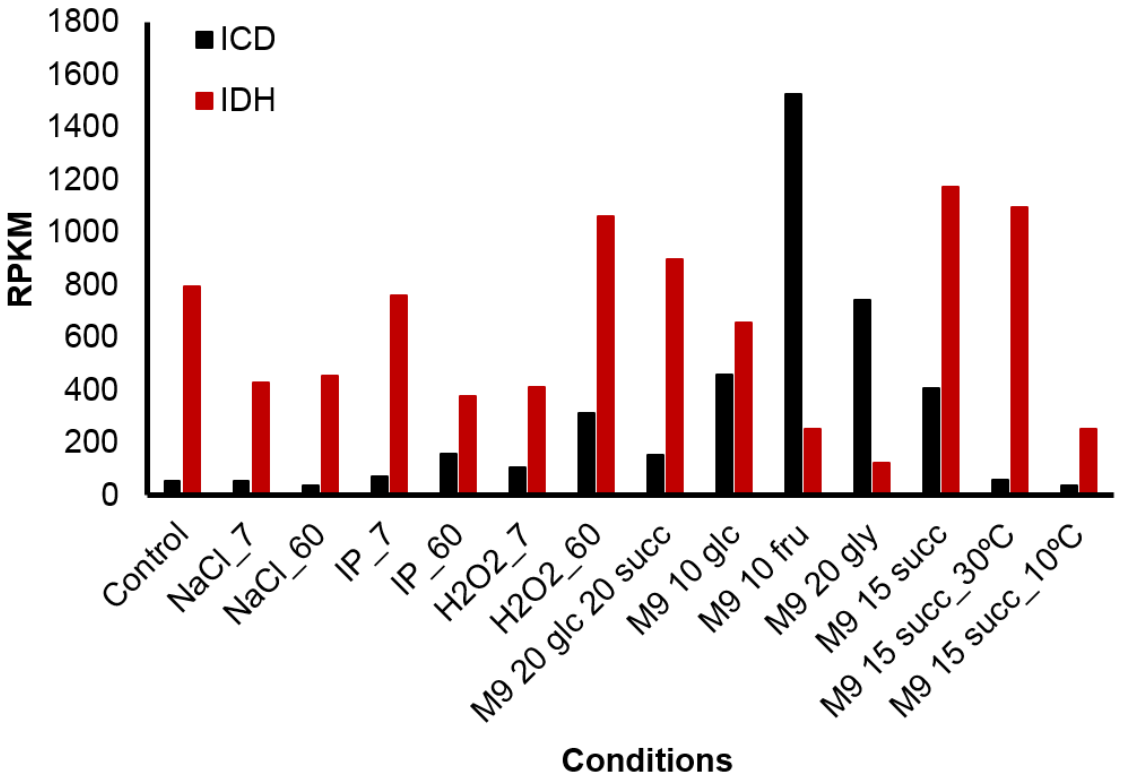

Figure 38. Transcriptomic data available on *P. putida* KT2440. The expression levels (RPKM values: reads-per-kb-per million read) of the dimeric ICD (black bars) and IDH (red bars) are shown. Different growth conditions were tested with data obtained under mid exponential growth published by different groups (Frank *et al.*, 2011; Kim *et al.*, 2013; La Rosa *et al.*, 2015; Bojanovič *et al.*, 2017). Conditions tested: Control: growth under M9 27.5 mM glucose, NaCl_7: growth under control conditions supplemented by 3% NaCl 7 min exposure, NaCl_60: growth under control conditions supplemented by 3% NaCl 60 min exposure, IP_7: growth under control conditions supplemented by 0.1 µg/ml of imipenem (IP) 7 min exposure, IP_60: growth under control conditions supplemented by 0.1 µg/ml of imipenem (IP) 60 min exposure, H_2O_2_7: growth under control conditions supplemented by 0.5 mM H_2O_2 7 min exposure, H_2O_2_60: growth under control conditions supplemented by 0.5 mM H_2O_2 60 min exposure (Bojanovič *et al.*, 2017); M9 20 mM glucose and 20 mM succinate (La Rosa *et al.*, 2015); M9 10 mM glucose, M9 10 mM fructose, M9 20 mM glycerol, M9 15 mM succinate (Kim *et al.*, 2013); M9 15 succinate grown on 30ºC, M9 15 mM succinate grown on 10ºC (Frank *et al.*, 2011).

In order to validate some of the available transcriptomic data, the expression level of both PIDH were further checked under different nutritional scenarios by means of qRT-PCR experiments. The expression levels of the *icd* and *idh* of *P. putida* growing on LB, citrate, succinate and glucose are shown in Figure 39. Overall, we found a carbon source dependent expression of both PIDH, where the monomeric *idh* showed higher expression levels compared to the dimeric *icd* in all the conditions tested. These results are in accordance to the observed behavior of these enzymes by transciptomic data

(Figure 38). In fact, when growing on LB and glucose, the *idh* gene showed up to 35 and 5 times more expression than the *icd*, respectively (Figure 39). However, no significant differences were found in the expression levels of both enzymes when citrate and succinate were used as sole carbon source.

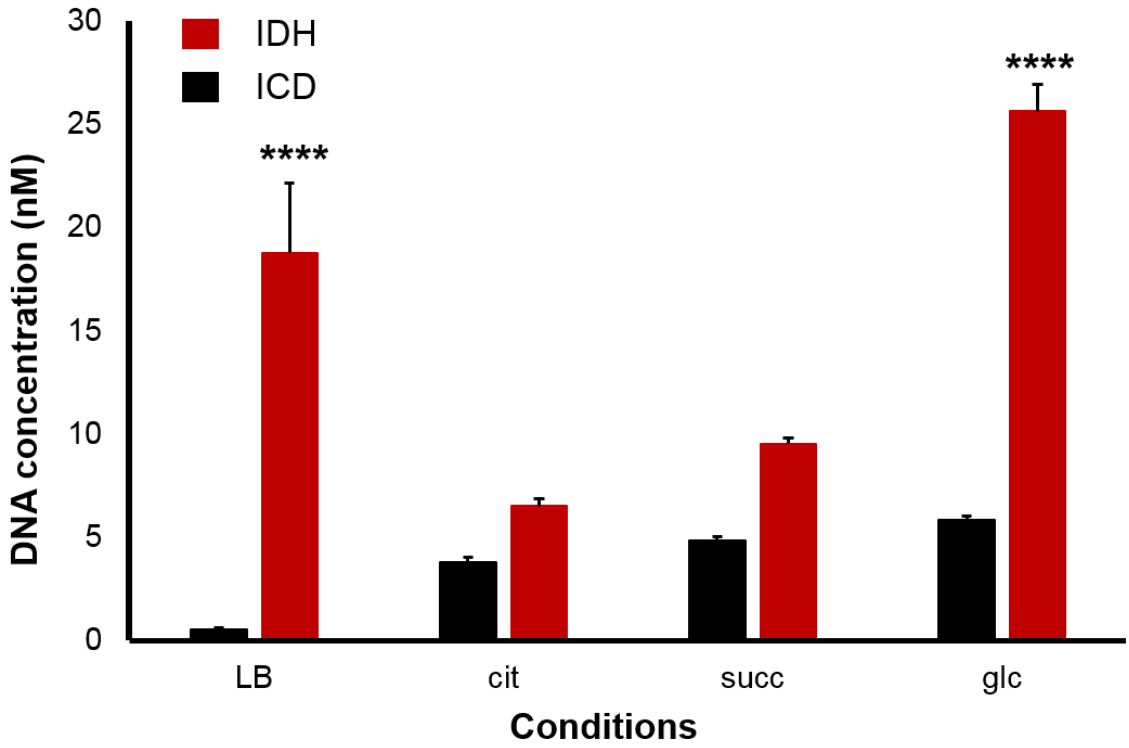

Figure 39. qRT-PCR experiments of KT2440 strain grown in different carbon sources. The absolute expression levels (nM) of dimeric ICD and monomeric IDH are shown in black and red colors, respectively. *P. putida* cells were grown in rich LB medium and minimal M63 medium supplemented with 10 mM citrate (cit), 15 mM succinate (succ) or 10 mM glucose (glc) and they were harvested when reached mid-exponential growth ($OD_{600\ nm}$: 0.5-0.6). One-way ANOVA analysis was performed and the significant differences compared to ICD are shown (*, $p<0.05$; **, $p<0.01$; ***, $p<0.001$; ****, $p<0.0001$).

Therefore, it can be confirmed that i) both genes were transcriptionally active in *P. putida* KT2440, ii) the expression of these genes is carbon-source-dependent and iii) it looks that there is a clear preference towards the expression of the monomeric *idh* gene.

4.2.2 The construction and phenotyping of *P. putida* KT2440 isocitrate dehydrogenase deletion mutants

In order to investigate the importance of having two PIDH in *P. putida* KT2440 and a probable divergent response towards stressors, single and double deletion mutants were designed. For deleting the *icd* gene (PP_4011), the pK18*mobsacB* system was used (Materials and Methods 3.4.4 section), resulting to MM18 strain. Unfortunately,

different attempts to delete the monomeric *idh* gene (PP_4012), using different approaches, including pK18*mob,* pK18*mobsacB* and I-Sce-I systems failed and the deletion mutant could not be obtained. Similarly, attempts to construct the double knockout strain were fruitless.

We decided to continue by phenotyping the MM18 strain using several carbon sources, in order to shed light in the role of these enzymes in *P. putida*. Therefore, MM18 strain was grown under different carbon sources and the growth profile was monitored using a multiwell reader (Figure 40). Despite the expression of the two isoenzymes was carbon source dependent (Figures 38-39), no differences were observed as far as it concerns the growth performance between the wild type and the MM18 strain in all the conditions tested (Figure 40). These results were somewhat expected in the case of glucose, given *idh* gene is highly expressed but not in the case of succinate, where similar *icd* and *idh* expression levels were observed previously. These observations could be explained by the presence of alternative (redundant) mechanisms. In other words, the monomeric IDH could replace the role of the dimeric ICD, by avoiding the collapse of the whole system. Further experiments need to be realized in order to validate this exciting hypothesis.

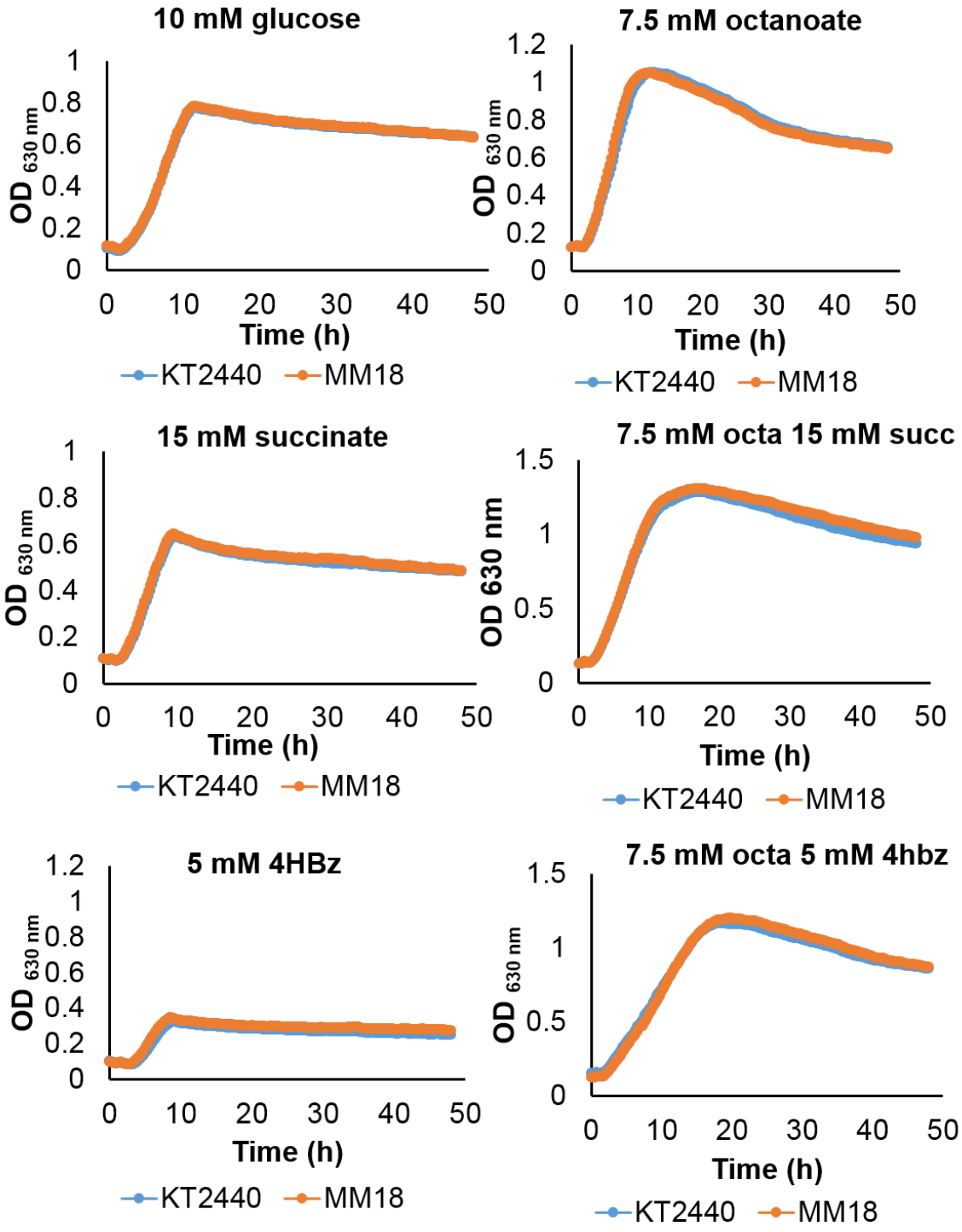

Figure 40. Growth curves on different carbon sources. Phenotyping of wild type strain (in blue color) and MM18 (null *icd*) strain (in orange color). The conditions tested were M63 supplemented with 7.5 mM octanoate,10 mM glucose,15 mM succinate, 7.5 mM octanoate +15 mM succinate, 5 mM 4hydroxybenzoate, 7.5 mM octanoate + 5 mM 4HBz.

4.2.3 Analysis of primary structure of *P. putida* PIDH

Since several deletion attempts of monomeric IDH of *P. putida* KT2440 were unsuccessful, we tried to get closer to the metabolic role of these enzymes through enzymatic approaches. As a first approach, we addressed the identification of the catalytic sites determinant for the enzymatic activities of *P. putida* PIDH. For this purpose alignments for the dimeric ICD and monomeric IDH were realized (Figures 41-42).

-Dimeric ICD

Based on the available crystal data on the dimeric ICD, the proposed binding sites for isocitrate, metal and $NADP^+$-coenzyme specificity for the dimeric ICD are summarized in the Table 11 (Chen and Yang, 2000; Yasutake *et al.*, 2002).

Proposed binding sites	Residues
for isocitrate	Ser113, Asn115, Arg119, Arg129, Arg153, Tyr160, Lys230´
for metal	Asp283´, Asp307, Asp311
for $NADP^+$ specificity	Arg292´, Lys344, Tyr345, Val351, Tyr391, Arg395
for phosphorylation	Ser113

Table 11. A summary of the proposed binding sites for isocitrate, metal and $NADP^+$-coenzyme specificity for the dimeric ICD. The prime sign indicates the second subunit.

Aimed by the architecture of the dimeric ICD coenzyme binding pocket, it was confirmed that the Lys344 and Tyr345 residues were the major determinants of the coenzyme specificity (Chen *et al.*, 1997; Chen and Yang, 2000). These residues are also conserved in ICD of *P. putida* KT2440.

Furthermore, the ICD of *E. coli* is reversibly phosphorylated at Ser113 by the action of kinase/phosphatase AceK. The P-Ser113 electrostatically repulses the isocitrate and prevents substrate binding (Walsh and Koshland, 1985; Dean *et al.*, 1989). Recently, it was found that ICD from *P. aeruginosa* is also inactivated by AceK but the monomeric IDH does not. This is due to the differently structured catalytic sites of IDH and the absence of AceK recognition segment from monomeric IDH, that are critical for the AceK recognition and binding (Crousilles *et al.*, 2018). This mechanism seems to be functional in the case of ICD from *P. putida* KT2440. An *aceK* gene (PP_4565) codifying for the isocitrate dehydrogenase kinase/phosphatase is also annotated in *P. putida* KT2440 genome.

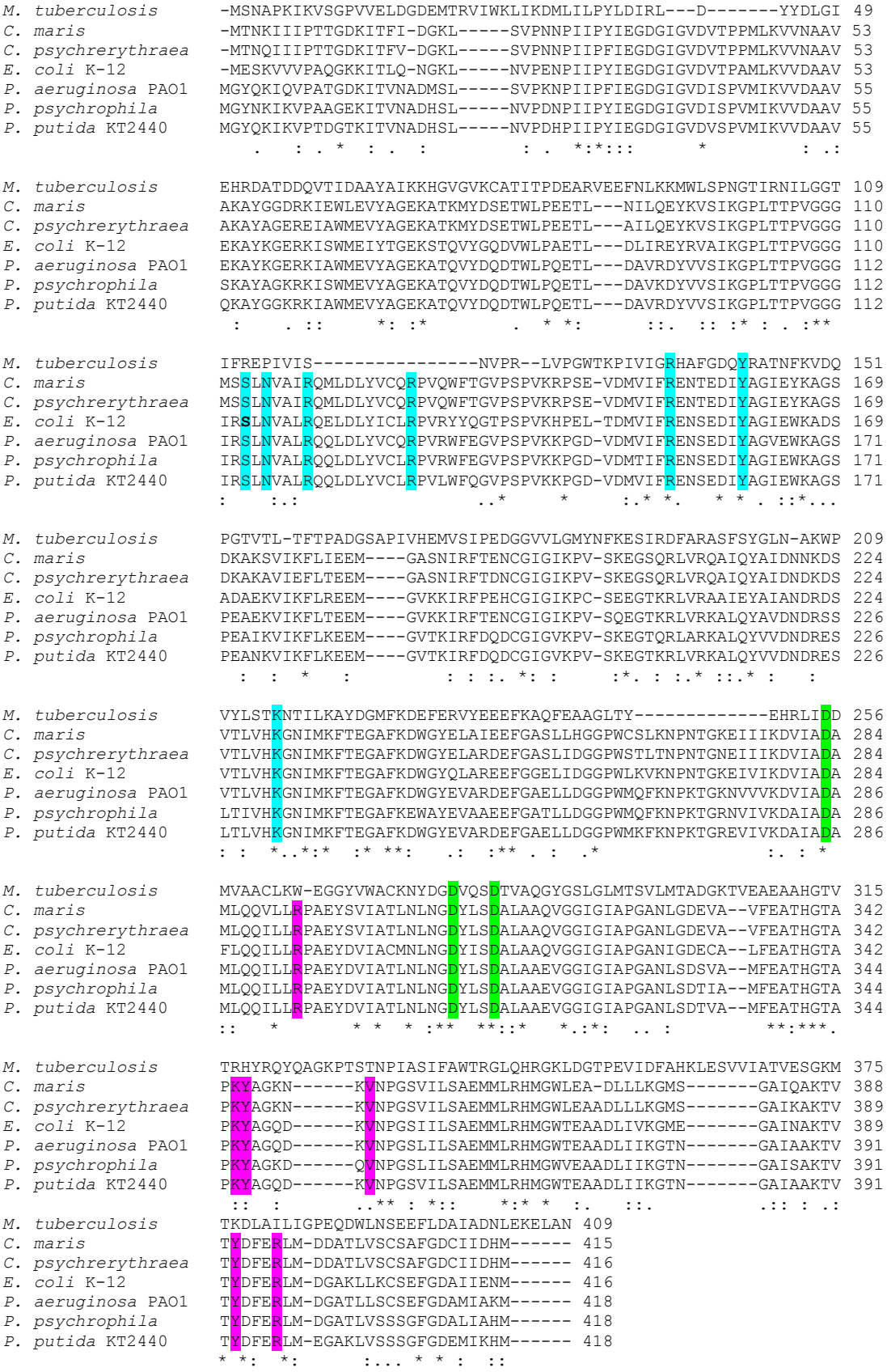

Figure 41. Dimeric isocitrate dehydrogenase multiple alignment using ClustalW. The amino acids that confer NADP$^+$- coenzyme specificity and are responsible for metal (Mg^{2+}, Mn^{2+}) and substrate binding are indicated in shaded pink, light green and blue colors, respectively. Phosphorylation sites by AceK are

indicated in bold letters. * (asterisk) indicates positions, which have a single, fully conserved residue; : (colon) indicates conservation between groups of strongly similar properties - scoring > 0.5 in the Gonnet PAM 250 matrix; . (period) indicates conservation between groups of weakly similar properties - scoring =< 0.5 in the Gonnet PAM 250 matrix. The database accession numbers are for *C. maris* (BAA03135), *C. psychrerythraea* 34H (AAZ24108), *P. psychrophila* (BAH80316), *P. aeruginosa* PAO1 (AAG06011), *P. putida* KT2440 (NP_746141), *M. tuberculosis* H37Rv (NP_217856) and *E. coli* K12 (BAA35958).

-Monomeric IDH

The proposed binding sites for isocitrate, metal and $NADP^+$-specificity for the monomeric IDH are summarized in the Table 12 (Chen and Yang, 2000; Yasutake *et al.*, 2002). Furthermore, previous experimental studies on psychrophilic bacteria identified the key amino acids residues involved in the mesophilic properties of the *P. psychrophila* IDH compared to the cold induced *C. maris* and *C. psychrerythraea* shown in the Figure 42 (Matsuo *et al.*, 2010; Kobayashi and Takada, 2014). The residues responsible for the mesophilic properties of the IDH of the *P. psychrophila* are conserved in IDH of *P. putida* KT2440.

Proposed binding sites	Residues
for isocitrate	Ser132, Asn135, Arg139, Arg145, Arg547, Tyr420, Lys255
for metal	Asp350, Asp548
for $NADP^+$ specificity	Arg358, Lys588, His589, Arg649

Table 12. A summary of the proposed binding sites for isocitrate, metal and $NADP^+$-coenzyme specificity for the monomeric IDH.

```
C. maris          MSTDNSKIIYTITDEAPALATYSLLPIIQAYTASSGINVETRDISLAGRILANFPKYLTK 60
34H               MSTDNSKIIYTITDEAPALATYSLLPIIQAYTASSGINVETRDISLAARILANFPKYLTK 60
A.vinelandii      --MSTPKIIYTLTDEAPALATYSLLPIIKAFTGSSGIAVETRDISLAGRLIATFPEYLTD 58
P. psychrophila   -MPNRSKIIYTFTDEAPALATYSLLPIIEAFTAPADIAVETRDISLAGRILASFPEQLGA 59
P. putida KT2440  -MPTRSKIIYTFTDEAPALATYSLLPIIEAFTASADIAVETRDISLAGRILAAFPEQLGA 59
P. aeruginosa     -MSIRSKITYTFTDEAPALATYSLLPIVKAFAASAGIDVETSDISLAGRILANFADRLEA 59
34H_2             ---MSSKIIYTYTDEAPLLATCSLLPIIKTFAASADIDIELKDISLASRVLSAFSDILPA 57
M. tuberculosis   MSAEQPTIIYTLTDEAPLLATYAFLPIVRAFAEPAGIKIEASDISVAARILAEFPDYLTE 60
                        .* ** ***** *** ::***:.:::  :.* :*  ***:*.*::: * . *

C. maris          EQRIDDALAELGELAQTPEANIIKLPNISASIPQLEAVIKELQAKGYDLPHYPAEPQNEA 120
34H               EQRVDDALSELGKLAKTPEANIIKLPNISASIPQLELAIKELQAKGYDLPHYPAEPQNEA 120
A.vinelandii      TQKISDDLAELGKLATTPDANIIKLPNISASVPQLKAAIKELQQQGYKLPDYPEEPKTDT 118
P. psychrophila   K-AVADHLAELGALAVTPEANIIKLPNISASVPQLQAAIKELQAQGFDIPDYPETVTTDA 118
P. putida KT2440  EKQVGDHLAELGQLATTPEANIIKLPNISASVPQLKAAIKELQGKGFNIPDYADEPATAE 119
P. aeruginosa     DQRIEDDLARLAVLATSPDANIIKLPNISASVPQLKGAIAELQGLGYKVPDFPEDPQTDE 119
34H_2             DQQVPDTLAELGALTHHPDTNIIKLPNISASIPQLKDVISELQAQGYAIPDYPESPKTDE 117
M. tuberculosis   EQRVPDNLAELGRLTQLPDTNIIKLPNISASVPQLVAAIKELQDKGYAVPDYPADPKTDQ 120
                     : * *:.*. *:  *::***********:***  .* ***  *: :*.:     .

C. maris          EESIKLTYAKILGSAVNPVLREGNSDRRAPASVKQYARNNPHSMGAWSKESKSHVAHMAS 180
34H               EESIKLTYAKVLGSAVNPVLREGNSDRRAPGSVKQYARNNPHSMGAWSPESKSHVAHMES 180
A.vinelandii      EKDVKARYDKIKGSAVNPVLREGNSDRRAPLSVKNYARKHPHKMGAWSADSKSHVAHMDN 178
P. psychrophila   DKEVKARYSKVMGSAVNPVLREGNSDRRAPLSVKNYARKHPHKMGAWAADSKSHVAHMSE 178
P. putida KT2440  EKESRARYDRIKGSAVNPVLREGNSDRRAPLSVKNYARKHPHKMGAWAADSKSHVAHMTQ 179
P. aeruginosa     EKEVRARYAKILGSAVNPVLREGNSDRRAPAAVKAYARKHPHSMGKWSMASRSHADYMRG 179
34H_2             DRSNEAKYSKTLGSAVNPVLREGNSDRRAPPSVKAFARKNPHSMGKWSQASRTHVSHMHS 177
M. tuberculosis   EKAIKERYARCLGSAVNPVLRQGNSDRRAPKAVKEYARKHPHSMGEWSMASRTHVAHMRH 180
                  :.  .  * :  *********:******** :** :**::**.** *:  *::*. :*
```

```
C. maris          GDFYGSEKSVTIDGATSVNIEFVAKNG-DVTLLKSKLPLLDKEIIDASVMSKSALVEFFE 239
34H               GDFYGSEKSVTIDGATSINIEFVAQNG-DVTLLKSKLPLLDKEIIDASVMSKSALIEFYE 239
A.vinelandii      GDFYGSEKAALIGAPGSVKIELIAKDG-SSTVLKAKTSVQAGEIIDSSVMSKNALRNFIA 237
P. psychrophila   GDFYASEKAALIEAPGSVKIELIAQDG-TTTVLKEKTAVQAGEIIDCSVMSKKALRQFVA 237
P. putida KT2440  GDFYGSEKAALIEADDSLRIELVGKDG-STTVLKEKTAVKAAEVIDCATMSRKALKAFIA 238
P. aeruginosa     GDFFSSEQSITMAKAGDVRIEFVGKDG-K-VEVKKQLSLQEGEVLDSMFMSCGKLRDFFE 237
34H_2             GDFYASEKCMTMDKACDVKIEFVAKDDGAVTVLKEKTSLQAGEIIDSMFMSKKILCEFLE 237
M. tuberculosis   GDFYAGEKSMTLDRARNVRMELLAKS-GKTIVLKPEVPLDDGDVIDSMFMSKKALCDFYE 239
                  ***:..*:.  :    .:.:*::.:.      :* :  :   :::*.  **   *  *

C. maris          TEINKAKEEDVLLSLHLKATMMKVSDPVMFGHAVRVFYKDVFAKHAATFEQLGVDADNGI 299
34H               TEINKAKEEDVLLSLHLKATMMKVSDPIMFGHAVKVFYKDVFTKHEATFDQLGVDADNGI 299
A.vinelandii      AEIEDAKKQGVLLSVHLKATMMKVSDPIMFGQIVSEFYKDALTKHAEVLKQIGFDVNNGI 297
P. psychrophila   AEIEDAKKQGVLFSVHLKATMMKVSDPIMFGQIVAEFYKDALEKHADILKEIGFNLNNGI 297
P. putida KT2440  EQIADAKAAGVLLSVHLKATMMKVSDPIMFGVIVEEFYNDVLTKHAAALAEVGFNANNGI 298
P. aeruginosa     KTLQDCKETGVMWSLHVKATMMKISHPIVFGHAVSVYYKDVFDKWGQLFEELGVNPNNGI 297
34H_2             QEMEDARETGVMFSFHVKATMMKVSHPIVFGHAVKVYYKDLFAKHAETFEKLGVNANDGV 297
M. tuberculosis   EQMQDAFETGVMFSLHVKATMMKVSHPIVFGHAVRIFYKDAFAKHQELFDDLGVNVNNGL 299
                    : ..   .*: *.*:******:*.*::**  *  :*:* : *    : .:*.: ::*:

C. maris          GDVYAKIARLPAAQKEEIEADLQAVYATRPEMAMVDSDKGITNLHVPSDVIIDASMPAAL 359
34H               GDVYAKIARLPAAQKAEIEADLQAVYATRPEMAMVDSDKGITNLHVPSDVIIDASMPAAL 359
A.vinelandii      GDLYARIKTLPEAKQKEIEADIQAVYAQRPQLAMVNSDKGITNLHVPSDVIVDASMPAMI 357
P. psychrophila   GDLYARIKALPAEKQAEIEADIQAVYANRPALAMVNSDKGITNLHVPSDVIVDASMPAMI 357
P. putida KT2440  GDLYARIKDLPADKQAEIEADIQALYAERPALAMVNSDKGITNLHVPSDVIVDASMPAMI 358
P. aeruginosa     SSVYDKIKSLPASQQEEILHDIHEVYSHRPEMAMVDSVKGITNLHIPSDVIVDASMPAMI 357
34H_2             SSIYEKVKQLPESWREEILADLHACYEKRPELAMVDSAKGISNLHTPNEVIVDASMPAMI 357
M. tuberculosis   SDLYSKIESLPASQRDEIIEDLHRCHEHRPELAMVDSARGISNFHSPSDVIVDASMPAMI 359
                  ..:* ::  **   : **  *::  :  ** :***:* :**:*:* *.:**:****** :

C. maris          RASGMMWGPDGKQKDTKFMIPDRNYAGVFSAVVDFCRENGAFNPATMGTVPNVGLMAQKA 419
34H               RASGMMWAPDGSQKDTKFMIPDRNYAGVFSAVVDFCRENGAFNPTTMGTVPNVGLMAQKA 419
A.vinelandii      RDSGKMWGPDGKLHDTKAVIPDRCYAGVYQVVIEDCKQHGAFDPTTMGSVPNVGLMAQKA 417
P. psychrophila   RDSGKMWNTEGQLQDTKAVIPDRCYATIYQATIEDCQKHGAFDPTTMGSVPNVGLMAQKA 417
P. putida KT2440  RDSGKMWNAAGELQDAKAVIPDRCYAGIYQATIEDCKVNGAFDPTTMGSVPNVGLMAQKA 418
P. aeruginosa     RNSGQMWGKDGKQKDTKAVMPESTYARIYQEMINFCKTNGAFDPTTMGSVPNVGLMAQKA 417
34H_2             RAGGKMWGPDGKLKDTKAVMPESTFARIYQEIINFCKTHGAFDPTTMGTVPNVGLMAQKA 417
M. tuberculosis   RAGGKMYGADGKLKDTKAVNPESTFSRIYQEIINFCKTNGQFDPTTMGTVPNVGLMAQQA 419
                  * .* *:   *. :*:* : *:  :: ::.  :: *: :* *:*:***:*********:*


C. maris          EEYGSHDKTFTMKAAGTVRVVN-SQGERLIEQEVAQGDIYRMCQVKDAPIQDWVKLAVTR 478
34H               EEYGSHDKTFTMSATGVVRVVN-DNGDILIEQNVAQGDIFRMCQVKDAPIQDWVKLAVTR 478
A.vinelandii      EEYGSHDKTFQIPADGVVRVTD-ESGKLLLEQSVEAGDIWRMCQAKDAPIQDWVKLAVNR 476
P. psychrophila   EEYGSHDKTFQIKTPGVVRVTD-SNGNVLMEQNVEEGDIWRMCQAKDAPIRDWVKLAVNR 476
P. putida KT2440  EEYGSHDKTFQIKADGVVRVVD-GKGNVVLEQNVEAGDIFRMCQTKDAPIQDWVKLAVNR 477
P. aeruginosa     EEYGSHDKTFEMTADGTMRVVL-ADGSVLMQHKVETGDIWRACQTKDAPIRDWVKLAVTR 476
34H_2             EEYGSHDKTFEVQGDGCIRIVDD-EGKTLLTMDVEEGDIWRMCQVKDAPIQDWVKLAVAR 476
M. tuberculosis   EEYGSHDKTFEIPEDGVANIVDVATGEVLLTENVEAGDIWRMCIVKDAPIRDWVKLAVTR 479
                  ********** :   *  .:.    *. ::  .*  ***:* * .*****:******* *

C. maris          ARATGTPTVFWLDENRGHDEQMIKKVNTYLADHDTTGLDIQILEPVKACEFTLARVAKGE 538
34H               AKATGTPTVFWLDENRGHDAEMIKKVNTYLADHDTNGLDIQILEPVKACEYTLARVAKGE 538
A.vinelandii      ARATNTPAVFWLDPARAHDAQVIAKVERYLKDYDTSGLDIRILSPVEATRFSLARIREGK 536
P. psychrophila   ARASNTPAVFWLDPKRSHDAEMIKKVETYLKDHDTSGLDIRIMAPVDAMKFTLERTRAGL 536
P. putida KT2440  ARLSNTPAVFWLDPARAHDGVMIEKVQKYLKDHDTTGLDIRILAPVDAIKFSLARIREGK 537
P. aeruginosa     ARQSDTPAIFWLDPERAHDRELRKKVELYLKDHDLTGLDISIMGYNEAIRVSMERLIRGK 536
34H_2             AKLSDTPAVFWLDEYRPHEAELIKKVKLYLKDHDLTGLDIQIMSQTRAMRYTLERILRGG 536
M. tuberculosis   ARISGMPVLFWLDPYRPHENELIKKVKTYLKDHDTEGLDIQIMSQVRSMRYTCERLVRGL 539
                  *: :. *.:****  * *:  :  **: ** *:*  **** *:    : . :  *   *

C. maris          DAISVTGNVLRDYLTDLFPILELGTSAKMLSIVPLMNGGGLFETGAGGSAPKHVQQFEKE 598
34H               DAISVTGNVLRDYLTDLFPILELGTSAKMLSIVPLMNGGGLFETGAGGSAPKHVQQFEKE 598
A.vinelandii      DTISVTGNVLRDYLTDLFPIMELGTSAKMLSIVPLMSGGGLFETGAGGSAPKHVQQFLEE 596
P. psychrophila   DTISVTGNVLRDYLTDLFPIMELGTSAKMLSIVPLMNGGGLFETGAGGSAPKHVQQLLEE 596
P. putida KT2440  DTISVTGNVLRDYLTDLFPIMELGTSAKMLSIVPLMNGGGLFETGAGGSAPKHVQQLVEE 597
P. aeruginosa     DTISVTGNVLRDYLTDLFPIMELGTSAKMLSIVPLMAGGGMYETGAGGSAPKHVQQLVEE 596
34H_2             DTISVTGNILRDYLTDLFPILELGTSAKMLSIVPLMAGGGLFETGAGGSAPKHVKQLIEE 596
M. tuberculosis   DTIAATGNILRDYLTDLFPILELGTSAKMLSVVPLMAGGGMYETGAGGSAPKHVKQLVEE 599
                  *:*:.***:***********:**********:**** ***::************:*: :*
```

```
C. maris          NHLRWDSLGEFLALAASLEHVAVTTGNARAQILADTLDAATGKFLDTNKSPSRKVGELDN 658
34H               NHLRWDSLGEFLALAASLEHVAISTGNAKAQVLADTLDSATGKFLDTNKSPSRRVGELDN 658
A.vinelandii      GYLRWDSLGEFLALAASLEHLGNAYKNPKALVLASTLDQATGKILDNNKSPARKVGEIDN 656
P. psychrophila   NFLRWDSLGEFLALAASLEHLGTTYNNPKALVLAKTLDQATGQFLDNNKSPSRKVGNIDN 656
P. putida KT2440  NFLRWDSLGEFLALAASLEHLGNTYDNPRAKVLANTLDQATGKFLDTNKSPSRKVGGIDN 657
P. aeruginosa     NYLRWDSLGEFLALAVSLEETGIKTGNAKAKLLGKALDEATGKLLDNNKSPSRKVGDIDN 656
34H_2             NHLRWDSLGEFLAISASLEDLGIKQDSAKAKLLAKTLDQATAELLENGKSPSRKTGELDN 656
M. tuberculosis   NHLRWDSLGEFLALGAGFEDIGIKTGNERAKLLGKTLDAAIGKLLDNDKSPSRKTGELDN 659
                  ..***********:...:*. .    . :* :*..:** * .::*:..***:*:.* :**

C. maris          RGSHFYLAMYWAQALAAQTTDTELQASFSSVAQALTKQEEKIVAELNAAQGPAIDLNGYY 718
34H               RGSHFYLAMYWAQAIAEQTTDTDLKESFTGVAQALTKQEEKIVAELNAAQGPAIDVNGYY 718
A.vinelandii      RGSHFYLALYWAQALAAQTEDKELQAQFTGIAKALTDNETKIVGELAAAQGKPVDIAGYY 716
P. psychrophila   RGSHFYLALYWAQALAAQTEDKELQAQFAPVAKAMAENEAKIVAELNAVQGKPVDIGGYY 716
P. putida KT2440  RGSHFYLTLYWAEALAAQTDDAALQARFAPLAKTLAENEATIVAELNAVQGKPADIGGYY 717
P. aeruginosa     RGSHFYLAMYWAQALAAQNEDAELKAHFAPLAKALTEQEATIVAELNAVQGKPAEIGGYY 716
34H_2             RGSHFYLALYWAKALAEQTEDTELQHHFAPLAQSLTENEAAIVSDLTTDQWHSVDIGGYY 716
M. tuberculosis   RGSQFYLAMYWAQELAAQTDDQQLAEHFASLADVLTKNEDVIVRELTEVQGEPVDIGGYY 719
                  ***:***::***: :* *. *  *   *: :*. ::.:*  ** :*   *    :: ***

C. maris          FADTKLAEKAMRPSETFNTILSALL- 743
34H               FADTQLTEKAMRPSETLNTILSALL- 743
A.vinelandii      HPNTDLTSKAIRPSATFNAALAPLA- 741
P. psychrophila   HADADKLSKVMRPSATLNAIIASLV- 741
P. putida KT2440  APDAELTAKVMRPSQTLNSAIAAL-- 741
P. aeruginosa     RSNPELTSKVMRPSATFNAAIDSLA- 741
34H_2             KADAKKIIEIMRPSKCFNEVLAAFK- 741
M. tuberculosis   APDSDMTTAVMRPSKTFNAALEAVQG 745
                    : .     :***  :*  :  .
```

Figure 42. Monomeric isocitrate dehydrogenase multiple alignment using Clustal W. The amino acids that confer $NADP^+$-coenzyme specificity and are responsible for metal (Mg^{2+}, Mn^{2+}) and substrate binding are indicated in shaded pink, light green and blue colors, respectively. The amino acid residues involved in the mesophilic properties of the *P. psychrophila* monomeric IDH are indicated in bold green letters. The amino acid residues that are different from *C. maris*/*C. psychrerythrea* and *P. psychrophila* are shown in bold blue letters (Matsuo *et al.*, 2010). The proposed amino acids responsible for the thermal properties are shown in shaded dark green color (Kobayashi and Takada, 2014). The point mutations realized in this study (pET29-PP_4012mut) are indicated in shaded yellow color. * (asterisk) indicates positions, which have a single, fully conserved residue; : (colon) indicates conservation between groups of strongly similar properties - scoring > 0.5 in the Gonnet PAM 250 matrix; . (period) indicates conservation between groups of weakly similar properties - scoring =< 0.5 in the Gonnet PAM 250 matrix. The database accession numbers are for *C. maris* (BAA03134), *C. psychrerythraea* 34H (AAZ27772/AAZ27953), *P. psychrophila* (BAH80317), *P. aeruginosa* PAO1 (AAG06012), *P. putida* KT2440 (NP_746142), *M. tuberculosis* H37Rv (NP_214580) and *A. vinelandii* (D73443/BAA11169).

4.2.4 Kinetic properties of the purified isocitrate dehydrogenase isozymes

Since several deletion attempts of the monomeric IDH were fruitless, we decided to inactivate its enzymatic activity by site-directed mutagenesis of some of the proposed catalytic sites for the substrate binding (Table 12 and Figures 42-43). Thus, the corresponding conserved residues in *P. putida* KT2440, Ser133, Asn136 and Arg140 were substituted by Ala, resulting in a mutated monomeric *idh* (PP_4012 mut, Figure 43).

To study the properties of the two native isocitrate dehydrogenase isoenzymes of *P. putida* KT2440 and the *idh* mutated version, these enzymes were heterologously overexpressed in *E. coli* using the traditional pET29a vectors (Materials and Methods 3.8.2 section). His-tagged protein versions were used in order to facillitate the proteins

purification process. Four different strains were obtained, a negative control with an empty pET29a plasmid, a pET29a-PP_4011 (that overexpresses the dimeric *icd*), a pET29a-PP_4012 (that overexpresses the monomeric *idh*) and a pET29a-PP_4012mut (that overexpresses the mutated monomeric *idh*).

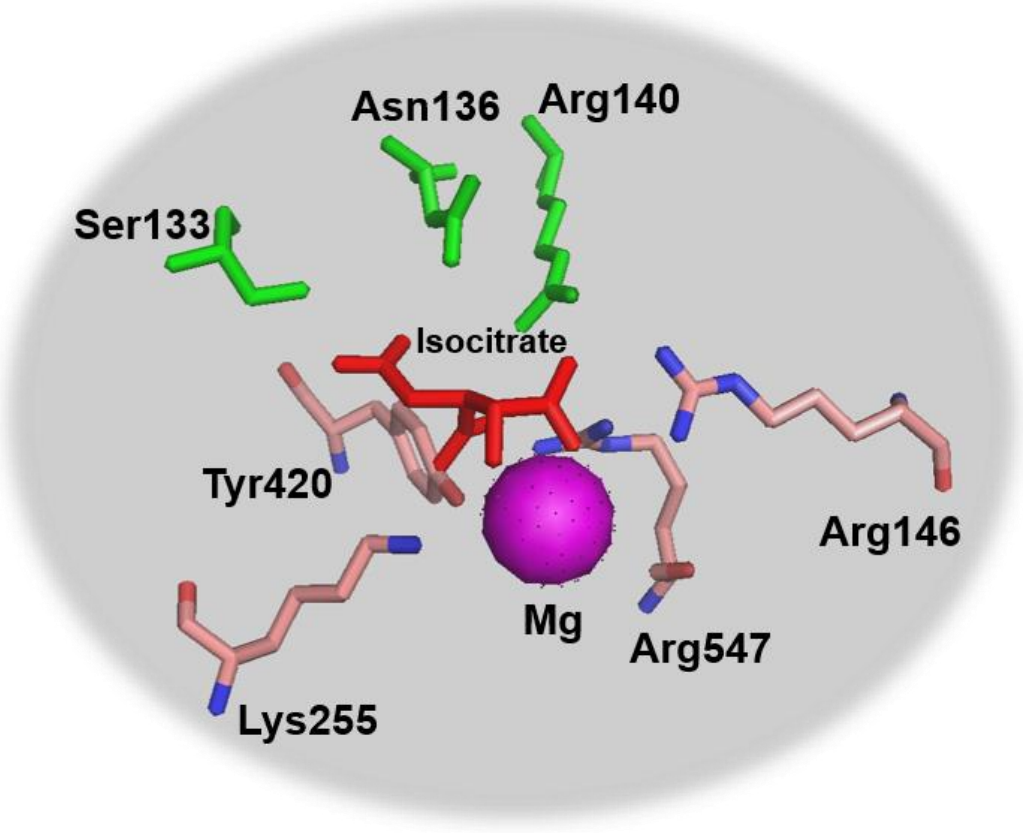

Figure 43. close-up view of the conserved active site residues of monomeric IDH in *P. putida* KT2440 are shown. The residues mutated in this study are shown in green color, the isocitrate in red color and the magnesium in pink color. For rendering and animating 3D structures the pyMol software was used.

The PIDH were successfully purified using the Quiagen Ni-NTA spin columns (Materials and Methods 3.8.2 section and Figure 44). The kinetic parameters for both PIDH were summarized in the Tables 13-14. Under standard assay conditions, the monomeric *idh* had higher specific activity than the dimeric *icd*. This observation is in accordance with previous work in *Pseudomonas psychrophila* (Matsuo *et al.*, 2010). The PP_4012mut (Ser133Ala, Asn136Ala, Arg140Ala) lost completely its enzymatic activity (Table 13). Furthermore, the monomeric *idh* had higher Km values for the isocitrate (56.5 µM) than the dimeric *icd* (34.7 µM). However, the influence of the construction in the monomeric *idh* cannot be discarded as responsible for the higher km values for isocitrate. No major differences were observed as far as it concerns the Km values for the $NADP^+$ on both IDHs (39.7 µM for dimeric versus 22.9 µM for the monomeric IDH). These km values for the $NADP^+$ indicate clear preference towards $NADP^+$, since standard

enzymatic assays with NAD^+, resulted in no detectable activity. Furthermore, the turnover values and catalytic activities for both isocitrate and $NADP^+$ were higher for the monomeric IDH than the dimeric ICD (Tables 13-14).

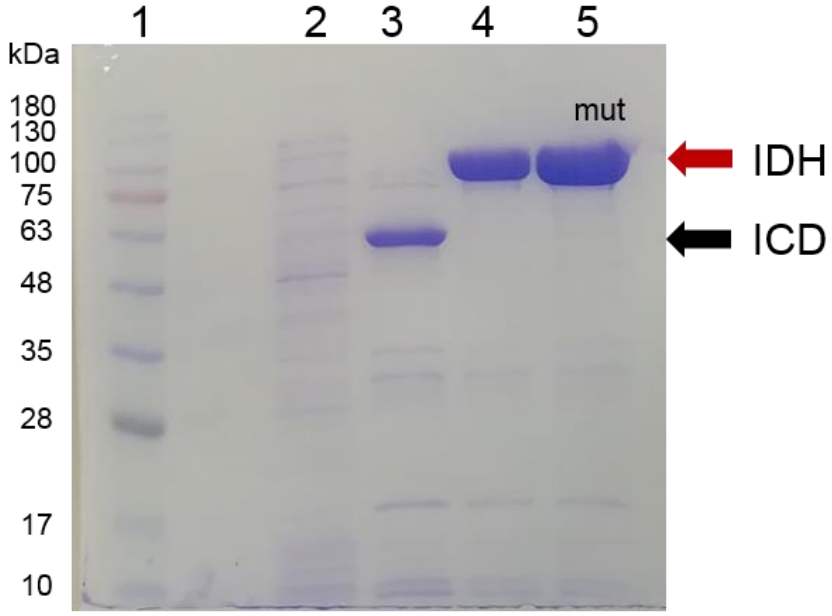

Figure 44. A 12.5% polyacrylamide gel of the purified PIDH using His-trap columns. 1. MW ladder, 2. empty pET29a (negative control), 3. pET29a-PP_4011 (dimeric *icd*), 4. pET29a-PP_4012 (monomeric *idh*), 5. pE29a-PP_4012 mut (monomeric *idh* mut).

Enzyme	Standard assay	Isocitrate			
	Specific activity ($\mu mol\ mg^{-1}\ min^{-1}$)	Km (μM)	Vmax ($\Delta mM/min$)	Kcat (s^{-1})	Kcat/Km ($s^{-1}\ \mu M^{-1}$)
PP_4011	22.4 ± 0.7	34.7 ± 3.0	0.05 ± 0.01	14.5 ± 2.4	0.4 ± 0.1
PP_4012	50.8 ± 6.3	56.5 ± 16.0	0.30 ± 0.04	94.7 ± 19.1	1.7 ± 0.2
PP_4012 mut	N.D.	N.A.	N.A.	N.A.	N.A.

Table 13. Kinetic parameterers for isocitrate at 30°C. The specific activity, the Km, Vmax, kcat and Kcat/Km are listed. N.A.: not determined, N.D.: not detected.

Enzyme	$NADP^+$			
	Km (μM)	Vmax ($\Delta mM/min$)	Kcat (s^{-1})	Kcat/Km ($s^{-1}\ \mu M^{-1}$)
PP_4011	39.7 ± 6.4	0.06 ± 0.01	19.9± 1.6	0.5 ± 0.0
PP_4012	22.9 ± 10.9	0.24 ± 0.05	73.4 ± 8.7	3.9 ± 1.5
PP_4012 mut	N.A.	N.A.	N.A.	N.A.

Table 14. Kinetic parameterers for $NADP^+$ at 30°C. The specific activity, the Km, Vmax, kcat and Kcat/Km are listed. N.A.: not determined.

The unsuccessful attempts to delete the monomeric IDH, could indicate that the activity of this enzyme is essential for growth in *P. putida* KT2440. However, this hypothesis is controversial because the dimeric isoenzymes is actively expressed and it is functional in *P. putida*. Thus, ICD could replace at least in part, the absence of the monomeric enzyme. In order to test whether the reason of the observed essentiality of IDH is other than its enzymatic activity, we tried to inactivate the monomeric IDH in *P. putida* by replacing the native gene by PP_4012mut by using pK18*mobsacB* second recombination process. However, various attempts to substitute the wild type PP_4012 by the mutated PP_4012mut failed and in all the cases the wild type phenotype was rescued. These results thus confirmed the essentiality of the IDH activity in *P. putida*, despite the presence of a functional ICD.

Summing up, in this chapter, we confirmed that both PIDH genes are transcriptionally active in *P. putida* KT2440, with a clear preference towards monomeric *idh* gene. Even though the expression of these enzymes is carbon source dependent, there is no apparent growth effect on the *icd*Δ deletion mutant (MM18). Additionally, by the kinetic properties characterization of the two enzymes, no major differences were observed. However, the results suggested that the monomeric IDH is more active than the dimeric ICD in *P. putida* KT2440. As far as it concerns the catalytic sites for isocitrate binding, Ser133Ala, Asn136Ala and Arg140Ala monomeric IDH mutant lost completely its enzymatic activity. Finally, since various deletions attempts of monomeric *idh* gene have been fruitless, it could be suggested that the monomeric *idh* could be an essential gene for *P. putida* KT2440 growth.

4.3 Chapter 3: Model-driven design and synthetic biology-assisted construction of growth-coupled *P. putida* KT2440 strains overproducing PHA

Introduction

Nowadays, there is an increasing interest in the revalorization of complex and recalcitrant polymers including lignin and oil-based plastics, such as polyethylene terephthalate (PET) and polyurethane (PU) (Danso *et al.*, 2019). Many of these heterogeneous substrates are degraded via the central intermediate protocatechuic acid (PCA) through the β-ketoadipate pathway (Figures 9 and 45). Monomers derived from the hydrolysis of these polymers have an intrinsic value, however the complete revalorization of these compounds require complex and expensive purification steps (Beckham *et al.*, 2016). Therefore, an ideal scenario is the conversion of this complex mix of monomers into a single high-value product such as PHA. These monomers as non-PHA related compounds render low PHA yields by using *de novo* fatty acid synthesis pathway for PHA synthesis (section 1.4.3). Another aspect to consider in the revalorization of these compounds is that these aromatic groups are highly toxic for the cell at high concentrations, thus hampering the traditional PHA production approaches based on unbalanced C/N ratio provoked by nitrogen limitation and carbon excess. Therefore, a new strategy is required in order to revalorize monomers derived from lignin and aromatic-based plastic into PHA.

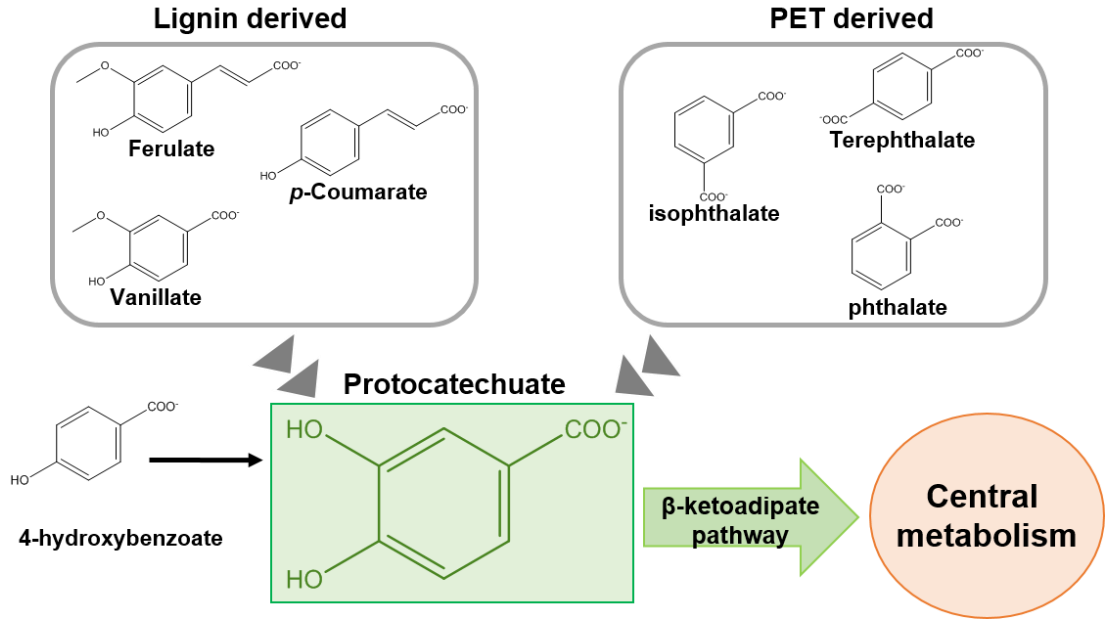

Figure 45. Schematic representation of the approach used in this study. The main aromatic compounds derived from lignin and PET hydrolysis are shown. The protocatechuate is the key intermediate of these compounds connecting with central metabolism.

Often, metabolic engineering endeavors and synthetic biology designs suffer metabolic limitations due to the introduction of non-native biochemical transformations in the host metabolic network, requiring a holistic approach for the final design of the chassis. Genome-scale models (GEMs) and constraint-based reconstruction and analysis (COBRA) methods rely on knowledge of the metabolic network and mass balance during steady state growth to predict the optimal distribution of metabolic flux for growth. Among other applications, GEMs have been shown to be able to predict with high accuracy byproduct secretions, such as in *E. coli* and *S. cerevisiae* (Famili *et al.*, 2003; Hoek and Merks, 2017). In addition, several computational methods have been developed to facilitate the overproduction of a given metabolite. In the context of GEMs, metabolic designs in which the target product must be secreted for optimal growth are called growth-coupled designs, and large number of algorithms have been recently developed to predict and engineer growth-coupled chemical production (King *et al.*, 2017). Growth-coupling is a highly desirable trait as it minimizes the effect of undesirable regulatory constraints, alleviates the genetic instability and selection problems that can result from classical metabolic engineering, and enables the use of adaptive laboratory evolution (ALE) to further increase the production rate (Conrad *et al.*, 2011).

In this Doctoral Thesis, we took the challenge to transform highly recalcitrant substrates derived from the hydrolysis of PET, lignin and PU into high-value added product, PHA. For this purpose, these monomeric constituents were checked using the *in silico i*JN1411 model, for PHA production. Then, the *in silico* designs were further implemented and phenotyped *in vivo*, resulting in *P. putida* KT2440 recombinant growth-coupled PHA overproducing strains from unrelated complex aromatic carbon sources. For the purpose of this work, DBTL cycles were used. These are interactive designs combining the advances in systems and synthetic biology towards rational strain modification and testing (1.3.3 chapter). The details of the two round DBTL cycle used in this work are shown in the Figure 46.

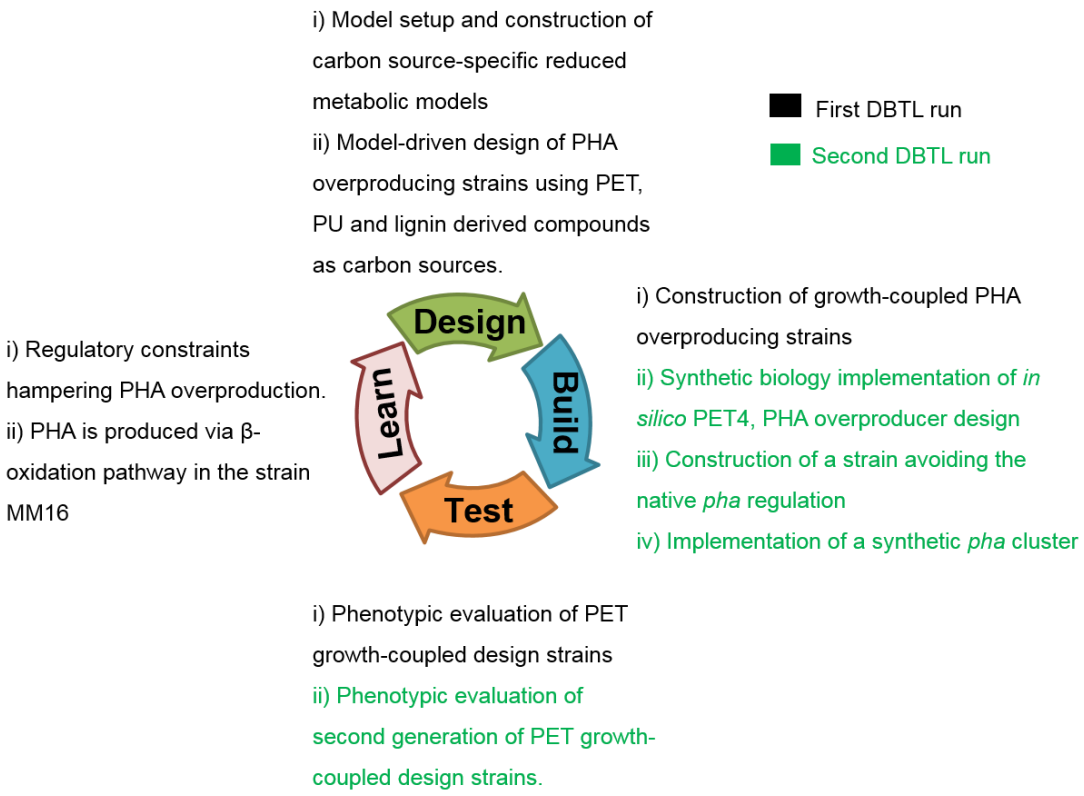

Figure 46. PHA overproducing DBTL cycle. First and second DBTL (Design Build Test Learn) run is shown in black and green colors, respectively.

Results

4.3.1 Model setup and construction of carbon source-specific reduced metabolic models.

The first step of this cycle (Design) included the model-based design of PHA overproducing *P. putida* strains based on growth-coupling using PET and PU as carbon source. It is worth to mention that *P. putida* KT2440 is not able to grow on PET either its monomers derived from hydrolysis, e.g., terephthalic acid (TPHTA) and ethylene glycol (EG) as sole carbon source. During the realization of this work, engineered *P. putida* strains were constructed for efficient EG utilization, shading light on the complex EG processing in *P. putida* KT2440 (Franden *et al.*, 2018).

In order to perform this analysis, the most comprehensive metabolic model of *P. putida* available so far, *i*JN1411 was used (Nogales *et al.*, 2017). *i*JN1411 (https://drive.google.com/file/d/1L-iVLsONX9qiReDmjVgRS_eDTL6sfJa9/view) was updated with the metabolic pathways involved in the metabolism of PET via terephthalate (TPHTA) and ethylene glycol (EG); and PU, via methylene diphenyl diisocyanate (MDI), EG, adipic acid (ADIPATE) and 1,4-butanediol (14DBO) (Figure 47). This update

resulted in the addition of 32 new reactions and 25 new metabolites (https://drive.google.com/file/d/16RK0bcaD9T9Q3V7T4qgoz11SPxpGCCH9/view). The resulting model, named *i*MM1412, was used for the subsequent analysis

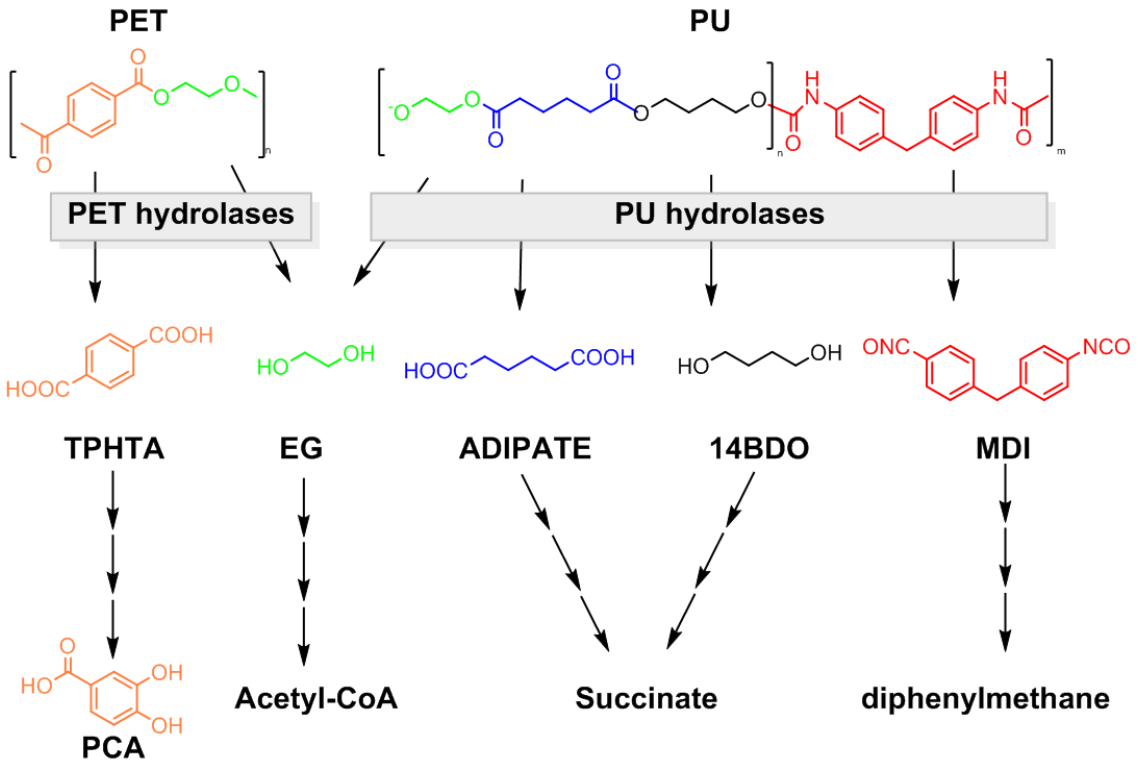

Figure 47. Biochemical overview of PET and PU hydrolysis. PET and PU wastes are depolymerised by PET and PU hydrolases. The resulting hydrolysis products were studied in this work. PET: polyethylene terephthalate, PU: polyurethane, TPHTA: terephthalate, EG: ethylene glycol, ADIPATE: adipic acid, 14BDO: 1,4-butanediol, MDI: 4,4-methylene diphenyl diisocyanate, PCA: protocatechuic acid. This figure was adapted from the P4SB European project (https://www.p4sb.eu/)

Subsequently and in order to reduce the computational complexity of the process, we proceeded to construct a simplified version of *i*MM1412, following the workflow shown in the Figure 48. The reduced model (Figure 48, dark green box) was constructed by applying two consecutive simplification steps e.g., model simplification and model reduction. This simplified model version included a less complex biomass equation and reduced PHA and alginate metabolism, e.g., only the final production of medium-chain length aliphatic PHA containing 8 carbon atoms (C8) and a specific single alginate (alginate with 3 units of acetylated D-mannuronate and 2 units of L-guluronate) were considered. Lumped reactions corresponding to pyruvate dehydrogenase and 2-oxoglutarate dehydrogenase were also removed from the simplified model. TOL plasmid reactions were removed excepting for the case of PU and MDI analyzes, in which reactions involved in complete incorporation of MDI (2-oxopent-4-enoate hydratase and 4-hydroxy-2-oxopentanoate aldolase) were maintained. In the following step the blocked

reactions in each condition were identified (defined as those with a minimum and maximum theoretical flux lower than 10^{-6} mmol·gDW^{-1}·h^{-1}) and removed from the simplified model.

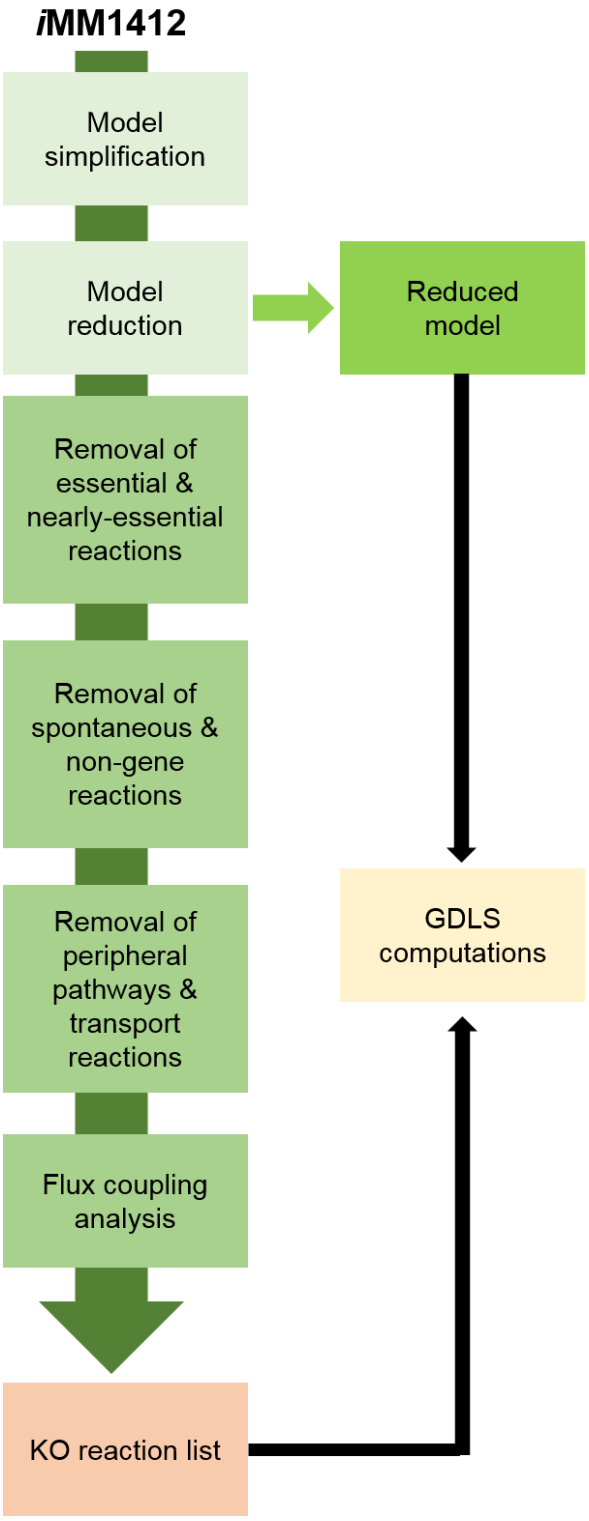

Figure 48. Workflow scheme for model reduction and KO reactions list generation. The reduced model (green box) was constructed by applying two consecutive simplification steps e.g., model simplification and model reduction. The content of these reduced models was dependent of the carbon source used for the analysis (Table 15).

Carbon source	Reduced model (reactions/metabolites)	KO reaction list (reactions)	Uptake ($mmol \cdot gDW^{-1} \cdot h^{-1}$)
PET	1394/1036	252	3.78
TPHTA	1388/1032	256	4.73
EG	1387/1031	283	13.6
PU	1413/1052	252	1.40
ADIPATE	1388/1032	244	6.30
MDI	1396/1039	253	2.52
PAC	1383/1028	238	4.73
14BDO	1389/1033	244	9.45

Table 15. Metabolic content, KO reaction list and uptake rate data for each carbon source-specific reduced model. All uptake values used were taken in order to be equivalent in number of carbons to the *P. putida* glucose uptake (6.3 $mmol \cdot gDW^{-1} \cdot h^{-1}$) (del Castillo *et al.*, 2007).

In order to create a reduced list of target reactions to be deleted, we applied four additional reduction steps including the removement of: i) reactions encoded by essential and/or nearly-essential genes, ii) all reactions without associated genes in the model, iii) peripheral and transport reactions, and iv) the sets of flux-coupled reactions were aggregated as a single reaction. These approaches allowed us to significantly reduce the number of reactions suitable to be deleted. A metabolic content of each carbon source-specific reduced model and the lists of suitable reactions for knockout in each carbon source are listed in the Table 15.

4.3.2 Model-driven design of PHA overproducing strains using PET and PU as carbon source.

We first addressed the identification of growth-coupled *in silico* overproducing PHA designs using PET as sole carbon source. Therefore, the GDLS algorithm was applied using an uptake rate of PET of 3.78 $mmol \cdot gDW^{-1} \cdot h^{-1}$ (Table 15) and the default parameters for GDLS (section 3.10.5). As corresponds with a local search algorithm, in each positive iteration (where target product is predicted to be produced), GDLS keeps those deleted reactions providing product secretion and initiates a new iteration in order to optimize the production. This way, individual paths with increasing number of knockouts are provided in each GDLS run. Following this procedure, several GDLS paths were identified and the most promising in terms of i) PHA yield, ii) Biomass-coupled product yield (BCPY), iii) number of knockouts and iv) physiological feasibility, was selected for further analysis as it is shown in the Figure 49 and Tables 16-17.

GDLS runs			
PET1	PET2	PET3	PET4
RHACOAE80	RHACOAE80	RHACOAE80	RHACOAE80
PHADPC80	PHADPC80	PHADPC80	PHADPC80
CYSS	CYSS	CYSS	CYSS
NACODA	NACODA	NACODA	NACODA
ALDD2x	ALDD2x	ALDD2x	ALDD2x
ENO	ENO	ENO	ICL
GHMT2	GHMT2	GHMT2	ICDHyr
HSK	HSK	HSK	PPCSCT
ICL	ICL	ICL	SUCOAS
	ICDHyr	ICDHyr	ORNCD
	PPCSCT	PPCSCT	PDHbr
	SUCOAS	SUCOAS	PDHcr
	TKT2	TKT2	ABUTD
		ORNCD	ALAR
		PDHbr	UPPN
		PDHcr	RBK
			ALATA_L
			FORGLUIH2
			MALS
			MCITL2
			OARGDC

Table 16. Key reactions identified to knocked out for PHA growth-coupled mutants using PET as carbon source. A signle path with 4 consecutive iterations (PET1-4) is shown. Model reaction abbreviations: ABUTD, aminobutyraldehyde dehydrogenase; ALAR, alanine racemase; ALATA_L, L-alanine transaminase; ALDD2x, aldehyde dehydrogenase acetaldehyde CYSS, cysteine synthase; ENO, enolase; FORGLUIH2, N-formimino-L-glutamate inimohydrolase; ICDHyr, isocitrate dehydrogenase NADP; ICL, isocitrate lyase; MALS, malate synthase; MCITL2, methylisocitrate lyase; NACODA, N-acetylornithine deacetylase; OARGDC, oxoarginine decarboxylase; ORNCD, ornithine cyclodeaminase; PDH, pyruvate dehydrogenase; PHADPC80, poly-3-hydroxyalkanoate depolymerase C80; PPCSCT, propanoyl CoA - succinate CoA-transferase; RBK, ribokinase; RHACOAE80, *R*-hydroxyacyl CoA-thioesterase C80; SUCOAS, succinyl-CoA synthetase ADP-forming; TKT2, transketolase; UPPN, b-ureidopropionase

Subsequently, the production envelopes of the model-driven designs obtained using PET as carbon source were plotted. As it could be expected, the more the number of gene knockouts is increased (from iteration PET1 to PET4), the higher the production of PHA is. Finally, a dynamic simulation of the behaviour of PET4 model (which included up to 21 reaction knockouts) was performed by using FBA analysis (Figure 49B). This simulation provided us with interesting predictions, such as the theoretical growth curve, growth rate, the theoretical PHA production and the biomass coupled product yield

(BCPY), listed in the Table 17. Interestingly, these model-based predictions suggested that a potential *P. putida* strain constructed on PET4 model deletions could accumulate more than 50% of biomass as PHA, even in absence of nitrogen limitation.

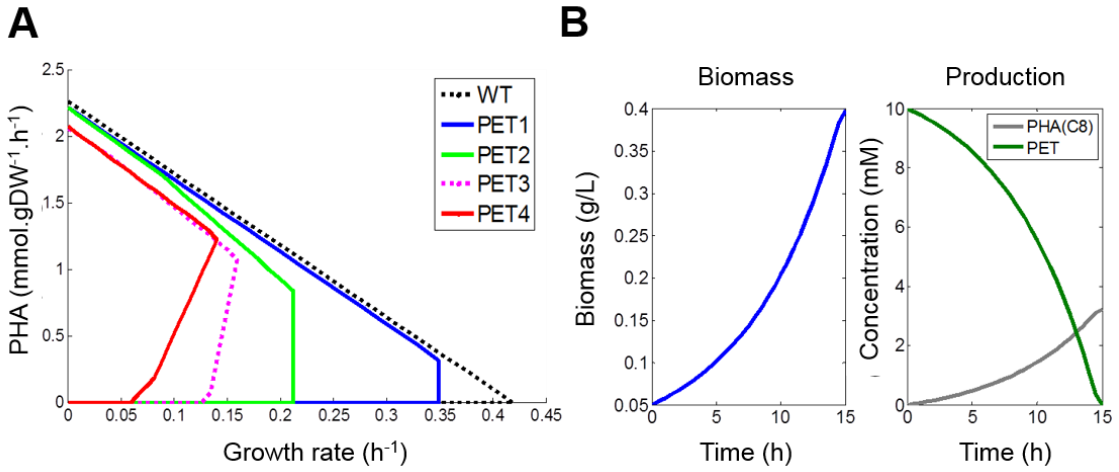

Figure 49. A. Production envelopes for wild-type and PET *P. putida* knockout strains belonging to more promising GDLS path. The production envelopes for each overproducer design are shown as a function of the biomass production rate of the wild-type *P. putida* network using PET as sole carbon source (black lines). PET1 (blue), PET2 (green), PET3 (magenta), PET4 (red). **B.** Production of biomass (blue), PET uptake rate (green) and PHA (grey) as a function of time of design PET4 as predicted with dynamic FBA are shown.

Design	PET1	PET2	PET3	PET4
Uptake rate (mmol·gDW^{-1}·h^{-1})	3.78	3.78	3.78	3.78
Knockouts	9	13	17	21
Growth rate (h^{-1})	0.35	0.21	0.16	0.14
Production Rate (min-max)	0 - 0.32	0 - 0.83	1.07-1.07	1.22-1.22
Residual Biomass (g/L)	1.64	0.56	0.44	0.40
PHA (mM)	N.D.	N.D.	2.82	3.23
PHA Biomass (g/L)	N.D.	N.D.	0.45	0.51
$Y_{p/s}$ (mmol/mmol)	0 - 0.08	0 - 0.22	0.28	0.32
BCPY (mmol·gDW^{-1}·h^{-1})	0 - 0.11	0 - 0.18	0.17	0.17
Biomass PHA (% CDW)	N.A.	N.A.	50.49	56.38

Table 17. Properties of the PHA growth-coupled overproducer designs using PET as substrate at 10 mM (2.26 g/L). (N.A..: not determined, N.D.: not detected). Uptake rate (mmol·gDW^{-1}·h^{-1}); Growth rate (h^{-1}); Production rate (mmol·gDW^{-1}·h^{-1}); $Y_{p/s,}$ Product yield (mmol product/mmol substrate); BCPY, Biomass coupled product yield (mmol·gDW^{-1}·h^{-1}).

Following similar approach, a collection of growth-coupled PHA overproducer designs was obtained using PU and the different metabolites derived from PET and PU hydrolysis, e.g., TPHTA, EG, 14DBO, ADIPATE, and MDI (Figure 50). The production envelopes and the properties of the PHA growth-coupled designs using PET and PU

hydrolysis products are listed in the Supplementary Figures S1-7 and the Supplementary Tables S12-S18. The best growth-coupled designs for each carbon source are shown in the Table 18 and the Figure 50.

Design	PET4	TPHTA4	EG4	PU4	ADIPATE5	14BDO4	MDI5	PAC5
Concentration (mM)	10	10	10	10	10	10	10	10
Knockouts	22	*14	26	*15	*16	*17	*21	*17
Growth rate (h^{-1})	0.14	0.20	0.17	0.34	0.30	0.31	0.25	0.27
Production rate ($mmol.gDW^{-1}.h^{-1}$)	1.22	1.22	0.53	1.07	1.64	1.63	1.16	1.35
Residual Biomass (g/L)	0.40	0.44	0.16	2.09	0.47	0.33	0.93	0.56
PHA Biomass (g/L)	0.51	0.32	0.06	1.22	0.43	0.27	0.73	0.46
$Y_{p/s}$ (mol/mol)	0.32	0.26	0.04	0.76	0.26	0.17	0.46	0.28
$Y_{p/s}$ (g/g)	0.23	0.20	0.10	0.25	0.30	0.30	0.29	0.34
Biomass PHA (% CDW)	56.38	42.16	27.50	36.80	47.46	45.01	44.07	44.87

Table 18. a summarised analysis of growth–coupled designs using different non-sustainable plastic wastes and their monomers, as a sole carbon source. The best designs are represented; PET4 (polyethylene terephtalate), TPHTA4 (terephthalate), EG4 (ethylene glycol), PU4 (polyurethane), ADIPATE5 (adipic acid), 14BDO4 (1, 4-butanediol), MDI5 (4, 4´-methylene diphenyl diisocyanate), PAC5 (phenylacetic acid). In the table, the concentration of each substrate and the needed knockouts in order to be able to produce polyhydroxyalkanoates (PHA) were indicated. Additional physiological parameters are shown such as growth rate, production rate, residual biomass (biomass free of PHA), PHA (g/L or %), Y p/s. * Indicates additional flux constraints.

Due to the heterogeneity of substrates used, the ambitiousness of the final goal and the completeness of our metabolic model, a large number of knockouts, ranging from 14 in the case of TPHTA to 26 for EG, were needed in order to achieve PHA growth-coupled designs (Table 18 and Figure 50, shown in black squares). Similarly, a large diversity was found in terms of the final yields, BCPY and amount of PHA produced. On average, the growth-coupled designs accumulated more than 40% of their biomass in form of PHA with the highest PHA% reached by PET4 design (Table 18). Therefore, the PHA growth-coupled designs present here represent an encouraging starting point for their further implementation *in vivo*.

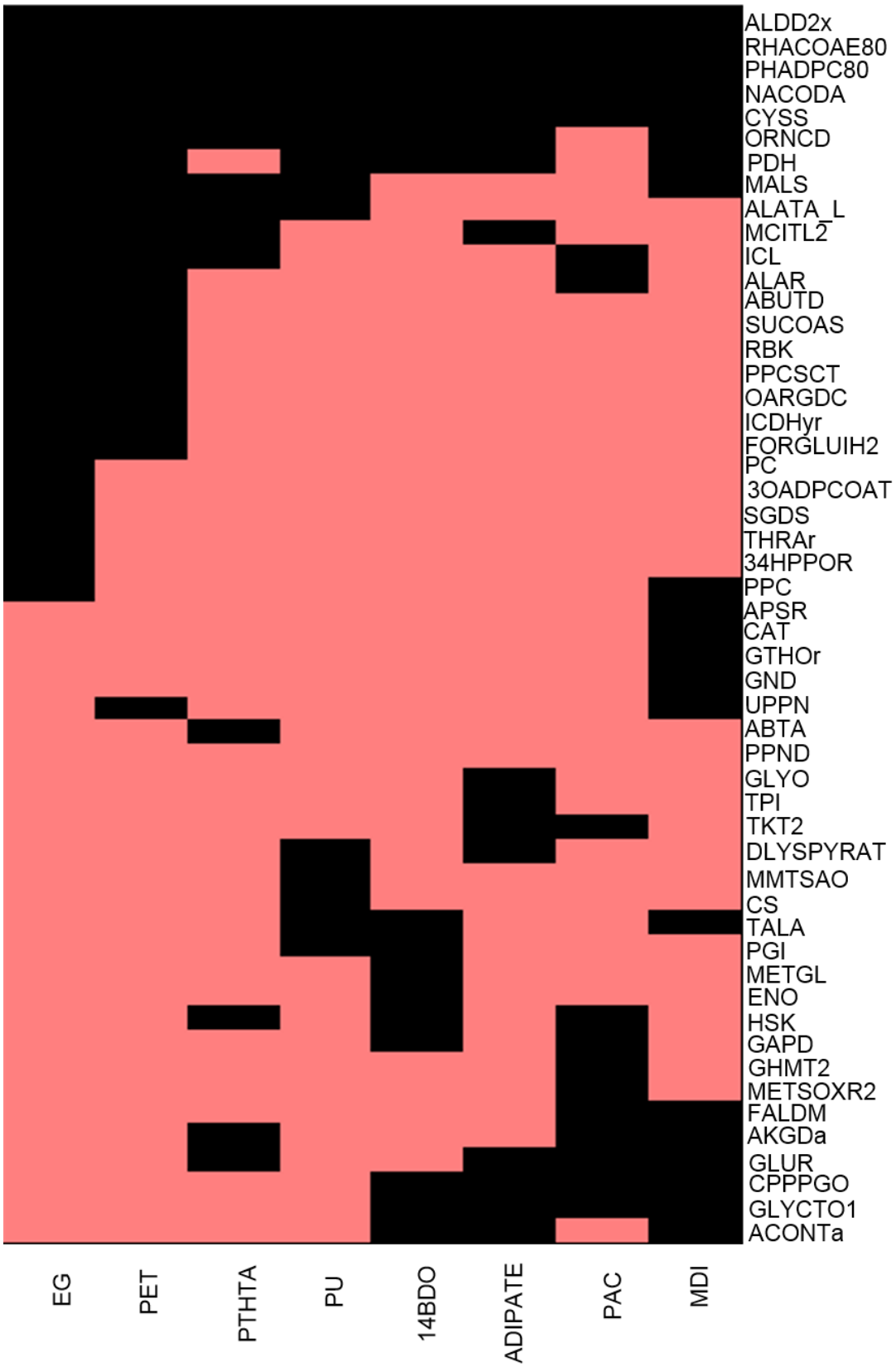

Figure 50. Clustering of the reactions required to be deleted (knockouts) in order to achieve the growth-coupled production of PHA in *P. putida* KT2440 using PET, PU and their derived substrates as carbon sources. The reactions removed in each carbon source are shown in black, while the one maintained are shown in red color. Model reaction abbreviations: 34HPPOR, 4

hydroxyphenylpyruvateoxygen oxidoreductase; 3OADPCOAT, 3-oxoadipate CoA-transferase; ABTA, 4 aminobutyrate transaminase; ABUTD, aminobutyraldehyde dehydrogenase; ACONTa, aconitase half reaction A citrate hydro lyase; AKGDa, oxoglutarate dehydrogenase lipoamide; ALAR, alanine racemase; ALATA_L, L-alanine transaminase; ALDD2x, aldehyde dehydrogenase acetaldehyde NAD; APSR, adenosine 5-phosphosulfate reductase; CAT, catalase; CPPPGO, coproporphyrinogen oxidase; CS, citrate synthase; CYSS, cysteine synthase; DLYSPYRAT, D-lysinepyruvate aminotransferase; ENO, enolase; FALDM, formaldehyde dismutase; FORGLUIH2, N-formimino-L-glutamate inimohydrolase; GAPD, glyceraldehyde 3-phosphate dehydrogenase; GHMT2, glycine hydroxymethyltransferase; GLUR, glutamate racemase; GLYCTO1, glycolate oxidase; GLYO, glycine oxidase; GND, phosphogluconate dehydrogenase; GTHOr, glutathione oxidoreductase; HSK, homoserine kinase; ICDHyr, isocitrate dehydrogenase NADP; ICL, isocitrate lyase; MALS, malate synthase; MCITL2, methylisocitrate lyase; METGL, methionine g-lyase; METSOXR2, L-methionine R-sulfoxide reductase; MMTSAO, S-methylmalonate semialdehydeNAD oxidoreductase CoA-propanoylating; NACODA, N-acetylornithine deacetylase; OARGDC, oxoarginine decarboxylase; ORNCD, ornithine cyclodeaminase; PC, pyruvate carboxylase; PDH, pyruvate dehydrogenase; PGI, glucose 6-phosphate isomerase; PHADPC80, poly-3-hydroxyalkanoate depolymerase C80; PPC, phosphoenolpyruvate carboxylase; PPCSCT, propanoyl CoA -succinate CoA-transferase; PPND, prephenate dehydrogenase; RBK, ribokinase; RHACOAE80, R-hydroxyacyl CoA-thioesterase C80; SGDS, succinylglutamate desuccinylase; SUCOAS, succinyl-CoA synthetase ADP-forming; TALA, transaldolase; THRAr, threonine aldolase; TKT2, transketolase; TPI, triose phosphate isomerase; UPPN, b-ureidopropionase.

Despite the diversification of the reactions deleted, in order to achieve the overproduction of PHA in each substrate, common patterns were found. For instance, the deletion of the reactions ALDD2x, RHACOAE80, PHADPC80, NACODA, ORNCD, PDH and CYSS was required in all cases, suggesting that the deletion of these reactions is needed to achieve the overproduction of PHA and that they would be the first reactions to be deleted *in vivo*. In addition, a set of deletions were specific of PET and its derived substrates such as MALS, ALATA_L, MCITL2 and ICL; while others were specific of PU and derived substrates e.g., TALA, AKGDa and GLUR. Therefore, these sets of reactions point the way for the *in vivo* implementation of PET- and PU-based PHA growth-coupled strains, respectively. For model reaction abbreviation see the footnote of the Figure 50.

Taken together, it could be concluded that PET4 design was the best growth-coupled design as far as it concerns the PHA (%) production (Table 18). Even though high PHA production was also obtained from PU and its monomers, PU´s composition variability would complicate its *in vivo* implementation. Furthermore, taking into account the feasibility of PET degradation and the advanced research on PET hydrolases, the PET4 is a promising design for further *in vivo* implementation (Wierckx *et al.*, 2018; Belisário-Ferrari *et al.*, 2019; Danso *et al.*, 2019; Salvador *et al.*, 2019). Finally, the PET4 design served for growth-coupled PHA production from simpler carbon sources derived

from lignin and PET hydrolysis (Figure 51). Therefore, the PET4 design was chosen for further *in vivo* validation.

Finally, in order to increase the scope of above growth-coupled designs to additional carbon sources, other than those already tested (PET, TPHTA, EG, 14DBO, ADIPATE, MDI and PAC), we tested the feasibility of the different designs for overproducing PHA by using the complete set of carbon sources supporting *i*JN1411 growth.

As an example, the carbon sources allowing growth of PET4 design when compared to the wild type model were shown (Figure 51). As it would be expected, the PET4 strain exhibited a reduced metabolic versatility. For instance, since glyoxylate shunt was deleted, PET4 strain was unable to grow on fatty acids as carbon sources. It was also observed that from the carbon sources supporting PET4 strain growth, only a few of them allowed growth-coupled PHA production (Figure 51, graph below). Interestingly, the most of the compounds allowing PHA production were aromatic compounds. The most promising were PU-derived metabolites, such as phenyl acetic acid related compounds (red), followed by the lignin-derived carbon source (in orange, such as ferulic acid) and the PET derived metabolites (in green, such as 4-hydroxybenzoic acid, vanillic acid and protocatechuic acid).

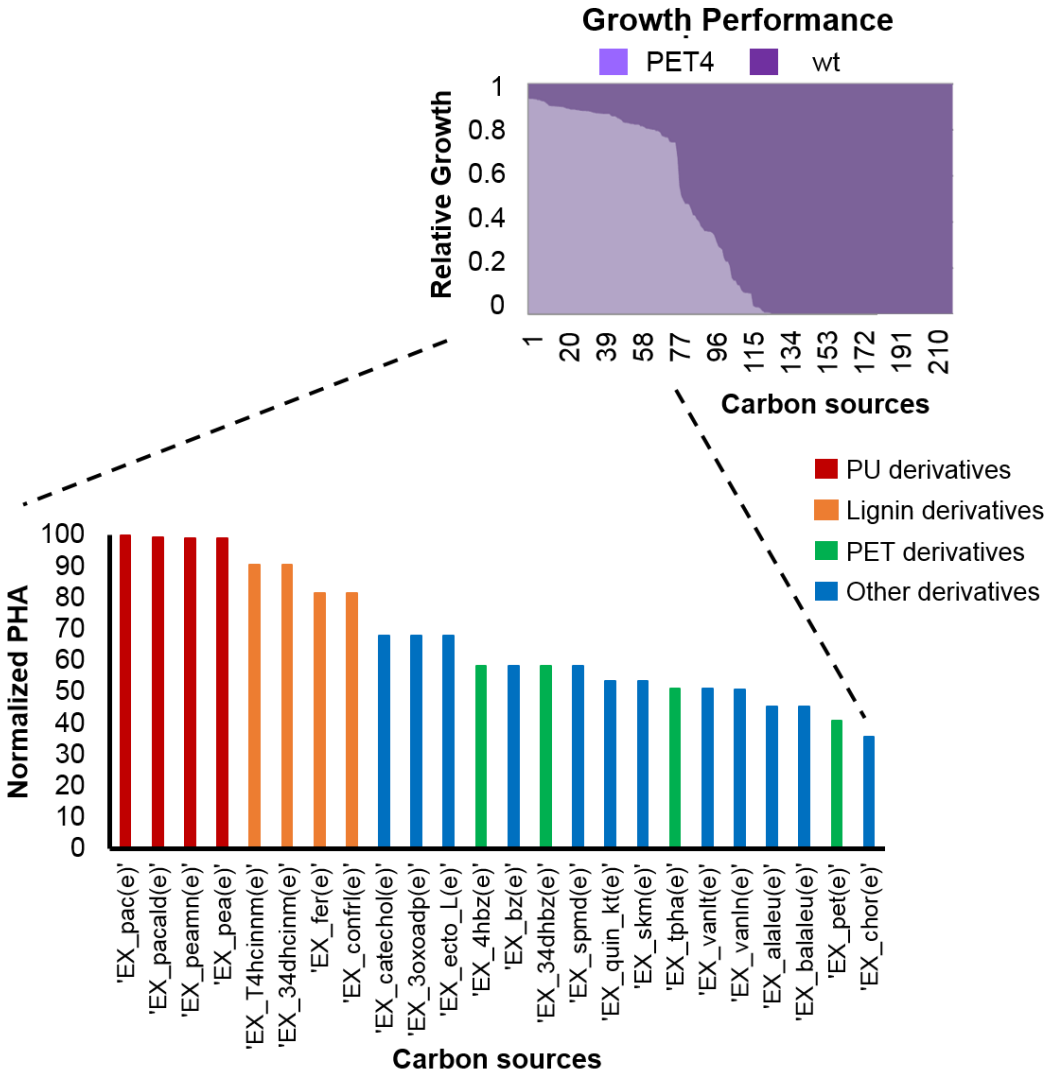

Figure 51. The growth performance of the PET4 strain (light purple) versus the wild type (dark purple) strain after *in silico* comparison of almost 210 carbon sources is shown. The PHA produced was normalized to the number of carbons of each substrate used in this analysis. From the carbon sources supporting PET4 growth, only a few allow growth-coupled PHA production (graph below). From these, PU like compounds (in red) are the more promising carbon sources. The lignin derived (in orange), the PET derived (in green) and other derivatives (in blue) are shown. The uptake rate for all the carbon sources was 5 mmol·gDW^{-1}·h^{-1}. For the PHA production normalization, the number of carbons of each substrate was taken into account. Model reaction abreviations: 'EX_pac(e)', Phenylacetic acid exchange; 'EX_pacald(e)', Phenylacetaldehyde exchange; 'EX_peamn(e)', Phenethylamine exchange; 'EX_pea(e)', Phenylethylalcohol exchange; 'EX_T4hcinnm(e)', trans 4 Hydroxycinnamate exchange; 'EX_34dhcinm(e)', 3 4 Dihydroxy trans cinnamate exchange; 'EX_fer(e)', Ferulate exchange; 'EX_confrl(e)', Coniferol exchange; 'EX_catechol(e)', Catechol exchange; 'EX_3oxoadp(e)', 3 Oxoadipate exchange; 'EX_ecto_L(e)', L Ectoine exchange, 'EX_4hbz(e)', 4 Hydroxybenzoate exchange; 'EX_bz(e)', Benzoate exchange; 'EX_34dhbz(e)', 3 4 Dihydroxybenzoate exchange; 'EX_spmd(e)', Spermidine exchange; 'EX_quin_kt(e)', Quinate exchange; 'EX_skm(e)', Shikimate exchange; 'EX_tpha (e)', Exchange terepthalate; 'EX_vanlt(e)', Vanillate exchange; 'EX_vanln(e)', Vanillin exchange; 'EX_alaleu(e)', L alaninylleucine exchange; 'EX_balaleu(e)', beta alanyl L leucine exchange; 'EX_pet(e)', PET Exchange; 'EX_chor(e)', chorismate exchange.

4.3.3 Synthetic Biology implementation of *in silico* PET4 PHA overproducer design.

The complete PET4 design was based on the deletion of 21 reactions, making challenging its *in vivo* implementation due to the large number of genetic modifications required. As a first step, a manual curation of PET4 design was performed, in order to identify the minimal number of knockouts still resulting in an efficient growth-coupled design. By this effort, the importance of each reaction towards growth-coupled PHA production was evaluated (Table 19). Some reactions including RHACOAE80, PHADPC80 among others, showed a dispensable behaviour for PHA production. Furthermore, the deletion of UPPN and ALATA_L reactions resulted in slight decrease in the PHA content and the PDH reaction showed a moderate decrease in the PHA production. Overall, from the initial list of 21 reaction knockouts required, only 9 reactions deletion were identified as completely essential for growth-coupled PHA production. Based on this analysis, it was feasible the identification of three possible growth-coupled designs accounting for an increasing number of knockouts, minimal, medium and complete (Figure 52 and Table 19). We proceeded to plot the production envelopes of each design in order to visualize the phenotype of these different *in silico* knockout strains (Figure 52). The production envelope of the wild type model is shown in black, while the minimal, medium and complete designs are shown in red, blue and green color, including 9, 12 and 21 knockouts, respectively. Despite the significant lower number of knockouts of the minimal design, it keeps the ability to overproduce a significant amount of PHA, so close as the complete design does.

Design		
Complete (function)	medium	minimal
RHACOAE80 (dispensable)	RHACOAE80	PHADPC80
PHADPC80 (dispensable)	PHADPC80	FORGLUIH2
FORGLUIH2 (essential)	FORGLUIH2	ICL
ICL (essential)	ICL	ICDHyr
ICDHyr (essential)	ICDHyr	MALS
MALS (essential)	MALS	MCITL2
MCITL2 (essential)	MCITL2	ORNCD
ORNCD (essential)	ORNCD	PPCSCT
PPCSCT (essential)	PPCSCT	SUCOAS
SUCOAS (essential)	SUCOAS	
CYSS (dispensable)	CYSS	
NACODA (dispensable)	NACODA	

UPPN (slight *pha* reduction)
RBK (dispensable)
OARGDC (dispensable)
ABUTD (dispensable)
ALATA_L (slight *pha* reduction)
ALDD2x (dispensable)
PDH (moderate *pha* reduction)
PDHbr (moderate *pha* reduction)
PDHcr (moderate *pha* reduction)

Table 19. Key reactions identified to knocked out for PHA growth-coupled mutants using PET as carbon source. The importance of each reaction to PHA production was validated by manual curation process and indicated in the complete model. Model reaction abbreviations: ABUTD, aminobutyraldehyde dehydrogenase; ALAR, alanine racemase; ALATA_L, L-alanine transaminase; ALDD2x, aldehyde dehydrogenase acetaldehyde CYSS, cysteine synthase; ENO, enolase; FORGLUIH2, N-formimino-L-glutamate inimohydrolase; ICDHyr, isocitrate dehydrogenase NADP; ICL, isocitrate lyase; MALS, malate synthase; MCITL2, methylisocitrate lyase; NACODA, N-acetylornithine deacetylase; OARGDC, oxoarginine decarboxylase; ORNCD, ornithine cyclodeaminase; PDH, pyruvate dehydrogenase; PHADPC80, poly-3-hydroxyalkanoate depolymerase C80; PPCSCT, propanoyl CoA-succinate CoA-transferase; RBK, ribokinase; RHACOAE80, *R*-hydroxyacyl CoA-thioesterase C80; SUCOAS, succinyl-CoA synthetase ADP-forming; TKT2, transketolase; UPPN, b-ureidopropionase

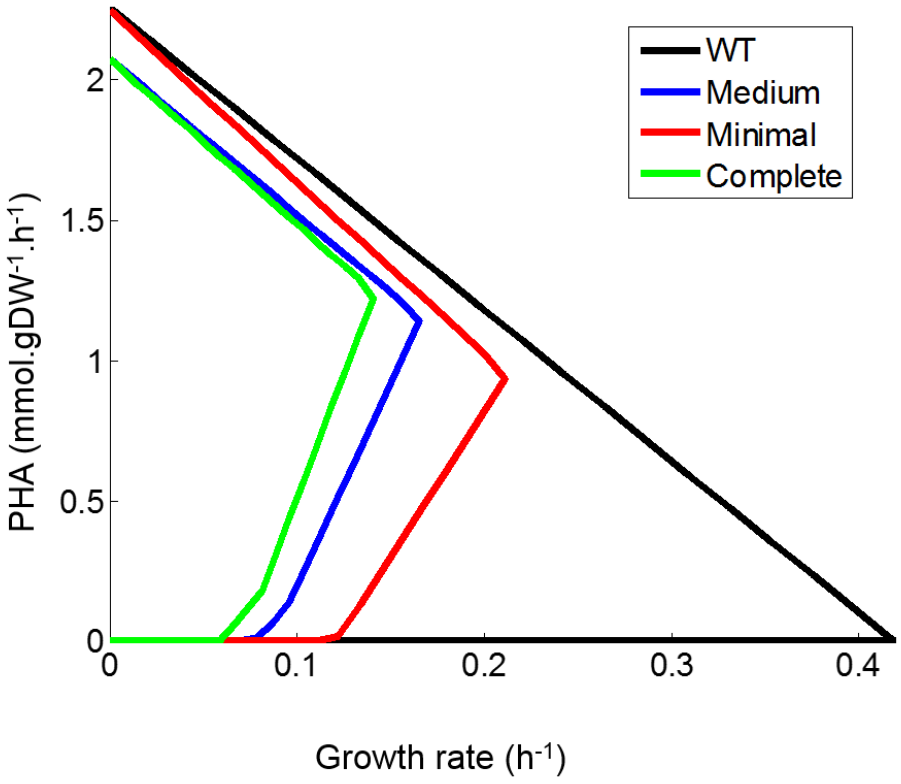

Figure 52. Manual curation of PET4 optimal design. Flux through PHA versus growth rate is represented. The wild type (in black), minimal (in red), medium (in blue) and complete (in green) designs are shown.

Therefore, the minimal´s PET4 design was used as a starting point for the *in vivo* implementation. These reactions were blocked sequentially by deleting the corresponding coding gene(s). We relied on a system for individual gene deletions (pK18*mobsacB*) and in order to accumulate all the necessary deletions in a single strain many successive rounds were performed (section 3.4.4). A logical order to delete the genes was planned based on the predicted weight of each deletion on PHA production (Table 20 and Figures 53-54). In order to facilitate the understanding, a workflow of the mutants construction is shown in the Figure 53.

Reaction deletion order	Reaction	Pathway	Annotation	Gene name(s)
1	2-methylisocitrate lyase	Succinate	PP_2334	*mmgF*
2	Propionyl-CoA:succinate-CoA transferase	Succinate	PP_0154	*scpC*
3	Succinyl-CoA synthetase subunit alpha/ beta	Succinate	PP_4185, PP_4186	*sucC, sucD*
4	Isocitrate lyase	Gyoxylate	PP_4116	*aceA*
5	Malate synthase G	Gyoxylate	PP_0356	*glcB*
6	Isocitrate dehydrogenase	TCA cycle	PP_4011, PP_4012	*icd, idh*
7	PHA depolymerase	PHA	PP_5004	*phaZ*
8	Ornithine cyclodeaminase	Amino acid metabolism	PP_3190, PP_3533, PP_4431	*ocd*
9	Formiminoglutamate deiminase	Amino acid metabolism	PP_5036	*hutF*

Table 20. Reactions and their corresponding genes deletd to achieve the PET growth-coupled design strain.

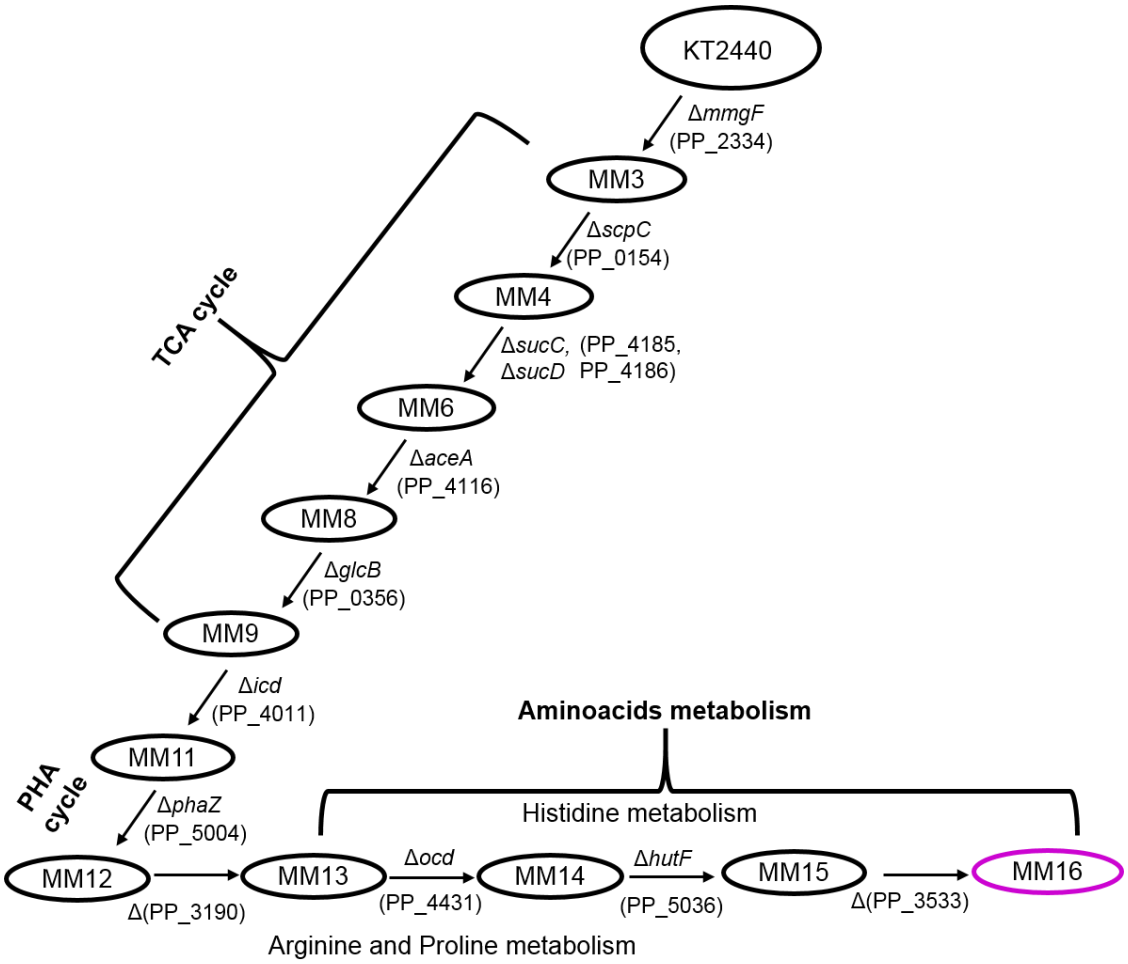

Figure 53. Workflow of the mutants' strategy construction. The obtained deletion mutants in *P. putida* KT2440 background called as MMxxx were shown.

In the *in silico* PET design strain, PET is degraded into TPHTA and EG with the action of PET hydrolases. TPHTA is catabolized via PCA and then into succinate and acetyl-CoA, while EG is assumed to be metabolized via acetyl-CoA (Figure 47). A detailed analysis of PET4 minimal design showed that PHA overproduction relies on blocking oxidation of succinate and acetyl-CoA at tricarboxylic acid cycle (TCA). According to model predictions, succinate was used as biomass building block and energy source via glycine oxidation, while acetyl-CoA was used mainly as a PHA precursor via PHA *de novo* fatty acid biosynthesis (Figure 54).

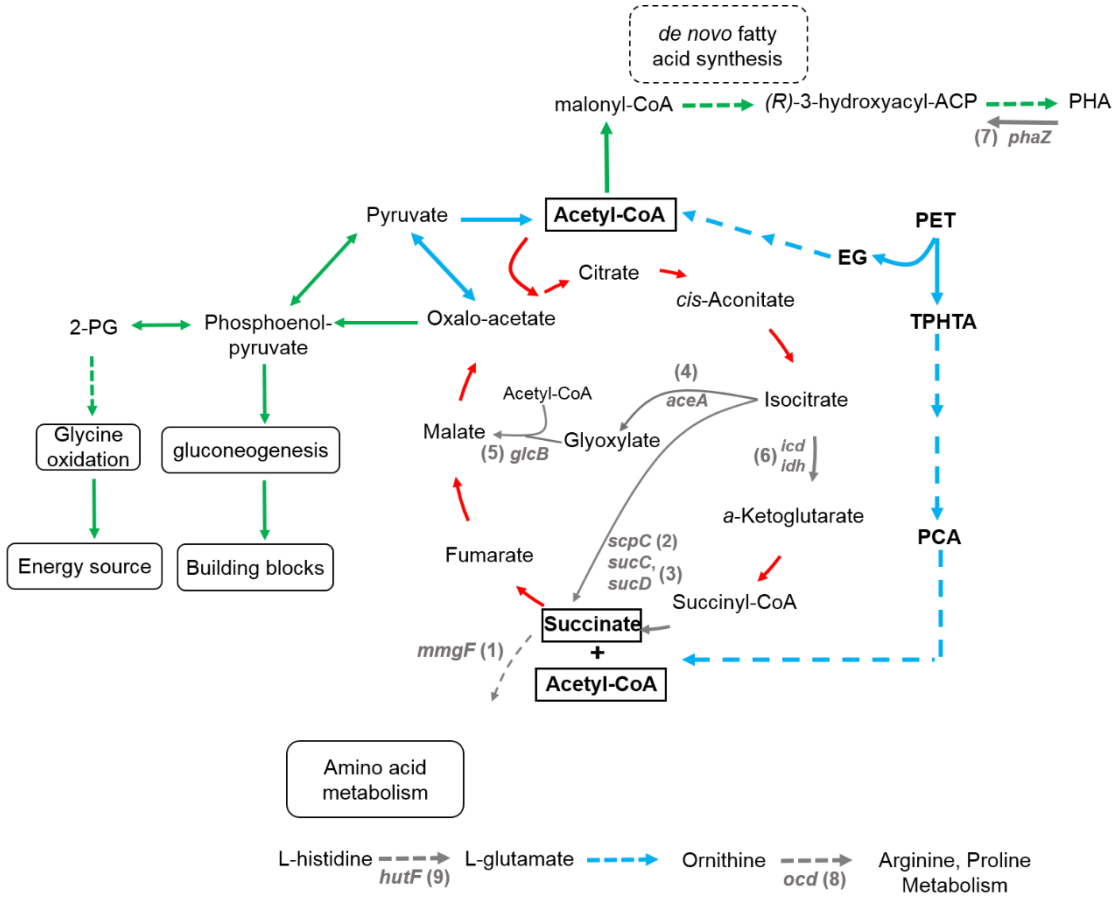

Figure 54. Predicted Carbon Flux Distribution in PET-growth optimized minimal design. The deleted reactions (in gray), the increased flux reactions (in green), the reduced flux reactions (in red) and the unaffected fluxes (in blue) are shown.

Therefore, the first three reactions deleted were those responsible of blocking in succinate metabolism, 2-methylisocitrate lyase, propionyl-CoA:succinate-CoA transferase and succinyl-CoA synthetase subunit alpha/beta (Figure 55). The next reactions knocked out were responsible of glyoxylate cycle, isocitrate lyase and malate synthase (Figure 56). Glyoxylate cycle is a variation on the TCA cycle in charge of the biosynthesis of 4-carbon metabolites from acetyl-CoA (Introduction 1.4.2.5 section). The subsequent deletion was the isocitrate dehydrogenase, that when taken together with the five previous deletions, it was expected to eliminate a substantial portion of the carbon flux through the TCA cycle (Figure 57). The seventh reaction that was sequentially deleted was the PHA depolymerase, PhaZ, which was expected to allow for increased PHA accumulation. However, the single *phaZ* mutant was made and has already been under active phenotypic investigation in our lab (Results chapter 1 and Figure 23, for mutant construction details). The last deletions were required in order to avoid alternative metabolism of acetyl-CoA and acetate secretion via amino acid

metabolism (Figure 58-59). The deletion strategy for all the knockout mutants and the remaining nucleotide sequence after the deletion is shown (Figures 55-59).

- **Blocking Succinate Metabolism**

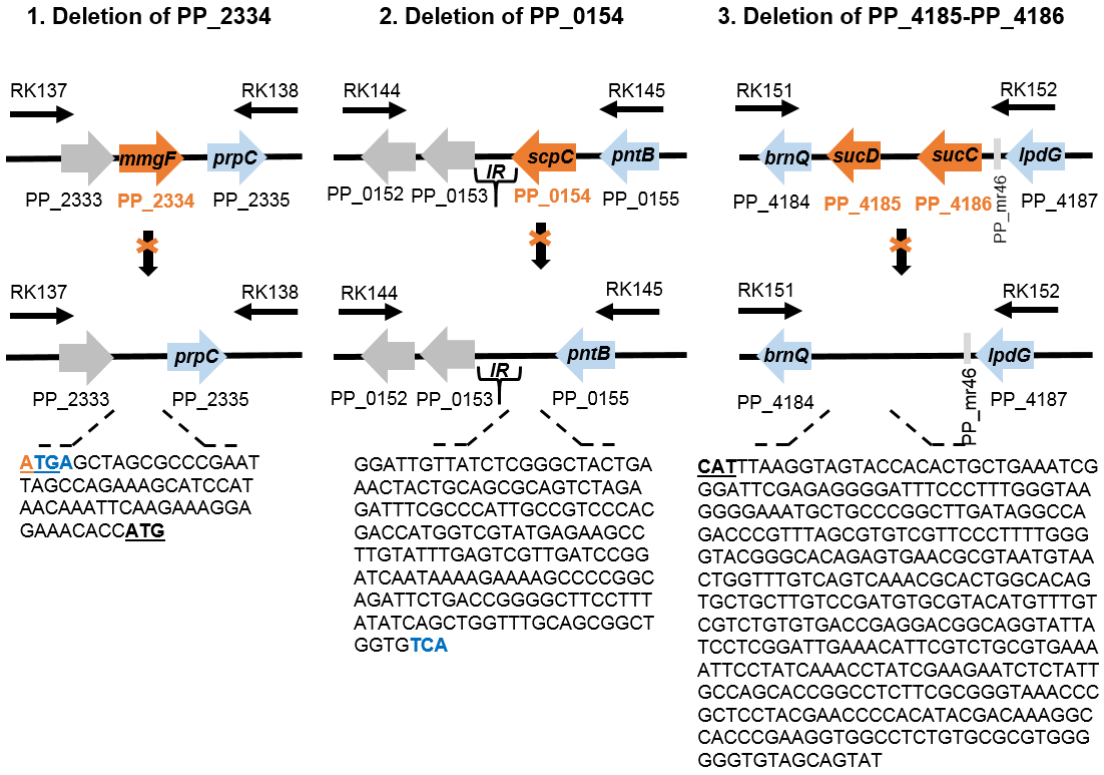

Figure 55. Succinate metabolism reactions deletion strategy. The deleted gene products at their corresponding locus are shown. The arms of homology used for recombinatorial deletion of each gene consist of the flanking upstream and downstream genes. Arrows above indicate the annealing location for primers used for colony PCR following the second recombination event to confirm the gene deletion. The remaining nucleotide sequence after the deletion is shown. The stop codons, the start codons are shown with bold blue and bold underlined, respectively. The remaining nucleotides of the deleted genes are shown in orange color. IR: intergenic region.

- **Blocking glyoxylate shunt**

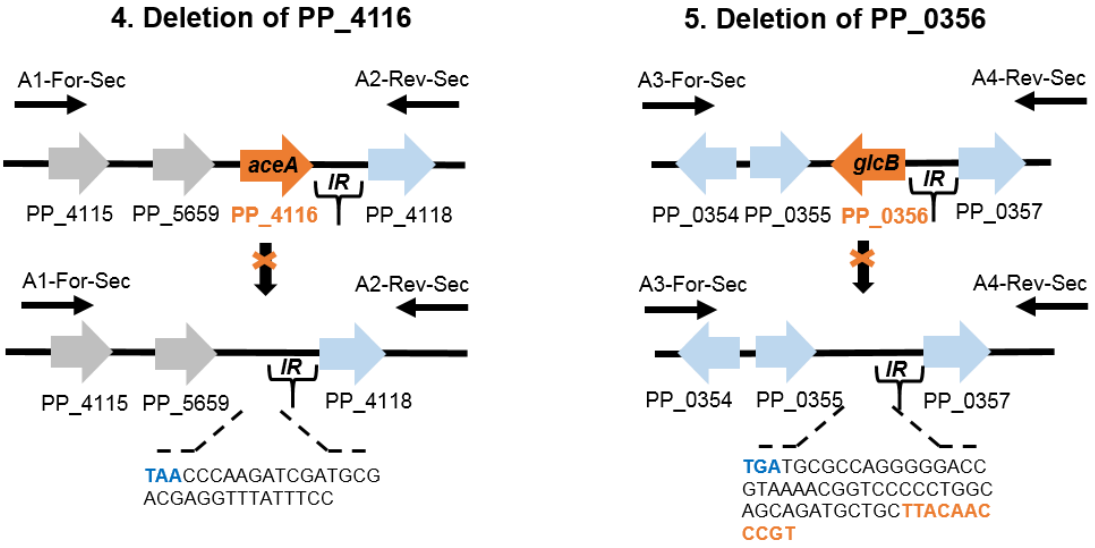

Figure 56. Glyoxylate shunt reactions deletion strategy. The deleted gene products at their corresponding locus are shown. The arms of homology used for recombinatorial deletion of each gene consist of the flanking upstream and downstream genes. Arrows above indicate the annealing location for primers used for colony PCR following the second recombination event to confirm the gene deletion. The remaining nucleotide sequence after the deletion is shown. The stop codons, the start codons are shown with bold blue and bold underlined, respectively. The remaining nucleotides of the deleted genes are shown in orange color. IR: intergenic region.

- **Blocking Isocitrate dehydrogenase**

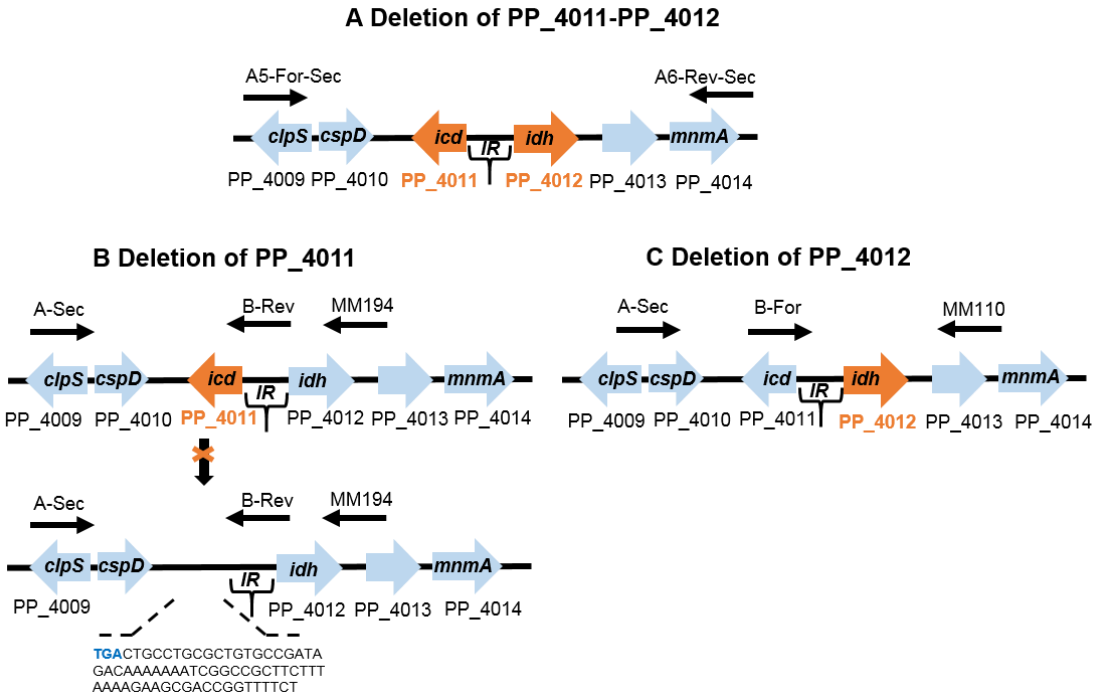

Figure 57. isocitrate dehydrogenase reaction deletion strategy. A. deletion strategy for both PP_4011 and PP_4012, **B.** deletion strategy for PP_4011 and **C.** deletion strategy for PP_4012. The deleted gene

products at their corresponding locus are shown. The arms of homology used for recombinatorial deletion of each gene consist of the flanking upstream and downstream genes. Arrows above indicate the annealing location for primers used for colony PCR following the second recombination event to confirm the gene deletion. The remaining nucleotide sequence after the deletion is shown. The stop codons are shown with bold blue color. IR: intergenic region.

- **Blocking Amino acids metabolism**

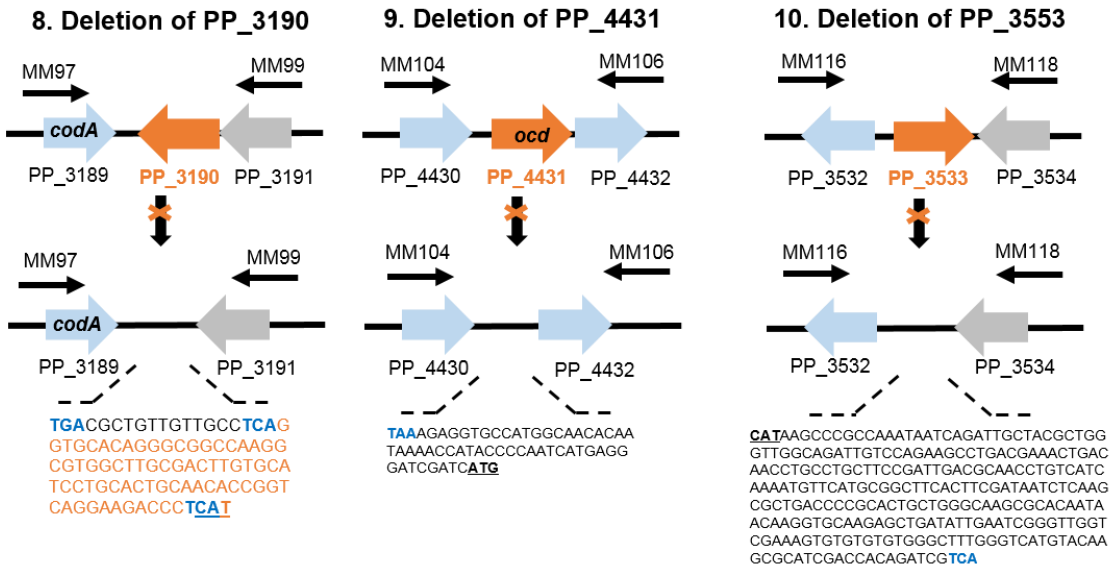

Figure 58. Ornithine cyclodeaminase reactions deletion strategy. The deleted gene products at their corresponding locus are shown. The arms of homology used for recombinatorial deletion of each gene consist of the flanking upstream and downstream genes. Arrows above indicate the annealing location for primers used for colony PCR following the second recombination event to confirm the gene deletion. The remaining nucleotide sequence after the deletion is shown. The stop codons, the start codons are shown with bold blue and bold underlined, respectively. The remaining nucleotides of PP_3190 are shown with orange color.

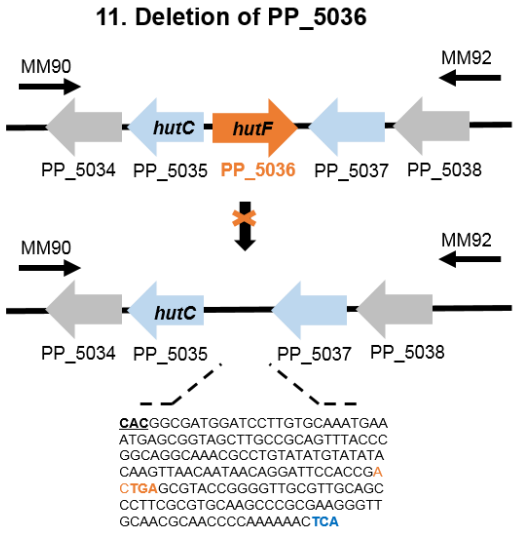

Figure 59. Formiminoglutamate deiminase reaction deletion strategy. The deleted gene products at their corresponding locus are shown. The arms of homology used for recombinatorial deletion of each gene

consist of the flanking upstream and downstream genes. Arrows above indicate the annealing location for primers used for colony PCR following the second recombination event to confirm the gene deletion. The remaining nucleotide sequence after the deletion is shown. The stop codons, the start codons are shown with bold blue and bold underlined, respectively. The remaining nucleotides of PP_5036 are shown with orange color.

4.3.4 Phenotypic evaluation of PET growth-coupled design strains.

Once the strains were constructed, the ideal scenario was to phenotypically evaluate their growth and PHA production capabilities under similar conditions to those previously simulated (PET). However, as we mentioned previously, *P. putida* KT2440 is not able to grow on PET either its monomers derived from hydrolysis, e.g., terephthalic acid (TPHTA) and ethylene glycol (EG) as carbon source. Thus, as a potentially equivalent substrate to the simulated conditions, protocatechuic acid (PCA) was chosen. PCA is an intermediate of TPHTA or PET degradation process (Figures 47 and 54). Since PCA is a very unstable substrate, due to its rapid oxidation in working conditions, sodium 4-hydroxybenzoate (4HBz) was used instead, which is metabolized in *P. putida* via PCA (Figure 9).

Phenotypic evaluation of MM16 strain was carried out by assessing growth on microtiter and batch growth experiments. The growth and PHA production capabilities of MM16 strain were monitored under both balanced and nitrogen limitation conditions. Some growth performance paramenters were monitored such as the growth rate, lag phase and maximum optical density reached (Table 21). As a control, wild type and KT40Z strains were used. MM16 strain exhibited a significantly higher lag phase in both conditions of growth when compared with the wild type and KT40Z strains. Under balanced conditions, MM16 strain showed a decrease in growth rate.

Using this strategy and under balanced conditions, the PHA polymer degradation is favored. It is noteworthy remark here that under balanced conditions, while the wild-type strain is able to depolymerize the polymer, KT40Z or MM16 strains are not, due to the lack of *phaZ*, among others. Therefore, it is reasonable to assume that under these conditions, the PHA accumulation would be favored in the knockout strains. However, no PHA production was observed in all the strains tested in any condition. This discrepancy to the *in silico* predictions is due likely to insufficient acetyl-CoA levels. In fact, PET4 design accounts also for EG utilization, which is metabolized to acetyl-CoA in the model. Summing up, PET utilization would result to 2 acetyl-CoA and 1 succinate, while PCA or 4HBz to 1 acetyl-CoA and 1 succinate. Therefore, it was considered that an extra pulse of acetyl-CoA would aim the PHA production.

Conditions	C/N ratio (mol/mol)	Strains	Lag phase (h)	growth rate (h^{-1})	OD max
M63 5 mM 4HBz	1.12	KT2440	1.75	0.30	0.34
		KT40Z	3.25	0.26	0.34
		MM16	4.75	0.18	0.31
M63 0.1 N 10 mM 4HBz	23.33	KT2440	2.58	0.15	0.54
		KT40Z	3.25	0.23	0.54
		MM16	6.50	0.15	0.48

Table 21. Growth characteristics under balanced and nitrogen limitation conditions. The results correspond to microtiter experiments.

We proceeded to add a pulse of octanoate as an acetyl-CoA precursor source, while 4HBz was used as carbon source in this new experiment. In this case, MM16 strain produced 33.7% of PHA/CDW compared to 7% of wild type and 25.2% of KT40Z strain (Figure 60 and Table 22). Even though, the single deletion of the depolymerase resulted in 25.2% PHA/CDW, the deletion of extra reactions in MM16 led to higher PHA production (33.7% vs 25.2%). Thus, it could be concluded that these growing conditions, which largely mimic the *in silico* PET metabolism used to design MM16 strain, can be used instead of PET as feasible culture conditions for phenotyping our knockout strains.

The above culture conditions were used in order to screen the impact of each individual and sequential deletions on PHA production (Figure 60 and Table 22) and to *in vivo* verify which reactions were essential to drive the PHA production. Thus, key knockout reactions leading to higher PHA content were the succinyl-CoA synthase, *sucC-sucD*, (in purple) and the isocitrate lyase, *aceA* (in orange). The special importance was the deletion of *sucCD* that increased the PHA production from 5% in MM4 strain to 22% in MM6 strain (Figure 60 and Table 22). The deletion of isocitrate lyase has been previously reported to improve the PHA production (Klinke *et al.*, 2000). At be best of our knowledge, this is the first time that the deletion of *sucCD* genes is related with improved PHA capabilities. The rest of knockouts only increased slightly the PHA production found in MM8 strain.

Overall, it could be concluded, that MM16 strain was able to efficiently produce PHA under balanced growth conditions (M63 3 mM octanoate 5 mM 4HBz), reaching up to 33.7% of PHA/CDW production, 4.8 times improvement when compared to the wild type strain. In fact, MM16 strain produced up to 0.2 g/L of PHA compared to 0.05 g/L of the wild type strain.

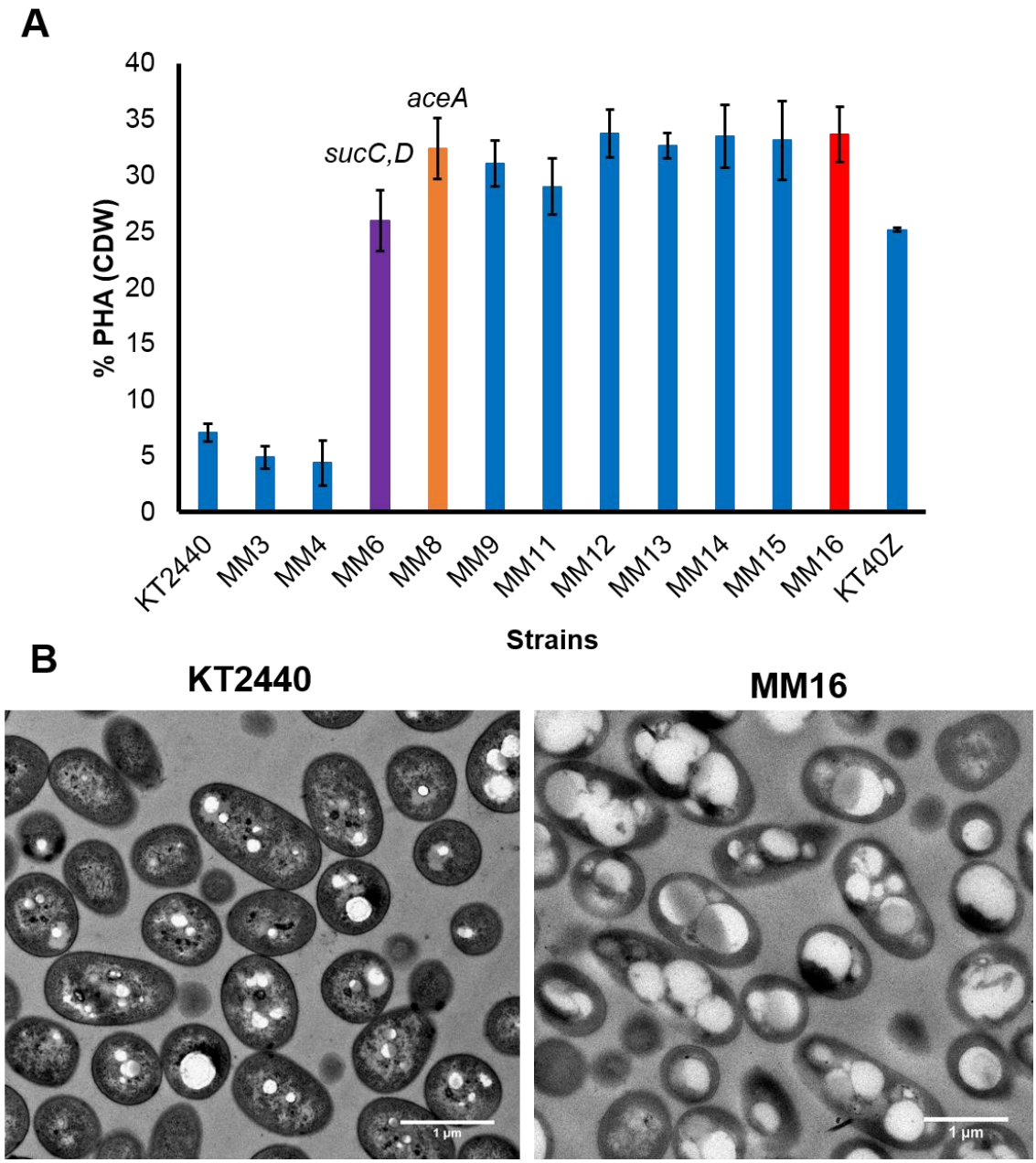

Figure 60. A. The PHA (% CDW) content after 24h of growth in M63 3 mM octanoate 5 mM 4-hydroxybenzoate (C/N ratio: 2 mol/mol) in the different deletion mutants background is demonstrated (see Figure 53 and Table 2 for the strains nomeclature). **B.** Electronic microscopy pictures of the KT2440 and MM16 strains after 24 h of growth under the above mentioned conditions are shown. The scale bar of the pictures is 1 µm.

Strains	Total biomass (g/L)	PHA (% CDW)	PHA (g/L)	Residual biomass (g/L)
KT2440	0.69 ± 0.05	7.09 ± 0.78	0.05 ± 0.01	0.63 ± 0.05
KT40Z	0.74 ± 0.03	25.19 ± 1.97	0.19 ± 0.02	0.56 ± 0.03
MM3	0.68 ± 0.05	4.90 ± 1.02	0.03 ± 0.01	0.64 ± 0.04
MM4	0.63 ± 0.04	4.38 ± 204	0.03 ± 0.01	0.60 ± 0.04
MM6	0.63 ± 0.02	22.56 ± 4.07	0.16 ± 0.03	0.47 ± 0.01
MM8	0.59 ± 0.01	32.41 ± 2.71	0.19 ± 0.02	0.40 ± 0.02
MM9	0.57 ± 0.02	31.10 ± 2.07	0.18 ± 0.02	0.39 ± 0.00
MM11	0.55 ± 0.04	29.05 ± 2.49	0.16 ± 0.00	0.42 ± 0.01
MM12	0.60 ± 0.03	33.79 ± 2.14	0.19 ± 0.01	0.41 ± 0.02
MM13	0.57 ± 0.04	32.68 ± 1.15	0.20 ± 0.01	0.40 ± 0.01
MM14	0.60 ± 0.02	33.53 ± 2.82	0.20 ± 0.02	0.40 ± 0.01
MM15	0.57 ± 0.04	33.15 ± 3.54	0.20 ± 0.02	0.38 ± 0.01
MM16	0.59 ± 0.03	33.70 ± 2.47	0.20 ± 0.02	0.39 ± 0.02

Table 22. Physiological parameters after 24 h of growth under M63 3 mM octanoate 5 mM 4HBz (C/N ratio: 2 mol/mol).

4.3.5 PHA is produced via β-oxidation pathway in the MM16 strain.

PHA can be produced either via β-oxidation or *de novo* fatty acid synthesis (Introduction sections 1.4.1 and 1.4.3). Since 4HBz is a non-PHA related carbon sources, the growth-coupled strains obtained are expected to follow the *de novo* fatty acid synthesis for PHA production. In order to assert the metabolic pathway responsible for the PHA production observed in the MM16 strain, octanoate was replaced by an odd fatty acid and the PHA monomers pattern was subsequently analyzed. Thus, if odd chain monomers were obtained, this unequivocally indicate that they came from the β-oxidation; however, if even chain monomers appear, this would suggest that they came from *de novo* fatty acid synthesis. Following this premise, the PHA content was quantified in KT2440, KT40Z and MM16 strains after 24 h of growth using 3 mM 10-undecenoic acid and 5 mM 4-hydroxybenzoate as carbon sources (Table 23). No significant differences were observed as far as it concerns the PHA monomeric pattern between the strains. Since only odd monomers were observed, it could be concluded that the pathway used for PHA synthesis in MM16 strain was the β-oxidation and not the *de novo* fatty acid synthesis as was expected by design.

Strains	KT2440	KT40Z	MM16
% OH-C6 (mM)	N.D.	N.D.	N.D.
% OH-C7:1 (mM)	3.23 ± 2.11	3.70 ± 1.75	2.46 ± 2.03
% OH-C8 (mM)	N.D.	N.D.	N.D.
% OH-C9:1 (mM)	63.83 ± 2.46	55.87 ± 1.22	53.47 ± 1.22
% OH-C10 (mM)	N.D.	N.D.	N.D.
% OH-C11:1 (mM)	32.94 ± 1.24	40.44 ± 0.82	44.07 ± 2.82

Table 23. The pattern of PHA monomers for the wild type KT2440, null *phaZ* (KT40Z), MM16 strains after 24 h of growth under M63 3mM 10-undecenoic acid and 5 mM 4-hydroxybenzoate was shown. N.D.: not detected.

This result strongly argued in favor of potential regulatory constraints avoiding the synthesis of PHA via *de novo* fatty acid synthesis pathway. In order to check the feasibility of this hypothesis, the transcription levels of key genes of *pha* cluster (*phaF* and *phaI*) as well as the *(R)*-3-hydroxydecanoyl-ACP:CoA transacylase *phaG* were checked in the MM16 strain (Figure 61). The *phaG* gene is a key connector between the fatty acid synthesis and PHA production (Introduction section 1.4.3).

Therefore, the expression levels of *phaF*, *phaI* and *phaG* were quantified by means of qRT-PCR experiments from total RNAs extracted of bacterial cultures of genes for the control strains (KT2440, KT40Z), and MM16, after 6 h of growth using 5 mM 4HBz (red bars) or 3 mM octanoate and 5 mM 4HBz (blue bars). Similar results were obtained for the *phaI* phasin. A standard balanced condition of growth was used as a positive control for the expression levels of the phasins for the control strains (M63 7.5 mM octanoate, shown in black bars). MM16 strain could not be analyzed under these conditions since it cannot grow on fatty acid as sole carbon source (Figure 50).

As it would be expected, the expression levels of *phaF*, for wild type and KT40Z strains were higher in the control condition (black bars) compared to the experimental (red and blue bars), since the strains were grown under PHA-related carbon source (fatty acid). Under this condition, PHA are being synthetized and the requirement of phasins increase accordingly in order to allocate the PHA into the growing granules both in the wild type and KT40Z strain. However, growth under 5 mM 4HBz 3 mM octa (blue bars) resulted in 1.3 and 1.7 fold decrease in the *phaF* expression levels in wild type and KT40Z strains, respectively compared to the control condition (black bars). Accordingly, MM16 strain showed 1.7 times decreased *phaF* expression compared to the corresponding values of the wild type strain. Finally, growth under 5 mM 4HBz (red bars), led to 2.2 fold decrease in the *phaF* expression levels of wild type and KT40Z strains. However, 3 fold decrease in its expression was observed by MM16 strain compared to

the corresponding levels of wild type strain. Thus, in the case of MM16 strain, the *phaF* expression levels were affected compared to the wild type. In addition, the *phaG* was barely expressed in all the strains and conditions tested.

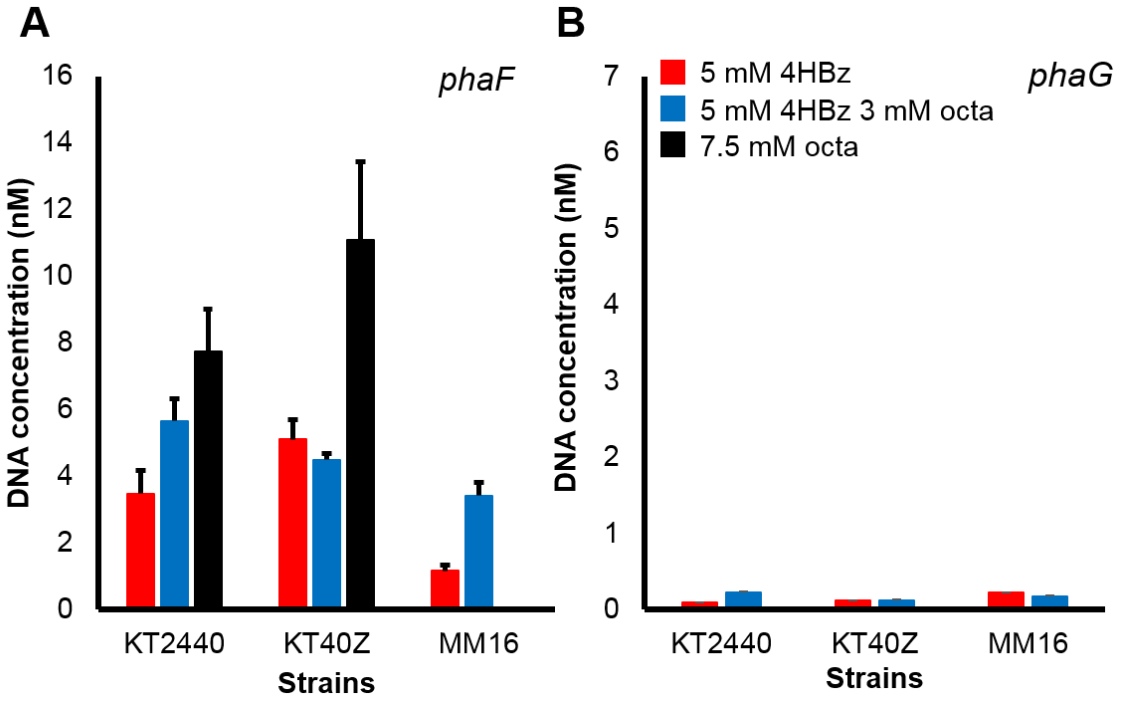

Figure 61. qRT-PCR experiments under M63 5 mM 4-hydroxybenzoate (5mM 4HBz; in red) and M63 5 mM 4-hydroxybenzoate 3 mM octanoate (5 mM 4HBz 3 mM octa; in blue) and M63 7.5 mM octanoate (7.5 mM octa; in black bars). The expression levels (DNA concentration) for the phasin *phaF* **(A)** and *phaG* genes **(B)** for the strains KT2440, KT40Z and MM16 strains are shown in the left and right graph, respectively.

Taking together, these results could explain, to some extent, the observed phenotypes. A plausible hypothesis could be that by increasing the expression levels of these critical genes, such as *phaC1* synthase, *phaF* phasin and the *phaG*, recombinant microorganisms capable of producing PHA from *de novo* fatty acid synthesis could be obtained.

4.3.6 Construcion of a second generation of PHA overproducer *P. putida* strains.

As despicted above, MM16 strain synthetizes PHA through the β-oxidation pathway (Table 23) and not through *de novo* fatty acid synthesis as it was designed, likely due to the lack of proper expression of both *pha* genes (*phaC1*, *phaF*), as well as *phaG* gene in our experimental conditions (Figure 61). Therefore, it was decided to completely avoid the native regulation on PHA metabolism in *P. putida*. For this, we

addressed a series of sequential genetic iterations. Figure 62 shows the strategy consisting in i) the deletion of the whole *pha* cluster (blue color) and ii) the expression of a synthetic PHA operon containing the minimal set of enzymes required for PHA production and those needed to reroute the carbon flux towards *de novo* fatty acid biosynthesis (pink color).

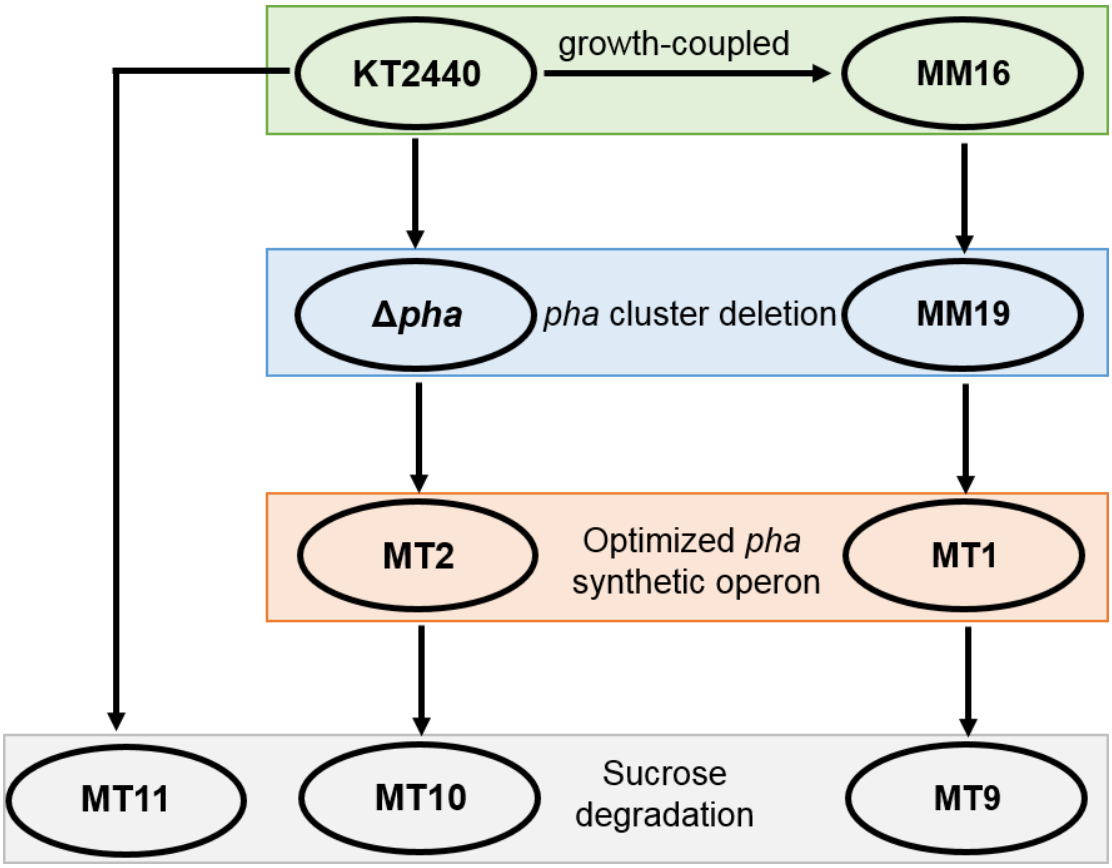

Figure 62. Schematic representation of second generation PHA overproducer strain construction. The obtained mutants in *P. putida* KT2440 background with the different interations are shown. The growth-coupled construction MM16 (green), *pha* cluster deletion (blue), optimized *pha* synthetic operon (pink) and genes required for sucrose degradation (gray) are indicated.

- ***pha* cluster deletion**

i) As mentioned in the introduction (section 1.4.5), the *pha* metabolism is subjected to a complex regulation including global and specific regulator. In order to avoid this native regulation, the whole *pha* cluster was deleted using pEMG deletion strategy (Materials and Methods section 3.4.4 and Figure 62). The KT2440 Δ*pha* strain has been constructed previously and it has already been under active phenotypic investigation in our lab (Results chapter 1). The *pha* deletion in MM16 strain resulted in MM19 strain (Figure 62, blue color).

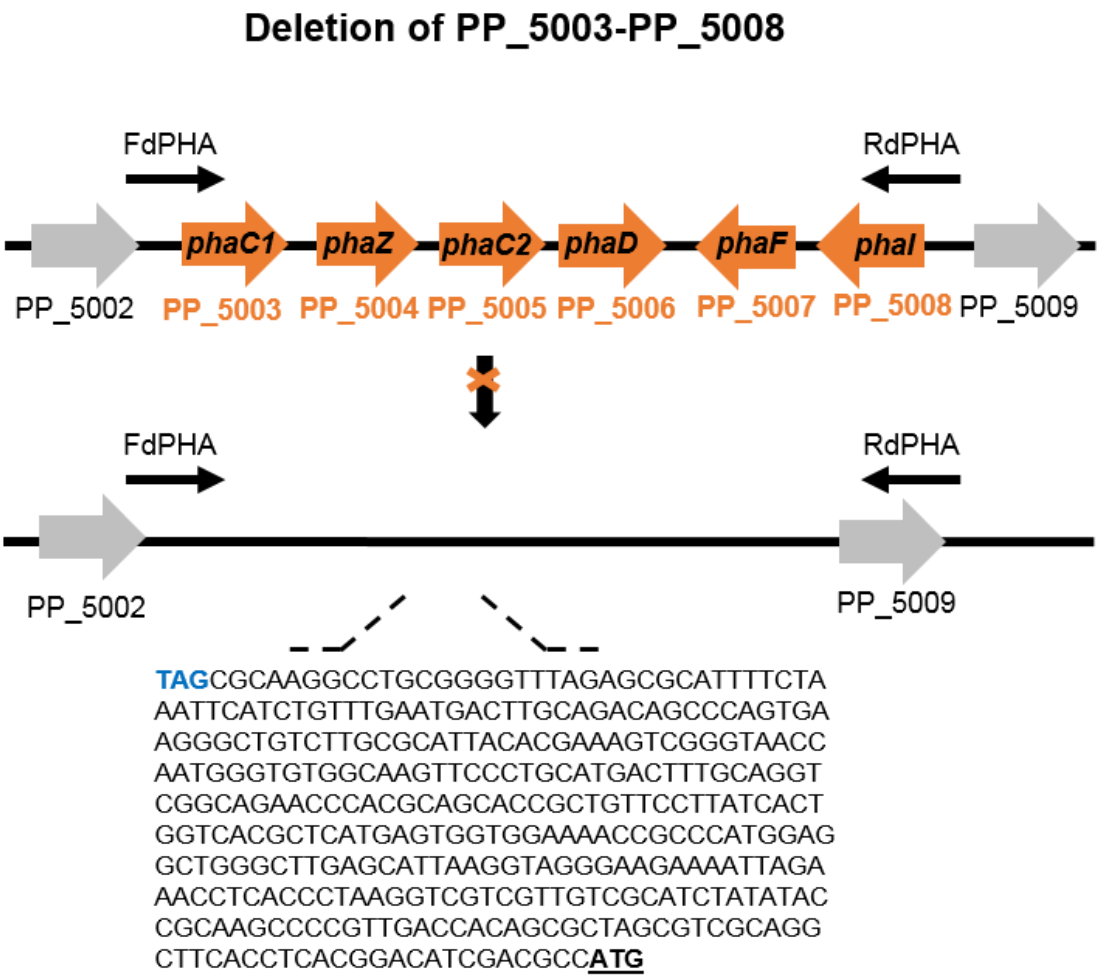

Figure 63. PHA cycle deletion strategy. The deleted gene products at their corresponding locus are shown. The arms of homology used for recombinatorial deletion of each gene consist of the flanking upstream and downstream genes. Arrows above indicate the annealing location for primers used for colony PCR (sequencing) following the second recombination counterselection to confirm the gene deletion. The remaining nucleotide sequence after the deletion is shown. The stop and start codons are shown with bold blue and bold underlined, respectively.

- **Optimized *pha* synthetic operon**

ii) As a second approach and in order to increase the preference of MM19 strain towards the *de novo* fatty acid synthesis, it was decided to overexpress key genes related with PHA synthesis. First, the *phaG* and the medium chain-fatty acid CoA ligase encoded by the gene PP_0763, were overexpressed. Our strategy was based on the previous work from Wang and collaborators that found high expression levels of *phaG* and PP_0763 genes associated to biosynthesis of mcl-PHAs from unrelated carbon sources (Q. Wang *et al.*, 2012). Second, based on the suboptimal expression of key *pha* genes (Figure 61), we proceeded to overexpress the key genes involved in the PHA production, e.g., the *phaC1* synthase and the phasin encoded by the *phaF* gene using Golden Gate assembly method (Materal and Methods 3.4.5 section).

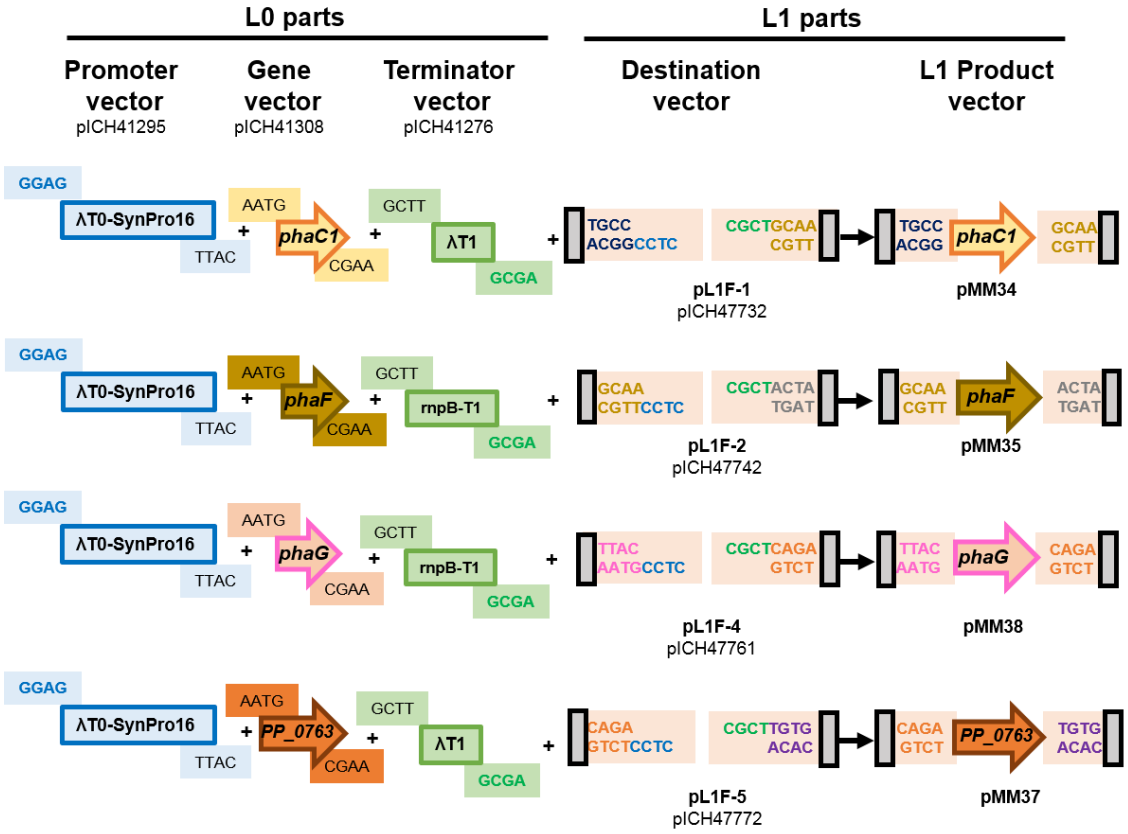

Figure 64. Golden Gate – MoClo Level 1 plasmid constructions. Level 0 parts, including promoter, gene and terminator, were mixed along with the Level 1 destination vector, BsaI and T4 DNA Ligase to form each Level 1 product vectors. This reaction takes place by complementation using fusion sites (sequences represented). The promoter part (and the corresponding fusion sites for this part), and the terminator part are demonstrated with blue and green color, respectively. The Golden Gate-MoClo vectors that were used as backbones and the resulting L1 Product vectors are shown.

Four Golden Gate-MoClo Level 1 reactions were carried out to create transcription unit constructs for the *phaC1*, *phaF*, *phaG* and PP_0763 (Figure 64). Correct Level 1 assemblies/plasmids were then mixed with the Level 2 plasmid and the appropriate Level 2 end-linker (Figure 65). This Level 2 Product vector (pMM55) contained an end-linker with the LacZ that maintained the construct opened, allowing the addition of extra transcription units if needed. The pMM55 plasmid was then transformed into *P. putida* MM19 and KT2440 Δ*pha* strains, generating MT1 and MT2 strains, respectively (Figure 62).

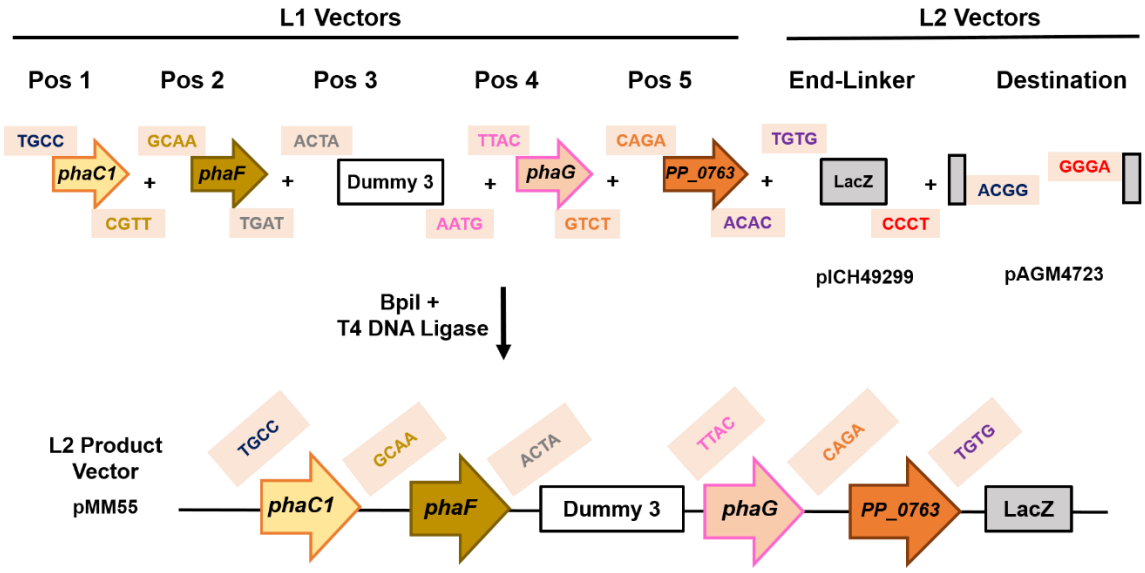

Figure 65. Golden Gate-MoClo Level 2 plasmid constructions. Level 1 transcription unit vectors are mixed along with the appropriate end-linker vector, the Level 2 destination vector, BpiI enzyme and T4 DNA Ligase to form each Level 2 product vector. This reaction takes place by complementation of unique fusion sites (sequences represented). The Golden Gate-MoClo vectors that were used as backbones and the resulting L2 Product vector are shown. Dummies can be used to assemble a multigene construct lacking a transcription unit at an internal position. For example, three transcription units previously cloned in level 1 vectors for positions 1,2 and 4, can be assembled in a multigene construct by using dummy 3 in the level 2 cloning reaction. The multigene construct obtained will contain 15 bp of sequence at position 3.

4.3.7 Phenotypic evaluation of second generation growth-coupled design strains using fatty acids and PHA-unrelated carbon sources.

The performance of these synthetic genes were tested on plasmid in the MT1, MT2 strains compared to the wild type KT2440 and the corresponding parental, MM19 and KT2440 Δ*pha* null strains, respectively. The phenotypic comparison and the physiological parameters of these strains after 24 h of growth under M63 minimal medium supplemented with 3 mM octanoate 5 mM 4-hydroxybenzoate (C/N= 2 mol/mol) are listed in the Table 24. As it would be expected, the MM19 strain, resulted in no PHA production, since the whole *pha* cluster has been deleted. The MT1 and MT2 strains, resulted in 46% and 26% PHA/CDW, respectively compared to 33.7% produced in MM16 strain. Slight higher amounts of C10 monomer was also observed in MT1 and MT2 background strains compared to the MM16 strain (Table 25). These results validate the functionality of the synthetic operon, since the overexpression of the *phaG* and PP_0763 genes would lead to an increased flux through the *de novo* fatty acid synthesis. Therefore, it would be interesting to test MT1 and MT2 growth-coupled PHA production using aromatic compounds derived from lignin and PET hydrolysis, as sole carbon

source. The PHA production in these strains was first analyzed by electronic microscopy pictures after 24 h of growth under the above-mentioned conditions (Figure 66).

Strains	Total Biomass (g/L)	PHA (% CDW)	PHA (g/L)	Residual Biomass (g/L)
KT2440	0.69 ± 0.05	7.09 ± 0.78	0.05 ± 0.01	0.63 ± 0.05
MM16	0.59 ± 0.03	33.70 ± 2.47	0.20 ± 0.02	0.39 ± 0.02
MM19	0.43 ± 0.01	N.D.	N.D.	0.43 ± 0.01
MT1	0.49 ± 0.04	46.05 ± 2.96	0.22 ± 0.01	0.26 ± 0.03
MT2	0.70 ± 0.03	26.14 ± 3.72	0.18 ± 0.03	0.51 ± 0.03

Table 24. Physiological parameters after 24 h of growth under M63 3 mM octanoate 5 mM 4HBz (C/N ratio: 2 mol/mol). N.D.: not detected.

Strains	%OH-C6 (mM)	%OH-C8 (mM)	%OH-C10 (mM)	%OH-C12:1 (mM)	%OH-C12 (mM)
KT2440	5.82 ± 0.27	88.62 ± 0.63	4.01 ± 1.84	N.D.	1.55 ± 2.20
MM16	6.71 ± 0.44	91.64 ± 0.77	1.42 ± 0.51	N.D.	0.24 ± 0.41
MT1	5.96 ± 0.38	76.49 ± 2.42	15.40 ± 1.59	0.79 ± 0.34	1.36 ± 0.54
MT2	6.25 ± 0.37	82.59 ± 1.52	9.79 ± 1.19	0.43 ± 0.24	0.94 ± 0.38

Table 25. PHA monomeric pattern after 24 h of growth under M63 minimal medium supplemented with 3 mM octanoate 5 mM 4HBz (C/N ratio: 2 mol/mol). N.D.: not detected.

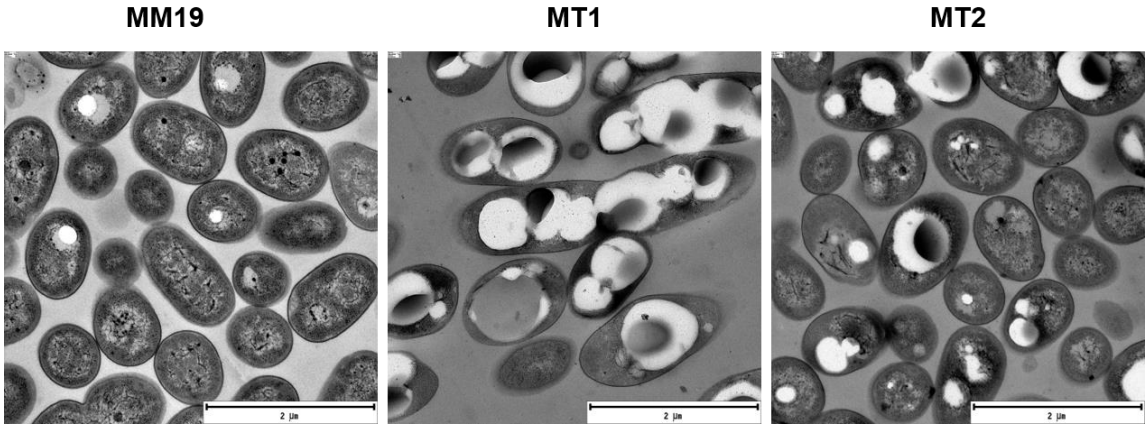

Figure 66. Designing the optimal chassis for *in vivo* PHA production. Electronic microscopy pictures of the cells grown after 24 h under M63 3 mM octanoate 5 mM 4HBz (C/N ratio: 2mol/mol)

Interestingly and contrary to the traditionally PHA overproducer strains that require unbalanced C/N ratio for efficient PHA production, strains MM16, MT1 and MT2 accumulate significant amounts of PHA under equilibrate nutrients conditions using octanoate plus 4-hydroxybenzoic acid (4HBz) (Table 24). Even more, strains MT1 and MT2 produced significant PHA using unrelated carbon sources in the absence of octanoate (Table 26 and Figure 67). For instance, while the wild type strain produced a

negligible amount of PHA using aromatic compounds derived of lignin and PET (such as *p*-coumaric, ferulic, vanillic or 4HBz), the strain MT2 accumulated PHA ranging 4-8% of total biomass and MT1 strain accumulated higher amounts (up to 19.68% using ferulic acid as carbon source). Validating *in silico* predictions that suggested phenyl acetic carbon source for PHA production (Figure 51), the MT1 strain was able to produce up to 14.7% of PHA after 72 h of cultivation (Table 26). Since the lignin, PET and PU derived monomers are PHA unrelated carbon sources, the *de novo* fatty acid synthesis is expected to be used for PHA production, leading to major production of C10, followed by C8 monomers. The monomeric pattern of the strains grown for 24 h using 4HBz are listed in the Table 27.

Conditions M63	Strains	Total Biomass (g/L)	PHA (% CDW)	PHA (g/L)	Residual Biomass (g/L)
Phenyl acetic acid (4.4 mM)	KT2440	0.32	N.D.	N.D.	0.32 ± 0.00
	MT2	0.33	4.13 ± 0.20	0.01 ± 0.00	0.31 ± 0.00
	MT1 (72 h)	0.28	14.67 ± 0.10	0.04 ± 0.00	0.24 ± 0.00
Ferulic acid (3.5 mM)	KT2440	0.37 ± 0.01	N.D.	N.D.	0.37 ± 0.01
	MT2	0.38 ± 0.00	7.78 ± 0.94	0.03 ± 0.00	0.35 ± 0.00
	MT1	0.30 ± 0.00	19.68 ± 0.27	0.06 ± 0.00	0.24 ± 0.00
p-Coumaric acid (3.9 mM)	KT2440	0.38 ± 0.00	N.D.	N.D.	0.38 ± 0.00
	MT2	0.38 ± 0.01	6.15 ± 0.94	0.02 ± 0.00	0.36 ± 0.01
	MT1	0.24 ± 0.04	14.23 ± 1.88	0.04 ± 0.01	0.21 ± 0.03
Vanillic acid (4.4 mM)	KT2440 (48 h)	0.27 ± 0.06	N.D.	N.D.	0.27 ± 0.05
	MT2 (48 h)	0.29 ± 0.03	7.68 ± 0.49	0.02 ± 0.00	0.27 ± 0.02
	MT1 (48 h)	0.26 ± 0.02	15.29 ± 0.33	0.04 ± 0.00	0.22 ± 0.01
4-HBz (5 mM)	KT2440	0.39 ± 0.02	N.D.	N.D.	0.39 ± 0.01
	MT2	0.34 ± 0.03	5.73 ± 2.16	0.02 ± 0.01	0.32 ± 0.03
	MT1	0.31 ± 0.03	17.65 ± 3.30	0.05 ± 0.01	0.26 ± 0.03

Table 26. PHA production of strains MT1 and MT2 using aromatic compounds compared with the wild type strain KT2440. In all the cases except where noted the PHA content was obtained after 24 h of growth. In all the cases the C/N ratio: 1.12 mol / mol was maintained. N.D.: not detected

Strains	%OH-C6 (mM)	%OH-C8 (mM)	%OH-C10 (mM)	%OH-C12:1 (mM)	%OH-C12 (mM)
MT1	0.66 ± 0.19	7.66 ± 1.35	80.75 ± 4.56	3.48 ± 1.11	6.79 ± 1.54
MT2	0.60 ± 0.11	5.69 ± 0.57	83.27 ± 2.15	2.85 ± 0.35	7.50 ± 1.28

Table 27. PHA monomeric pattern after 24 h of growth under M63 minimal medium supplemented with 5 mM 4HBz (C/N ratio: 1.12 mol/mol). Traces of %OH-C14 (mM) were detected in both strains.

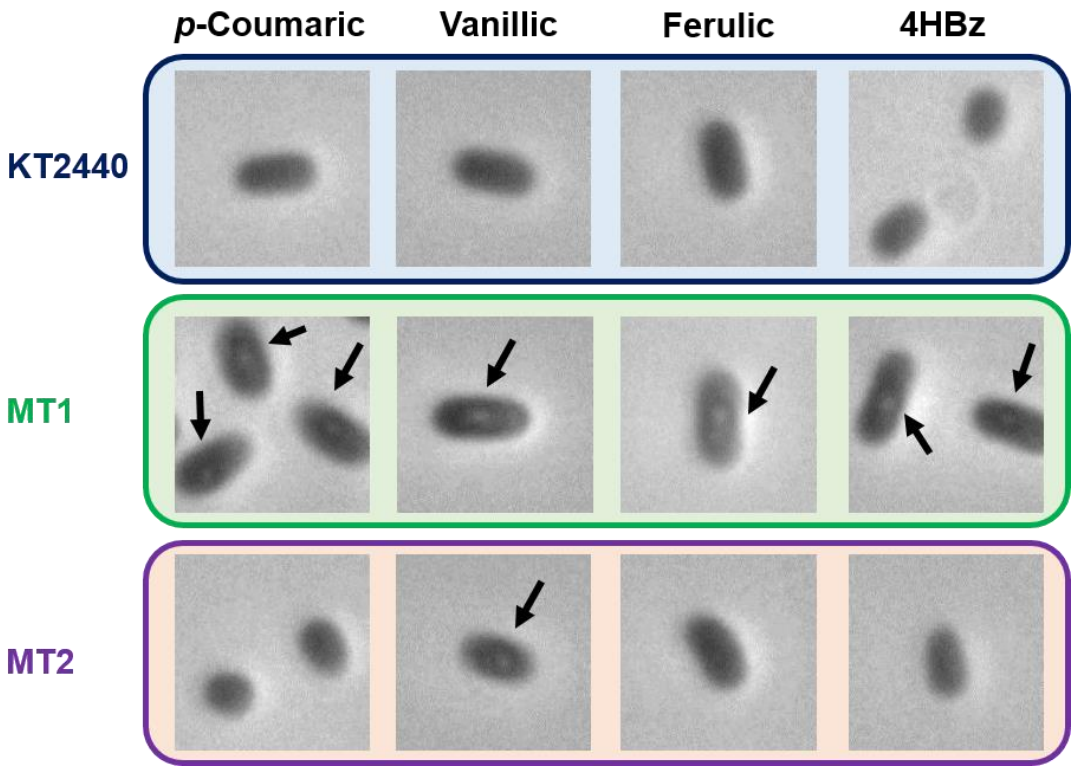

Figure 67. Phase contrast microscopy pictures after 24 h of growth under the corresponding conditions. The C/N ratio was maintained at 2 mol/mol. With arrows the PHA granules are indicated. KT2440, MT1 and MT2 are shown in blue, green and purple colors respectively. The scale bar is 2 µm.

4.3.8 Optimal chassis for *in vivo* PHA production from cheap carbon sources.

Lignin valorization and plastic degration towards high-value added bioplastics, PHA is an interesting and promising biotechnological field. However, PHA production from these recalcitrant carbon sources is extremely challenging for scale-up processes. This is mainly due to the scarce accesibility of these aromatic compounds as industrial feedstock, since there are found in form of complex polymers, such as PET or lignin. Furthermore, since almost 50% of the PHA production costs are dependent on the applied carbon source, cheap and abundant substrates are diserable for industrial scale PHA production. For this purpose, we faced the challenge of expanding the PET4 design (MM16 strain) for PHA production from aromatics to inexensive and abundant substrates, such as sugars. In order to test whether this was the case, a series of phenotypic assays were realized under balanced growth conditions supplemented with 10 mM glucose or 20 mM glycerol.

No PHA accumulation was observed under balanced medium conditions supplemented with 10 mM glucose, from the parental strains, KT2440 Δ*pha* and MM19,

since these two strains lack of a functional *pha* cluster. Additionally, under these conditions the growh-coupled PHA MT1 strain, reached 27.5% PHA, being 17.5 fold higher than that produced by wt (Figure 68 and Table 28). Surprisingly, the KT2440 Δ*pha* background mutant, MT2 exhibited 14% PHA, respectively, being 8.9 times increased compared to the wt. Since glucose is a PHA-unrelated carbon source, the de novo fatty acid synthesis is used for PHA production (Table 29). As it would be expected, MT1 and MT2 strains had higher flux through the *de novo* fatty acid synthesis, due to the presence of the optimized pha synthetic operon. In fact, almost 20% higher amounts of C10 monomers were observed in the MT1 and MT2 strains compared to wild type strain (Table 29).

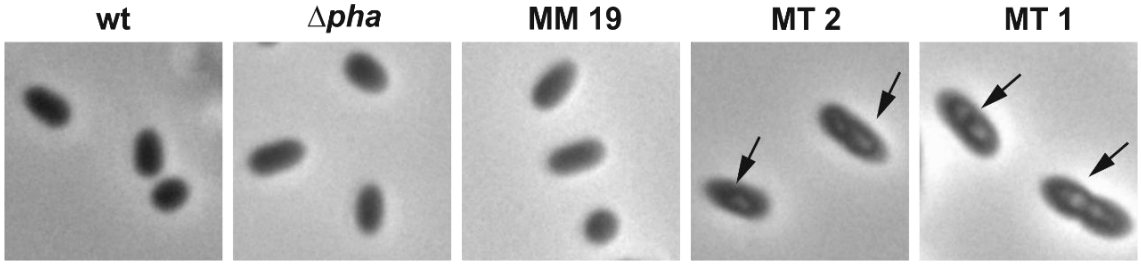

Figure 68. Phase contrast microscopy pictures after 24 h of growth under M63 10 mM glucose. The C/N ratio was maintained at 2 mol/mol. With arrows the PHA granules are indicated. wt (KT2440), Δ*pha* (KT2440 Δ*pha*) strains. The scale bar is 2 µm.

Strains	Total Biomass (g/L)	PHA (% CDW)	PHA (g/L)	Residual Biomass (g/L)
KT2440	0.91 ± 0.02	1.57 ± 0.89	0.01 ± 0.01	0.90 ± 0.01
KT2440 Δ*pha*	0.93 ± 0.01	N.D.	N.D.	0.93 ± 0.00
MM19	0.83 ± 0.04	N.D.	N.D.	0.83 ± 0.03
MT2	0.90 ± 0.02	14.04 ± 0.73	0.12 ± 0.01	0.76 ± 0.01
MT1	0.57 ± 0.03	27.48 ± 2.45	0.15 ± 0.02	0.42 ± 0.02

Table 28. Physiological data after 24h of growth under M63 10 mM glucose. The C/N ratio was maintained at 2 mol/mol. N.D.: not detected.

Strains	%OH-C6 (mM)	%OH-C8 (mM)	%OH-C10 (mM)	%OH-C12:1 (mM)	%OH-C12 (mM)
KT2440	N.A.	N.A.	N.A.	N.A.	N.A.
MT1	0.67 ± 0.10	8.70 ± 0.56	77.99 ± 3.54	3.83 ± 0.95	7.62 ± 1.40
MT2	0.67 ± 0.21	8.79 ± 2.17	79.11 ± 4.75	3.45 ± 1.70	7.33 ± 2.63

Table 29. PHA monomeric pattern after 24 h of growth under M63 minimal medium supplemented with 5 mM 4HBz (C/N ratio: 1.12 mol/mol). Traces of %OH-C14 (mM) were detected in MT1 and MT2 strains. Since the % PHA/CDW content of wild type strain is very low, in this case the PHA monomeric pattern characterization is not reliable (N.A.).

No PHA production was observed from the wt strain under balanced medium conditions supplemented with 20 mM glycerol, in good agreement with previous observations from our group (Escapa *et al.*, 2013). The addition of small amounts of glucose (1.33 mM, equivalent to octanoate concentration) or octanoate (1 mM) to the cultures of 20 mM glycerol, was necessary in order to avoid the long lag phase observed under glycerol growth conditions (Wang and Nomura, 2010; Escapa *et al.*, 2013). Similarly, as it would be expected, wt, Δ*pha* and MM19 strains did not show detectable amounts of PHA production under balanced medium conditions supplemented by glycerol (plus glucose or octanoate; Figures 69-70 and Tables 30-31).

In addition, growth-coupled MT1 mutant and MT2 strain reached up to 30% and 9.7% PHA, respectively, after 24 h of growth using glycerol and 1.33 mM glucose (Figure 69 and Table 30). These PHA quantities correspond to significant and highly encouranging PHA production improvements under balanced medium conditions, compared to the wt strain.

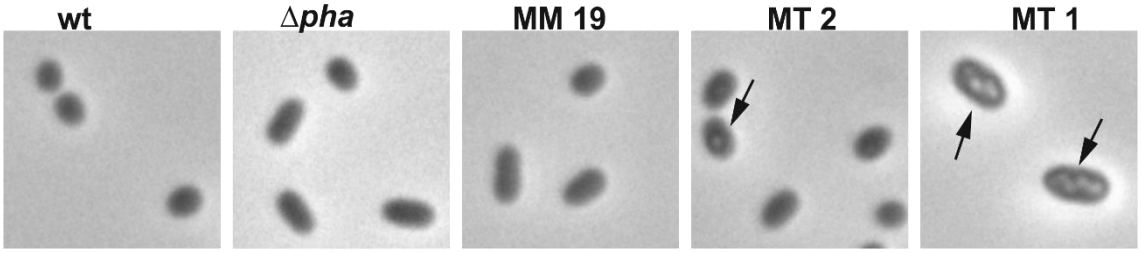

Figure 69. Phase contrast microscopy pictures after 24 h of growth under M63 1.33 mM glucose and 20 mM glycerol. The C/N ratio was maintained at 2.26 mol/mol. With arrows the PHA granules are indicated. wt (KT2440), Δ*pha* (KT2440 Δ*pha*) strains. The scale bar is 2 μm.

Strains	Total Biomass (g/L)	PHA (% CDW)	PHA (g/L)	Residual Biomass (g/L)
KT2440	1.02 ± 0.02	N.D.	N.D.	1.02 ± 0.02
MT2	0.96 ± 0.04	9.73 ± 1.11	0.09 ± 0.01	0.87 ± 0.02
MT1	0.39 ± 0.05	29.98 ± 4.28	0.10 ± 0.03	0.28 ± 0.01

Table 30. Physiological data after 24h of growth under M63 1.33 mM glucose and 20 mM glycerol. The C/N ratio was maintained at 2.26 mol/mol. N.D.: not detected.

Moreover, high amounts of PHA were observed under balanced conditions using glycerol and 1 mM octanoate by MT2 strain reaching 14% PHA. Even higher amounts of PHA were observed by the growth-coupled MT1 strain, reaching up to 51.8% PHA after 24 h of growth (Figure 70 and Table 31). Similarly, these PHA production properties were, by far, improved to the reported ones (Escapa *et al.*, 2013).

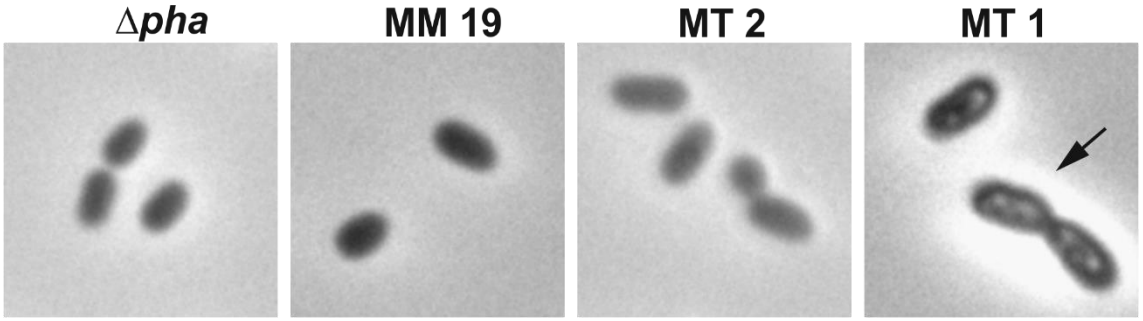

Figure 70. Phase contrast microscopy pictures after 24 h of growth under M63 1 mM octanoate and 20 mM glycerol. The C/N ratio was maintained at 2.26 mol/mol. With arrows the PHA granules are indicated. Δ*pha* (KT2440 Δ*pha*) strain. The scale bar is 2 µm.

Strains	Total Biomass (g/L)	PHA (% CDW)	PHA (g/L)	Residual Biomass (g/L)
MM19	0.93	0.09 ± 0.12	<0.01	0.92 ± 0.00
MT2	0.75	13.97 ± 4.07	0.11 ± 0.03	0.65 ± 0.03
MT1	0.27	51.79 ± 3.06	0.14 ± 0.01	0.13 ± 0.01

Table 31. Physiological data after 24h of growth under M63 1 mM octanoate and 20 mM glycerol. The C/N ratio was maintained at 2.26 mol/mol.

Summing up, it can be concluded that MT1 and MT2 strains have the catabolic potential expanded, being able to use cheap PHA unrelated compounds as sole carbon source, while accumulating significant amounts of PHA under nutritional balanced conditions. However, from the observed PHA data, it could be suggested that the PHA productivity remained the same among MT1 and MT2 strain, since similar PHA (g/L) is obtained. Even though, higher %PHA/CDW is produced in MT1 strain compared to MT2 and wild type strains, its low residual biomass is a disadvantage for further scale up processes.

4.3.9 Expanding the growth-coupled designs to non-native carbon sources.

In order to expand the repertory of suitable substrates to produce PHA, to non-native carbon sources such as sucrose, the genes needed for its degradation were additionally added to the previous recombinant strains.

In brief, a subcloning of the *cscAcscB* genes to pSEVA621 was performed, resulting to pMM66 plasmid. MT1, MT2 and KT2440 strains were electroporated with the obtained pMM66 plasmid resulting to MT9, MT10 and MT11 strains, respectively (Figures 62 and 71).

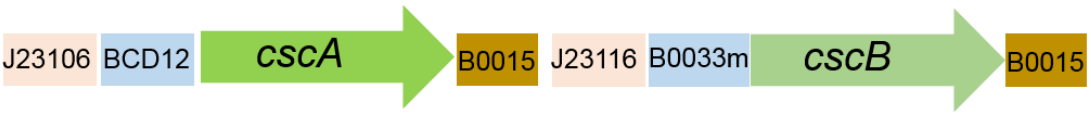

Figure 71. Schematic representation of the pMM66 plasmid constructed for sucrose degradation. The genes needed for the sucrose degradation (*cscA*, *cscB*; in dark green colors) are based on previous work realized in *E. coli* W (Archer *et al.*, 2011; Sabri *et al.*, 2013). The J23106 and J23116 are the promoters used in this work, based on the available Anderson library http://parts.igem.org/Promoters/Catalog/Anderson (Iverson *et al.*, 2016); BCD12 and B0033m are the RBS and B0015 the terminator used in this case (Mutalik *et al.*, 2013).

The cells were grown under balanced conditions supplemented with 5 mM sucrose. Similarly to glucose, the wild type strain, MT11 was not able to accumulate PHA, while the growth-coupled mutant, MT9 exhibited 34.5% PHA/CDW production after 24 h of growth versus the 17.8% PHA/CDW produced by the MT10 strrain (Figure 72 and Table 32). These PHA quantities obtained by MT9 and MT10 strains were highly improved to the wild type.

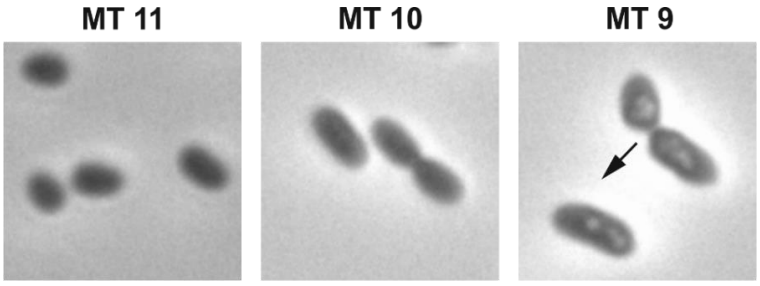

Figure 72. Phase contrast microscopy picture after 24 h of growth under M63 5 mM sucrose. The C/N ratio was maintained at 2 mol/mol. With arrows the PHA granules are indicated. The scale bar is 2 µm.

Strains	Total Biomass (g/L)	PHA (% CDW)	PHA (g/L)	Residual Biomass (g/L)
MT11	0.79 ± 0.00	N.D.	N.D.	0.79 ± 0.00
MT10	0.31	17.74 ± 1.12	0.05 ± 0.00	0.25 ± 0.00
MT9	0.30 ± 0.04	34.47 ± 1.98	0.10 ± 0.01	0.20 ± 0.02

Table 32. Physiological data after 24h of growth under M63 5 mM sucrose. N.D.: not detected

In summary, MT1 not only can be considered as a great candidate for PHA production using several aromatic and cheap substrates under balanced growth conditions, but it is a nice example of how the application of a DBTL cycles can improve significantly biotechnological output. However, further DBTL runs targeted on strain optimization via additional genetic iterations and/or evolutionary engineering via Adaptive Laboratory Experiments (ALE) could be performed to ameliorate certain growth parameters such as growth rate, biomass yield and PHA production (Fong *et al.*, 2005b; Conrad *et al.*, 2011; Dragosits and Mattanovich, 2013).

5. INTEGRATED DISCUSSION

5 INTEGRATED DISCUSSION

PHA are biodegradable polymers with similar properties to the petrochemical derived polymers. There is an increasing interest over the years about their production and the molecular basis of the PHA metabolism regulation. PHA are reserve storage granules generally considered to play a role as sink for carbon and reducing equivalents when other nutrients are limited (De Eugenio *et al.*, 2010a; Prieto *et al.*, 2016). The buffering role of PHA cycle by maintaining active the recirculation of key metabolites of central metabolism has been proposed previously (Ren *et al.*, 2009; De Eugenio *et al.*, 2010a; Nogales *et al.*, 2017). As it will be discussed, this characteristic could provide stability in fitness and metabolic robustness under fluctuating environmental conditions.

In this Doctoral Thesis, we checked the impact of tuning the flux through the PHA cycle in conferring metabolic robustness to *P. putida* KT2440 physiology (Results chapter 1). Among the mechanisms providing biological robustness, the redundant (alternative) mechanisms have been also proposed (Kitano, 2004). The presence of two isocitrate dehydrogenase isoenzymes in *P. putida* KT2440 was, investigated (Results Chapter 2). In the final Results chapter, recombinant microorganisms have been obtained, able to reroute the carbon flux provided by recalcitrant and inexpensive abundant carbon sources towards high-value added product production, such as PHA.

5.1 Chapter 1: PHA cycle tuning contributes to *P. putida* KT2440 metabolic robustness

In this chapter, we focused on the effect of PHA cycle on the overall metabolism, as biological robustness in *P. putida* KT2440. For this purpose several mutant strains on key *pha* genes were obtained. First of all, in order to avoid the PHA cycle turnover in *P. putida* cells, the *phaZ* depolymerase null mutant strain (KT40Z) was constructed and the absence of polar effects on downstream *pha* genes was verified by qRT-PCR experiments (Figures 22-23). Higher *phaF* and *phaI* transcription levels were observed in KT40Z null background compared to wild type strain (Figure 23). Similar observation was reported previously by Cai and collaborators (Cai *et al.*, 2009), where the *phaC2* transcription levels were higher in the *phaZ* null mutant compared to the parental KT2442 strain under PHA accumulation conditions, probably due to the higher amounts of PHA in the *phaZ* null mutant strain. Additionally, in order to avoid the whole *pha* cluster complex native regulation, a null *pha* strain was obtained and used as a control strain in this study (http://xurl.es/35c8f).

To increase the flux through the *phaZ* depolymerase reaction, a battery of strains, M0 to M4 driving differential *phaZ* depolymerase expression levels were constructed in a KT40Z background (Figure 24 and Table 5). The resulting strains were further validated by Western blot experiments (Figure 25) and, as it would be expected, the PhaZ production levels were correlated to the strength of the applied promoters (Zobel *et al.*, 2015).

To investigate the impact of tuning the PhaZ production levels on the carbon metabolism of the cell, a battery of phenotyping analyses were performed under PHA mobilization and PHA accumulation conditions (Figures 26-28). Under the former conditions, where the PHA degradation is favored, no major differences were observed in all the strains tested, in terms of growth characteristics (growth rate, viable cell number, cell size) (Figure 26 and Table 6). For instance, as it could be expected, the only strain able to accumulate PHA content after 24 h of growth under these conditions was the KT40Z, since the *phaZ* depolymerase was not present to degrade the polymer, reaching up to 29% PHA (Figure 26 and Table 6).

However, under PHA accumulation conditions large differences were found regarding the PHA accumulation properties of the different cells tested. In fact, with higher PhaZ production levels, the trend was towards no PHA accumulation, resulting to one log increase in viable cell number and twice smaller cell size (Figure 27). Similar observations have been described previously in *pha* mutant strains (De Eugenio *et al.*, 2010a). Furthermore, the strains with higher PhaZ production levels, favored the PHA degradation resulting in releasing free monomers (*(R)*-HAs; Tables 7-10) to the culture medium supernatant. These results are in accordance to previous observations from our laboratory with a *phaZ* overproduction strain in *P. putida* KT2442 (De Eugenio *et al.*, 2010a) and in *P. putida* U by (Sandoval *et al.*, 2005). Interestingly, after 24 h of growth under PHA accumulation conditions, we were able to produce 2.5 times more *(R)*-HAs in the M2-M4 strains compared to the wild type. Additionally, the strains with higher PhaZ expression levels (M2-M4) had less total biomass due to no PHA production, that results in loss of carbon either in form of accumulation of extracellular metabolites or in an increased CO_2 production. In order to check the accumulation of metabolite originated from an unbalanced carbon metabolism, the culture supernatant of the strains after 24 h of growth under PHA accumulation conditions was analyzed by HPLC. However, no significant amounts of any of the metabolites tested were detected, as reported previously in other *pha* mutant strains (Escapa *et al.*, 2012).

To get a glance of the impact of PHA cycle tuning on the overall *P. putida* metabolism, the experimental data (Tables 7-10 and Figures 27-30) were contextualized in the *in silico i*JN1411 genome-scale model. In order to cover the whole range of growth

phases (A, B, C) observed, three condition-specific models for each strain were constructed (Figures 29 and 31). Based on the results observed in Figure 31, it can be concluded that the *in silico* model *i*JN1411 predicts accurently what is happening *in vivo* and it is a useful tool in order to study the metabolism. Previous metabolic flux analysis using stoichiometric model for a pseudo steady state period (4-8.5 hours of growth under PHA accumulation conditions) of KT2442 and KT42C1 strains has been performed in our group (Escapa *et al.*, 2012). To be best of our knowledge, this is the first study where a detailed *in silico* modeling of PHA metabolism was performed throughout the whole growth curves including different growth phases.

By flux analyses such as random sampling of Monte Carlo (Schellenberger and Palsson, 2009), we studied how PHA cycle tuning affects *P. putida* metabolism. Modifying the PHA cycle leads to significant metabolic changes (Figure 31), which are reflected on the differential strains response throughout the growth phases A, B and C (Figures 32-35 and Supplementary Tables S8-S10). Interestingly, the null *phaZ* (KT40Z) and M1 (strain with low PhaZ levels) strains have higher flux through key reactions affecting the TCA cycle, the energy conservation and the CO_2 production compared to wild type strain, during the growth phase A (Figure 32 and Table S8). Thus, these strains could be a promising tool for metabolic engineering processes affecting the TCA cycle such as, TCA metabolite production, e.g., succinate or proteinogenic amino acids (Molina-Henares *et al.*, 2010)

Furthermore, the strains with higher PhaZ levels maintained higher flux distribution through key reactions involved in gluconeogenesis, β-oxidation, TCA cycle, energy generation and CO_2 production compared to wild type strain during phase C (Figure 34 and Table S10). Thus, these *P. putida* recombinant cells were still metabolically active even during stationary phase, an interesting and promising quality that it could be useful for maintaining the cells alive for longer periods. Maintenance of viability is a desirable feature for prokaryotic cell array assays, as tools in toxicity testing (Elad *et al.*, 2008). Additionally, these strains could demonstrate higher resistance to environmental stresses and they could be a valuable tool in experiments using resting cells. Finally, this library of strains with tuning PhaZ production levels exhibited higher *(R)*-HAs monomers production compared to wild type strain and they could be promising biotechnological candidates for scaling up process to produce these enantiopure products.

The *(R)*-HAs monomers have been considered really valuable substrates, since they can be used as building blocks for a variety of biotechnological applications such as, for the synthesis of antibiotics, polyesters, vitamins, flavors and pheromones (Ruth *et al.*, 2007; De Eugenio *et al.*, 2010a). It was also reported that some *(R)*-HAs could act as antimicrobial, insecticidal, antiviral agents (Sandoval *et al.*, 2005; Ruth *et al.*, 2007;

De Eugenio *et al.*, 2010a; Koskimäki *et al.*, 2016). Furthermore, It was reported that intracellular concentration of 3HB monomer in *C. necator* was 16.5 times higher than in mutant incapable of PHA biosynthesis, serving as a potent chemical chaperone protecting proteins and other molecules from denaturation during low and high temperatures, heavy metals and oxidative stress. It was also proposed to be an efficient cryo-protectant (Obruca *et al.*, 2016a; Obruca *et al.*, 2016c). To test if *(R)*-HAs could protect against oxidative stress in *P. putida* KT2440, the sensitivity to oxidative stress was checked in plate assays. In fact, in both growth conditions, these preliminary results showed that the M4 strain resulted in 1.3 to 1.5 more tolerance to oxidative stress compared to the other strains tested (data not shown).

Key interrelated aspects to be considered for a competitive *(R)*-HA production at large scale are substrate cost, product purification and strain fitness. Previous studies in our laboratory characterized a KTZ1 strain able to produce 10 fold higher amounts of *(R)*-HAs than the wild type strain, in a regulable expression system driven by *Pm*/*XylS* inducible by benzoate. This strain was suggested to be an interesting biotechnological candidate for scaling up process (De Eugenio *et al.*, 2010a). In the M4 strain, the expression levels of *phaZ* are under the control of a constitutive strong promoter (14g) without the need of extrernal inductor and its chromosomal location is known due to the specific integration event using mini-Tn*7* system compared to mini-Tn*5* in the case of KTZ1 strain, that it was inserted randomly. Thus, the M4 strain could also be an interesting tool for large-scale production of HAs and further biotechnological applications.

It could be concluded that by modulating the carbon flux through the PHA cycle, *Pseudomonas putida* physiology could be varied. PHA metabolism balances global biomass, including PHA carbon/energy storage, cell division and energy spillage. It acts as a metabolic buffer cycle by absorbing and releasing carbon as required. Thus, PHA is not only a source of carbon during carbon starvation (Obruca *et al.*, 2016b), but rather a key element in resource balancing that guarantees efficient growth.

The impact of PHA cycle in cell physiology and stress resistance has been studied previously in several microorganisms (Introduction section 1.5 and reviewed recently by (Obruca *et al.*, 2018)). There are controversial studies on whether just the presence of PHA granule (Goh *et al.*, 2014), or the ability to accumulate and/or mobilize the PHA could attribute to stress resistance. For instance, it was reported that just the presence of PHA granules provided protection against oxidative stress provoked by photoactivated TiO_2 in *Delftia acidovorans*. Additionally, it cannot be discarded that phasins were involved in conferring resistance to stress (due to the chaperone-like activity), apart from their primary function to cover the PHA granule. This might contribute to the protective

mechanism of PHA in their natural producers. Protective effect of the PHA granules was observed in engineered strains where the phasins and depolymerase were absent (Wang *et al.*, 2009; Goh *et al.*, 2014). Thus, in this work it is proposed that PHA cycle in *P. putida* KT2440 contributes to metabolic robustness.

5.2 Chapter 2: Isocitrate dehydrogenase isoenzymes play a crutial role in *P. putida* KT2440 robustness

Among the alternative mechanisms of robustness, the gene functional redundancy properties have been proposed (Kitano, 2004; Nogales *et al.*, 2017). The existence of more than one similar mechanisms that can replace each other when needed, such as response to environmental perturbations, guarantees the integrity of the whole system. In this work, the presence and physiological roles of isocitrate dehydrogenase isoenzymes (PIDH) in *P. putida* KT2440 have been studied.

Isocitrate dehydrogenase is a key enzyme of the TCA cycle, highly conserved and widely observed from bacteria to humans. Generally speaking, there are two isocitrate dehydrogenases; the $NADP^+$-dependent IDH and NAD^+-dependent IDH (majorly found in eukaryotic organisms). $NADP^+$-dependent IDH could either form a dimeric structure composed of identical subunits of 40-50 kDa or/and monomeric one with molecular weight of 80-100 kDa (Gálvez and Gadal, 1995).

From evolutionary studies, it was suggested that the eubacterial $NADP^+$-isocitrate dehydrogenase was evolved from NAD^+-IDH about 3.5 billion years ago as a result of an adaptive event (Dean and Golding, 1997). Most prokaryotic IDHs (PIDH) are $NADP^+$-dependent. It has been proposed that this coenzyme discrimination has a biological significance. For instance, bacteria able to grow on acetate, generate up to 90% of the NADPH necessary for biosynthesis by using $NADP^+$-PIDH. However, bacteria harboring NAD^+-IDH variants such as the obligate methylotroph *Methylobacillus falgellatus* are not able to grow on acetate and lack either a respiratory chain or a complete TCA cycle due to absence of an a-ketoglutarate dehydrogenase (Romkina and Kiriukhin, 2017). Following this different cofactor usage, in the recent years, there is a great interest towards the coenzyme specificity swapping by site-directed mutagenesis such as on *E. coli* or *Bifidobacterium longum* (Huang *et al.*, 2016; Armingol *et al.*, 2018). This was possibile due to the identification of the amino acid that confer $NADP^+$-coenzyme specificity based on the available crystal data (Tables 11-12). In fact, the key amino acid responsible for the $NADP^+$-specificity are for the dimeric ICD of *E. coli* Arg292´, Lys344, Tyr345, Val351, Tyr391 and Arg395, with the major determinants being the Lys344 and

Tyr345 (Chen *et al.*, 1997; Chen and Yang, 2000), while for the monomeric IDH of *A. vinelandii* were the Arg358, Lys588, His589 and Arg649 (Yasutake *et al.*, 2002, 2003).

Furthermore, the majority of prokaryotes tend to have only one type of PIDH mostly dimeric, such as *E. coli*, or monomeric, such as *A. vinelandii*. Multiple alignment of the dimeric and monomeric PIDH from the widely studied organisms was performed (Figures 41-42). These two types of PIDH share only 8% of identity in amino acid structure-based sequence alignment. This could apply that both PIDH have evolved convergently. However, Yasutake and collaborators, suggested that monomeric IDH may have evolved through the duplication of domains (B-C) in an ancestral dimeric ICD. Using the available crystal data of *A. vinelandii*, it was observed that the amino acid residues responsible for the binding of isocitrate and metal cation are identical between the monomeric and dimeric PIDH (Figures 41-43 and Tables 11-12). The interaction of the monomeric IDH with $NADP^+$ should be different from the dimeric ICD, since the amino acid residues are not completely identical in both PIDH (Yasutake *et al.*, 2002, 2003).

Interestingly, some organisms possess both types of PIDH such as *C. maris*, *C. psychrerythraea* strain NRC1004 or 34H and *P. psychrophila* (Ochiai *et al.*, 1979; Maki *et al.*, 2006; Matsuo *et al.*, 2010). Having two PIDH was majorly found in psychrophilic microorganisms, providing them probably advantage to survive in these extreme environments (Ochiai *et al.*, 1979; Ishii *et al.*, 1993; Suzuki *et al.*, 1995; Watanabe *et al.*, 2005; Yasuda *et al.*, 2013; Kobayashi and Takada, 2014). Studies on the *C. maris* and *C. phychrerythraea* concluded that the dimeric ICD were typical mesophilic and acetate induced enzymes, while the monomeric IDH were cold-adapted and thermolabile. Furthermore, different promoters independently regulated the two PIDH (see Figure 37 for their DNA chromosomal location). However, this can not be taking as an universal rule. For instance, in the case of *P. psychrophila* both PIDH were mesophilic enzymes with slight inductions by cold or acetate in the expression of monomeric and dimeric PIDH, respectively (Matsuo *et al.*, 2010).

At the beginning of this study, we found interesting the fact that *P. putida* KT2440 also possesses two PIDH, despite the fact that it is mainly a characteristic observed in psychrophiles. Until now, there is not enough information available about these PIDHs in pseudomonads and has not been studied on *P. putida* KT2440. We confirmed that both PIDH genes were transcriptionally active in *P. putida* and the expression of these enzymes was carbon source dependent (Figures 38-39). Additionally, it seems like there is a clear preference towards the monomeric *idh*, since it exhibited higher transcription levels than the dimeric i*cd* in all the conditions tested by qRT-PCR experiments (Figure 39).

In order to study the physiological importance of this enzyme duplication, we proposed to construct single and double deletion mutants of these PIDH. Unfortunately, only the dimeric ICD deletion mutant was obtained (PP_4011), resulting to MM18 strain. A similar result was observed in *Mycobacterium tuberculosis*, where Murina and collaborators concluded that maybe the monomeric isocitrate dehydrogenase is essential for the microorganism growth (Murima *et al.*, 2016). However, checking for gene essentiality studies in *P. aeruginosa*, different transposon insertions mutants were identified, suggesting that the monomeric *idh* in *P. aeruginosa* and probably in *P. putida* is not an essential gene (Jacobs *et al.*, 2003; Lewenza, 2005). Moreover, the PIDH are not among the conditionally essential genes for growth identified in *P. putida* KT2440 (Molina-Henares *et al.*, 2010). Finally, there are not considered as possible bottleneck for the strain performance, since there were not among the 300 genes deleted by Martínez and collaborators (Martínez-García *et al.*, 2014).

Phenotypic evaluation of growth performance of dimeric *icd* deletion mutant, MM18 strain using several carbon sources, resulted in no major differences when compared to wild type strain (Figure 40). Since several deletions attempts of the monomeric IDH were fruitless, we tried to get closer to the metabolic role of these enzymes through enzymatic approaches. Thus, the monomeric *idh* and dimeric *icd* genes of *P. putida* were heterologously overexpressed in *E.coli* by using pET29a vectors and His tagged purification of both PIDH was performed. In this work, we addressed the identification and confirmation of the catalytic sites determinant for the enzymatic activity of the monomeric IDH. Therefore, by site-directed mutagenesis on Ser133Ala, Asn136Ala and Arg140Ala in the monomeric IDH (PP_4012mut strain; Figures 43-44 and Table 13), the enzymatic activity was lost completely, demonstrating that these predicted amino acid residues were critical for the IDH enzymatic activity in *P. putida* KT2440. Previous work on *C. glutamicum*, demonstrated that the mutant Lys253Met in the monomeric IDH, lost its enzymatic activity too (Chen and Yang, 2000).

During the realization of this study, two interesting works have been published in *M. tuberculosis* and *P. aeruginosa* possessing both PIDH (Murima *et al.*, 2016; Crousilles *et al.*, 2018). Comparing the monomeric IDH of both organisms to that of *P. putida*, 60.3% (*M. tuberculosis*) and 66.3% (*P. aeruginosa*) of identity was observed. Under standard assay conditions, the monomeric IDH had more specific activity than the dimeric ICD, which is in accordance to previous observations in *P. psychrophila* (82.1% identity) (Matsuo *et al.*, 2010). Furthermore, the monomeric IDH (PP_4012) presented higher values of turnover (kcat) and catalytic activity (kcat/km) than the dimeric ICD (PP_4011). However, opposite results have been described in *P. aeruginosa* (Crousilles *et al.*, 2018). As far as it concerns the km values for $NADP^+$, no major differences were observed

between monomeric and dimeric isoenzymes, which is in accordance to previous observations in *P. aeruginosa* (Crousilles *et al.*, 2018). The low km values for $NADP^+$ indicate the clear preference towards it. Finally, higher km values for isocitrate have been observed in the monomeric IDH compared to the dimeric one. These km values for isocitrate in the case of the monomeric IDH have been higher than the previously reported in *C. gluramicum*, *A. vinelandii* and *P. aeruginosa* (Chen and Yang, 2000; Watanabe *et al.*, 2005; Crousilles *et al.*, 2018).

In the recent years, there is also an interest on determining the key amino acid residues responsible for the thermal properties of the monomeric IDH (Watanabe *et al.*, 2005; Matsuo *et al.*, 2010; Kobayashi and Takada, 2014). Matsuo and collaborators identified some different key amino acid residues between the mesophilic and cold-adapted monomeric IDH of *P. psychrophila* and *C. maris (and C. psychrerythraea)* respectively (Matsuo *et al.*, 2010). Between those amino acids His158Asn, Pro490Glu, Glu595Lys and Pro709Ala, but only the Glu55Lys resulted in the decreased thermolability, suggesting that Glu55 is involved in the mesophilic properties of *P. psychrophila* monomeric IDH. All these residues are also conserved in *P. putida* KT2440, explaining the mesophilic properties of monomeric IDH. A recent update of the amino acids responsible for the thermal properties in *C. maris* y *P. psychrophila* is available (Nagai and Takada, 2019).

So far, it is not clear why *P. putida* KT2440 has two PIDH and how it is regulated the competition for isocitrate by ICL and the two PIDH. In the recent work by Crousilles and collaborators in *P. aeruginosa* showed that the AceK, encoding the ICD kinase/phosphatase, phosphorylates and inactivates at 75% the dimeric ICD and not the monomeric IDH. This is due to structural differences on the P-loop and AceK recognition segment which are absent in monomeric IDH (Crousilles *et al.*, 2018). They also proposed a “rheostatic control”, where high amounts of gluconeogenic precursors such as succinate and glyoxylate could inhibit ICL and activate the AceK phosphatase activity by stimulation of ICD activity and therefore greater flux through the TCA cycle for biomass production. However, the opposite result is obtained with low amounts of oxaloacetate and pyruvate that inhibit ICD by activating ICL when there is an increase demand of gluconeogenesis. Finally, another “rheostat mechanism” was described in *M. tuberculosis* that also possesses ICL, ICD and IDH but lacks AceK (absence of ICD phosphorylation) (Murima *et al.*, 2016). Murima and collaborators demonstrated that only the monomeric IDH has an important physiological role under all the condition tested and there is a “cross-activation” of the IDH by the glyoxylate partitioning the flux between the TCA cycle and the glyoxylate shunt. It is possible that this is the case for the monomeric

IDH of *P. putida* KT2440. Further investigation, need to be realized in order to figure out the physiological importance of the two PIDH in *P. putida* KT2440.

5.3 Chapter 3: *P. putida* KT2440 strains overproducing PHA from PHA unrelated carbon sources

PHA are accumulated in microorganism as energy and carbon source stores under unbalanced nutritional conditions, mainly including an excess of carbon together the lack of other nutrients (such as phosphorus, nitrogen, and oxygen). A large effort has been done to optimize the production of PHA by using chemical or metabolic engineering approaches.

Over the past decade, one crucial design principle for metabolic engineering and computational strain design is to couple cellular growth with the production of a desired functionality (metabolite/growth). The goal is to make the desired metabolite a mandatory by-product of growth and its production an integral part of the organism´s metabolic fuction. Thus, growth of the organism becomes a driving force of production (von Kamp and Klamt, 2017). This dependent production usually possesses a burden on the organism resulting to longer lag phases and less growth rates than the wild type strains. In this way, without coupling the functionality that is needed for production, it could be lost from a production strain, that adapts to a higher growth rate at this functionality. Finally, when a growth-coupled strain has been designed, its production capabilities could be improved through ALE by selecting for maximum growth or desired metabolite production. A variety of *E. coli* mutant strains has successfully been constructed using growth coupling approaches for the production of lactic acid (Fong *et al.*, 2005a), ethanol (Trinh and Srienc, 2009), malonyl-CoA (Xu *et al.*, 2011) and itaconic acid (Harder *et al.*, 2016), among others.

In this Doctoral Thesis, growth-coupled strategies were used to obtain PHA overproducer *P. putida* strains. Previously other works involving Pseudomonas strains have been described. For instance, the growth of *Pseudomonas pseudoalcaligenes* in jewelry industry wastewater containing cyanide was coupled to PHA production in batch reactors (Manso Cobos *et al.*, 2015). Recently, in *P. putida* KT2440 coupling the growth to PHA production was realized on fed-batch cultures from a mixture of fatty acids (Andin *et al.*, 2017). In this work, the *P. putida* growth was coupled to PHA production by using non-PHA related carbon sources, such as aromatic compounds derived from lignin or PET degradation processes. The mutant strains are forced to produce PHA in order to be able to grow with maximal growth rate.

Our growth coupled designs were based on blocking the succinate and acetyl-CoA metabolism, the TCA cycle, the PHA metabolism and amino acid metabolism. These deletions focused on rerouting the carbon flux towards the PHA production (Figure 54). An *in vivo* validation of the sequential deletion mutants was realized after 24 h of growth using M63 minimal medium supplemented by 3 mM octanoate and 5 mM 4-hydroxybenzoate (Figure 60 and Table 22). Key reactions that led to a PHA production increase were succinyl-CoA synthase *sucC, D* and isocitrate lyase *aceA*. Even though, the beneficiary role of *aceA* to PHA production was previously proposed (Klinke *et al.*, 2000), the deletion of *sucCD* genes related to improved PHA capabilitites. Finally, the resulting MM16 strain produced 4.8 times more PHA than the wild type strain, in terms of % of CDW (Figure 60 and Table 22) under balanced growth conditions and this PHA originated from the β-oxidation pathway (Table 23).

As confirmed by qRT-PCR experiments (Figure 61), the transcription levels of key enzymes for PHA production from non-fatty acid precursors were downregulated in MM16 strain compared to KT2440 and KT40Z strains. This phenotype was expected, as metabolic models do not take into account regulation processes. In order to obtain an optimized expression of the key enzymes responsible for PHA production, the *phaC1*, *phaF*, *phaG* and PP_0763 genes were overexpressed under the constitutive SynPro16 promoter, using Golden-Gate Moclo approaches (Figures 64-65) (Engler and Marillonnet, 2011; Tiso *et al.*, 2016). The resulting MT1 and MT2 strains were tested for PHA production using M63 minimal medium supplemented with aromatic compounds derived of lignin or PET hydrolysis (Figure 66 and Tables 24-26). MT1 accumulated 14.7-19.7% of PHA/CDW under these conditions compared to 4.1-7.8% of MT2 and traces of KT2440 (Table 26).

Previous work in *E. coli* have shown that the co-expression of acyl-CoA ligase PP_0763 with *phaG* from *P. putida* KT2440 led to an increase on the PHA production from glucose, as sole carbon source (Q. Wang *et al.*, 2012). Recently, recombinant *P. putida* strains have been obtained, able to produce high yields of PHA from aromatic compounds and lignin. In fact, these strains lacked the *phaZ* and the *fadBA* genes, involved in PHA depolymerization and β-oxidation pathway, respectively (Salvachúa *et al.*, 2020). Additionally, in order to increase the flux towards PHA production, Salvachúa and collaborators, realized a codon-optimized overexpression of the *phaC1*, *phaC2* synthases, *phaG* and PP_0763 genes. This construct was overexpressed under the P*tac* promoter and chromosomically integrated in the PP_0545 region of *P. putida* (Salvachúa *et al.*, 2020). These recombinant microorganisms reached significant amounts of PHA (0.95 g/L) after 72 h of growth under N limited conditions supplemented by *p*-coumaric

acid (C/N ratio: 55.6 mol/mol, Table 33). To favor the PHA production fed-batch and high-cell-densitiy approaches were applied (Salvachúa *et al.*, 2020).

Growth and PHA production from lignin derived and enriched compounds (APL) combined with nitrogen limitation have been studied before in *P. putida* KT2440 (Linger *et al.*, 2014; Salvachúa *et al.*, 2015; Beckham *et al.*, 2016; Ravi *et al.*, 2017) *and P. putida* Gpo1 and *P. putida* JCM 13063 strains (Tomizawa *et al.*, 2014). Selected examples describing PHA production from lignin-derived aromatic substrates are listed in the Table 33.

In fact, during the realization of this study, several works have been published using different lignin derived substrates. Two different studies have been performed in *P. putida* A514 focusing on lignin valorization towards PHA production (Lin *et al.*, 2016; X. Wang *et al.*, 2018). These authors designed three functional modules affecting the dye peroxidase-based enzymatic system, several peripheral and central catabolism pathways and up–down regulated the β-oxidation and the *de novo* fatty acid synthesis, respectively. As a result, they reached up to 37% (under N excess) and 73% (under N limitation) of cell dry weight PHA production from M9 minimal medium supplemented with 15 mM vanillic acid. However, this study provided incomplete data as far as it concerns the conditions of PHA production and its corresponding characterization. The *P. putida* A514 strain was proposed as a more robust bacteria than other *P. putida* strains (such as CA-3) for PHA production under N excess (Lin *et al.*, 2016). However, this Doctoral Thesis is the first study in *P. putida* KT2440 where PHA production is obtained from lignin derivated compounds without N limitation. The second study on *P. putida* A514 is more complete than the previous one, providing a battey of strains overexpressing the *phaJ4 phaC1* genes or *phaG alkK phaC1* genes under the constitutive Pvan or strong indusible PxylA promoter. The authors provide promising results under N excess and limitation conditions supplied by 15 mM vanillic acid (X. Wang *et al.*, 2018). Some of these results are listed in the Table 33.

In our work, the PHA properties characterization, suggested that the strains MT1 and MT2 had the same PHA productivity (PHA production in g/L), even though the MT1 strain reached higher %PHA/CDW. The low residual biomass of MT1 strain is a drawback compared to MT2 and wild type strain and an aspect to consider for further scale up processes. Therefore, MT1 strain is a great candidate for PHA production using several aromatic substrates derived from PET or lignin degradation. However, further strain optimization and possible ALE experiments should be performed to ameliorate certain growth parameters such as growth rate, biomass yield and PHA production (Fong *et al.*, 2005b; Conrad *et al.*, 2011; Dragosits and Mattanovich, 2013).

Microorganism	Substrate (mM)	Fermentation Mode (hours)	CDW (g/L)	PHA (g/L)	PHA (% CDW)	References
P. putida JCM13063	Vanillic acid (59.5)	Batch (72 h)	0.21	Traces	<1	(Tomizawa *et al.*, 2014)
P. putida Gpo1	Vanillic acid (59.5)	Batch (72 h)	0.14	Traces	<1	(Tomizawa *et al.*, 2014)
P. putida A514	Vanillic acid (14.9)	Batch (50)	0.66	0.01	1.7	(X. Wang *et al.*, 2018)
P. putida A514 Axyl_*alkKphaGC1*	Vanillic acid (14.9)	Batch (50)	0.71	0.25	34.4	(X. Wang *et al.*, 2018)
P. putida A514	Vanillic acid (14.9)	Batch (50)	0.13	0.02	17.3	(X. Wang *et al.*, 2018)
P. putida A514 Axyl_*alkKphaGC1*	Vanillic acid (14.9)	Batch (50)	0.18	0.01	66.3	(X. Wang *et al.*, 2018)
P. putida Gpo1	*p*-coumaric acid (61)	Batch (72 h)	0.27	Traces	<1	(Tomizawa *et al.*, 2014)
P. putida KT2440	*p*-coumaric acid (12.2)	Batch (48 h)	0.47	0.16	34	(Linger *et al.*, 2014)
P. putida KT2440	*p*-coumaric acid (12.2)	Batch (72 h)	0.38	0.16	41	(Salvachúa *et al.*, 2020)
P. putida KT2440 AG2162	*p*-coumaric acid (12.2)	Fed-Batch (72 h)	0.48	0.24	50	(Salvachúa *et al.*, 2020)
P. putida KT2440 AG2162	*p*-coumaric acid (12.2)	Fed-Batch, HCD (85 h)	1.76	0.95	54.2	(Salvachúa *et al.*, 2020)
P. putida Gpo1	Ferulic acid (51.5)	Batch (72 h)	0.15	Traces	<1	(Tomizawa *et al.*, 2014)
P. putida KT2440	Ferulic acid (10.3)	Batch (48 h)	0.44	0.17	39	(Linger *et al.*, 2014)
P. putida Gpo1	4HBz (72.4)	Batch (72 h)	0.22	Traces	<1	(Tomizawa *et al.*, 2014)

Table 33. Selected examples describing mcl-PHA production from lignin-derived aromatic substrates using native and engineered pseudomonads strains. In all the cases N limitation was used except in the case of *P. putida* A514 strain (shown by shaded grey color).

Nowadays, there is an increasing interest on the development of sustainable approaches towards PHA synthesis. For industrial scale PHA production, a significant factor to consider is the cost of the process. Several variables contribute to this cost such as the type of substrate, the microbial fermentation and the PHA extraction approaches, among others. The carbon substrate price account for about 50% of the overall production costs (Koller *et al.*, 2010; Gomez *et al.*, 2012). The choise of the adequate

carbon source strongly depends on the location of the intented production plant, in order to save costs for transportation and facilities. Furthermore, the seasonal availability and in sufficient quantity of to be used resources are other factors to consider (Koller *et al.*, 2010). Thus, the need for PHA production from cheap substrates has arised, using waste streams alternatives, highly available in Europe. Moving towards economic feasibility, the PHA production prices are estimated below 2-3 €/kg (Koller and Braunegg, 2018). Previous works in different bacterial species successfully led to PHA production from industrial and agricultural substrates that do not require extensive purification steps, such as milk whey (Nikel *et al.*, 2006; Bustamante *et al.*, 2019), sugarcane molasses (Park *et al.*, 2015; Löwe *et al.*, 2017a; Löwe *et al.*, 2017b) and biodiesel derived glycerol (Escapa *et al.*, 2013; Fu *et al.*, 2014; Beckers *et al.*, 2016). Similarly, in this Doctoral Thesis we provided recombinant *P. putida* KT2440 microorganisms capable to transform inexpensive and available carbon sources to PHA production such as glycerol and sucrose.

Over the last decade, it was observed an increased biodiesel production in several countries all over the world, with 85% coming from the European Union (www.ebb-eu.org/studiesreports/EMISIA_Contribution_Biofuels_transport_sustainability.pdf). As a consequence, considerable amounts of its major side stream, glycerol have been generated, leading to a significant decrease in glycerol price (10 kg of crude glycerol is generated for every 100 kg of biodiesel produced). Thus, in order to improve the viability of biofuel industry, glycerol was applied as the preferred substrate in microbial fermentation processes (recently reviewed (Poblete-Castro *et al.*, 2019)). It has been demonstrated that glycerol facilitate the polymer synthesis over glucose or lactose, due to its higher degree of reduction (γ=4.7 vs γ=4 in glucose). Thus, since less carbon has to be oxidized into CO_2 for reducing power generation, higher substrate yield could be available for PHA production (Gomez *et al.*, 2012; Poblete-Castro *et al.*, 2019). There are several studies realized in pseudomonads, testing the impact of glycerol on growth performance, metabolic response, PHA production among others. The activation of both glucolytic and gluconeogenic pathways has been proposed by transcriptomic analyses using glycerol as carbon source (Nikel *et al.*, 2014a). Some of the genes transcriptionally upregulated were the glycerol transport and catabolic genes (such as *glp* gene cluster) and an activation of gluconeogenic response has been observed. Additionally, alternative pathways for carbon processing have been downregulated including TCA cycle and gluconate/2-ketogluconate loop for hexoses oxidation (Nikel *et al.*, 2014a).

In order to expand the carbon substrates for PHA production, the engineered *P. putida*, MT1 and MT2 strains were used for further phenotypic analyses and PHA quantification under balanced conditions using glucose or glycerol as carbon sources

(Figures 68-70 and Tables 28-31). Since glucose is not a PHA related substrate, *P. putida* KT2440 is able to reach from 13.4 to almost 25% PHA under PHA accumulation condition (Poblete-Castro *et al.*, 2013; Fonseca *et al.*, 2014). However, as it would be expected and previously reported, wild-type strain produced insignificant amount of PHA (less than 2%) under balanced growth conditions (Figure 68 and Table 28). Interestingly, the MT2 and MT1 strains reached up to 14% and 27.5% PHA production after 24 h of growth using 10 mM glucose, compared to the insignificant PHA amount observed by the wild type strain (C/N ratio: 2 mol/mol, Figure 68 and Table 28).

Several *P. putida* recombinant strains were also tested for PHA productions using glycerol as carbon source. *P. putida* KT2440 grows slowly and with long lag phase, when glycerol is applied as sole carbon source (Wang and Nomura, 2010; Escapa *et al.*, 2013). This long lag-phase can be avoided by co-feeding strategies, by supplying small amounts of octanoate and glucose, or by creating a *glpR* regulator knock-out mutant (Escapa *et al.*, 2013). In this work, co-substrate of 1 mM or 1.33 mM of octanoate or glucose were applied, respectively allowing faster growth and higher PHA production (C/N ratio: 2.26 mol/mol; Figures 69-70 and Tables 30-31). In fact, MT2 and MT1 strains, reached up to 9.7% and 30% PHA/CDW after 24 h of growth using 20 mM glycerol supplemented by 1.33 mM glucose, while similar amounts of PHA were reached with octanoate adding (Figure 69 and Table 30).

Selected bibliographic examples describing PHA production from glycerol are listed in the Table 34. A variety of PHA pattern was observed, probably due to the different metabolic regulation among strains and culture conditions (Table 34).

Microorganism	Fermentation Mode (hours)	PHA (g/L)	PHA (% CDW)	Yield (g/g)	References
P. putida GO16	Fed-batch (48 h)	6.3	33	0.16	(Kenny *et al.*, 2012)
P. putida LS46	Batch (72 h)	0.6	16.3	0.02	(Fu *et al.*, 2014)
P. mosselii TO7	Batch (48 h)	1.3	9.9*	N.A.	(Liu *et al.*, 2018)
P. putida KT2440	Batch (72 h)	1.5	34.5	0.05	(Poblete-Castro *et al.*, 2014)
P. putida KT2440 Δ*phaZ*	Batch (72 h)	2.0	46.8	0.07	(Poblete-Castro *et al.*, 2014)
P. putida KT2440	Batch (46 h)	0.15	19	N.A.	(Escapa *et al.*, 2013)
P. putida KT2440 Δ*glpR*	Batch (46 h)	0.34	34	N.A.	(Escapa *et al.*, 2013)

Table 34. Selected examples describing mcl-PHA production from glycerol using native and engineered pseudomonads strains. * The %PHA varies depending glycerol concentration reaching up to 48% when 12% glycerol was used. N.A.: not determined.

Wastes from lignocellulosic feedstocks, starch, or sugar industry such as molasses are abundant for industrial biotechnology demands. Since the sugar extraction is not economically viable process, low-grade molasses (inappropriate for food applications) have been used as alternative carbon substrates for PHA production by diverse Gram negative and positive bacteria (Gomez *et al.*, 2012). Recently, recombinant *C. necator* strains reached up to 20% and 73% of PHA/CDW production, when cultured under defined medium containing 20 g/L sucrose (Park *et al.*, 2015). During the realization of this work, engineered *P. putida* KT2440 strains were obtained conferring sucrose consumption (Löwe *et al.*, 2017a). For this purpose, broad-host range mini-transposons were constructed bearing *cscA* and *cscB* genes of *E. coli* W encoding for the sucrose invertase and the sucrose permease, respectively. Interestingly, based on this system these authors successfully produced 0.16 g/L PHA applying a synthetic bacterial co-culture composed of two-biomodules. From one hand the cyanobacterial strain *Synechococcus elongatus* bearing *cscB* gene, able to fix CO_2 and convert it to sucrose and export it to the culture supernatant by the help of CscB. From the other hand, *P. putida cscAcscB* can efficiently metabolize the secreted sucrose and produce PHA (Löwe *et al.*, 2017a). Aimed by these studies, similar recombinant *P. putida* strains were obtained in this Doctoral Thesis (MT9-MT11 strains; Figures 62 and 71) leading up to 34.5% of PHA/CDW production using 5 mM sucrose under balanced medium conditions (Figure 72 and Table 32). So far, these are encouraging results for further scale-up approaches, however, further strains optimization need to be realized.

Summing up, in this Doctoral Thesis, interactive designs combining the advances in synthetic and systems biology were applied in order to achieve the planned objectives. Then, recombinant microorganisms capable of producing high amounts of *(R)*-HAs were provided and *P. putida´s* physiology was varied depending on the PHA cycle dosis. The significance of the isocitrate dehydrogenase isoenzymes in the *P. putida* KT2440 physiology leading to robustness properties, was studied. Finally, aimed by cutting edge synthetic biology approaches, a high number of gene knockouts and knockins was carried out, in order to systematically remove all the potential competing pathways and to reroute the carbon flux towards PHA production. Therefore, recombinant microorganisms capable of producing high amounts of PHA from unrelated and inexpensive carbon sources were provided. In fact, we used recalcitrant carbon sources derived from PET, PU or lignin hydrolysis (4-hydroxybenzoic acid, vanillic acid, *p*-coumaric acid and phenylacetic acid) and cheap-abundant substrates (glucose, sucrose and glycerol). Furthermore, the engineered organisms are able to produce PHA in the absence of nutritional limitations. This constitutes a first evidence of *P. putida* producing PHA from unrelated carbon source under balanced C/N ratio conditions. Therefore, the

envisioned PHA production bioprocess supported by these strains constitutes a significant improvement with respect to wild type strain. However, further strains optimization, via metabolic engineering and ALE approaches, is a necessity for future scale-up processes.

6. CONCLUSIONS

6 CONCLUSIONS

1. By finely modulating the carbon flux through the PHA cycle, we can gradually vary important physiological parameters in *P. putida*. Strains harboring high constitutive PhaZ depolymerase levels tend to have one log increase in the viable cell number, smaller cell size and increased *(R)*-HAs production compared to the wild type strain.
2. High flux through the *pha* cycle drives a residual oxidative metabolism under stationary phase. This metabolism provides an increased capability of *P. putida* as biocatalyst at stationary phase.
3. M4 *P. putida* strain, harboring the highest flux through PhaZ depolymerase, is a highly valuable biotechnological strain, as source of enantiopure *(R)*-HAs.
4. *P. putida* has two genes encoding for isocitrate dehydrogenase that are transcriptionally active under the conditions tested. The expression of these genes is carbon-source-dependent and there is a clear preference towards the monomeric IDH production The presence of both isoenzymes likely responds to a robustness mechanism, focusing on functional redundancy.
5. The biochemical characterization confirms the enzymatic functionality of both enzymes. Km values for the $NADP^+$ could indicate clear preference towards this cofactor, compared to NAD^+. Furthermore, we provide here the first experimental evidence supporting the role of residues Ser133, Asn136 and Arg140, as essential for the monomeric IDH activity.
6. Genetics evidence based on the several fruitless deletion attempts of the monomeric *idh*, strongly suggested that this isoenzyme is an essential gene for *P. putida* under various growth conditions, irrespective of the functionality of the dimeric isoform.
7. Model-driven designs of PHA-growth-coupled overproducing strains using complex polymers such as PET, lignin, PU and its monomers substrates have been successfully obtained *in silico*. PET4 is the best design for further *in vivo* implementation in terms of PHA yield, biomass-coupled product yield, number of knockouts and physiological feasibility.
8. MM16 growth–coupled strain can efficiently produce PHA under balanced growth conditions due to the engineering carbon flux rerouting towards PHA production. While the PHA is produced in this strain via β-oxidation pathway, *de novo* fatty acid biosynthesis pathway is hampered by regulatory constraints under these culture conditions.
9. MT1 strain is a great candidate for PHA production using several recalcitrant substrates under balanced growth conditions, reaching up to 20% of PHA/cell dry weight

production. The superior performance of MT1 was achieved by avoiding the natural regulation of PHA gene cluster and by engineering a growth-coupled and constitutive expression of optimized synthetic genes required for PHA production.

10. By expanding the natural metabolic versatility of *P. putida* towards new carbon sources, by using synthetic biology approaches, it has been possible to construct a *P. putida* strain, MT9, overproducing PHA using inexpensive and abundant disaccharides, such as sucrose, as carbon source under balanced growth conditions, reaching up to 35% of PHA/cell dry weight production.

6 CONCLUSIONES

1. La modulación precisa del flujo de carbono a través del ciclo de PHA permite variar parámetros fisiológicos clave en *P. putida* gradualmente de forma controlada. Las cepas que producen constitutivamente altos niveles de PhaZ tienden a aumentar un log el número de células viables, tienen un tamaño de célula más pequeño y presentan una mayor producción de *(R)*-HA, en comparación con la cepa de tipo salvaje.
2. Un alto flujo metabólico a través del ciclo del PHA favorece la emergencia de un metabolismo oxidativo residual en la fase estacionaria. Esto proporciona a *P. putida* una mayor capacidad como biocatalizador en esta fase de crecimiento.
3. La cepa *P. putida* M4, que presenta el flujo de carbono más alto dirigido por la despolimerasa PhaZ, es una cepa muy valiosa como fuente de *(R)*-HA desde un punto de vista biotecnológico.
4. *P. putida* tiene dos genes que codifican la isocitrato deshidrogenasa, que son transcripcionalmente activos en las condiciones probadas, y su expresión depende de la fuente de carbono. Los resultados indican que existe una clara preferencia hacia la producción de la IDH monomérica. La presencia de ambas isoenzimas probablemente responde a un mecanismo de robustez basado en redundancia funcional.
5. La caracterización bioquímica confirma la funcionalidad de ambas enzimas. Los valores de Km para $NADP^+$, indica una clara preferencia hacia este cofactor en lugar de NAD^+. Este trabajo proporciona la primera evidencia experimental que apoya el papel de los residuos Ser133, Asn136 y Arg140, como esenciales para la actividad monomérica de la IDH.
6. Evidencias genéticas basadas en varios intentos fallidos de eliminación de la IDH monomérica sugieren que esta isoenzima es un gen esencial para *P. putida* en diversas condiciones de crecimiento. Esta esencialidad es independientemente de la funcionalidad de la isoforma dimérica.
7. Utilizando como base un modelo metabólico a escala genómica, se han obtenido con éxito diseños *in silico* de cepas super-productoras de PHA, en las que la producción está acoplada al crecimiento bacteriano. Las fuentes de carbono utilizadas en los diseños son polímeros complejos como PET, lignina, PU y sus sustratos de monómeros. PET4 es el mejor diseño para su posterior implementación *in vivo* en términos de rendimiento de PHA, rendimiento acoplado en la biomasa, en el número de deleciones y en la viabilidad fisiológica.
8. La cepa MM16 presenta un re-direccionamiento del flujo de carbono que le permite producir PHA acoplada al crecimiento de manera eficiente en condiciones de

crecimiento equilibradas. El PHA se produce en esta cepa a través de la vía de β-oxidación. Sin embargo, la vía de biosíntesis *de novo* de ácidos grasos está disminuida por restricciones reguladoras en estas condiciones de cultivo.

9. La cepa MT1 es un candidato óptimo para la producción de PHA a partir de varios sustratos recalcitrantes en condiciones de crecimiento equilibrado, alcanzando hasta un 20% de producción de PHA respecto al peso seco total. Este alto rendimiento alcanzado por la cepa MT1 se logró al anular la regulación natural de los genes *pha*, y el posterior diseño e implementación de un sistema de expresión constitutiva, y acoplada al crecimiento, de los genes necesarios para la producción de PHA que previamente fueron optimizados y sintetizados.

10. Mediante la expansión de la versatilidad metabólica natural de *P. putida* hacia la utilización de nuevas fuentes de carbono, utilizando aproximaciones de biología sintética, ha sido posible construir la cepa de *P. putida* MT9 que produce PHA utilizando como fuente de carbono disacáridos abundantes y económicos como la sacarosa en condiciones de crecimiento equilibrado. La producción alcanza hasta un 35% de PHA respecto a su peso seco.

7. REFERENCES

7 REFERENCES

Alhasawi, A., Castonguay, Z., Appanna, N.D., Auger, C., and Appanna, V.D. (2015) Glycine metabolism and anti-oxidative defence mechanisms in *Pseudomonas fluorescens*. *Microbiological Research* **171**: 26-31.

Anderson, J.C., Dueber, J.E., Leguia, M., Wu, G.C., Arkin, A.P., and Keasling, J.D. (2010) BglBricks: A flexible standard for biological part assembly. *Journal of Biological Engineering* **4**: 1-12.

Andin, N., Longieras, A., Veronese, T., Marcato, F., Molina-Jouve, C., and Uribelarrea, J.-L. (2017) Improving carbon and energy distribution by coupling growth and medium chain length polyhydroxyalkanoate production from fatty acids by *Pseudomonas putida* KT2440. *Biotechnology Bioprocess Engineering* **22**: 308-318.

Anjum, A., Zuber, M., Zia, K.M., Noreen, A., Anjum, M.N., and Tabasum, S. (2016) Microbial production of polyhydroxyalkanoates (PHAs) and its copolymers: A review of recent advancements. *International Journal of Biological Macromolecules* **89**: 161-174.

Aparicio, T., de Lorenzo, V., and Martínez-García, E. (2015) Broadening the SEVA Plasmid Repertoire to Facilitate Genomic Editing of Gram-Negative Bacteria. In, McGenity,T.J., Timmis,K.N., and Nogales,B. (eds), *Hydrocarbon and Lipid Microbiology Protocols*. Berlin, Heidelberg: Springer Berlin Heidelberg, pp. 9-27.

Archer, C.T., Kim, J.F., Jeong, H., Park, J.H., Vickers, C.E., Lee, S.Y., and Nielsen, L.K. (2011) The genome sequence of *E. coli* W (ATCC 9637): comparative genome analysis and an improved genome-scale reconstruction of *E. coli*. *BMC Genomics* **12**: 9.

Arias, S., Sandoval, A., Arcos, M., Cañedo, L.M., Maestro, B., Sanz, J.M., *et al*. (2008) Poly-3-hydroxyalkanoate synthases from *Pseudomonas putida* U: substrate specificity and ultrastructural studies. *Microbial Biotechnology* **1**: 170-176.

Armingol, E., Tobar, E., and Cabrera, R. (2018) Understanding the impact of the cofactor swapping of isocitrate dehydrogenase over the growth phenotype of *Escherichia coli* on acetate by using constraint-based modeling. *PLOS ONE* **13**: e0196182.

Baart, G.J.E. and Martens, D.E. (2012) Genome-Scale Metabolic Models: Reconstruction and Analysis. In, Christodoulides,M. (ed), *Neisseria meningitidis*. Totowa, NJ: Humana Press, pp. 107-126.

Bagdasarian, M., Lurz, R., Rückert, B., Franklin, F.C., Bagdasarian, M.M., Frey, J., and Timmis, K.N. (1981) Specific-purpose plasmid cloning vectors. II. Broad host range, high copy number, RSF1010-derived vectors, and a host-vector system for gene cloning in *Pseudomonas*. *Gene* **16**: 237-247.

Becker, S.A., Feist, A.M., Mo, M.L., Hannum, G., Palsson, B.Ø., and Herrgard, M.J. (2007) Quantitative prediction of cellular metabolism with constraint-based models: the COBRA Toolbox. *Nature Protocols* **2**: 727-738.

Beckers, V., Poblete-Castro, I., Tomasch, J., and Wittmann, C. (2016) Integrated analysis of gene expression and metabolic fluxes in PHA-producing *Pseudomonas putida* grown on glycerol. *Microbial Cell Factories* **15**: 1-18.

Beckham, G.T., Johnson, C.W., Karp, E.M., Salvachúa, D., and Vardon, D.R. (2016) Opportunities and challenges in biological lignin valorization. *Current Opinion in Biotechnology* **42**: 40-53.

Beld, J., Lee, D.J., and Burkart, M.D. (2015) Fatty acid biosynthesis revisited: structure elucidation and metabolic engineering. *Molecular bioSystems* **11**: 38-59.

Belda, E., van Heck, R.G.A., José Lopez-Sanchez, M., Cruveiller, S., Barbe, V., Fraser, C., *et al*. (2016) The revisited genome of *Pseudomonas putida* KT2440 enlightens its value as a robust metabolic chassis. *Environmental Microbiology* **18:** 3403-3424.

Belisário-Ferrari, M.R., Wei, R., Schneider, T., Honak, A., and Zimmermann, W. (2019) Fast Turbidimetric Assay for Analyzing the Enzymatic Hydrolysis of Polyethylene Terephthalate Model Substrates. *Biotechnology Journal* **14**: 1800272.

Best, E.A. and Knauf, V.C. (1993) Organization and nucleotide sequences of the genes encoding the biotin carboxyl carrier protein and biotin carboxylase protein of *Pseudomonas aeruginosa* acetyl coenzyme A carboxylase. *Journal of Bacteriology* **175**: 6881-6889.

Bojanovič, K., D'Arrigo, I., and Long, K.S. (2017) Global transcriptional responses to osmotic, oxidative, and imipenem stress conditions in *Pseudomonas putida*. *Applied and Environmental Microbiology* **83:** e03236-16**.**

Borrero-de Acuña, J.M., Bielecka, A., Häussler, S., Schobert, M., Jahn, M., Wittmann, C., *et al*. (2014) Production of medium chain length polyhydroxyalkanoate in metabolic flux optimized *Pseudomonas putida*. *Microbial cell factories* **13**: 88.

Boyer, H.W. and Roulland-Dussoix, D. (1969) A complementation analysis of the restriction and modification of DNA in *Escherichia coli*. *Journal of Molecular Biology* **41**: 459-472.

Bradford, M.M. (1976) A Rapid and Sensitive Method for the Quantitation of Microgram Quantities of Protein Utilizing the Principle of Protein-Dye Binding. *Analytical Biochemistry* **72**: 248-254.

Bresan, S., Sznajder, A., Hauf, W., Forchhammer, K., Pfeiffer, D., and Jendrossek, D. (2016) Polyhydroxyalkanoate (PHA) granules have no phospholipids. *Scientific Reports* **6**.

Bustamante, D., Segarra, S., Tortajada, M., Ramón, D., del Cerro, C., Prieto, M.A., *et al.* (2019) *In silico* prospection of microorganisms to produce polyhydroxyalkanoate from whey: *Caulobacter segnis* DSM 29236 as a suitable industrial strain. *Microbial Biotechnology* **12**: 487-501.

Cai, L., Yuan, M.Q., Liu, F., Jian, J., and Chen, G.Q. (2009) Enhanced production of medium-chain-length polyhydroxyalkanoates (PHA) by PHA depolymerase knockout mutant of *Pseudomonas putida* KT2442. *Bioresource Technology* **100**: 2265-2270.

Campbell, J.W. and Cronan, J.E. (2001) Bacterial Fatty Acid Biosynthesis: Targets for Antibacterial Drug Discovery. *Annual Review of Microbiology* **55**: 305-332.

del Castillo, T., Ramos, J.L., Rodriguez-Herva, J.J., Fuhrer, T., Sauer, U., and Duque, E. (2007) Convergent Peripheral Pathways Catalyze Initial Glucose Catabolism in *Pseudomonas putida*: Genomic and Flux Analysis. *Journal of Bacteriology* **189**: 5142-5152.

Castro-Sowinski, S., Burdman, S., Matan, O., and Okon, Y. (2010) Natural Functions of Bacterial Polyhydroxyalkanoates. In, Chen,G.G.-Q. (ed), *Plastics from Bacteria*. Berlin, Heidelberg: Springer Berlin Heidelberg, pp. 39-61.

Cebolla, A. and Arévalo-Rodríguez, M. (2010) Genetic Analysis of Gram-Negative Bacteria Using Mini Tn*5* Transposons. In, Timmis,K.N. (ed), *Handbook of Hydrocarbon and Lipid Microbiology*. Berlin, Heidelberg: Springer Berlin Heidelberg, pp. 4243-4254.

Chen, G.-Q. (2009) A microbial polyhydroxyalkanoates (PHA) based bio- and materials industry. *Chemical Society Reviews* **38**: 2434-2446.

Chen, R., Greer, A.F., and Dean, A.M. (1997) Structural Constraints in Protein Engineering. The Coenzyme Specificity of *Escherichia coli* Isocitrate Dehydrogenase. *European Journal of Biochemistry* **250**: 578-582.

Chen, R. and Yang, H. (2000) A highly specific monomeric isocitrate dehydrogenase from *Corynebacterium glutamicum*. *Archives of Biochemistry and Biophysics* **15**: 238-245.

Choi, K.-H., Gaynor, J.B., White, K.G., Lopez, C., Bosio, C.M., Karkhoff-Schweizer, R.R., and Schweizer, H.P. (2005) A Tn*7*-based broad-range bacterial cloning and expression system. *Nature Methods* **2**: 443-448.

Choi, K.-H. and Kim, K.-J. (2009) Applications of Transposon-Based Gene Delivery System in Bacteria. *Journal of Microbiolal Biotechnology* **19:** 217-228.

Choi, K.H., Kumar, A., and Schweizer, H.P. (2006) A 10-min method for preparation of highly electrocompetent *Pseudomonas aeruginosa* cells: Application for DNA fragment transfer between chromosomes and plasmid transformation. *Journal of Microbiological Methods* **64**: 391-397.

Choi, K.-H. and Schweizer, H.P. (2006) mini-Tn*7* insertion in bacteria with single *att*Tn*7* sites: example *Pseudomonas aeruginosa*. *Nature Protocols* **1**: 153-161.

Clarke, P.H. (1982) The metabolic versatility of pseudomonads. *Antonie van Leeuwenhoek* **48**: 105-130.

Cobb, R.E., Wang, Y., and Zhao, H. (2015) High-Efficiency Multiplex Genome Editing of *Streptomyces* Species Using an Engineered CRISPR/Cas System. *ACS Synthetic Biology* **4**: 723-728.

Conrad, T.M., Lewis, N.E., and Palsson, B.O. (2011) Microbial laboratory evolution in the era of genome-scale science. *Molecular Systems Biology* **7**: 509.

Cook, T.B., Rand, J.M., Nurani, W., Courtney, D.K., Liu, S.A., and Pfleger, B.F. (2018) Genetic tools for reliable gene expression and recombineering in *Pseudomonas putida*. *Journal of Industrial Microbiology & Biotechnology* **45**: 517-527.

Cozzone, A.J. and El-Mansi, M. (2005) Control of Isocitrate Dehydrogenase Catalytic Activity by Protein Phosphorylation in *Escherichia coli*. *Journal of Molecular Microbiology and Biotechnology* **9**: 132-146.

Cronan, Jr., J.E. and Rock, C.O. (2008) Biosynthesis of Membrane Lipids. *EcoSal Plus* **3**.

Crousilles, A., Dolan, S.K., Brear, P., Chirgadze, D.Y., and Welch, M. (2018) Gluconeogenic precursor availability regulates flux through the glyoxylate shunt in *Pseudomonas aeruginosa*. *Journal of Biological Chemistry* **293**: 14260-14269.

Danso, D., Chow, J., and Streit, W.R. (2019) Plastics: Environmental and Biotechnological Perspectives on Microbial Degradation. *Applied and Environmental Microbiology* **85**: e01095-19.

De Eugenio, L.I., García, P., Luengo, J.M., Sanz, J.M., Román, J.S., García, J.L., and Prieto, M.A. (2007) Biochemical evidence that *phaZ* gene encodes a specific intracellular medium chain length polyhydroxyalkanoate depolymerase in *Pseudomonas putida* KT2442: Characterization of a paradigmatic enzyme. *Journal of Biological Chemistry* **282**: 4951-4962.

De Eugenio, L.I., Escapa, I.F., Morales, V., Dinjaski, N., Galán, B., García, J.L., and Prieto, M.A. (2010a) The turnover of medium-chain-length polyhydroxyalkanoates in *Pseudomonas putida* KT2442 and the fundamental role of PhaZ depolymerase for the metabolic balance. *Environmental Microbiology* **12**: 207-221.

De Eugenio, L.I., Galán, B., Escapa, I.F., Maestro, B., Sanz, J.M., García, J.L., and Prieto, M.A. (2010b) The PhaD regulator controls the simultaneous expression of the *pha* genes involved in polyhydroxyalkanoate metabolism and turnover in *Pseudomonas putida* KT2442. *Environmental Microbiology* **12**: 1591-1603.

Dean, A.M. and Golding, G.B. (1997) Protein engineering reveals ancient adaptive replacements in isocitrate dehydrogenase. *Proceedings of the National Academy of Sciences* **94**: 3104-3109.

Dean, A.M., Lee, M.H., and Koshland, D.E. (1989) Phosphorylation inactivates *Escherichia coli* isocitrate dehydrogenase by preventing isocitrate binding. *Journal of Biological Chemistry* **264**: 20482-20486.

Dinjaski, N. and Prieto, M.A. (2013) Swapping of Phasin Modules To Optimize the *In Vivo* Immobilization of Proteins to Medium-Chain-Length Polyhydroxyalkanoate Granules in *Pseudomonas putida*. *Biomacromolecules* **14**: 3285-3293.

Dragosits, M. and Mattanovich, D. (2013) Adaptive laboratory evolution - principles and applications for biotechnology. *Microbial Cell Factories* **12**: 64.

Duque, E., Molina-Henares, A.J., Torre, J. de la, Molina-Henares, M.A., Castillo, T. del, Lam, J., and Ramos, J.L. (2007) Towards a Genome-Wide Mutant Library of *Pseudomonas putida* Strain KT2440. In, Ramos,J.-L. and Filloux,A. (eds), *Pseudomonas*. Dordrecht: Springer Netherlands, pp. 227-251.

Durham, D.R. and Phibbs, P.V. (1982) Fractionation and characterization of the phosphoenolpyruvate: fructose 1-phosphotransferase system from *Pseudomonas aeruginosa*. *Journal of Bacteriology* **149**: 534-541.

Durner, R., Witholt, B., and Egli, T. (2000) Accumulation of Poly[*(R)*-3-hydroxyalkanoates] in *Pseudomonas oleovorans* during growth with octanoate in continuous culture at different dilution rates. *Applied Environmental Microbiology* **66**: 3408-3414.

Edwards, J.S. and Palsson, B.O. (1999) Systems Properties of the *Haemophilus influenzae* Rd Metabolic Genotype. *Journal of Biolological Chemistry* **274**: 17410-17416.

Eguchi, H., Wakagi, T., and Oshima, T. (1989) A highly stable NADP-dependent isocitrate dehydrogenase from *Thermus thermophilic* HB8: purification and general properties. *Biochimica et Biophysica Acta (BBA) - General Subjects* **990**: 133-137.

Eikmanns, B.J., Rittmann, D., and Sahm, H. (1995) Cloning, sequence analysis, expression, and inactivation of the *Corynebacterium glutamicum icd* gene encoding isocitrate dehydrogenase and biochemical characterization of the enzyme. *Journal of Bacteriology* **177**: 774-782.

Elad, T., Lee, J.H., Belkin, S., and Gu, M.B. (2008) Microbial whole-cell arrays. *Microbial Biotechnology* **1**: 137-148.

Elmore, J.R., Furches, A., Wolff, G.N., Gorday, K., and Guss, A.M. (2017) Development of a high efficiency integration system and promoter library for rapid modification of *Pseudomonas putida* KT2440. *Metabolic Engineering Communications* **5:** 1-8.

Encarnacion, S., del Carmen Vargas, M., Dunn, M.F., Davalos, A., Mendoza, G., Mora, Y., and Mora, J. (2002) AniA Regulates Reserve Polymer Accumulation and Global Protein Expression in *Rhizobium etli*. *Journal of Bacteriology* **184**: 2287-2295.

Engler, C., Kandzia, R., and Marillonnet, S. (2008) A one pot, one step, precision cloning method with high throughput capability. *PLoS ONE* **3**: e3647.

Engler, C. and Marillonnet, S. (2011) Generation of families of construct variants using golden gate shuffling. *Methods in Molecular Biology* **729**: 167-181.

Escapa, I.F., García, J.L., Bühler, B., Blank, L.M., and Prieto, M.A. (2012) The polyhydroxyalkanoate metabolism controls carbon and energy spillage in *Pseudomonas putida*. *Environmental Microbiology* **14**: 1049-1063.

Escapa, I.F., del Cerro, C., García, J.L., and Prieto, M.A. (2013) The role of GlpR repressor in *Pseudomonas putida* KT2440 growth and PHA production from glycerol: *Pseudomonas putida* growth and PHA production from glycerol. *Environmental Microbiology* **15**: 93-110.

Famili, I., Forster, J., Nielsen, J., and Palsson, B.O. (2003) *Saccharomyces cerevisiae* phenotypes can be predicted by using constraint-based analysis of a genome-scale reconstructed metabolic network. *Proceedings of the National Academy of Sciences* **100**: 13134-13139.

Fiedler, S., Steinbuchel, A., and Rehm, B.H.A. (2000) PhaG-Mediated Synthesis of Poly(3-Hydroxyalkanoates) Consisting of Medium-Chain-Length Constituents from Nonrelated Carbon Sources in Recombinant *Pseudomonas fragi*. *Applied and Environmental Microbiology* **66**: 2117-2124.

Fiedler, S., Steinbüchel, A., and Rehm, B. (2002) The role of the fatty acid β-oxidation multienzyme complex from *Pseudomonas oleovorans* in polyhydroxyalkanoate biosynthesis: molecular characterization of the *fadBA* operon from *P. oleovorans* and of the enoyl-CoA hydratase genes *phaJ* from *P. oleovorans* and *Pseudomonas putida*. *Archives of Microbiology* **178**: 149-160.

Fong, S.S., Burgard, A.P., Herring, C.D., Knight, E.M., Blattner, F.R., Maranas, C.D., and Palsson, B.O. (2005a) *In silico* design and adaptive evolution of *Escherichia coli* for production of lactic acid. *Biotechnology and Bioengineering* **91**: 643-648.

Fong, S.S., Joyce, A.R., and Palsson, B.Ø. (2005b) Parallel adaptive evolution cultures of *Escherichia coli* lead to convergent growth phenotypes with different gene expression states. *Genome Research* **15**: 1365-1372.

Fonseca, P., de la Peña, F., and Prieto, M.A. (2014) A role for the regulator PsrA in the polyhydroxyalkanoate metabolism of *Pseudomonas putida* KT2440. *International Journal of Biological Macromolecules* **71**: 14-20.

Franden, M.A., Javakodv, L.N., Li, W.J., Cleveland, N.S., Michener, W.E., Hauer, B., *et al*. (2018) Engineering *Pseudomonas putida* KT2440 for efficient ethylene glycol utilization. *Metabolic Engineering* **48**: 197-207.

Frank, S., Klockgether, J., Hagendorf, P., Geffers, R., Schöck, U., Pohl, T., *et al.* (2011) *Pseudomonas putida* KT2440 genome update by cDNA sequencing and microarray transcriptomics: *P. putida* KT2440 genome update. *Environmental Microbiology* **13**: 1309-1326.

Fu, J., Sharma, U., Sparling, R., Cicek, N., and Levin, D.B. (2014) Evaluation of medium-chain-length polyhydroxyalkanoate production by *Pseudomonas putida* LS46 using biodiesel by-product streams. *Canadian Journal of Microbiology* **60**: 461-468.

Fukunaga, N., Sasaki, S., Minowa, O., Mizuno, Y., Shiokawa, H., and Science, I. (1987) Isozymes Psychrophilic of Isocitrate Bacterium, Dehydrogenase *Vibrio* Strain an Obligately and Modulation of Activities by Growth Conditions and quaternary homogeneous state from an obligately psychrophilic marine chromatography was an efficient procedure. *Journal of Biochemistry* **102**: 1489-1498.

Galán, B., Dinjaski, N., Maestro, B., De Eugenio, L.I., Escapa, I.F., Sanz, J.M., *et al. (*2011) Nucleoid-associated PhaF phasin drives intracellular location and segregation of polyhydroxyalkanoate granules in *Pseudomonas putida* KT2442. *Molecular Microbiology* **79**: 402-418.

Gálvez, S. and Gadal, P. (1995) On the function of the NADP-dependent isocitrate dehydrogenase isoenzymes in living organisms. *Plant Science* **105**:1-14.

Gao, X., Chen, J.C., Wu, Q., and Chen, G.Q. (2011) Polyhydroxyalkanoates as a source of chemicals, polymers, and biofuels. *Current Opinion in Biotechnology* **22**: 768-774.

Gellatly, S.L. and Hancock, R.E.W. (2013) *Pseudomonas aeruginosa* : new insights into pathogenesis and host defenses. *Pathogens and Disease* **67**: 159-173.

Gemperlein, K., Zipf, G., Bernauer, H.S., Müller, R., and Wenzel, S.C. (2016) Metabolic engineering of *Pseudomonas putida* for production of docosahexaenoic acid based on a myxobacterial PUFA synthase. *Metabolic Engineering* **33**: 98-108.

Ghisla, S. and Thorpe, C. (2004) Acyl-CoA dehydrogenases. A mechanistic overview. *European Journal of Biochemistry* **271**: 494-508.

Gibson, D.G., Young, L., Chuang, R.-Y., Venter, J.C., Hutchison, C.A., and Smith, H.O. (2009) Enzymatic assembly of DNA molecules up to several hundred kilobases. *Nature Methods* **6**: 343-345.

Goh, L.K., Purama, R.K., and Sudesh, K. (2014) Enhancement of Stress Tolerance in the Polyhydroxyalkanoate Producers without Mobilization of the Accumulated Granules. *Applied Biochemistry and Biotechnology* **172**: 1585-1598.

Gomez, J.G.C., S., B., I., P., Julia, M., A., M., and F., L. (2012) Making Green Polymers Even Greener:Towards Sustainable Production of Polyhydroxyalkanoates from Agroindustrial By-Products. In, Petre,M. (ed), *Advances in Applied Biotechnology*. InTech, Rijeka, Croatia.

Graf, N. and Altenbuchner, J. (2011) Development of a Method for Markerless Gene Deletion in *Pseudomonas putida*. *Applied Environmenal Microbiology* **77**: 5549-5552.

Grant, S.G., Jessee, J., Bloom, F.R., and Hanahan, D. (1990) Differential plasmid rescue from transgenic mouse DNAs into *Escherichia coli* methylation-restriction mutants. *Proceedings of the National Academy of Sciences* **87**: 4645-4649.

Gu, C., Kim, G.B., Kim, W.J., Kim, H.U., and Lee, S.Y. (2019) Current status and applications of genome-scale metabolic models. *Genome Biology* **20**: 121.

Guzik, M.W., Narancic, T., Ilic-Tomic, T., Vojnovic, S., Kenny, S.T., Casey, W.T., *et al*. (2014) Identification and characterization of an acyl-CoA dehydrogenase from *Pseudomonas putida* KT2440 that shows preference towards medium to long chain length fatty acids. Microbiology 160: 1760-71.

Hampton, M.L. and Hanson, R.S. (1969) Regulation of isocitrate dehydrogenase from Thiobacillus thiooxidans and *Pseudomonas fluorescens*. *Biochemical and Biophysical Research Communications* **36**: 296-305.

Han, J., Hou, J., Liu, H., Cai, S., Feng, B., Zhou, J., and Xiang, H. (2010) Wide Distribution among Halophilic Archaea of a Novel Polyhydroxyalkanoate Synthase Subtype with Homology to Bacterial Type III Synthases. *Applied and Environmental Microbiology* **76**: 7811-7819.

Handrick, R., Reinhardt, S., Kimmig, P., and Jendrossek, D. (2004) The "Intracellular" Poly(3-Hydroxybutyrate) (PHB) Depolymerase of *Rhodospirillum rubrum* Is a Periplasm-Located Protein with Specificity for Native PHB and with Structural Similarity to Extracellular PHB Depolymerases. *Journal of Bacteriology* **186**: 7243-7253.

Harder, B.-J., Bettenbrock, K., and Klamt, S. (2016) Model-based metabolic engineering enables high yield itaconic acid production by *Escherichia coli*. *Metabolic Engineering* **38**: 29-37.

Heath, R.J. and Rock, C.O. (1996) Roles of the FabA and FabZ β-Hydroxyacyl-Acyl Carrier Protein Dehydratases in *Escherichia coli* Fatty Acid Biosynthesis. *Journal of Biological Chemistry* **271**: 27795-27801.

Heirendt, L., Arreckx, S., Pfau, T., Mendoza, S.N., Richelle, A., Heinken, A., *et al.* (2019) Creation and analysis of biochemical constraint-based models using the COBRA Toolbox v.3.0. *Nature Protocols* **14**: 639-702.

Herrero, M., De Lorenzo, V., and Timmis, K.N. (1990) Transposon vectors containing non-antibiotic resistance selection markers for cloning and stable chromosomal insertion of foreign genes in gram-negative bacteria. *Journal of Bacteriology* **172**: 6557-6567.

Hickman, A.B. and Dyda, F. (2016) DNA Transposition at Work. *Chemical Reviews* **116**: 12758-12784.

Hirota, R., Tsubouchi, K., and Takada, Y. (2017) $NADP^+$-dependent isocitrate dehydrogenase from a psychrophilic bacterium, *Psychromonas marina*. *Extremophiles* **21**: 711-721.

Hoang, T.T. and Schweizer, H.P. (1999) Characterization of *Pseudomonas aeruginosa* enoyl-acyl carrier protein reductase (FabI): a target for the antimicrobial triclosan and its role in acylated homoserine lactone synthesis. *Journal of Bacteriology* **181**: 5489-5497.

Hoek, M.J.A. van and Merks, R.M.H. (2017) Emergence of microbial diversity due to cross-feeding interactions in a spatial model of gut microbial metabolism. *BMC Systems Biology* **11**: 56.

Hoffmann, N. and Rehm, B.H.A. (2004) Regulation of polyhydroxyalkanoate biosynthesis in *Pseudomonas putida* and *Pseudomonas aeruginosa*. *FEMS Microbiology Letters* **237**: 1-7.

Hoffmann, N., Steinbüchel, A., and Rehm, B.H. (2000) Homologous functional expression of cryptic *phaG* from *Pseudomonas oleovorans* establishes the transacylase-mediated polyhydroxyalkanoate biosynthetic pathway. *Applied Microbiolial Biotechnology* **54**: 665-670.

Howard, L. and Becker, R.R. Isolation and Some Properties of the Triphosphopyridine Nucleotide Isocitrate Dehydrogenase from *Bacillus stearothermophilus*. J*ournal of Biological Chemistry* **245**: 3186-3194.

Huang, S.P., Cheng, H.M., Wang, P., and Zhu, G.P. (2016) Biochemical characterization and complete conversion of coenzyme specificity of isocitrate dehydrogenase from *Bifidobacterium longum*. *International Journal of Molecular Sciences* **17**.

Huisman, G.W., Wonink, E., Meima, R., Kazemier, B., Terpstra, P., and Witholt, B. (1991) Metabolism of poly(3-hydroxyalkanoates) (PHAs) by *Pseudomonas oleovorans*. Identification and sequences of genes and function of the encoded proteins in the synthesis and degradation of PHA. *Journal of Biological Chemistry* **266**: 2191-2198.

Ishii, A., Suzuki, M., Sahara, T., Takada, Y., Sasaki, S., and Fukunaga, N. (1993) Genes encoding two isocitrate dehydrogenase isozymes of a psychrophilic bacterium, *Vibrio* Genes Encoding Two Isocitrate Dehydrogenase Isozymes of a Psychrophilic Bacterium, *Vibrio* sp . Strain ABE-1. *Journal of Bacteriology* **175**: 6873-6880.

Iverson, S.V., Haddock, T.L., Beal, J., and Densmore, D.M. (2016) CIDAR MoClo: Improved MoClo Assembly Standard and New *E. coli* Part Library Enable Rapid Combinatorial Design for Synthetic and Traditional Biology. *ACS Synthetic Biology* **5**: 99-103.

Jacobs, M.A., Alwood, A., Thaipisuttikul, I., Spencer, D., Haugen, E., Ernst, S., *et al.* (2003) Comprehensive transposon mutant library of *Pseudomonas aeruginosa*. *Proceedings of the National Academy of Sciences* **100**: 14339-14344.

Jahreis, K., Bentler, L., Bockmann, J., Hans, S., Meyer, A., Siepelmeyer, J., and Lengeler, J.W. (2002) Adaptation of Sucrose Metabolism in the *Escherichia coli* Wild-Type Strain EC3132. *Journal of Bacteriology* **184**: 5307-5316.

Jendrossek, D. and Pfeiffer, D. (2014) New insights in the formation of polyhydroxyalkanoate granules (carbonosomes) and novel functions of poly(3-hydroxybutyrate). *Enironmental Microbiology* **16**: 2357-2373.

Jimenez, J.I., Minambres, B., Garcia, J.L., and Diaz, E. (2002) Genomic analysis of the aromatic catabolic pathways from *Pseudomonas putida* KT2440. *Environmental Microbiology* **4**: 824-841.

Jiménez, J.I., Miñambres, B., García, J.L., and Díaz, E. (2004) Genomic Insights in the Metabolism of Aromatic Compounds in *Pseudomonas*. In, Ramos,J.-L. (ed), *Pseudomonas*. Boston, MA: Springer US, pp. 425-462.

Jiménez, J.I., Nogales, J., García, J.L., and Díaz, E. (2010) A Genomic View of the Catabolism of Aromatic Compounds in Pseudomonas. In, Timmis,K.N. (ed), *Handbook of Hydrocarbon and Lipid Microbiology*. Berlin, Heidelberg: Springer Berlin Heidelberg, pp. 1297-1325.

Johnson and Beckham (2015) Aromatic catabolic pathway selection for optimal production of pyruvate and lactate from lignin. *Metabolic Engineering* **28**: 240-247.

Kadouri, D., Burdman, S., Jurkevitch, E., and Okon, Y. (2002) Identification and Isolation of Genes Involved in Poly(β-Hydroxybutyrate) Biosynthesis in *Azospirillum brasilense* and Characterization of a *phbC* Mutant. *Applied and Environmental Microbiology* **68**: 2943-2949.

Kadouri, D., Jurkevitch, E., and Okon, Y. (2003a) Involvement of the Reserve Material Poly-β-Hydroxybutyrate in *Azospirillum brasilense* Stress Endurance and Root Colonization. *Applied and Environmental Microbiology* **69**: 3244-3250.

Kadouri, D., Jurkevitch, E., and Okon, Y. (2003b) Poly β-hydroxybutyrate depolymerase (PhaZ) in *Azospirillum brasilense* and characterization of a *phaZ* mutant. *Archives of Microbiology* **180**: 309-318.

Kadouri, D., Jurkevitch, E., Okon, Y., and Castro-Sowinski, S. (2005) Ecological and Agricultural Significance of Bacterial Polyhydroxyalkanoates. *Critical Reviews in Microbiology* **31**: 55-67.

von Kamp, A. and Klamt, S. (2017) Growth-coupled overproduction is feasible for almost all metabolites in five major production organisms. *Nature Communications* **8**: 15956.

Kampers, L.F.C., Volkers, R.J.M., and Martins dos Santos, V.A.P. (2019) *Pseudomonas putida* KT2440 is HV 1 certified, not GRAS. *Microbial Biotechnology* **12**: 845-848.

Kanao, T., Kawamura, M., Fukui, T., Atomi, H., and Imanaka, T. (2002) Characterization of isocitrate dehydrogenase from the green sulfur bacterium *Chlorobium limicola*: A carbon dioxide-fixing enzyme in the reductive tricarboxylic acid cycle. *European Journal of Biochemistry* **269**: 1926-1931.

Kang, Y., Nguyen, D.T., Son, M.S., and Hoang, T.T. (2008) The *Pseudomonas aeruginosa* PsrA responds to long-chain fatty acid signals to regulate the *fadBA*5-oxidation operon. *Microbiology* **154**: 1584-1598.

Kenny, S.T., Runic, J.N., Kaminsky, W., Woods, T., Babu, R.P., and O'Connor, K.E. (2012) Development of a bioprocess to convert PET derived terephthalic acid and biodiesel derived glycerol to medium chain length polyhydroxyalkanoate. *Applied Microbiology and Biotechnology* **95**: 623-633.

Keshavarz-Tohid, V., Vacheron, J., Dubost, A., Prigent-Combaret, C., Taheri, P., Tarighi, S., *et al.* (2019) Genomic, phylogenetic and catabolic re-assessment of the *Pseudomonas putida* clade supports the delineation of *Pseudomonas alloputida* sp. nov., *Pseudomonas inefficax* sp. nov., *Pseudomonas persica* sp. nov., and *Pseudomonas shirazica* sp. nov. *Systematic and Applied Microbiology* **42**: 468-480.

Kessler, B., de Lorenzo, V., and Timmis, K.N. (1992) A general system to integrate *lacZ* fusions into the chromosomes of gram-negative eubacteria: regulation of the P_m promoter of the TOL plasmid studied with all controlling elements in monocopy. *Molecular Genetics and Genomics* **233**: 293-301.

Kim, J., Oliveros, J.C., Nikel, P.I., de Lorenzo, V., and Silva-Rocha, R. (2013) Transcriptomic fingerprinting of *Pseudomonas putida* under alternative physiological regimes. *Environmental Microbiology Reports* **5**: 883-891.

Kim, T.Y., Sohn, S.B., Kim, Y.B., Kim, W.J., and Lee, S.Y. (2012) Recent advances in reconstruction and applications of genome-scale metabolic models. *Current Opinion in Biotechnology* **23**: 617-623.

King, Z.A., O'Brien, E.J., Feist, A.M., and Palsson, B.O. (2017) Literature mining supports a next-generation modeling approach to predict cellular byproduct secretion. *Metabolic Engineering* **39**: 220-227.

Kitano, H. (2004) Biological robustness. *Nature Reviews Genetics* **5**: 826–837.

Kitano, H. (2007) Towards a theory of biological robustness. *Molecular Systems Biology* **3**: 137.

Klinke, S., Dauner, M., Scott, G., Kessler, B., and Witholt, B. (2000) Inactivation of isocitrate lyase leads to increased production of medium-chain-length poly(3-hydroxyalkanoates) in *Pseudomonas putida. Applied and Environmental Microbiology* **66**: 909-913.

Kniewel, R., Revelles Lopez, O., and Prieto, M.A. (2017) Biogenesis of Medium-Chain-Length Polyhydroxyalkanoates. In, Geiger,O. (ed), *Biogenesis of Fatty Acids, Lipids and Membranes*. Cham: Springer International Publishing, pp. 1-25.

Kobayashi, M. and Takada, Y. (2014) Effects of the combined substitutions of amino acid residues on thermal properties of cold-adapted monomeric isocitrate dehydrogenases from psychrophilic bacteria. *Extremophiles* **18**: 755-762.

Kohlstedt, M. and Wittmann, C. (2019) GC-MS-based 13C metabolic flux analysis resolves the parallel and cyclic glucose metabolism of *Pseudomonas putida* KT2440 and *Pseudomonas aeruginosa* PAO1. *Metabolic Engineering* **54**: 35-53.

Kojic, M. and Venturi, V. (2001) Regulation of *rpoS* Gene Expression in *Pseudomonas*: Involvement of a TetR Family Regulator. *Journal of Bacteriology* **183**: 3712-3720.

de Kok, A., Hengeveld, A.F., Martin, A., and Westphal, A.H. (1998) The pyruvate dehydrogenase multi-enzyme complex from Gram-negative bacteria. *Biochimica et biophysica acta* **1385**: 353-366.

Koller, M., Atlić, A., Dias, M., Reiterer, A., and Braunegg, G. (2010) Microbial PHA Production from Waste Raw Materials. In, Chen,G.G.-Q. (ed), *Plastics from Bacteria: Natural Functions and Applications*. Berlin, Heidelberg: Springer Berlin Heidelberg, pp. 85-119.

Koller, M. and Braunegg, G. (2018) Advanced approaches to produce polyhydroxyalkanoate (PHA) biopolyesters in a sustainable and economic fashion. *The EuroBiotech Journal* **2**: 89-103.

Koskimäki, J.J., Kajula, M., Hokkanen, J., Ihantola, E.L., Kim, J.H., Hautajärvi, H., *et al.* (2016) Methyl-esterified 3-hydroxybutyrate oligomers protect bacteria from hydroxyl radicals. *Nature Chemical Biology* **12**: 332-338.

Krebs, H.A. and Johnson, W.A. (1980) The role of citric acid in intermediate metabolism in animal tissues. *FEBS Letters* **117**: K2-K10.

Kukurugya, M.A., Mendonca, C.M., Solhtalab, M., Wilkes, R.A., Thannhauser, T.W., and Aristilde, L. (2019) Multi-omics analysis unravels a segregated metabolic flux network that tunes co-utilization of sugar and aromatic carbons in *Pseudomonas putida*. *Journal of Biological Chemistry* **294**: 8464-8479.

Kutchma, A.J., Hoang, T.T., and Schweizer, H.P. (1999) Characterization of a *Pseudomonas aeruginosa* fatty acid biosynthetic gene cluster: purification of acyl carrier protein (ACP) and malonyl-coenzyme A:ACP transacylase (FabD). *Journal of Bacteriology* **181**: 5498-5504.

La Rosa, R., de la Peña, F., Prieto, M.A., and Rojo, F. (2014) The Crc protein inhibits the production of polyhydroxyalkanoates in *Pseudomonas putida* under balanced carbon/nitrogen growth conditions: Crc control of PHA production in *P. putida*. *Environmental Microbiology* **16**: 278-290.

La Rosa, R., Nogales, J., and Rojo, F. (2015) The Crc/CrcZ-CrcY global regulatory system helps the integration of gluconeogenic and glycolytic metabolism in *Pseudomonas putida*: Crc controls succinate and glucose co-metabolism. *Environmental Microbiology* **17**: 3362-3378.

Lambertsen, L., Sternberg, C., and Molin, S. (2004) Mini-Tn*7* transposons for site-specific tagging of bacteria with fluorescent proteins. *Environmental Microbiology* **6**: 726-732.

Lee, S.Y., Wong, H.H., Choi, J., Lee, S.H., Lee, S.C., and Han, C.S. (2000) Production of medium-chain-length polyhydroxyalkanoates by high-cell-density cultivation of *Pseudomonas putida* under phosphorus limitation. *Biotechnology and Bioengineering* **68**: 466-470.

Lee, T., Krupa, R.A., Zhang, F., Hajimorad, M., Holtz, W.J., Prasad, N., *et al. (*2011) BglBrick vectors and datasheets: A synthetic biology platform for gene expression. *Journal of Biological Engineering* **5**: 12.

Lemoigne, M. (1926) Products of dehydration and of polymerization of β-hydroxybutyric acid. *Bulletin de la Société de chimie biologique* **8**: 770-782.

Leprince, A., de Lorenzo, V., Völler, P., van Passel, M.W.J., and Martins dos Santos, V.A.P. (2012) Random and cyclical deletion of large DNA segments in the genome of *Pseudomonas putida*: Random genomic deletions in *Pseudomonas putida*. *Environmental Microbiology* **14**: 1444-1453.

Lewenza, S. (2005) Construction of a mini-Tn*5*-luxCDABE mutant library in *Pseudomonas aeruginosa* PAO1: A tool for identifying differentially regulated genes. *Genome Research* **15**: 583-589.

Li, M.Z. and Elledge, S.J. (2012) SLIC: A Method for Sequence- and Ligation-Independent Cloning. In, Peccoud,J. (ed), *Gene Synthesis*. Totowa, NJ: Humana Press, pp. 51-59.

Li, Z., Yang, J., and Loh, X.J. (2016) Polyhydroxyalkanoates: opening doors for a sustainable future. *NPG Asia Materials* **8**: e265-e265.

Lin, L., Cheng, Y., Pu, Y., Sun, S., Li, X., Jin, M., *et al.* (2016) Systems biology-guided biodesign of consolidated lignin conversion. *Green Chemistry* **18**: 5536–5547.

Linger, J.G., Vardon, D.R., Guarnieri, M.T., Karp, E.M., Hunsinger, G.B., Franden, M.A., *et al.* (2014) Lignin valorization through integrated biological funneling and chemical catalysis. *Proceedings of the National Academy of Sciences* **111**: 12013-12018.

Liu, M.H., Chen, Y.J., and Lee, C.Y. (2018) Characterization of medium-chain-length polyhydroxyalkanoate biosynthesis by *Pseudomonas mosselii* TO7 using crude glycerol. *Bioscience, Biotechnology, and Biochemistry* **82**: 532-539.

Liu, R., Bassalo, M.C., Zeitoun, R.I., and Gill, R.T. (2015) Genome scale engineering techniques for metabolic engineering. *Metabolic Engineering* **32**: 143-154.

de Lorenzo, V., Herrero, M., Jakubzik, U., and Timmis, K.N. (1990) Mini-Tn*5* transposon derivatives for insertion mutagenesis, promoter probing, and chromosomal insertion of cloned DNA in gram-negative eubacteria. *Journal of Bacteriology* **172**: 6568-6572.

Löwe, H., Hobmeier, K., Moos, M., Kremling, A., and Pflüger-Grau, K. (2017a) Photoautotrophic production of polyhydroxyalkanoates in a synthetic mixed culture of *Synechococcus elongatus cscB* and *Pseudomonas putida cscAB*. *Biotechnology for Biofuels* **10**: 1-11.

Löwe, H., Schmauder, L., Hobmeier, K., Kremling, A., and Pflüger-Grau, K. (2017b) Metabolic engineering to expand the substrate spectrum of *Pseudomonas putida* toward sucrose. *MicrobiologyOpen* **6**: 1-9.

Lu, X., Zhang, J., Wu, Q., and Chen, G.-Q. (2003) Enhanced production of poly(3-hydroxybutyrate- *co* -3-hydroxyhexanoate) via manipulating the fatty acid β-oxidation pathway in *E. coli*. *FEMS Microbiology Letters* **221**: 97-101.

Lun, D.S., Rockwell, G., Guido, N.J., Baym, M., Kelner, J.A., Berger, B., *et al.* (2009) Large-scale identification of genetic design strategies using local search. *Molecular Systems Biology* **5**: 296.

Luo, X., Yang, Y., Ling, W., Zhuang, H., Li, Q., and Shang, G. (2016) *Pseudomonas putida* KT2440 markerless gene deletion using a combination of λ Red recombineering and Cre/loxP site-specific recombination. *FEMS Microbiology Letters* **363**.

Lv, P., Tang, W., Wang, P., Cao, Z., and Zhu, G. (2018) Enzymatic characterization and functional implication of two structurally different isocitrate dehydrogenases from *Xylella fastidiosa*: Two Isocitrate Dehydrogenases from *Xylella*. *Biotechnology and Applied Biochemistry* **65**: 230-237.

Maestro, B., Galán, B., Alfonso, C., Rivas, G., Prieto, M.A., and Sanz, J.M. (2013) A new family of intrinsically disordered proteins: structural characterization of the major phasin PhaF from *Pseudomonas putida* KT2440. *PLoS ONE* **8**: e56904.

Maki, S., Yoneta, M., and Takada, Y. (2006) Two isocitrate dehydrogenases from a psychrophilic bacterium, *Colwellia psychrerythraea*. *Extremophiles* **10**: 237-249.

Manso Cobos, I., Ibáñez García, M.I., de la Peña Moreno, F., Sáez Melero, L.P., Luque-Almagro, V.M., Castillo Rodríguez, F., *et al.* (2015) *Pseudomonas pseudoalcaligenes* CECT5344, a cyanide-degrading bacterium with by-product (polyhydroxyalkanoates) formation capacity. *Microbial Cell Factories* **14**: 77.

Martínez, V., Jurkevitch, E., García, J.L., and Prieto, M.A. (2013) Reward for *Bdellovibrio bacteriovorus* for preying on a polyhydroxyalkanoate producer. *Environmental Microbiology* **15**: 1204-1215.

Martínez-García, E. and de Lorenzo, V. (2011) Engineering multiple genomic deletions in Gram-negative bacteria: Analysis of the multi-resistant antibiotic profile of *Pseudomonas putida* KT2440. *Environmental Microbiology* **13**: 2702-2716.

Martínez-García, E. and de Lorenzo, V. (2012) Transposon-Based and Plasmid-Based Genetic Tools for Editing Genomes of Gram-Negative Bacteria. In, Weber,W. and Fussenegger,M. (eds), *Synthetic Gene Networks*. Totowa, NJ: Humana Press, pp. 267-283.

Martínez-García, E., Nikel, P.I., Aparicio, T., and de Lorenzo, V. (2014) *Pseudomonas* 2.0: genetic upgrading of *P. putida* KT2440 as an enhanced host for heterologous gene expression *Microbial Cell Factories* **13**: 159.

Martínez-García, E., Aparicio, T., Goñi-Moreno, A., Fraile, S., and de Lorenzo, V. (2015) SEVA 2.0: an update of the Standard European Vector Architecture for de-/re-construction of bacterial functionalities. *Nucleic Acids Research* **43**: D1183-D1189.

Martínez-García, E., Aparicio, T., de Lorenzo, V., and Nikel, P.I. (2017) Engineering Gram-Negative Microbial Cell Factories Using Transposon Vectors. In, Reeves,A. (ed), *In Vitro Mutagenesis*. New York, NY: Springer New York, pp. 273-293.

Mato, A., Tarazona, N.A., Hidalgo, A., Cruz, A., Jiménez, M., Pérez-Gil, J., and Prieto, M.A. (2019) Interfacial Activity of Phasin PhaF from *Pseudomonas putida* KT2440 at Hydrophobic–Hydrophilic Biointerfaces. *Langmuir* **35**: 678-686.

Matsuo, S., Shirai, H., and Takada, Y. (2010) Isocitrate dehydrogenase isozymes from a psychrotrophic bacterium, *Pseudomonas psychrophila*. *Archives of Microbiology* **192**: 639-650.

McDermott, T.R. and Kahn, M.L. (1992) Cloning and mutagenesis of the *Rhizobium meliloti* isocitrate dehydrogenase gene. *Journal of Bacteriology* **174**: 4790–4797.

McMahon, B., Gallagher, M.E., and Mayhew, S.G. (2005) The protein coded by the PP2216 gene of *Pseudomonas putida* KT2440 is an acyl-CoA dehydrogenase that oxidises only short-chain aliphatic substrates. *FEMS Microbiology Letters* **250**: 121-127.

McMahon, B. and Mayhew, S.G. (2007) Identification and properties of an inducible phenylacyl-CoA dehydrogenase in *Pseudomonas putida* KT2440. *FEMS Microbiology Letters* **273**: 50-57.

Miller, J.H., (1972) Experiments in Molecular Genetics. Cold Spring Harbor Laboratory Press: Cold Spring Harbor, NY.

Moldes, C., García, P., García, J.L., and Prieto, M.A. (2004) *In Vivo* Immobilization of Fusion Proteins on Bioplastics by the Novel Tag BioF. *Applied Environmental Microbiology* **70**: 3205-3212.

Molina-Henares, M.A., de la Torre, J., García-Salamanca, A., Molina-Henares, A.J., Herrera, M.C., Ramos, J.L., and Duque, E. (2010) Identification of conditionally essential genes for growth of *Pseudomonas putida* KT2440 on minimal medium through the screening of a genome-wide mutant library. *Environmental Microbiology* **12**: 1468-1485.

Monk, J., Nogales, J., and Palsson, B.O. (2014) Optimizing genome-scale network reconstructions. *Nature Biotechnology* **32**: 447-452.

Morris, C.E., Sands, D.C., Vinatzer, B.A., Glaux, C., Guilbaud, C., Buffière, A., *et al.* (2008) The life history of the plant pathogen *Pseudomonas syringae* is linked to the water cycle. *The ISME Journal* **2**: 321-334.

Murima, P., Zimmermann, M., Chopra, T., Pojer, F., Fonti, G., Dal Peraro, M., *et al.* (2016) A rheostat mechanism governs the bifurcation of carbon flux in mycobacteria. *Nature Communications* **7**: 12527.

Mutalik, V.K., Guimaraes, J.C., Cambray, G., Lam, C., Christoffersen, M.J., Mai, Q.A., *et al*. (2013) Precise and reliable gene expression via standard transcription and translation initiation elements. *Nature Methods* **10**: 354-360.

Nagai, S. and Takada, Y. (2019) Analysis of amino acid residues involved in the thermal properties of isocitrate dehydrogenases from a psychrophilic bacterium, *Colwellia maris*, and a psychrotrophic bacterium, *Pseudomonas psychrophila*. *Journal of Bioscience and Bioengineering* doi: 10.1016/j.jbiosc.2019.09.014.

Nakazawa, T. (2002) Travels of a Pseudomonas, from Japan around the world. *Environmental Microbiology* **4**: 782-786.

Nelson, K.E., Weinel, C., Paulsen, I.T., Dodson, R.J., Hilbert, H., Martins dos Santos, V.A.P., *et al.* (2002) Complete genome sequence and comparative analysis of the metabolically versatile *Pseudomonas putida* KT2440. *Environmental Microbiology* **4**: 799-808.

Nikel, P.I., de Almeida, A., Melillo, E.C., Galvagno, M.A., and Pettinari, M.J. (2006) New Recombinant *Escherichia coli* Strain Tailored for the Production of Poly(3-Hydroxybutyrate) from Agroindustrial By-Products. *Applied and Environmental Microbiology* **72**: 3949-3954.

Nikel, P.I., Kim, J., and de Lorenzo, V. (2014a) Metabolic and regulatory rearrangements underlying glycerol metabolism in *Pseudomonas putida* KT2440: Glycerol metabolism in *P* . *putida*. *Environmental Microbiology* **16**: 239-254.

Nikel, P.I., Martínez-García, E., and De Lorenzo, V. (2014b) Biotechnological domestication of pseudomonads using synthetic biology. *Nature Reviews Microbiology* **12**: 368-379.

Nikel, P.I., Chavarría, M., Fuhrer, T., Sauer, U., and De Lorenzo, V. (2015) *Pseudomonas putida* KT2440 strain metabolizes glucose through a cycle formed by enzymes of the Entner-Doudoroff, Embden-Meyerhof-Parnas, and pentose phosphate pathways. *Journal of Biological Chemistry* **290**: 25920-25932.

Nikel, P.I., Chavarría, M., Danchin, A., and de Lorenzo, V. (2016) From dirt to industrial applications: *Pseudomonas putida* as a Synthetic Biology chassis for hosting harsh biochemical reactions *Current Opinion in Chemical Biology* **34**: 20-29.

Nogales, J., Macchi, R., Franchi, F., Barzaghi, D., Fernández, C., García, J.L., *et al.* (2007) Characterization of the last step of the aerobic phenylacetic acid degradation pathway. *Microbiology* **153**: 357-365.

Nogales, J., Palsson, B.Ø., and Thiele, I. (2008) A genome-scale metabolic reconstruction of *Pseudomonas putida* KT2440: *i*JN746 as a cell factory. *BMC Systems Biology* **2**: 79.

Nogales, J., Canales, Á., Jiménez-Barbero, J., Serra, B., Pingarrón, J.M., García, J.L., and Díaz, E. (2011) Unravelling the gallic acid degradation pathway in bacteria: the *gal* cluster from *Pseudomonas putida*: Aerobic gallic acid degradation. *Molecular Microbiology* **79**: 359-374.

Nogales, J. (2014) A Practical Protocol for Genome-Scale Metabolic Reconstructions. In, McGenity,T.J., Timmis,K.N., and Nogales,B. (eds), *Hydrocarbon and Lipid Microbiology Protocols*. Berlin, Heidelberg: Springer Berlin Heidelberg, pp. 197-221.

Nogales, J. and Agudo, L. (2015) A Practical Protocol for Integration of Transcriptomics Data into Genome-Scale Metabolic Reconstructions. *Hydrocarbon and Lipid Microbiology Protocols*. Berlin, Heidelberg: Springer, Berlin, Heidelberg, pp. 135-152.

Nogales, J., Gudmundsson, S., Duque, E., Ramos, L., and Bernhard, O. (2017) Expanding the computable reactome in *Pseudomonas putida* reveals metabolic cycles providing robustness. *bioRxiv* doi: https://doi.org/10.1101/139121.

Nogales, J., Mueller, J., Gudmundsson, S., Canalejo, F.J., Duque, E., Monk, J., *et al.,* (2020) High-quality genome-scale metabolic modelling of *Pseudomonas putida* highlights its broad metabolic capabilities *Environmental microbiology* **22**(1): 255-269

Nomura, C.T., Taguchi, K., Gan, Z., Kuwabara, K., Tanaka, T., Takase, K., and Doi, Y. (2005) Expression of 3-Ketoacyl-Acyl Carrier Protein Reductase (*fabG*) Genes Enhances Production of Polyhydroxyalkanoate Copolymer from Glucose in Recombinant *Escherichia coli* JM109. *Applied and Environmental Microbiology* **71**: 4297-4306.

Oberhardt, M.A., Puchałka, J., Martins dos Santos, V.A.P., and Papin, J.A. (2011) Reconciliation of Genome-Scale Metabolic Reconstructions for Comparative Systems Analysis. *PLoS Computational Biology* **7**: e1001116.

Obruca, S., Sedlacek, P., Mravec, F., Samek, O., and Marova, I. (2016a) Evaluation of 3-hydroxybutyrate as an enzyme-protective agent against heating and oxidative damage and its potential role in stress response of poly(3-hydroxybutyrate) accumulating cells. *Applied Microbiology and Biotechnology* **100**: 1365-1376.

Obruca, S., Doskocil, L., Krzyzanek, V., Hrubanova, K., Sedlacek, P., Mravec, F., *et al.* (2016b) Polyhydroxyalkanoates in Bacterial Cells - More Than just Storage Materials. *Materials Science Forum* **851**: 20-25.

Obruca, S., Sedlacek, P., Krzyzanek, V., Mravec, F., Hrubanova, K., Samek, O., *et al.* (2016c) Accumulation of Poly(3-hydroxybutyrate) Helps Bacterial Cells to Survive Freezing. *PLOS ONE* **11**: e0157778.

Obruca, S., Sedlacek, P., Koller, M., Kucera, D., and Pernicova, I. (2018) Involvement of polyhydroxyalkanoates in stress resistance of microbial cells: Biotechnological consequences and applications. *Biotechnology Advances* **36**: 856-870.

Ochiai, T., Fukunaga, N., and Sasaki, S. (1979) Purification and some properties of two $NADP^+$-specific isocitrate dehydrogenases from an obligately psychrophilic marine bacterium, *Vibrio* sp., strain ABE-1. *Journal of Biochemistry* **86**: 377-384.

Olivera, E.R., Carnicero, D., García, B., Miñambres, B., Moreno, M.A., Cañedo, L., *et al.* (2001a) Two different pathways are involved in the beta-oxidation of n-alkanoic and n-phenylalkanoic acids in *Pseudomonas putida* U: genetic studies and biotechnological applications. *Molecular Microbiology* **39**: 863-874.

Olivera, E.R., Carnicero, D., Jodra, R., Miñambres, B., García, B., Abraham, G.A., *et al.* (2001b) Genetically engineered *Pseudomonas*: a factory of new bioplastics with broad applications. *Environmental Microbiology* **3**: 612-618.

Olivera, E.R., Arcos, M., Naharro, G., and Luengo, J.M. (2010) Unusual PHA Biosynthesis. In, Chen,G.G.-Q. (ed), *Plastics from Bacteria*. Berlin, Heidelberg: Springer Berlin Heidelberg, pp. 133-186.

Orth, J.D., Thiele, I., and Palsson, B.O. (2010) What is flux balance analysis? *Nature Biotechnology* **28**: 245-248.

Ouyang, S.-P., Luo, R.C., Chen, S.-S., Liu, Q., Chung, A., Wu, Q., and Chen, G.-Q. (2007) Production of polyhydroxyalkanoates with high 3-hydroxydodecanoate monomer content by *fadB* and *fadA* knockout mutant of *Pseudomonas putida* KT2442. *Biomacromolecules* **8**: 2504-2511.

Palleroni, N.J. (2010) The *Pseudomonas* Story: Editorial. *Environmental Microbiology* **12**: 1377-1383.

Palsson, B.O. (2015) Systems Biology: Constraint-Based Reconstruction and Analysis, Cambridge and New York: Cambridge University Press.

Park, S.J., Jang, Y.-A., Noh, W., Oh, Y.H., Lee, H., David, Y., *et al.* (2015) Metabolic engineering of *Ralstonia eutropha* for the production of polyhydroxyalkanoates from sucrose: Engineered *R. eutropha* Producing PHA From Sucrose. *Biotechnology and Bioengineering* **112**: 638-643.

Parlane, N.A., Gupta, S.K., Rubio-Reyes, P., Chen, S., Gonzalez-Miro, M., Wedlock, D.N., and Rehm, B.H.A. (2017) Self-Assembled Protein-Coated Polyhydroxyalkanoate Beads: Properties and Biomedical Applications. *ACS Biomaterials Science & Engineering* **3**: 3043-3057.

Poblete-Castro, I., Escapa, I.F., Jäger, C., Puchalka, J., Chi Lam, C.M., Schomburg, D., *et al*. (2012) The metabolic response of *P. putida* KT2442 producing high levels of polyhydroxyalkanoate under single- and multiple-nutrient-limited growth: Highlights from a multi-level omics approach. *Microbial Cell Factories* **11**: 1-21.

Poblete-Castro, I., Binger, D., Rodrigues, A., Becker, J., Martins Dos Santos, V.A.P., and Wittmann, C. (2013) *In-silico*-driven metabolic engineering of *Pseudomonas putida* for enhanced production of poly-hydroxyalkanoates. *Metabolic Engineering* **15**: 113-123.

Poblete-Castro, I., Binger, D., Oehlert, R., and Rohde, M. (2014) Comparison of mcl-Poly(3-hydroxyalkanoates) synthesis by different *Pseudomonas putida* strains from crude glycerol: citrate accumulates at high titer under PHA-producing conditions. *BMC biotechnology* **14**: 962.

Poblete-Castro, I., Wittmann, C., and Nikel, P.I. (2019) Biochemistry, genetics and biotechnology of glycerol utilization in *Pseudomonas* species. *Microbial Biotechnology* **13**: 32-53.

Pohlmann, A., Fricke, W.F., Reinecke, F., Kusian, B., Liesegang, H., Cramm, R., *et al.* (2006) Genome sequence of the bioplastic-producing “Knallgas” bacterium *Ralstonia eutropha* H16. *Nature Biotechnology* **24**: 1257-1262.

Pötter, M. and Steinbüchel, A. (2006) Biogenesis and Structure of Polyhydroxyalkanoate Granules. In, *Inclusions in Prokaryotes*, Microbiology Monographs. Springer, Berlin, Heidelberg, pp. 109-136.

Pramanik, A., Pawar, S., Antonian, E., and Schulz, H. (1979) Five different enzymatic activities are associated with the multienzyme complex of fatty acid oxidation from *Escherichia coli*. *Journal of Bacteriology* **137**: 469-473.

Prieto, M.A., Bühler, B., Jung, K., Witholt, B., and Kessler, B. (1999) PhaF, a polyhydroxyalkanoate-granule-associated protein of *Pseudomonas oleovorans* GPo1 involved in the regulatory expression system for *pha* genes. *Journal of Bacteriology* **181**: 858-868.

Prieto, M.A., Eugenio, L.I. De, Galàn, B., Luengo, J.M., and Witholt, B. (2007) Synthesis and Degradation of Polyhydroxyalkanoates. In, *Pseudomonas*. Dordrecht: Springer Netherlands, pp. 397-428.

Prieto, A. (2016) To be, or not to be biodegradable\ldots that is the question for the bio-based plastics. *Microbial Biotechnology* **9**: 652-657.

Prieto, A., Escapa, I.F., Martínez, V., Dinjaski, N., Herencias, C., de la Peña, F., *et al.* (2016) A holistic view of polyhydroxyalkanoate metabolism in *Pseudomonas putida*. *Environmental Microbiology* **18**: 341-357.

Puchałka, J., Oberhardt, M.A., Godinho, M., Bielecka, A., Regenhardt, D., Timmis, K.N., *et al.* (2008) Genome-Scale Reconstruction and Analysis of the *Pseudomonas putida* KT2440 Metabolic Network Facilitates Applications in Biotechnology. *PLoS Computational Biology* **4**: e1000210.

Rai, R., Keshavarz, T., Roether, J.A., Boccaccini, A.R., and Roy, I. (2011) Medium chain length polyhydroxyalkanoates, promising new biomedical materials for the future. *Materials Science and Engineering: R: Reports* **72**: 29-47.

Ravi, K., García-Hidalgo, J., Gorwa-Grauslund, M.F., and Lidén, G. (2017) Conversion of lignin model compounds by *Pseudomonas putida* KT2440 and isolates from compost. *Applied Microbiology and Biotechnology* **101**: 5059-5070.

Raza, Z.A., Abid, S., and Banat, I.M. (2018) Polyhydroxyalkanoates: Characteristics, production, recent developments and applications. *International Biodeterioration & Biodegradation* **126**: 45-56.

Reeves, H.C., O'Neil, S., and Weitzman, P.D.J. (1983) Modulation of isocitrate dehydrogenase activity in *Acinetobacter calcoaceticus* by acetate. *FEBS Letters* **163**: 265-268.

Reeves, H.C., O'Neil, S., and Weitzman, P.D.J. (1986) Changes in NADP-isocitrate dehydrogenase isoenzyme levels in *Acinetobacter calcoaceticus* in response to acetate. *FEMS Microbiology Letters* **35**: 229-232.

Rehm, B.H., Krüger, N., and Steinbüchel, A. (1998) A new metabolic link between fatty acid *de novo* synthesis and polyhydroxyalkanoic acid synthesis. The *phaG* gene from *Pseudomonas putida* KT2440 encodes a 3-hydroxyacyl-acyl carrier protein-coenzyme a transferase. *Journal of Biological Chemistry* **273**: 24044-24051.

Rehm, B.H.A. (2003) Polyester synthases: natural catalysts for plastics. *Biochemistry Journal* **376**: 15-33.

Rehm, B.H.A. (2010) Bacterial polymers: biosynthesis, modifications and applications. *Nature Reviews Microbiology* **8**: 578-592.

Ren, Q., Kessler, B., van der Leij, F., and Witholt, B. (1998) Mutants of *Pseudomonas putida* affected in poly-3-hydroxyalkanoate synthesis. *Applied Microbiology and Biotechnology* **49**: 743-750.

Ren, Q., Sierro, N., Witholt, B., and Kessler, B. (2000) FabG, an NADPH-Dependent 3-Ketoacyl Reductase of *Pseudomonas aeruginosa*, Provides Precursors for Medium-Chain-Length Poly-3-Hydroxyalkanoate Biosynthesis in *Escherichia coli*. *Journal of Bacteriology* **182**: 2978-2981.

Ren, Q., De Roo, G., Ruth, K., Witholt, B., Zinn, M., and Thöny-Meyer, L. (2009) Simultaneous accumulation and degradation of polyhydroxyalkanoates: Futile cycle or clever regulation? *Biomacromolecules* **10**: 916-922.

Revelles, O., Tarazona, N., García, J.L., and Prieto, M.A. (2016) Carbon roadmap from syngas to polyhydroxyalkanoates in *Rhodospirillum rubrum*. *Environmental Microbiology* **18**: 708-720.

Rojo, F. (2010) Carbon catabolite repression in *Pseudomonas* : optimizing metabolic versatility and interactions with the environment. *FEMS Microbiology Reviews* **34**: 658-684.

Romkina, A.Y. and Kiriukhin, M.Y. (2017) Biochemical and molecular characterization of the isocitrate dehydrogenase with dual coenzyme specificity from the obligate methylotroph *Methylobacillus flagellatus*. *PLOS ONE* **12**: e0176056.

Rothermich, M.M., Guerrero, R., Lenz, R.W., and Goodwin, S. (2000) Characterization, seasonal occurrence, and diel fluctuation of poly(hydroxyalkanoate) in photosynthetic microbial mats. *Applied Enironmental Microbiology* **66**: 4279-4291.

Roy, S.O. and Packard, T.T. (1998) NADP-Isocitrate Dehydrogenase from *Pseudomonas nautica*: Kinetic Constant Determination and Carbon Limitation Effects on the Pool of Intracellular Substrates. *Applied Enironmental Microbiology* **64**: 4958-4964.

Ruth, K., Grubelnik, A., Hartmann, R., Egli, T., Zinn, M., and Ren, Q. (2007) Efficient production of *(R)*-3-hydroxycarboxylic acids by biotechnological conversion of polyhydroxyalkonoates and their purification. *Biomacromolecules* **8**: 279-286.

Ruth, K., Roo, G. de, Egli, T., and Ren, Q. (2008) Identification of Two Acyl-CoA Synthetases from *Pseudomonas putida* GPo1: One is Located at the Surface of Polyhydroxyalkanoates Granules. *Biomacromolecules* **9**: 1652-1659.

Sabri, S., Nielsen, L.K., and Vickers, C.E. (2013) Molecular Control of Sucrose Utilization in *Escherichia coli* W, an Efficient Sucrose-Utilizing Strain. *Applied Environmental Microbiology* **79**: 478-487.

Salvachúa, D., Karp, E.M., Nimlos, C.T., Vardon, D.R., and Beckham, G.T. (2015) Towards lignin consolidated bioprocessing: simultaneous lignin depolymerization and product generation by bacteria. *Green Chemistry* **17**: 4951-4967.

Salvachúa, D., Rydzak, T., Auwae, R., De Capite, A., Black, B.A., Bouvier, J.T., *et al.* (2020) Metabolic engineering of *Pseudomonas putida* for increased polyhydroxyalkanoate production from lignin. *Microbial Biotechnology* **13**: 290-298.

Salvador, M., Abdulmutalib, U., Gonzalez, J., Kim, J., Smith, A.A., Faulon, J.-L., *et al.* (2019) Microbial Genes for a Circular and Sustainable Bio-PET Economy. *Genes* **10**: 373.

Sambrook, J, and Russell D.W. (2001). Molecular cloning: a laboratory manual. *Cold Spring Harb Lab Press Cold Spring Harb NY.*

Sandoval, Á., Arias-Barrau, E., Bermejo, F., Cañedo, L., Naharro, G., Olivera, E.R., and Luengo, J.M. (2005) Production of 3-hydroxy-n-phenylalkanoic acids by a genetically engineered strain of *Pseudomonas putida*. *Applied Microbiology and Biotechnology* **67**: 97-105.

Sandoval, Á., Arias-Barrau, E., Arcos, M., Naharro, G., Olivera, E.R., and Luengo, J.M. (2007) Genetic and ultrastructural analysis of different mutants of *Pseudomonas putida* affected in the poly-3-hydroxy-n-alkanoate gene cluster. *Environmental Microbiology* **9**: 737-751.

dos Santos, V.A.P.M., Heim, S., Moore, E.R.B., Stratz, M., and Timmis, K.N. (2004) Insights into the genomic basis of niche specificity of *Pseudomonas putida* KT2440. *Environmental Microbiology* **6**: 1264-1286.

Saravolac, E.G., Taylor, N.F., Benz, R., and Hancock, R.E. (1991) Purification of glucose-inducible outer membrane protein OprB of *Pseudomonas putida* and reconstitution of glucose-specific pores. *J Bacteriol* **173**: 4970-4976.

Sato, S., Kanazawa, H., and Tsuge, T. (2011) Expression and characterization of *(R)*-specific enoyl coenzyme A hydratases making a channeling route to polyhydroxyalkanoate biosynthesis in *Pseudomonas putida*. *Applied Microbiology and Biotechnology* **90**: 951-959.

Schäfer, A., Tauch, A., Jäger, W., Kalinowski, J., Thierbach, G., and Pühler, A. (1994) Small mobilizable multi-purpose cloning vectors derived from the *Escherichia coli* plasmids pK18 and pK19: selection of defined deletions in the chromosome of *Corynebacterium glutamicum*. *Gene* **145**: 69-73.

Schellenberger, J. and Palsson, B. (2009) Use of randomized sampling for analysis of metabolic networks. *Journal of Biological Chemistry* **27**: 5457-5461.

Schellenberger, J., Que, R., Fleming, R.M.T., Thiele, I., Orth, J.D., Feist, A.M., *et al.* (2011) Quantitative prediction of cellular metabolism with constraint-based models: the COBRA Toolbox v2.0. *Nature Protocols* **6**: 1290-1307.

Schmid, K., Ebner, R., Altenbuchner, J., Schmitt, R., and Lengeler, J.W. (1988) Plasmid-mediated sucrose metabolism in *Escherichia coli* K12: mapping of the *scr* genes of pUR400. *Molecular Microbiology* **2**: 1-8.

Schweizer, H.P. (2004) Fatty Acid Biosynthesis and Biologically Significant Acyl Transfer Reactions in Pseudomonads. In, Ramos,J.-L. (ed), *Pseudomonas*. Boston, MA: Springer US, pp. 83-109.

Segura, D., Guzmán, J., and Espín, G. (2003) *Azotobacter vinelandii* mutants that overproduce poly-beta-hydroxybutyrate or alginate. *Applied Microbiology and Biotechnology* **63**: 159-163.

Silva-Rocha, R., Martínez-García, E., Calles, B., Chavarría, M., Arce-Rodríguez, A., De Las Heras, A., *et al.* (2013) The Standard European Vector Architecture (SEVA): A coherent platform for the analysis and deployment of complex prokaryotic phenotypes. *Nucleic Acids Research* **41**: 666-675.

Silva-Rocha, R. and de Lorenzo, V. (2014) Chromosomal Integration of Transcriptional Fusions. In, Filloux,A. and Ramos,J.-L. (eds), *Pseudomonas Methods and Protocols*. New York, NY: Springer New York, pp. 479-489.

Singh, A.K. and Mallick, N. (2009) SCL-LCL-PHA copolymer production by a local isolate, *Pseudomonas aeruginosa* MTCC 7925. *Biotechnology Journal* **4**: 703-711.

Singh S., B., Grewal, A., and Kumar, P. (2014) Biotechnological Production of Polyhydroxyalkanoates: A Review on Trends and Latest Developments. *Chinese Journal of Biology* **2014**: 1-18.

Singh, S.K., Matsuno, K., LaPorte, D.C., and Banaszak, L.J. (2001) Crystal Structure of *Bacillus subtilis* Isocitrate Dehydrogenase at 1.55 Å: insights into the nature of substrate specificity exhibited by *Esherichia coli* isocitrate dehydrogenase kinase/phosphatase. *Journal of Biological Chemistry* **276**: 26154-26163.

Singh, S.K., Miller, S.P., Dean, A., Banaszak, L.J., and LaPorte, D.C. (2002) *Bacillus subtilis* Isocitrate Dehydrogenase: A substrate analogue for *Esherichia coli* isocitrate dehydrogenase kinase/phosphatase. *Journal of Biological Chemistry* **277**: 7567-7573.

Sivaraman, J., Li, Y., Banks, J., Cane, D.E., Matte, A., and Cygler, M. (2003) Crystal Structure of *Escherichia coli* PdxA, an Enzyme Involved in the Pyridoxal Phosphate Biosynthesis Pathway. *Journal of Biological Chemistry* **278**: 43682-43690.

Slepecky, R.A. and Law, J.H. (1961) Synthesis and degradation of poly-3-hydroxybutyric acid in connection with sporulation of *Bacillus megaterium*. Journal of Bacteriology **82**: 37-42.

Sohn, S.B., Kim, T.Y., Park, J.M., and Lee, S.Y. (2010) In silico genome-scale metabolic analysis of *Pseudomonas putida* KT2440 for polyhydroxyalkanoate synthesis, degradation of aromatics and anaerobic survival. *Biotechnology Journal* **5**: 739-750.

Stanier, R.Y., Palleroni, N.J., and Doudoroff, M. (1966) The Aerobic Pseudomonads a Taxonomic Study. *Journal of General Microbiology* **43**: 159-271.

Steen, I.H., Madsen, M.S., Birkeland, N.K., and Lien, T. (1998) Purification and characterization of a monomeric isocitrate dehydrogenase from the sulfate-reducing bacterium *Desulfobacter vibrioformis* and demonstration of the presence of a monomeric enzyme in other bacteria. *FEMS Microbiology Letters* **160**: 75-79.

Sudesh, K., Abe, H., and Doi, Y. (2000) Synthesis, structure and properties of polyhydroxyalkanoates: biological polyesters. *Progress in Polymer Science* **25**: 1503-1555.

Sullivan, S.A., Schweizer, H.P., Hoang, T.T., and Cusick, J.K. (2002) β-Ketoacyl acyl carrier protein reductase (FabG) activity of the fatty acid biosynthetic pathway is a determining factor of 3-oxo-homoserine lactone acyl chain lengths. *Microbiology* **148**: 3849-3856.

Suzuki, K. and Takada, Y.T. (2016) Characterization of $NADP^+$-dependent isocitrate dehydrogenase isozymes from a psychrophilic bacterium, *Colwellia psychrerythraea* strain 34H. *Bioscience, Biotechnology and Biochemistry* **80**: 1492-1498.

Suzuki, M., Sahara, T., Tsuruha, J.I., Takada, Y., and Fukunaga, N. (1995) Differential expression in *Escherichia coli* of the *Vibrio* sp. strain ABE-1 *icdI* and *icdII* genes encoding structurally different isocitrate dehydrogenase isozymes. *Journal of Bacteriology* **177**: 2138-2142.

Taguchi, K., Aoyagi, Y., Matsusaki, H., Fukui, T., and Doi, Y. (1999) Co-expression of 3-ketoacyl-ACP reductase and polyhydroxyalkanoate synthase genes induces PHA production in *Escherichia coli* HB101 strain. *FEMS Microbiology Letters* **176**: 183-190.

Tan, S.Z., Reisch, C.R., and Prather, K.L.J. (2018) A Robust CRISPR Interference Gene Repression System in *Pseudomonas*. *Journal of Bacteriology* **200**: e00575-17.

Tarazona, N.A., Maestro, B., Revelles, O., Sanz, J.M., and Prieto, M.A. (2019a) Role of leucine zipper-like motifs in the oligomerization of Pseudomonas putida phasins. *Biochimica et Biophysica Acta - General Subjects* **1863**: 362-370.

Tarazona, N.A., Machatschek, R., Schulz, B., Prieto, M.A., and Lendlein, A. (2019b) Molecular Insights into the Physical Adsorption of Amphiphilic Protein PhaF onto Copolyester Surfaces. *Biomacromolecules* **20**: 3242-3252.

Timmis, K.N. (2002) *Pseudomonas putida*: a cosmopolitan opportunist par excellence. *Environmental Microbiology* **4**: 779-781.

Tiso, T., Sabelhaus, P., Behrens, B., Wittgens, A., Rosenau, F., Hayen, H., and Blank, L.M. (2016) Creating metabolic demand as an engineering strategy in *Pseudomonas putida* – Rhamnolipid synthesis as an example. *Metabolic Engineering Communications* **3**: 234-244.

Tobin, K.M., O'Leary, N.D., Dobson, A.D.W., and O'Connor, K.E. (2007) Effect of heterologous expression of *phaG* [*(R)*-3-hydroxyacyl-ACP-CoA transferase] on polyhydroxyalkanoate accumulation from the aromatic hydrocarbon phenylacetic acid in *Pseudomonas* species. *FEMS Microbiology Letters* **268**: 9-15.

Tomizawa, S., Chuah, J.A., Matsumoto, K., Doi, Y., and Numata, K. (2014) Understanding the limitations in the biosynthesis of polyhydroxyalkanoate (PHA) from lignin derivatives. *ACS Sustainable Chemistry and Engineering* **2**: 1106-1113.

Trinh, C.T. and Srienc, F. (2009) Metabolic Engineering of Escherichia coli for Efficient Conversion of Glycerol to Ethanol. *Applied and Environmental Microbiology* **75**: 6696-6705.

Tsuge, T., Taguchi, K., Seiichi, Taguchi, and Doi, Y. (2003) Molecular characterization and properties of *(R)*-specific enoyl-CoA hydratases from *Pseudomonas aeruginosa*: metabolic tools for synthesis of polyhydroxyalkanoates via fatty acid ß-oxidation. *International Journal of Biological Macromolecules* **31**: 195-205.

Valappil, S.P., Misra, S.K., Boccaccini, A.R., and Roy, I. (2006) Biomedical applications of polyhydroxyalkanoates: an overview of animal testing and in vivo responses. *Expert Review of Medical Devices* **3**: 853-868.

Vo, M.T., Lee, K.W., Jung, Y.M., and Lee, Y.H. (2008) Comparative effect of overexpressed *phaJ* and *fabG* genes supplementing *(R)*-3-hydroxyalkanoate monomer units on biosynthesis of mcl-polyhydroxyalkanoate in *Pseudomonas putida* KCTC1639. *Journal of Bioscience and Bioengineering* **106**: 95-98.

Walsh, K. and Koshland, D.E. (1985) Branch point control by the phosphorylation state of isocitrate dehydrogenase. A quantitative examination of fluxes during a regulatory transition. *Journal of Biological Chemistry* **260**: 8430-8437.

Walsh, K. and Koshland, D.E. (1984) Determination of flux through the branch point of two metabolic cycles. The tricarboxylic acid cycle and the glyoxylate shunt. *Journal of Biol Chem* **259**: 9646-9654.

Wang, J.-P., Wu, L.-X., Xu, F., Lv, J., Jin, H.-J., and Chen, S.-F. (2010) Metabolic engineering for ethylene production by inserting the ethylene-forming enzyme gene (efe) at the 16S rDNA sites of *Pseudomonas putida* KT2440. *Bioresource Technology* **101**: 6404-6409.

Wang, P., Jin, M., and Zhu, G. (2012) Biochemical and molecular characterization of NAD^+-dependent isocitrate dehydrogenase from the ethanologenic bacterium *Zymomonas mobilis*. *FEMS Microbiology Letters* **327**: 134-141.

Wang, P., Lv, C., and Zhu, G. (2015) Novel Type II and Monomeric NAD^+ Specific Isocitrate Dehydrogenases: Phylogenetic Affinity, Enzymatic Characterization, and Evolutionary Implication. *Scientific Reports* **5**: 1-11.

Wang, P., Song, P., Jin, M., and Zhu, G. (2013) Isocitrate Dehydrogenase from Streptococcus mutans: Biochemical Properties and Evaluation of a Putative Phosphorylation Site at Ser102. *PLoS ONE* **8**: e58918.

Wang, P., Wu, Y., Liu, J., Song, P., Li, S., Zhou, X., and Zhu, G. (2018) Crystal Structure of the Isocitrate Dehydrogenase 2 from *Acinetobacter baumannii* (AbIDH2) Reveals a Novel Dimeric Structure with Two Monomeric-IDH-Like Subunits. *International Journal of Molecular Sciences* **19**: 1131.

Wang, Q., Yu, H., Xia, Y., Kang, Z., and Qi, Q. (2009) Complete PHB mobilization in *Escherichia coli* enhances the stress tolerance: a potential biotechnological application. *Microbial Cell Factories* **8**: 47.

Wang, Q. and Nomura, C.T. (2010) Monitoring differences in gene expression levels and polyhydroxyalkanoate (PHA) production in *Pseudomonas putida* KT2440 grown on different carbon sources. *Journal of Bioscience and Bioengineering* **110**: 653-659.

Wang, Q., Tappel, R.C., Zhu, C., and Nomura, C.T. (2012) Development of a new strategy for production of medium-chain-length polyhydroxyalkanoates by recombinant *Escherichia coli* via inexpensive non-fatty acid feedstocks. *Applied and Environmental Microbiology* **78**: 519-527.

Wang, X., Lin, L., Dong, J., Ling, J., Wang, W., Wang, H., *et al.* (2018) Simultaneous Improvements of *Pseudomonas* Cell Growth and Polyhydroxyalkanoate Production from a Lignin Derivative for Lignin-Consolidated Bioprocessing. *Applied Environmental Microbiology* **84**: e01469-18.

Wang, Z.X., Brämer, C., and Steinbüchel, A. (2003) Two phenotypically compensating isocitrate dehydrogenases in *Ralstonia eutropha*. *FEMS Microbiology Letters* **227**: 9-16.

Watanabe, S., Yasutake, Y., Tanaka, I., and Takada, Y. (2005) Elucidation of stability determinants of cold-adapted monomeric isocitrate dehydrogenase from a psychrophilic bacterium, *Colwellia maris*, by construction of chimeric enzymes. *Microbiology* **151**: 1083-1094.

Weber, E., Engler, C., Gruetzner, R., Werner, S., and Marillonnet, S. (2011) A modular cloning system for standardized assembly of multigene constructs. *PLoS ONE* **6**: e16765.

Wierckx, N., Narancic, T., Eberlein, C., Wei, R., Drzyzga, O., Magnin, A., *et al.* (2018) Plastic Biodegradation: Challenges and Opportunities. In, Steffan,R. (ed), *Consequences of Microbial Interactions with Hydrocarbons, Oils, and Lipids: Biodegradation and Bioremediation*. Cham: Springer International Publishing, pp. 1-29.

Williams, P.A. and Murray, K. (1974) Metabolism of Benzoate and the Methylbenzoates by *Pseudomonas putida* (arvilla) mt-2: Evidence for the Existence of a TOL Plasmid. *Journal of Bacteriology* **120**: 416-423.

Wong, J.X. and Rehm, B.H.A. (2018) Design of Modular Polyhydroxyalkanoate Scaffolds for Protein Immobilization by Directed Ligation. *Biomacromolecules* **19**: 4098-4112.

Wong, S.M. and Mekalanos, J.J. (2000) Genetic footprinting with mariner-based transposition in *Pseudomonas aeruginosa*. *Proceedings of the National Academy of Sciences* **97**: 10191-10196.

Xu, P., Ranganathan, S., Fowler, Z.L., Maranas, C.D., and Koffas, M.A.G. (2011) Genome-scale metabolic network modeling results in minimal interventions that cooperatively force carbon flux towards malonyl-CoA. *Metabolic Engineering* **13**: 578-587.

Yasuda, W., Kobayashi, M., and Takada, Y. (2013) Analysis of amino acid residues involved in cold activity of monomeric isocitrate dehydrogenase from psychrophilic bacteria, *Colwellia maris* and *Colwellia psychrerythraea*. *Journal of Bioscience and Bioengineering* **116**: 567-572.

Yasutake, Y., Watanabe, S., Yao, M., Takada, Y., Fukunaga, N., and Tanaka, I. (2002) Structure of the Monomeric Isocitrate Dehydrogenase. *Structure* **10**: 1637–1648.

Yasutake, Y., Watanabe, S., Yao, M., Takada, Y., Fukunaga, N., and Tanaka, I. (2003) Crystal Structure of the Monomeric Isocitrate Dehydrogenase in the Presence of $NADP^+$: insight into the cofactor recognition catalysis and evolution. *Journal of Biological Chemistry* **278**: 36897-36904.

Yuan, Q., Huang, T., Li, P., Hao, T., Li, F., Ma, H., *et al.* (2017) Pathway-Consensus approach to metabolic network reconstruction for *Pseudomonas putida* KT2440 by systematic comparison of published models. *PLoS ONE* **12**: e0169437.

Zhang, B., Wang, B., Wang, P., Cao, Z., Huang, E., Hao, J., *et al.* (2009) Enzymatic characterization of a monomeric isocitrate dehydrogenase from *Streptomyces lividans* TK54. *Biochimie* **91**: 1405-1410.

Zhao, Y.H., Li, H.M., Qin, L.F., Wang, H.H., and Chen, G.-Q. (2007) Disruption of the polyhydroxyalkanoate synthase gene in *Aeromonas hydrophila* reduces its survival ability under stress conditions. *FEMS Microbiology Letters* **276**: 34-41.

Zhu, G., Golding, G.B., and Dean, A.M. (2005) The Selective Cause of an Ancient Adaptation. Science **307**: 1279-1282.

Zinn, M., Witholt, B., and Egli, T. (2001) Occurrence, synthesis and medical application of bacterial polyhydroxyalkanoate. *Advanced Drug Delivery Reviews* **53**: 5-21.

Zobel, S., Benedetti, I., Eisenbach, L., De Lorenzo, V., Wierckx, N., and Blank, L.M. (2015) Tn*7*-Based Device for Calibrated Heterologous Gene Expression in *Pseudomonas putida*. *ACS Synthetic Biology* **4**: 1341-1351.

Zou, H., Shi, M., Zhang, T., Li, Lei, Li, Liangzhi, and Xian, M. (2017) Natural and engineered polyhydroxyalkanoate (PHA) synthase: key enzyme in biopolyester production. *Applied Microbiology and Biotechnology* **101**: 7417-7426.

8. ANNEXS

8 ANNEXS

Gene	Enzymatic activity	Annotation
fadL	Long chain fatty acid transporter (LCFAs)	PP_1689
?	Short chain fatty acid transporter	PP_3124
fadD	Acyl-CoA synthetase	PP_2213/PP_4549 / PP_4550
fadE	Acyl-CoA dehydrogenase	PP_0368/PP_1893/PP_2039/ PP_2048/PP_2216/PP_2437
	Multienzymatic activities of the FadBA complex:	PP_2047/PP_2136/PP_2214
fadB	Enoyl-CoA hydratase	
	3-hydroxyacyl-CoA dehydrogenase	
	Cis-Δ^3-trans-Δ^2-enoyl-CoA isomerase	
	3-hydroxyacyl-CoA epimerase	
fadA	3-ketoacyl-CoA thiolase	PP_2137/PP_2215/PP_4636
phaJ	Enoyl-CoA hydratase, *R* strereoselectivity	PP_0580/PP_4552/PP_4817
fabG	3-oxoacyl-ACP reductase subunit	PP_1914

Table S 1. Genes names, enzymatic activities and genes ID of *P. putida* KT2440 involved in β-oxidation pathway.

Pathway	Gene	Enzymatic activity	Annotation
	glk	glucokinase	PP_1011
	pgi-1 / pgi-2	Glucose-6-P isomerase	PP_1808
			PP_4701
	fbp	Fructose 1,6-biphosphate	PP_5040
	fda	Fructose-1,6-P2 aldolase	PP_4960
			PP_1791
			PP_2871
			PP_3224
	tpiA	Triose phosphate isomerase	PP_4715
EMP	*gap-1 / gap-2*	Glyceraldehyde-3-P	PP_1009
		dehydrogenase	PP_2149
			PP_0665
			PP_3443
	pgk	Phosphoglycerate kinase	PP_4963
	pgm	Phosphoglycerate mutase	PP_5056
			PP_2243
			PP_3923
			PP_4450
	eno	Phosphopyruvate hydratase	PP_1612

	pykA / *pykF*	Pyruvate kinase	PP_1362 PP_4301
ED	*edd*	6-Phosphogluconate dehydratase	PP_1010
	eda	2-keto-3-deoxy-6-phosphogluconate aldolase	PP_1024
PPP	*zwf-1, zwf-2, zwf-3*	Glucose-6-P-1-dehydrogenase	PP_1022 PP_4042 PP_5351
	pgl	6-phosphogluconolactonase	PP_1023
	gnd	6-phosphogluconate dehydrogenase	PP_4043
	rpe	Ribulose-5-*P*-3-epimerase	PP_0415
	rpiA	Ribose-5-*P*-3-epimerase	PP_5150
	tktA	Transketolase	PP_4965
	talA	Transaldolase B	PP_2168
Peripheral	*gcd*	Glucose dehydrogenase	PP_1444
	gad	Gluconate 2-dehydrogenase	PP_3382 PP_3384 PP_3623 PP_4232
	oprB-1	Carbohydrate-selective porin	PP_1019
	gtsA/B/C/D	Mannose/glucose ABC transporter substrate-binding protein	PP_1015 PP_1016 PP_1017 PP_1018
	gntP	D-gluconate transporter	PP_3417
	gnuk	Gluconate kinase	PP_3416
	kguT	2-ketogluconate transporter, putative	PP_3377
	kguk	2-ketogluconate kinase	PP_3378
	kguD	2-ketogluconate-6-P reductase	PP_3376

Table S 2. Genes, enzymatic activities and *P. putida* KT2440 genome database annotation involved in the EMP (Embden-Meyerhof-Parnas Pathway), ED (Entner-Doudoroff), PPP (Pentose phosphate pathway) and peripheral pathways.

Gene	Enzymatic activity	Annotation
oprB-1	Carbohydrate-selective porin	PP_1019
glpF	Aquaglyceroporin	PP_1076
glpK	Glycerol kinase	PP_1075
glpD	Aerobic glycerol-3-phosphate dehydrogenase	PP_1073
glpR	DNA-binding transcriptional repressor	PP_1074

Table S 3. The involved genes, their enzymatic activity and their corresponding *P. putida* KT2440 database annotation are listed for the glycerol catabolism pathways.

Pathway	Gene	Enzymatic activity	Annotation
β-ketoadipate	*pcaG/pcaH*	protocatechuate 3,4-dioxygenase subunit alpha/beta	PP_4655 PP_4656
	pcaI/pcaJ	3-oxoadipate CoA-transferase subunit A	PP_3951 PP_3952
	pcaB	3-carboxy-cis,cis-muconate cycloisomerase	PP_1379
	pcaD	3-oxoadipate enol-lactonase	PP_1380
	pcaC	4-carboxymuconolactone decarboxylase	PP_1381
	pcaF	beta-ketoadipyl-CoA thiolase	PP_1377
	pcaR	*pca* regulon transcriptional regulator	PP_1375
	pcaK	4-hydroxybenzoate transporter	PP_1376
	pcaT	alpha-ketoglutarate permease	PP_1378
	pcaP	porin	PP_1382
Peripheral	*ech*	enoyl-CoA hydratase/aldolase	PP_2217
	fcs	feruloyl-CoA-synthetase	PP_3356
	vdh	vanillin dehydrogenase	PP_3357
	vanA	vanillate O-demethylase oxygenase subunit	PP_3736
	vanB	vanillate O-demethylase oxidoreductase	PP_3737
	vanR	transcriptional regulator VanR	PP_3738
	galP-IV	porin like	PP_3739
	vanK	MFS transporter	PP_3740
	pobA	4-hydroxybenzoate 3-monooxygenase	PP_3537
	pobR	transcriptional regulator	PP_3538
Phenylacetate Degradation	*paaE*	ring 1,2-phenylacetyl-CoA epoxidase reductase subunit	PP_3274
	paaD	1,2-phenylacetyl-CoA epoxidase subunit D	PP_3275
	paaC	ring 1,2-phenylacetyl-CoA epoxidase subunit beta	PP_3276
	paaB	ring 1,2-phenylacetyl-CoA epoxidase regulatory subunit	PP_3277

	paaA	ring 1,2-phenylacetyl-CoA epoxidase subunit alpha	PP_3278
	paaK	phenylacetate-CoA ligase	PP_3279
	paaJ	3-oxoadipyl-CoA/3-oxo-5,6-dehydrosuberyl-CoA thiolase	PP_3280
	paaI	hydroxyphenylacetyl-CoA thioesterase	PP_3281
	paaH	3-hydroxyacyl-CoA dehydrogenase PaaC	PP_3282
	paaG	2-(1,2-epoxy-1,2-dihydrophenyl)acetyl-CoA isomerase	PP_3283
	paaF	enoyl-CoA hydratase/isomerase	PP_3284
	paaY	phenylacetate degradation pathway detoxifying thioesterase	PP_3285
	paaX	DNA-binding transcriptional repressor PaaX	PP_3286
	phaK	phenylacetic acid-specific porin	PP_3271

Table S 4. The involved genes, their enzymatic activity and their corresponding *P. putida* KT2440 database annotation are listed for the aromatic compounds catabolism pathways.

Pathway	Gene	Enzymatic activity	Annotation
TCA	*gltA*	citrate synthase	PP_4194
	acnA-I/II	aconitate hydratase	PP_2112/PP_2336
	acnB		PP_2339
	icd/idh	$NADP^+$-dependent isocitrate dehydrogenase	PP_4011/PP_4012
	lpdG	Dihydrolipoyl dehydrogenase (E3)	PP_4187
	sucB (kgdB)	2-oxoglutarate dehydrogenase dihydrolipoyltranssuccinylase subunit (E2)	PP_4188
	sucA	2-oxoglutarate dehydrogenase subunit E1	PP_4189
	sucD	succinyl-CoA synthetase subunit alpha	PP_4185
	sucC	bifunctional succinyl-CoA synthetase subunit beta/glutaryl-CoA synthetase subunit beta	PP_4186
	scpC	propionyl-CoA:succinate CoA transferase	PP_0154
	sdhB/sdhA/ sdhD/sdhC	succinate dehydrogenase iron-sulfur subunit	PP_4190/PP_4191 PP_4192/PP_4193
	fumA	class 1 fumarate hydratase	PP_0897

	fumC-I/ fumC-II	class 2 fumarate hydratase	PP_0944/PP_1755
	mdh	malate dehydrogenase	PP_0654
	mqo-I/II/III	malate:quinone oxidoreductase	PP_0751/PP_1251/ PP_2925
Glyoxylate shunt	*aceA*	isocitrate lyase	PP_4116
	glcB	malate synthase G	PP_0356
	maeB	malic enzyme B	PP_5085

Table S 5. The involved genes, their enzymatic activity and their corresponding *P. putida* KT2440 database annotation are listed for the TCA cycle and the glyoxylate shunt.

Gene	Enzymatic activity	Annotation
accABCD	accABCD complex: Acetyl-CoA carboxylase	PP_1607/PP_0559/PP_0558 /PP_1996
fabD	Malonyl-CoA transacylase	PP_1913
fabB	3-oxoacyl-ACP-synthase	PP_4175
fabF	beta-ketoacyl-ACP-synthase II	PP_1916/PP_3303
fabH	3-ketoacyl-ACP-synthase III	PP_4379/PP_4545
fabG	3-oxoacyl-ACP-reductase subunit	PP_0581/PP_1852/PP_1914 (*fabG*)/PP_2540/ PP_2783
fabA	3*R*-3-hydroxydecanoyl-ACP dehydratase	PP_4174
fabZ	3-hydroxyacyl-ACP dehydratase FabZ	PP_1602
?	Enoyl-ACP reductase	PP_1852
phaG	3-hydroxyacyl-CoA-ACP transferase	PP_1408
?	3-hydroxyacyl-CoA ligase	PP_0763

Table S 6. The involved genes, their enzymatic activity and their corresponding *P. putida* KT2440 database annotation are listed for the *de novo* fatty acid synthesis.

Oligonucleotide	Sequence (5´-3´)	Utility	Genomic locus
AvrII-BCD2-*phaZ*	CCTAGGGCCCAAGTTCACTTAAAA AGGAGATCAACAATGAAAGCAATT TTCGTACTGAAACATCTTAATCAT GCTAAGGAGGTTTTCTAATGCCG CAACCCTATATTTTC	To obtain BCD2-*phaZ* fusion	PP_5004
phaZ-BamHI-Rev	GCTGTTGGATCCTCACCCCCCCG AGGCCG	To obtain BCD2-*phaZ* fusion	
pBG-For	CAAGGTTCTGGACCAGTTGCG	Sequencing pBG plasmids	-
pBG-Rev	GGTTTTCCCAGTCACGACGC	Sequencing pBG plasmids	-
pBGXX-Sec	CCCGAGGCATAGGCTGTAC	Sequencing pBG plasmids	-
pBG-Sec-Rev	GGCAACCGAGCGTTCTGAAC	Sequencing pBG plasmids	-
5-Pput-glmSUP	AGTCAGAGTTACGGAATTGTAGG	Verification of Tn*7* insertion	-
3-Tn7L	ATTAGCTTACGACGCTACACCC	Verification of Tn*7* insertion	-
RK132	CGCAAGCTTCCTCGTTTATC	Cloning PCR	
RK133	CTTTCTGGCTAATTCGGGCGGGC GCTAGCTCATTTCTCACCTCGTGT GC	Cloning PCR	
RK134	GCTAGCGCCCGAATTAGCC	Cloning PCR	
RK135	TTTGGATCCACGACTTCCATT	Cloning PCR	
RK136	AAGGCGACTACGACTTCCATT	Sequencing primer, Genome PCR verification	PP_2334 Deletion
RK137	GCATTGCAAGGTTCTAGGCAAG	Sequencing primer, Genome PCR verification	
RK138	CAGACGAAGATCGGGGTGAA	Sequencing primer, Genome PCR verification	
RK139	TTTAAGCTTGTGACAACGAAACTG GTGGC	Cloning PCR	
RK140	TTTCAGTAGCCCGAGATAACAATC CTCCGGATGTGGTACGGAACG	Cloning PCR	PP_0154 Deletion

RK141	GGATTGTTATCTCGGGCTAC	Cloning PCR	
RK142	TTTGGATCCTACAGTGCCTTCACC CTGAT	Cloning PCR	
RK143	ACCCTACTGTTGCACTCGAA	Sequencing primer, Genome PCR verification	
RK144	GAAGGAAGAGCTCACGTCGG	Sequencing primer, Genome PCR verification	
RK145	TGAACCTGATCCTTGGCCTG	Sequencing primer, Genome PCR verification	
RK146	TTTAAGCTTCGGAACAGGCTGATG TAGACC	Cloning PCR	
RK147	GTACCTAACGAAGACGGTAAAAA GCATACTGCTACACCCCCCCACG	Cloning PCR	
RK148	GCTTTTTACCGTCTTCGTTA	Cloning PCR	
RK149	TTTGGATCCCAAGAAAGTCGAAGT CACCA	Cloning PCR	
RK150	AAGCGCAAACGTCATAAAGCC	Sequencing primer, Genome PCR verification	PP_4185-4186 Deletion
RK151	TGTACGTAGGCATGCAGCAC	Sequencing primer, Genome PCR verification	
RK152	AACGGCGTCACTTCGATCCAG	Sequencing primer, Genome PCR verification	
A1-For	GGGCGGAATTCCATTCAAAGCAA CACCGAATACC	Cloning PCR	
A1-Rev	CTTTGTTCAACGGCAACCCACTAG GAAATAAACCTCGTCGCATCG	Cloning PCR	
A2-For	TAGTGGGTTGCCGTTGAACAAAG	Cloning PCR	PP_4116 Deletion
A2-Rev	GCCAGGATCCGTAGGCGAGGATG ATCAGGTAC	Cloning PCR	
A1-For-Sec	CATGCAACAGGTACAAGCCAG	Sequencing primer, Genome PCR verification	

A1-For-Sec-ins	TCGCATTAGACCAAAGATGTAGT	Sequencing primer, Genome PCR verification	
A2-Rev-Sec	TCAATACTTTATCGGTTGAGCGA	Sequencing primer, Genome PCR verification	
A3-For	AGGTGGAATTCGCTGTGCTCCATCTGATTGAAC	Cloning PCR	
A3-Rev	CTGAGCAGAGTGAGGCAAGCAACGGGTTGTAAGCAGCATCTG	Cloning PCR	
A4-For	TGCTTGCCTCACTCTGCTCAG	Cloning PCR	
A4-Rev	CGCAGGATCCCTTCTGTGGAAAACCGCTCGAC	Cloning PCR	
A3-For-Sec	CAGGTTTGACGATGCTTTCAC	Sequencing primer, Genome PCR verification	PP_0356 Deletion
A3-For-Sec-ins	TTGGTGCTGGTGGTGGATGA	Sequencing primer, Genome PCR verification	
A4-Rev-Sec	TTCTTCCAGCGGCAAGGTCAA	Sequencing primer, Genome PCR verification	
A-For	TTTAAGCTTATTTCATCATGAGCGTCAGGTTA	Cloning PCR	
A-Rev	GACAGCGGAGTAGTGCAAGCAGAAAACCGGTCGCTTCTTTTAA	Cloning PCR	
B-For	GCTTGCACTACTCCGCTGTC	Cloning PCR	
B-Rev	TTTGGATCCCGGGTTAACTCTCTGTGTGCTG	Cloning PCR	PP_4011 Deletion
A-Sec	AATCCATTGGTGTGTAGTCATCG	Sequencing primer, Genome PCR verification	
A-Sec-Ins	GGTATTCAACATCGTCCAGGG	Sequencing primer, Genome PCR verification	
Z1-*phaZ*-For	CCTCTAGAACCCTGCTGGTCAGCGTGCTGGAC	Cloning PCR	
Z1-*phaZ*-Rev	GATCCATTTCCCCTGTCAGGCCGCAGCTGTTTATAGGGTTGCGGCATGC	Cloning PCR	PP_5004 Deletion

Z3-*phaZ*-For	AACAGCTGCGGCCTGACAGGGGAAATGGATC	Cloning PCR	
Z3-*phaZ*-Rev	CCAAGCTTAGCCGCTTTTGAGCATGTACTGGACGAAGC	Cloning PCR	
phaC1-For	GCATCACTTGTACCGCACTGG	Sequencing primer, Genome PCR verification	
phaC2-Rev	ATTCACGGTGGCGTGGGT	Sequencing primer, Genome PCR verification	
MM93	GCGGAATTCATCGTCGGTGAAGTTTCTGATGG	Cloning PCR	
MM94	AGGCCGTTCAATGAGGGTCTTCCTGACCGGTGTTGCAGTG	Cloning PCR	
MM95	AAGACCCTCATTGAACGGCCT	Cloning PCR	
MM96	AAAGGATCCCGGCATACAAAACAGAGGCAATG	Cloning PCR	
MM97	GCTGATCGACCTGCAGATTGTC	Sequencing primer, Genome PCR verification	PP_3190 Deletion
MM98	CTGGACCTGATTACCGACAACAG	Sequencing primer, Genome PCR verification	
MM99	CACACCGGTTCGTTCAAGTTTC	Sequencing primer, Genome PCR verification	
MM100	GCGGAATTCTCTGGGAGTAGTAACCGCTTCAA	Cloning PCR	
MM101	GGGTATGGTTTTATTGTGTTGCCATGGCACCTCTTTAAGCACGTG	Cloning PCR	
MM102	GGCAACACAATAAAACCATACCC	Cloning PCR	
MM103	AAAGGATCCCCGACCTTGAATGGAGAGTCATC	Cloning PCR	PP_4431 Deletion
MM104	CCGTGTACCTCAAGCTGGAATG	Sequencing primer, Genome PCR verification	
MM105	TCGACCGAGTGATTTTGCTCAAT	Sequencing primer, Genome PCR verification	

MM106	CCAGGTAAACAGTTCGGGACAG	Sequencing primer, Genome PCR verification	
MM112	GCGGAATTCGGTCACATCTTGTAGGTCGAA	Cloning PCR	
MM113	CGACCAACCCGATTCAATATCAGCTCTTGCACCTTGTTATTGTG	Cloning PCR	
MM114	CTGATATTGAATCGGGTTGGTCG	Cloning PCR	
MM115	TTTGGATCCCACAGGTGAAGCTCGAAGTGA	Cloning PCR	
MM116	GTGTGTGGCAGATGAAACCA	Sequencing primer, Genome PCR verification	PP_3533 Deletion
MM117	TAATCAGATTGCTACGCTGGGTT	Sequencing primer, Genome PCR verification	
MM118	CAACCGTGACGTACTGCCG	Sequencing primer, Genome PCR verification	
MM86	GCGGAATTCTCATTTGCTGAAACGTCCTTCC	Cloning PCR	
MM87	GCAACCCCGGTACGCTCAGTCGGTGGAATCCTGTTATTGTTAA	Cloning PCR	
MM88	CTGAGCGTACCGGGGTTGC	Cloning PCR	
MM89	TTTAAGCTTCCAAGATCAAGGCCGGTATGAACA	Cloning PCR	
MM90	CGGGTGATCTCTTCGGTGAAA	Sequencing primer, Genome PCR verification	PP_5036 Deletion
MM91	GCGATGGATCCTTGTGCAAATG	Sequencing primer, Genome PCR verification	
MM92	CCACTCGCCTGTATCATCTTTCA	Sequencing primer, Genome PCR verification	
TS1F	ACCTGCCCGCCGAATTCCTGC	Cloning PCR	PP_5003-PP_5008 Deletion
TS1R	GTTTTCCACCACTCATGAGCGTGACCAGTGATAAGGAACA	Cloning PCR	
TS2F	GCTCATGAGTGGTGGAAAACCGC	Cloning PCR	

TS2R	ATGCAGGATCCTGAATTTGAAACA CATGGGGT	Cloning PCR	
FdPHA	TCCCGAGAGATTCTGCCCAT	Sequencing primer, Genome PCR verification	
RdPHA	AGCCCGTTCCAGAAGCCGAT	Sequencing primer, Genome PCR verification	
RK198	TTTGAAGACGTaatgAGTAACAAGA ACAACGATGAGCTACAGC	Level 0, Pp_*phaC1*_ Golden Gate MoClo	PP_5003
RK199	TTTGAAGACGTaagcTCAACGCTC GTGAACGTAGG	Level 0, Pp_*phaC1*_ Golden Gate MoClo	
RK153	CACCTACATCGATGCGCTGA	qRT-PCR-sequencing primer_ *phaC1* gene	
RK154	GTACAAGTGATGCCACCGGA	qRT-PCR-sequencing primer_ *phaC1* gene	
RK173	TTTGAAGACACaatgGCTGGCAAG AAGAACACCGA	Level 0, *phaF*_ Golden Gate MoClo	PP_5007
RK174	TTTGAAGACACcgaTGACTTGGCA GTCTCGGC	Level 0, *phaF*_ Golden Gate MoClo	
RK175	TTTGAAGACAGAtcgACCACTTCG CGGGTGTCGG	Level 0, *phaF*_ Golden Gate MoClo	
RK176	TTTGAAGACAGaagcTCAGATCAG GGTACCGGTGCC	Level 0, *phaF*_ Golden Gate MoClo	
MM170	GCTTCTCGATCTGCTTGGTCA	qRT-PCR_*phaF* gene	
MM171	AAGATGTTGCCGAGACTGCC	qRT-PCR_*phaF* gene	
MM168	TTGTCGAGTTGAATTTCTACCTTG C	qRT-PCR_*phaI* gene	PP_5008
MM169	CAGGAAGGCGCTGACTACTT	qRT-PCR_*phaI* gene	
MM203	TTTGAAGACCTaatgAGGCCAGAAA TCGCTGTACT	Level 0, *phaG*_ Golden Gate MoClo	PP_1408
MM204	TTTGAAGACCTtTtcCTTGCTGATC AGCCGTT	Level 0, *phaG*_ Golden Gate MoClo	

MM205	TTTGAAGACGT**gaAa**CCGAGGCGC ATATCCT	Level 0, *phaG*_ Golden Gate MoClo	
MM206	TTTGAAGACGT**aagc**TCAGATGGC AAATGCATGCT	Level 0, *phaG*_ Golden Gate MoClo	
MM174	TGTCCAGGCTGCTCACATG	qRT-PCR_*phaG* gene	
MM175	GTTCTCGCCAGTGATCAACGA	qRT-PCR_*phaG* gene	
MM207	TTTGAAGACAG**aatg**TTGCAGACAC GCATCATC	Level 0, PP_0763_ Golden Gate MoClo	
MM208	TTTGAAGACAG**gtcC**TCGGCATGG TTCATGGTGT	Level 0, PP_0763_ Golden Gate MoClo	
MM209	TTTGAAGACGT**Ggac**CGCGTGGTG CTGGTC	Level 0, PP_0763_ Golden Gate MoClo	
MM210	TTTGAAGACGT**cCtc**CAGGTCGAG CGAGGAAA	Level 0, PP_0763_ Golden Gate MoClo	PP_0763
MM211	TTTGAAGACCA**gaGg**ACCTGATCA GCCGCCA	Level 0, PP_0763_ Golden Gate MoClo	
MM212	TTTGAAGACCA**aagc**TTACAACGTG GAAAGGAACGCG	Level 0, PP_0763_ Golden Gate MoClo	
MM222	GTCTGGTCGGCGAGTATGAG	Level 0, PP_0763_sequencing primer	
RK246	TTTGAAGACAC**ggag**CTTGGACTC CTGTTGATAGATCC	Level 0, λT0-SynPro16 promoter_ Golden Gate MoClo	-
RK247	TTTGAAGACAC**catt**TAGAACCCCC TCGTACGCTC	Level 0, λT0-SynPro16 promoter_Golden Gate MoClo	-
RK189	TTTGAAGACGA**gctt**TCTAGGGCGG CGGATTTGTC	Level 0, λT1-terminator_Golden Gate MoClo	-
RK190	TTTGAAGACGA**agcg**GGCATCAAA TAAAACGAAAGGC	Level 0, λT1-terminator_Golden Gate MoClo	-
RK205	TTTGAAGACAG**gctt**TCGGTCAGTT TCACCTGATT	Level 0, rnpBT1-terminator_Golden Gate MoClo	-

RK206	TTTGAAGACAGagcgGACAGTCATTCATCTTTCTGCC	Level 0, rnpBT1-terminator_Golden Gate MoClo	-
RK207	TTTGAAGACGTgcttGTAATCGTTAATCCGCAAATAA	Level 0, rpoC-term terminator_Golden Gate MoClo	-
RK208	TTTGAAGACGTagcgTGACAAATGCTCTTTCCCTA	Level 0, rpoC-term-terminator_Golden Gate MoClo	-
RK81	GGAAGAGCGCCCAATACG	Confirm Golden Gate/MoClo cloning in pL0	-
RK82	AAAGTGCCACCTGACGTCTA	Confirm Golden Gate/MoClo cloning in pL0	-
RK155	GAACCCTGTGGTTGGCATGCACATAC	Confirm Golden Gate/MoClo cloning in pL1	-
RK156	CTGGTGGCAGGATATATTGTGGTG	Confirm Golden Gate/MoClo cloning in pL1	-
RK157	GTGGTGTAAACAAATTGACGC	Confirm Golden Gate/MoClo cloning in pL2	-
RK158	GGATAAACCTTTTCACGCCC	Confirm Golden Gate/MoClo cloning in pL2	-
MM152	CATAAGCTTCATGTGTTTGATCATTTCATCGC	Cloning PCR_PP_4011	PP_4011
MM153	CATGGATCCATGGGATACCAGAAAATCAAGGTTC	Cloning PCR_PP_4011	
MM201	CTTGGTACCCTCCTTCGACAC	qRT-PCR_PP_4011	
MM154	CATGGATCCATGCCCACCCGTTCCAAGATC	Cloning PCR_PP_4012	PP_4012
MM155	CATAAGCTTCAGGGCAGCGATGGCG	Cloning PCR_PP_4012	
MM202	CGGTCTTTTCTTTCAGCACGG	qRT-PCR_PP_4012	

MM158	CATCTACCAGGCCACCATCG	PP_4012_Sequencing primer	
MM225	GCCCCGGTGCTGGC	PP_4012_Sequencing primer	
MM226	GTCCTTGATGCGGGCGTA	PP_4012_Sequencing primer	
MM223	G**GC**GTCGGAGTTGCCTTCG**GC**CAGCACCGGG**GC**CACGGCGG**C**GCCCTTGATGCGGTCGTAG	Cloning PCR_PP_4012 point mutations	
MM224	**G**CCGCCGTG**GC**CCCGGTGCTG**G****C**CGAAGGCAACTCCGAC**GC**C	Cloning PCR_PP_4012 point mutations	
F24	CGCCAGGGTTTTCCCAGTCACGAC	Sequencing primer, PCR verification	-
R24	AGCGGATAACAATTTCACACAGGA	Sequencing primer, PCR verification	-
T7prom	TAATACGACTCACTATAGGG	pET29a (+) sequencing primer	-
TT7	GCTAGTTATTGCTCAGCGG	pET29a (+) sequencing primer	-

Table S 7. Oligonucleotides used in this work. Underlined sequence means the restriction site for restriction enzymes, bold small red letters means the fusion sites used in level 0 golden gate process, with bold capital letters the point mutations are shown. The following restriction enzymes were used: AvrII (CCTAGG), BamHI-HF (GGATCC), EcoRI-HF (GAATTC), HindIII-HF (AAGCTT), XbaI (TCTAGA) and BpiI (GAAGAC).

Pathway	Reactions	KT2440	Δ*pha*	KT40Z	M1	M2	M3	M4
EMP	PGI	0.0	-0.1	-0.1	-0.1	0.0	0.0	0.0
	FBP	0.3	0.4	0.6	0.5	0.3	0.3	0.3
	FBA	-0.3	-0.4	-0.6	-0.5	-0.3	-0.3	-0.3
	TPI	-0.4	-0.6	-0.7	-0.6	-0.4	-0.4	-0.4
Pay-off	GAPD	-0.8	-1.2	-1.4	-1.2	-0.8	-0.8	-0.8
	PGK	0.8	1.2	1.4	1.2	0.8	0.8	0.8
	PGM	1.4	1.9	2.2	1.9	1.4	1.4	1.4
	ENO	-1.4	-1.9	-2.2	-1.9	-1.4	-1.4	-1.4
	PYK	0.2	0.3	0.4	0.3	0.2	0.2	0.2
	PPS	0.0	0.1	0.2	0.1	0.0	0.0	0.0
	PDHa	0.0	0.0	0.0	0.0	0.0	0.0	0.0
	PDHbr	0.0	0.0	0.0	0.0	0.0	0.0	0.0
	PDHcr	0.1	1.8	3.3	2.8	0.0	0.1	0.0
ED	EDA	0.0	0.0	0.1	0.0	0.0	0.0	0.0
	EDD	0.0	0.0	0.1	0.0	0.0	0.0	0.0
Gluconeogenesis	PPC	0.0	0.1	0.1	0.0	0.0	0.0	0.0
	PPCK	1.9	2.5	3.0	2.6	1.8	1.9	1.8
	OAADC	0.5	0.5	0.5	0.5	0.6	0.6	0.6
	PC	0.0	0.1	0.2	0.2	0.0	0.0	0.0
	ME2	0.3	0.2	0.2	0.3	0.2	0.2	0.2
PPP	G6PDH2	0.0	0.0	0.1	0.0	0.0	0.0	0.0
	GND	0.0	0.0	0.1	0.0	0.0	0.0	0.0
	RPE	-0.3	-0.3	-0.3	-0.3	-0.3	-0.3	-0.3
	RPI	-0.3	-0.3	-0.3	-0.3	-0.2	-0.3	-0.2
	TKT1	-0.1	0.0	0.0	0.0	-0.1	-0.1	-0.1
	TKT2	-0.2	-0.2	-0.2	-0.2	-0.2	-0.2	-0.2
	TALA	-0.1	0.0	0.0	0.0	-0.1	-0.1	-0.1
TCA	CS	4.0	6.5	8.5	7.5	3.9	4.0	3.9
	ACONTa	4.0	6.5	8.5	7.5	3.9	4.0	3.9
	ACONTb	4.0	6.5	8.5	7.5	3.9	4.0	3.9
	ICDHyr	0.5	2.3	3.7	3.2	0.4	0.5	0.4
	AKGDa	0.1	1.8	3.2	2.7	0.0	0.1	0.0
	AKGDbr	0.1	1.8	3.2	2.7	0.0	0.1	0.0
	SUCDi	3.6	6.2	8.4	7.3	3.5	3.6	3.5
	FUM	3.9	6.8	9.1	7.9	3.8	4.0	3.8
	MDH	7.2	10.6	13.2	11.5	7.1	7.3	7.1
	MDH2	0.0	0.1	0.1	0.1	0.0	0.0	0.0
	ICL	3.5	4.2	4.8	4.3	3.4	3.6	3.4
	MALS	3.5	4.1	4.5	4.0	3.4	3.5	3.4

de novo fatty acid biosynthesis	ACCOAC	0.4	1.4	2.2	1.8	0.4	0.4	0.4
	MCOATA	0.4	1.4	2.2	1.8	0.4	0.4	0.4
	MACPD	0.0	0.1	0.1	0.1	0.0	0.0	0.0
	ACOATA	0.0	0.0	0.0	0.0	0.0	0.0	0.0
	KAS15	0.0	0.0	0.0	0.0	0.0	0.0	0.0
	3OAR80	0.0	0.0	0.0	0.1	0.0	0.0	0.0
	3HAACOAT80	-0.1	-0.1	-0.1	-0.1	-0.1	-0.1	-0.1
	EAR80y	0.1	0.2	0.2	0.2	0.1	0.1	0.1
	3OAS80	0.0	0.0	0.0	0.1	0.0	0.0	0.0
β-oxidation	FACOAL80t2pp	4.0	2.9	4.0	5.0	3.2	3.2	3.3
	ACOAD1f	2.0	2.8	3.4	3.0	2.0	2.1	2.0
	ACOAD2f	2.0	2.8	3.4	3.0	2.0	2.1	2.0
	ACOAD3f	4.0	2.9	4.1	5.1	3.2	3.2	3.3
	ECOAH3	-1.8	-5.3	-2.0	-1.8	-4.3	-4.3	-3.8
	RHACOAR80	-0.2	2.5	-1.5	-1.3	2.3	2.2	1.8
	RECOAH3	-2.2	2.4	-2.2	-3.4	1.0	1.0	0.5
	HACD3i	1.8	5.3	2.0	1.8	4.3	4.3	3.8
	KAT3	2.0	2.8	3.4	3.0	2.0	2.1	2.0
	RECOAH3	-2.2	2.4	-2.2	-3.4	1.0	1.0	0.5
PHA cycle	PHAP2C80	1.9	0.0	0.6	2.0	1.1	1.1	1.2
	PHADPC80	1.1	0.0	0.0	1.3	1.1	1.1	1.2
	ACSPHAC80	0.0	0.0	0.0	0.0	0.0	0.0	0.0
	EX_R_3hocta(e)	1.1	0.0	0.0	1.3	1.1	1.1	1.2
	sink_PHAg	-0.8	0.0	-0.6	-0.7	0.0	0.0	0.0
Exchange reactions	EX_h(e)	0.2	0.4	-0.7	-0.7	0.9	0.9	0.9
	EX_octa(e)	-4.0	-2.9	-4.0	-5.0	-3.2	-3.2	-3.3
	EX_co2(e)	3.9	8.7	12.7	10.9	3.7	3.9	3.7
	EX_o2(e)	-10.6	-16.8	-22.8	-20.6	-10.0	-10.4	-10.1
Energy conservation	NADTRHD	0.4	1.6	0.6	0.7	0.6	0.5	0.6
	CYTBDpp	0.0	0.1	1.4	0.9	0.0	0.0	0.0
	CYTBO3_4pp	16.3	24.8	31.8	26.4	14.2	14.9	14.6
	CYO1_KT	4.9	7.1	9.0	11.0	5.8	5.8	5.5
	NADH16pp	9.3	14.0	14.3	11.4	9.1	9.4	9.1
	ATPS4rpp	26.9	38.1	44.8	40.9	25.6	26.5	25.7

Table S 8. Carbon flux distribution during phase A. The median values of reaction fluxes (mmol·gDW^{-1}·h^{-1}) were obtained by random sampling of Monte Carlo using the condition-specific models of the phase A. The reactions affecting key metabolic pathways, such as EMP, Pay-off, ED, Gluconeogenesis, PPP, TCA, key exchange reactions, PHA cycle, Fatty acid cycle, reactions are shown. For the model reaction nomenclature extra information can be found in the following link https://drive.google.com/file/d/1L-iVLsONX9qiReDmjVgRS_eDTL6sfJa9/view.

Pathway	Reactions	KT2440	Δ*pha*	KT40Z	M1	M2	M3	M4
EMP	PGI	-0.2	-0.2	-0.2	-0.1	-0.2	-0.2	-0.1
	FBP	0.4	0.5	0.4	0.3	0.3	0.4	0.3
	FBA	-0.4	-0.5	-0.4	-0.3	-0.3	-0.4	-0.3
	TPI	-0.5	-0.6	-0.5	-0.4	-0.5	-0.5	-0.4
Pay-off	GAPD	-0.9	-1.1	-0.9	-0.8	-0.8	-0.9	-0.6
	PGK	0.9	1.1	0.9	0.8	0.8	0.9	0.6
	PGM	1.6	1.9	1.7	1.3	1.4	1.6	1.1
	ENO	-1.6	-1.9	-1.7	-1.3	-1.4	-1.6	-1.1
	PYK	0.1	0.2	0.2	0.2	0.1	0.1	0.1
	PPS	0.1	0.2	0.2	0.1	0.1	0.1	0.1
	PDHa	0.0	0.1	0.0	0.0	0.0	0.0	0.0
	PDHbr	0.0	0.1	0.0	0.0	0.0	0.0	0.0
	PDHcr	3.8	4.2	4.4	3.2	3.7	3.8	2.7
ED	EDA	0.1	0.1	0.1	0.1	0.1	0.1	0.0
	EDD	0.1	0.1	0.1	0.1	0.1	0.1	0.0
Gluconeogenesis	PPC	0.1	0.1	0.1	0.0	0.1	0.1	0.0
	PPCK	2.0	2.5	2.1	1.7	1.8	1.9	1.4
	OAADC	0.2	0.3	0.2	0.2	0.1	0.2	0.1
	PC	0.4	0.6	0.4	0.3	0.4	0.4	0.3
	ME2	0.1	0.1	0.1	0.1	0.1	0.1	0.1
PPP	G6PDH2	0.1	0.1	0.1	0.1	0.1	0.1	0.1
	GND	0.1	0.1	0.1	0.0	0.0	0.1	0.0
	RPE	-0.1	-0.1	-0.1	-0.1	-0.1	-0.1	-0.1
	RPI	-0.1	-0.2	-0.2	-0.1	-0.1	-0.1	-0.1
	TKT1	0.0	0.0	0.0	0.0	0.0	0.0	0.0
	TKT2	-0.1	-0.1	-0.1	-0.1	-0.1	-0.1	-0.1
	TALA	0.0	0.0	0.0	0.0	0.0	0.0	0.0
TCA	CS	6.6	7.4	7.3	5.6	6.0	6.4	4.6
	ACONTa	6.6	7.4	7.3	5.6	6.0	6.4	4.6
	ACONTb	6.6	7.4	7.3	5.6	6.0	6.4	4.6
	ICDHyr	4.0	4.4	4.5	3.3	3.8	3.9	2.8
	AKGDa	3.7	4.1	4.3	3.1	3.6	3.7	2.6
	AKGDbr	3.7	4.1	4.3	3.1	3.6	3.7	2.6

	SUCDi	6.9	7.7	7.5	5.7	6.3	6.6	4.7
	FUM	7.4	8.3	8.2	6.5	6.8	7.1	5.1
	MDH	9.3	10.6	10.3	8.2	8.4	8.9	6.5
	MDH2	0.1	0.1	0.1	0.1	0.1	0.1	0.1
	ICL	2.5	2.9	2.6	2.2	2.2	2.3	1.8
	MALS	2.3	2.7	2.4	2.0	2.0	2.2	1.6
	ACCOAC	2.4	2.8	2.4	1.7	2.2	2.2	1.6
	MCOATA	2.4	2.8	2.4	1.7	2.2	2.2	1.6
	MACPD	0.1	0.1	0.1	0.0	0.1	0.1	0.1
	ACOATA	0.0	-0.1	0.0	0.0	0.0	0.0	0.0
de novo fatty acid	KAS15	0.0	0.0	0.0	0.0	0.0	0.0	0.0
biosynthesis	3OAR80	0.1	0.1	0.1	0.1	0.1	0.1	0.0
	3HAACOAT80	-0.1	-0.1	-0.1	0.0	0.0	0.0	0.0
	EAR80y	0.1	0.2	0.2	0.1	0.1	0.1	0.1
	3OAS80	0.1	0.1	0.1	0.1	0.1	0.1	0.0
	FACOAL80t2pp	3.8	2.5	3.3	3.2	2.6	3.0	2.2
	ACOAD1f	2.2	2.6	2.4	1.9	2.0	2.2	1.6
	ACOAD2f	2.2	2.5	2.4	1.9	2.0	2.1	1.6
	ACOAD3f	3.9	2.6	3.5	3.2	2.7	3.0	2.3
	ECOAH3	-4.4	-4.9	-1.9	-2.1	-1.9	-2.4	-2.3
β-oxidation	RHACOAR80	2.1	2.3	-0.6	0.1	-0.2	0.2	0.7
	RECOAH3	0.4	2.2	-1.6	-1.2	-0.9	-0.8	0.0
	HACD3i	4.4	4.9	1.9	2.1	1.9	2.4	2.3
	KAT3	2.2	2.5	2.4	1.9	2.0	2.1	1.6
	RECOAH3	0.4	2.2	-1.6	-1.2	-0.9	-0.8	0.0
	PHAP2C80	1.7	0.0	1.0	1.3	0.7	0.9	0.7
	PHADPC80	0.2	0.0	0.0	0.4	0.7	0.9	0.7
PHA cycle	ACSPHAC80	0.1	0.0	0.0	0.0	0.1	0.1	0.0
	EX_R_3hocta(e)	0.1	0.0	0.0	0.4	0.7	0.9	0.7
	sink_PHAg	-1.5	0.0	-0.9	-0.9	0.0	0.0	0.0
	EX_h(e)	-2.8	-1.3	-2.3	-1.7	-1.2	-1.3	-0.8
	EX_octa(e)'	-3.8	-2.5	-3.3	-3.2	-2.6	-3.0	-2.2
Exchange reactions	EX_co2(e)	12.7	13.9	13.7	10.1	11.7	12.3	8.6
	EX_o2(e)	-19.8	-21.1	-21.2	-16.2	-17.8	-18.8	-13.4
	NADTRHD	0.5	1.5	0.3	0.3	0.6	0.7	0.5

Energy conservation	CYTBDpp	2.2	1.9	5.9	2.0	2.0	2.1	1.3
	CYTBO3_4pp	21.4	27.1	23.7	20.9	20.8	21.8	16.0
	CYO1_KT	12.0	9.6	8.1	6.4	9.2	9.8	6.9
	NADH16pp	9.1	16.9	15.6	9.6	10.8	11.2	8.2
	ATPS4rpp	34.0	41.1	35.2	28.2	30.8	31.9	23.9

Table S 9. Carbon flux distribution during phase B. The median values of reaction fluxes (mmol·gDW^{-1}·h^{-1}) were obtained by random sampling of Monte Carlo using the condition-specific models of the phase B. The reactions affecting key metabolic pathways, such as EMP, Pay-off, ED, Gluconeogenesis, PPP, TCA, key exchange reactions, PHA cycle, Fatty acid cycle, reactions are shown. For the model reaction nomenclature extra information can be found in the following link https://drive.google.com/file/d/1L-iVLsONX9qiReDmjVgRS_eDTL6sfJa9/view.

Pathway	Reactions	KT2440	Δ*pha*	KT40Z	M1	M2	M3	M4
EMP	PGI	0.0	-0.1	0.0	0.0	-0.1	0.0	-0.1
	FBP	0.0	0.2	0.0	0.0	0.1	0.1	0.1
	FBA	0.0	-0.2	0.0	0.0	-0.1	-0.1	-0.1
	TPI	0.0	-0.2	0.0	0.0	-0.2	-0.1	-0.2
Pay-off	GAPD	0.0	-0.4	0.0	0.0	-0.3	-0.2	-0.3
	PGK	0.0	0.4	0.0	0.0	0.3	0.2	0.3
	PGM	0.0	0.7	0.0	0.1	0.6	0.4	0.6
	ENO	0.0	-0.7	0.0	-0.1	-0.6	-0.4	-0.6
	PYK	0.0	0.1	0.0	0.0	0.1	0.0	0.0
	PPS	0.0	0.1	0.0	0.0	0.0	0.0	0.1
	PDHa	0.0	0.0	0.0	0.0	0.0	0.0	0.0
	PDHbr	0.0	0.0	0.0	0.0	0.0	0.0	0.0
	PDHcr	0.1	1.8	0.2	0.3	1.5	1.0	1.7
ED	EDA	0.0	0.0	0.0	0.0	0.0	0.0	0.0
	EDD	0.0	0.0	0.0	0.0	0.0	0.0	0.0
Gluconeogenesis	PPC	0.0	0.0	0.0	0.0	0.0	0.0	0.0
	PPCK	0.0	0.9	0.0	0.1	0.7	0.5	0.7
	OAADC	0.0	0.0	0.0	0.0	0.1	0.0	0.0
	PC	0.0	0.2	0.0	0.0	0.2	0.1	0.2
	ME2	0.0	0.0	0.0	0.0	0.0	0.0	0.0
PPP	G6PDH2	0.0	0.0	0.0	0.0	0.0	0.0	0.0
	GND	0.0	0.0	0.0	0.0	0.0	0.0	0.0
	RPE	0.0	0.0	0.0	0.0	0.0	0.0	0.0
	RPI	0.0	-0.1	0.0	0.0	0.0	0.0	0.0
	TKT1	0.0	0.0	0.0	0.0	0.0	0.0	0.0
	TKT2	0.0	0.0	0.0	0.0	0.0	0.0	0.0
	TALA	0.0	0.0	0.0	0.0	0.0	0.0	0.0

TCA	CS	0.1	2.8	0.3	0.4	2.3	1.7	2.6
	ACONTa	0.1	2.8	0.3	0.4	2.3	1.7	2.6
	ACONTb	0.1	2.8	0.3	0.4	2.3	1.7	2.6
	ICDHyr	0.1	1.8	0.2	0.3	1.5	1.1	1.7
	AKGDa	0.1	1.7	0.2	0.3	1.4	1.0	1.6
	AKGDbr	0.1	1.7	0.2	0.3	1.4	1.0	1.6
	SUCDi	0.1	3.0	0.3	0.4	2.5	1.7	2.7
	FUM	0.1	3.2	0.3	0.4	2.7	1.8	2.9
	MDH	0.1	3.9	0.3	0.5	3.3	2.3	3.5
	MDH2	0.0	0.1	0.0	0.0	0.0	0.0	0.0
	ICL	0.0	1.0	0.1	0.1	0.8	0.6	0.8
	MALS	0.0	0.9	0.0	0.1	0.8	0.5	0.8
de novo fatty acid biosynthesis	ACCOAC	0.0	1.2	0.1	0.1	0.8	0.5	1.0
	MCOATA	0.0	1.2	0.1	0.1	0.8	0.5	1.0
	MACPD	0.0	0.1	0.0	0.0	0.0	0.0	0.0
	ACOATA	0.0	0.0	0.0	0.0	0.0	0.0	0.0
	KAS15	0.0	0.0	0.0	0.0	0.0	0.0	0.0
	3OAR80	0.0	0.0	0.0	0.0	0.0	0.0	0.0
	3HAACOAT80	0.0	0.0	0.0	0.0	0.0	0.0	0.0
	EAR80y	0.0	0.1	0.0	0.0	0.0	0.0	0.0
	3OAS80	0.0	0.0	0.0	0.0	0.0	0.0	0.0
β-oxidation	FACOAL80t2pp	0.3	0.9	0.6	0.3	0.8	0.6	0.8
	ACOAD1f	0.0	0.9	0.1	0.1	0.8	0.6	0.8
	ACOAD2f	0.0	0.9	0.1	0.1	0.8	0.6	0.8
	ACOAD3f	0.3	0.9	0.6	0.3	0.9	0.7	0.9
	ECOAH3	-3.0	-7.7	-2.5	-3.2	-4.3	-2.5	-5.2
	RHACOAR80	3.0	6.7	2.4	3.0	3.5	2.0	4.3
	RECOAH3	2.7	6.7	1.9	2.9	3.4	1.8	4.2
	HACD3i	3.0	7.7	2.5	3.2	4.3	2.5	5.2
	KAT3	0.0	0.9	0.1	0.1	0.8	0.6	0.8
	RECOAH3	2.7	6.7	1.9	2.9	3.4	1.8	4.2
PHA cycle	PHAP2C80	0.3	0.0	0.5	0.2	0.1	0.1	0.1
	PHADPC80	0.0	0.0	0.0	0.0	0.1	0.1	0.1
	ACSPHAC80	0.0	0.0	0.0	0.0	0.0	0.0	0.0
	EX_R_3hoct a(e)	0.0	0.0	0.0	0.0	0.1	0.1	0.1
	sink_PHAg	-0.3	0.0	-0.5	-0.2	0.0	0.0	0.0

Exchange reactions	EX_h(e)	-0.3	-0.6	-0.6	-0.3	-0.5	-0.3	-0.6
	EX_octa(e)'	-0.3	-0.9	-0.6	-0.3	-0.8	-0.6	-0.8
	EX_co2(e)	0.2	5.6	0.5	0.7	4.6	3.1	5.2
	EX_o2(e)	-0.5	-8.2	-1.0	-1.2	-6.9	-4.7	-7.6
Energy conservation	NADTRHD	0.3	1.2	0.4	0.4	0.4	0.5	0.4
	CYTBDpp	0.0	0.6	0.0	0.2	0.8	0.5	1.3
	CYTBO3_4pp	0.7	10.4	0.6	1.3	6.9	6.5	8.6
	CYO1_KT	0.3	3.9	1.2	0.6	4.6	1.8	3.7
	NADH16pp	0.4	6.6	0.7	0.9	4.2	3.5	5.8
	ATPS4rpp	1.2	15.9	2.1	2.3	11.9	8.0	13.2

Table S 10. Carbon flux distribution during phase C. The median values of reaction fluxes (mmol·gDW^{-1}·h^{-1}) were obtained by random sampling of Monte Carlo using the condition-specific models of the phase C. The reactions affecting key metabolic pathways, such as EMP, Pay-off, ED, Gluconeogenesis, PPP, TCA, key exchange reactions, PHA cycle, Fatty acid cycle, reactions are shown. For the model reaction nomenclature extra information can be found in the following link https://drive.google.com/file/d/1L-iVLsONX9qiReDmjVgRS_eDTL6sfJa9/view.

Organism	Reference
Dimeric IDH	
Echerichia coli	(Cozzone and El-Mansi, 2005; Watanabe *et al.*, 2005)
Bacillus subtillis	(Singh *et al.*, 2001, 2002)
Bacillus stearothermophilus	(Howard and Becker)
Methylobacillus flagellatus	(Romkina and Kiriukhin, 2017)
Thermus thermophilus HB8	(Eguchi *et al.*, 1989)
Streptococcus mutans	(Wang *et al.*, 2013)
Ostreococcus lucimarinus CCE9901	(Wang *et al.*, 2015)
Micromonas sp RCC299	(Wang *et al.*, 2015)
Bifidobacterium longum	(Huang *et al.*, 2016)
Zymomonas mobilis	(P. Wang *et al.*, 2012)
Monomeric IDH	
Corynebacterium glutamicum	(Eikmanns *et al.*, 1995; Chen and Yang, 2000)
Azotobacter vinelandii	(Yasutake *et al.*, 2002, 2003; Watanabe *et al.*, 2005)
Psychromonas marina	(Hirota *et al.*, 2017)
Vibrio parahaemolyticus	(Fukunaga *et al.*, 1987)
Acinetobacter calcoaceticus	(Reeves *et al.*, 1983, 1986)
Acinetobacter baumannii	(P. Wang *et al.*, 2018)
Rhizobium meliloti	(McDermott and Kahn, 1992),
Streptomyces lividans TK54	(Zhang *et al.*, 2009)
Desulfobacter vibrioformis	(Steen *et al.*, 1998)
Chlorobium limicola	(Kanao *et al.*, 2002)
Monomeric and Dimeric IDH	
Colwellia maris (formally *Vibrio* sp ABE-1)	(Ochiai *et al.*, 1979; Ishii *et al.*, 1993; Suzuki *et al.*, 1995; Watanabe *et al.*, 2005; Yasuda *et al.*, 2013; Kobayashi and Takada, 2014)
Colwellia psychrerythraea NRC1004	(Maki *et al.*, 2006; Kobayashi and Takada, 2014)
Colwellia psychrerythraea 34H	(Suzuki and Takada, 2016)
Mycobacterium tuberculosis	(Murima *et al.*, 2016)
Mycobacterium bovis	(Murima *et al.*, 2016)
Cupriavidus necator	(Wang *et al.*, 2003)
Xyllela fastidiosa	(Lv *et al.*, 2018)
Pseudomonas nautica	(Roy and Packard, 1998)
Pseudomonas psychrophila	(Matsuo *et al.*, 2010)
Pseudomonas aeruginosa PAO1	(Crousilles *et al.*, 2018)

Table S 11. Selected examples of bacteria with dimeric, monomeric and both $NADP^+$ isocitrate dehydrogenase are listed.

Growth-coupled designs using terephthalate as substrate

The GDLS algorithm using *i*MM1412 was applied using an uptake rate of TPHTA of 4.725 mmol·gDW^{-1}·h^{-1} and the default parameters for GDLS. The optimal GDLS path results are shown in Table S12 and Figure S1.

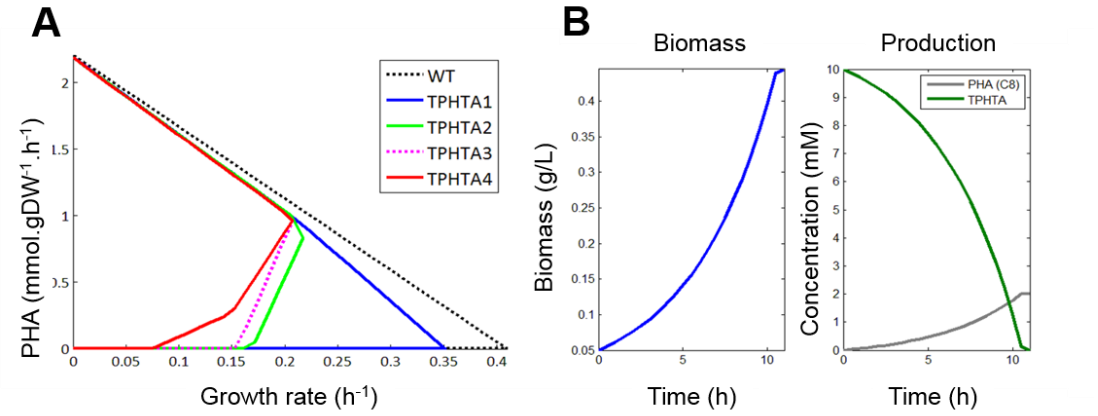

Figure S 1. A. Production envelopes for wild-type and TPHTA *P. putida* knockout strains belonging to more promising GDLS path. The production envelopes for each overproducer design are shown as a function of the biomass production rate of the wild-type *P. putida* network using TPHTA as sole carbon source (black lines). TPHTA1 (blue), TPHTA2 (green), TPHTA3 (magenta), TPHTA4 (red). **B.** Production of biomass (blue) and PHA (grey) of design TPHTA4 as predicted with dynamic FBA is shown in the center and right panels, respectively, as a function of time and TPHTA uptake (green).

Design	TPHTA1	TPHTA2	TPHTA3	TPHTA4
Uptake rate (mmol·gDW^{-1}·h^{-1})	4.73	4.73	4.73	4.73
Knockouts	9	11	14	*14
Growth rate (h^{-1})	0.35	0.22	0.21	0.21
Production Rate (min-max)	0.00	0.84	0.96	1.22
Residual Biomass (g/L)	0.70	0.47	0.44	0.44
PHA (mM)	0.00	1.78	2.04	2.04
PHA Biomass (g/L)	0.00	0.28	0.32	0.32
$Y_{p/s}$ (mmol/mmol)	0.00	0.18	0.20	0.26
BCPY (mmol·gDW^{-1}·h^{-1})	0.00	0.18	0.20	0.25
Biomass PHA (%)	0.00	37.80	42.16	42.16

Table S 12. Properties of the PHA growth-coupled overproducer designs using TPHTA as substrate at 10 mM (1.64 g/L). * Indicates additional flux constraints. Uptake rate (mmol·gDW^{-1}·h^{-1}); Growth rate (h^{-1}); Production rate (mmol·gDW^{-1}·h^{-1}); $Y_{p/s,}$ Product yield (mmol product/mmol substrate); BCPY, Biomass coupled product yield (mmol·gDW^{-1}·h^{-1}).

Growth-coupled designs using EG as substrate

The GDLS algorithm using *i*MM1412 was applied using an uptake rate of EG of 13.16-13.60 mmol·gDW^{-1}·h^{-1} (without other nutrient limitations) using default parameters for GDLS. The optimal GDLS path results are shown in the Table S13 and Figure S2.

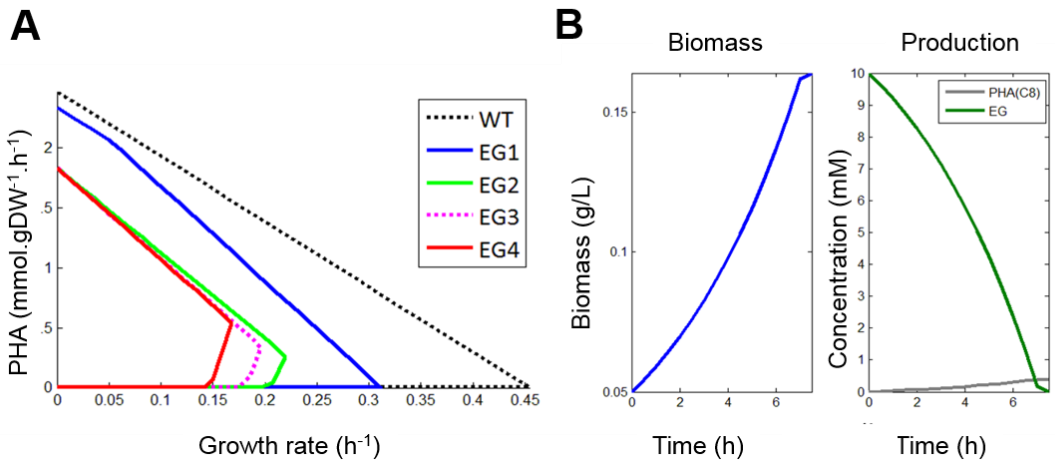

Figure S 2. A. Production envelopes for wild-type and EG *P. putida* knockout strains belonging to more promising GDLS path**.** The production envelopes for each overproducer design are shown as a function of the biomass production rate of the wild-type *P. putida* network using EG as sole carbon source (black lines). EG1 (blue), EG2 (green), EG3 (magenta), EG4 (red). **B.** Production of biomass (blue) and PHA (grey) of design EG4 as predicted with dynamic FBA is shown in the center and right panels, respectively, as a function of time and EG uptake (green).

Design	EG1	EG2	EG3	EG4
Uptake rate (mmol·gDW^{-1}·h^{-1})	13.60	13.26	13.16	13.53
Knockouts	10	20	22	26
Growth rate (h^{-1})	0.31	0.22	0.20	0.17
Production Rate (min-max)	0.00	0.26	0.33	0.53
Residual Biomass (g/L)	0.20	0.20	0.16	0.16
PHA (mM)	0.00	0.20	0.25	0.39
PHA Biomass (g/L)	0.00	0.03	0.04	0.06
$Y_{p/s}$ (mmol/mmol)	0.00	0.02	0.02	0.04
BCPY (mmol·gDW^{-1}·h^{-1})	0.00	0.06	0.06	0.09
Biomass PHA (%)	0.00	13.49	19.44	27.50

Table S 13. Properties of the PHA growth-coupled overproducer designs using EG as substrate at 10 mM (0.62 g/L). Uptake rate (mmol·gDW^{-1}·h^{-1}); Growth rate (h^{-1}); Production rate (mmol·gDW^{-1}·h^{-1}); $Y_{p/s,}$ Product yield (mmol product/mmol substrate); BCPY, Biomass coupled product yield (mmol·gDW^{-1}·h^{-1}).

Growth-coupled designs using PU as substrate

The GDLS algorithm using *i*MM1412 was applied using an uptake rate of PU of 1.4 mmol·gDW^{-1}·h^{-1} using default parameters for GDLS. The optimal GDLS path results are shown in the Table S14 and Figure S3.

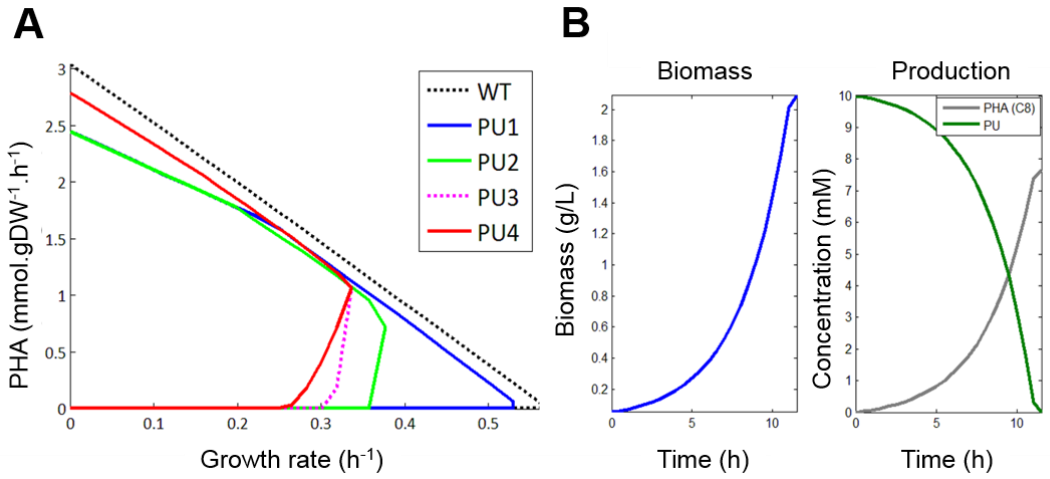

Figure S 3. A. Production envelopes for wild-type and PU *P. putida* knockout strains belonging to more promising GDLS path**.** The production envelopes for each overproducer design are shown as a function of the biomass production rate of the wild-type *P. putida* network using PU as sole carbon source (black lines). PU1 (blue), PU2 (green), PU3 (magenta), PU4 (red). **B.** Production of biomass (blue) and PHA (grey) of design PU4 as predicted with dynamic FBA is shown in the center and right panels, respectively, as a function of time and PU uptake (green).

Design	PU1	PU2	PU3	PU4
Uptake rate (mmol·gDW^{-1}·h^{-1})	1.40	1.40	1.40	1.40
Knockouts	8	11	15	*15
Growth rate (h^{-1})	0.53	0.38	0.34	0.34
Production Rate (min-max)	0 - 0.07	0.72	1.07	1.07
Residual Biomass (g/L)	3.07	2.30	2.09	2.09
PHA (mM)	N.D.	5.17	7.65	7.65
PHA Biomass (g/L)	N.D.	0.82	1.22	1.22
$Y_{p/s}$ (mmol/mmol)	0 - 0.05	0.51	0.76	0.76
BCPY (mmol·gDW^{-1}·h^{-1})	0 - 0.04	0.27	0.36	0.36
Biomass PHA (%)	N.D.	26.30	36.79	36.79

Table S 14. Properties of the PHA growth-coupled overproducer designs using PU as substrate at 10 mM (4.94 g/L). * Indicates additional flux constraints. (N.D.: not determined). Uptake rate (mmol·gDW^{-1}·h^{-1}); Growth rate (h^{-1}); Production rate (mmol·gDW^{-1}·h^{-1}); $Y_{p/s,}$ Product yield (mmol product/mmol substrate); BCPY, Biomass coupled product yield (mmol·gDW^{-1}·h^{-1}**).**

Growth-coupled designs using ADIPATE as substrate

The GDLS algorithm using *i*MM1412 was applied using an uptake rate of ADIPATE of 6.3 mmol·gDW^{-1}·h^{-1} using the default parameters for GDLS. The optimal GDLS path results are shown in the Table S15 and Figure S4 .

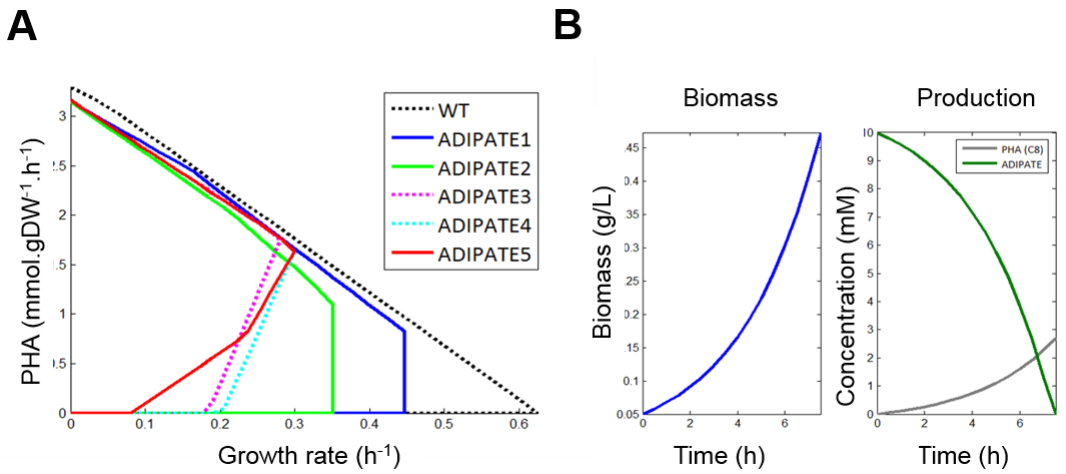

Figure S 4. A. Production envelopes for wild-type and ADIPATE *P. putida* knockout strains belonging to more promising GDLS path**.** The production envelopes for each overproducer design are shown as a function of the biomass production rate of the wild-type *P. putida* network using ADIPATE as sole carbon source (black lines). ADIPATE1 (blue), ADIPATE2 (green), ADIPATE3 (magenta), ADIPATE4 (cyan), ADIPATE5 (red). **B.** Production of biomass (blue) and PHA (grey) of design ADIPATE5 as predicted with dynamic FBA is shown in the center and right panels, respectively, as a function of time and ADIPATE uptake (green).

Design	ADIPATE1	ADIPATE2	ADIPATE3	ADIPATE4	ADIPATE5
Uptake rate (mmol·gDW^{-1}·h^{-1})	6.30	6.30	6.30	6.30	6.30
Knockouts	8	11	15	16	*16
Growth rate (h^{-1})	0.45	0.35	0.28	0.30	0.30
Production Rate (min-max)	0 - 0.83	0 - 1.10	1.75	1.64	1.64
Residual Biomass (g/L)	0.63	0.52	0.44	0.47	0.47
PHA (mM)	N.D.	N.D.	2.80	2.69	2.69
PHA Biomass (g/L)	N.D.	N.D.	0.45	0.43	0.43
$Y_{p/s}$ (mmol/mmol)	0 - 0.13	0 - 0.18	0.28	0.26	0.26
BCPY (mmol·gDW^{-1}·h^{-1})	0 - 0.37	0 - 0.39	0.49	0.49	0.49
Biomass PHA (%)	N.D.	N.D.	50.19	47.46	47.46

Table S 15. Properties of the PHA growth-coupled overproducer designs using ADIPATE as substrate at 10 mM (1.44 g/L). * Indicates additional flux constraints. (N.D.: not determined). Uptake rate (mmol·gDW^{-1}·h^{-1}); Growth rate (h^{-1}); Production rate (mmol·gDW^{-1}·h^{-1}); $Y_{p/s,}$ Product yield (mmol product/mmol substrate); BCPY, Biomass coupled product yield (mmol·gDW^{-1}·h^{-1}).

Growth-coupled designs using MDI as substrate

The GDLS algorithm using *i*MM1412 was applied using an uptake rate of MDI of 2.52 mmol·gDW^{-1}·h^{-1} and using the default parameters for GDLS. The optimal GDLS path results are shown in the Table S16 and Figure S5.

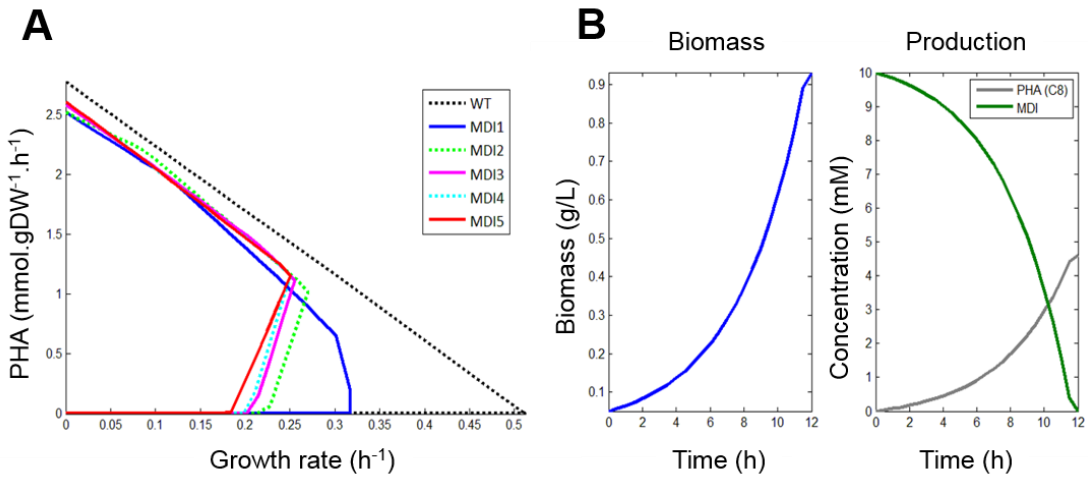

Figure S 5. A. Production envelopes for wild-type and MDI *P. putida* knockout strains belonging to more promising GDLS path. The production envelopes for each overproducer design are shown as a function of the biomass production rate of the wild-type *P. putida* network using MDI as sole carbon source (black lines). MDI1 (blue), MDI2 (green), MDI3 (magenta), MDI4 (cyan), MDI5 (red). **B.** Production of biomass (blue) and PHA (grey) of design MDI5 as predicted with dynamic FBA is shown in the center and right panels, respectively, as a function of time and MDI uptake (green).

Design	MDI1	MDI2	MDI3	MDI4	MDI5
Uptake rate (mmol·gDW^{-1}·h^{-1})	2.52	2.52	2.52	2.52	2.52
Knockouts	8	9	10	21	*21
Growth rate (h^{-1})	0.32	0.27	0.26	0.25	0.25
Production Rate (min-max)	0.00	1.02	1.11	1.16	1.16
Residual Biomass (g/L)	1.15	0.99	0.94	0.93	0.93
PHA (mM)	0.00	4.06	4.43	4.62	4.62
PHA Biomass (g/L)	0.00	0.65	0.70	0.73	0.73
$Y_{p/s}$ (mmol/mmol)	0.00	0.41	0.44	0.46	0.46
BCPY (mmol·gDW^{-1}·h^{-1})	0.00	0.28	0.28	0.29	0.29
Biomass PHA (%)	0.00	39.60	42.84	44.06	44.07

Table S 16. Properties of the PHA growth-coupled overproducer designs using MDI as substrate at 10 mM (0.62 g/L). * Indicates additional flux constraints. Uptake rate (mmol·gDW^{-1}·h^{-1}); Growth rate (h^{-1}); Production rate (mmol·gDW^{-1}·h^{-1}); $Y_{p/s,}$ Product yield (mmol product/mmol substrate); BCPY, Biomass coupled product yield (mmol·gDW^{-1}·h^{-1}).

Growth-coupled designs using PAC as substrate

The GDLS algorithm using *i*MM1412 was applied using an uptake rate of PAC of 4.725 mmol·gDW^{-1}·h^{-1} and using the default parameters for GDLS. The optimal GDLS path results are shown in the Table S17 and Figure S6.

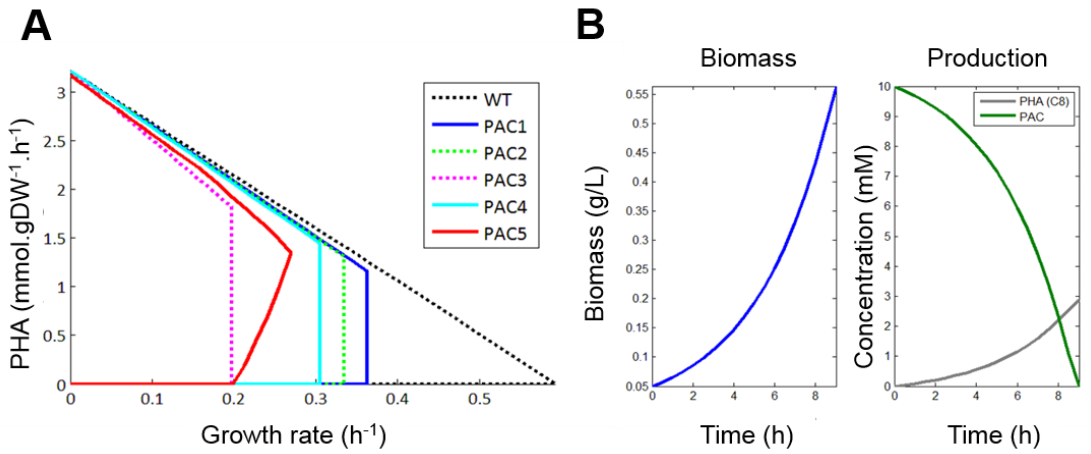

Figure S 6. A. Production envelopes for wild-type and PAC *P. putida* knockout strains belonging to more promising GDLS path. The production envelopes for each overproducer design are shown as a function of the biomass production rate of the wild-type *P. putida* network using PAC as sole carbon source (black lines). PAC1 (blue), PAC2 (green), PAC3 (magenta), PAC4 (cyan), PAC5 (red). **B.** Production of biomass (blue) and PHA (grey) of design PAC5 as predicted with dynamic FBA is shown in the center and right panels, respectively, as a function of time and PAC uptake (green).

Design	PAC1	PAC2	PAC3	PAC4	PAC5
Uptake rate (mmol·gDW^{-1}·h^{-1})	4.73	4.73	4.73	4.73	4.73
Knockouts	7	8	9	15	*17
Growth rate (h^{-1})	0.36	0.34	0.20	0.31	0.27
Production Rate (min-max)	0 - 1.16	0 - 1.31	0 - 1.82	0 - 1.44	1.35
Residual Biomass (g/L)	0.71	0.66	0.43	0.61	0.56
PHA (mM)	N.D.	N.D.	N.D.	N.D.	2.89
PHA Biomass (g/L)	N.D.	N.D.	N.D.	N.D.	0.46
$Y_{p/s}$ (mmol/mmol)	0 - 0.25	0 - 0.28	0 - 0.39	0 - 0.31	0.28
BCPY (mmol·gDW^{-1}·h^{-1})	0 - 0.42	0 - 0.44	0 - 0.36	0 - 0.44	0.36
Biomass PHA (%)	N.D.	N.D.	N.D.	N.D.	44.87

Table S 17. Properties of the PHA growth-coupled overproducer designs using PAC as substrate at 10 mM (1.35 g/L). * Indicates additional flux constraints. (N.D.: not determined). Uptake rate (mmol·gDW^{-}

^{1}·h^{-1}); Growth rate (h^{-1}); Production rate (mmol·gDW^{-1}·h^{-1}); $Y_{p/s,}$ Product yield (mmol product/mmol substrate); BCPY, Biomass coupled product yield (mmol·gDW^{-1}·h^{-1}).

Growth-coupled designs using 14BDO as substrate

The GDLS algorithm using *i*MM1412 was applied using an uptake rate of 14DBO of 9.45 mmol·gDW^{-1}·h^{-1} and using the default parameters for GDLS. The optimal GDLS path results are shown in the Table S18 and Figure S7.

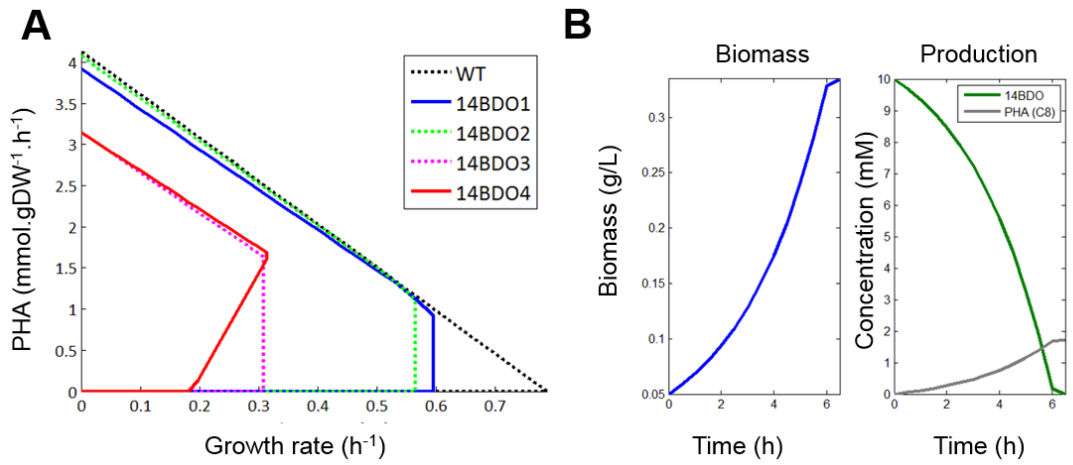

Figure S 7. A. Production envelopes for wild-type and 14BDO *P. putida* knockout strains belonging to more promising GDLS path. The production envelopes for each overproducer design are shown as a function of the biomass production rate of the wild-type *P. putida* network using 14DBO as sole carbon source (black lines). 14DBO1 (blue), 14DBO2 (green), 14DBO3 (magenta), 14DBO4 (cyan), 14DBO5 (red). **B.** Production of biomass (blue) and PHA (grey) of design 14DBO5 as predicted with dynamic FBA is shown in the center and right panels, respectively, as a function of time and 14DBO uptake (green).

Design	14BDO1	14BDO2	14BDO3	14BDO4
Uptake rate (mmol·gDW^{-1}·h^{-1})	9.45	9.45	9.45	9.45
Knockouts	8	9	11	*17
Growth rate (h^{-1})	0.60	0.57	0.31	0.31
Production Rate (min-max)	0 - 0.92	0 - 1.11	0 - 1.63	1.63
Residual Biomass (g/L)	0.54	0.51	0.33	0.33
PHA (mM)	N.D.	N.D.	N.D.	1.72
PHA Biomass (g/L)	N.D.	N.D.	N.D.	0.27
$Y_{p/s}$ (mmol/mmol)	0 - 0.10	0 - 0.12	0 - 0.17	0.17
BCPY (mmol·gDW^{-1}·h^{-1})	0 - 0.55	0 - 0.63	0 - 0.50	0.51
Biomass PHA (%)	ND	ND	ND	45.01

Table S 18. Properties of the PHA growth-coupled overproducer designs using 14DBO as substrate at 10 mM (0.9 g/L). * Indicates additional flux constraints. (N. D.: not determined). Uptake rate (mmol·gDW^{-1}·h^{-1}); Growth rate (h^{-1}); Production rate (mmol·gDW^{-1}·h^{-1}); $Y_{p/s,}$ Product yield (mmol product/mmol substrate); BCPY, Biomass coupled product yield (mmol·gDW^{-1}·h^{-1}).